Mechanical properties of crosslinked actin filament networks

by

Xiaobo Wang

Thesis submitted in partial fulfilment for the degree of

Doctor of Philosophy

Cardiff School of Engineering

Cardiff University

2020

I earnestly dedicate this to my parents, my family, my supervisors and my friends who always encourage and support me.

Acknowledgements

I would like to express my earnest thanks to my supervisors, Dr. Hanxing Zhu and Prof. David Kennedy who have given me a lot of supports and encouragement during the past few years. They are so erudite and kind hearted. They not only help me with my research program but also my daily life. Their professionalism, persistence and passion in research affect me a lot, which are invaluable treasure in my life. Especially, I would like to thank Dr. Hanxing Zhu for his kind help throughout my PhD program. He always gives me precious suggestions on developing models and conducting analyse, which is crucial for the completion of this research. He also spends considerable time and effort helping me to complete research papers.

I would like to thank my colleagues who have given me continuous help and supports during the past few years. It is the happiest and most exciting time when discussing academic questions with them. This contributes very much to my research work.

I would like to thank my friends who always go together with me, which brings me interminable warmness. It is an unforgettable memory to spend my spare time with them in UK.

I would like to acknowledge the supports from School of Engineering, Cardiff University and China Scholarship Council. With their supports, I can put my heart and soul into my research work.

I would like to convey my great thanks to my parents and my family for their unconditional support to my choices. They always support me and believe in me when I encounter difficulties.

Abstract

As a substructure of cell cytoskeleton, the crosslinked actin filament networks (CAFNs) play a major role in different cell functions, however, the mechanical properties and the deformation mechanisms of CAFNs still remain to be understood. In this research, numerical simulations have been performed on a three-dimensional (3D) finite element (FE) model to mimic the mechanical properties of actin filament (F-actin) networks crosslinked by filamin A (FLNA).

The simulation results indicate that although the Young's moduli of CAFNs varies in different directions for each random model, the statistical mean value is in-plane isotropic. The crosslinking density and the actin filament volume fraction are found to strongly affect the in-plane shear modulus of CAFNs. In addition, a cantilever beam model is developed for dimensional analysis on the shear stiffness of CAFNs, which indicates that the in-plane shear modulus of CAFNs is mainly dominated by FLNA (i.e., crosslinkers). The dimensional analysis results agree well with the simulation results. In addition, the deformation mechanism of the CAFNs is also investigated by performing dimensional analysis and conducting numerical simulations.

In physiological conditions, cells can undergo large deformation to respond to external stimulations and to support different cell functions. In large deformation situations, the CAFNs always show strong nonlinear elasticity to maintain the cell shape and integrity, which is known as strain stiffening. In this research, the nonlinear elastic properties of CAFNs are also studied by conducting numerical simulations. According to the results of numerical simulations, it can be demonstrated that the nonlinear elastic properties of crosslinked actin filament networks can be greatly influenced by the actin filament volume fraction, crosslinking density and components' properties. The stress strain relationship of crosslinked actin filament networks is obtained and compared with experimental measurements reported in literature. In addition, the negative normal stresses of CAFNs are obtained from simulations, and the effects of the components' properties on the negative normal stresses are discussed. In addition, to study the deformation mechanism of CAFNs in large strain regime, the effects of the components' bending, torsional and tensile stiffnesses on the stress-strain curves of CAFNs are investigated.

Most of the biopolymer networks are proved to be viscoelastic and their mechanical properties are highly dependent on time and frequency. In physiological conditions, the viscoelastic behaviour of CAFNs could greatly affect the mechanical responses of cells, and different cell functions. Thus, it is important to study the viscoelasticity of CAFNs. The viscoelastic properties of actin filament networks crosslinked by filamin A are also investigated by conducting numerical simulations in this research. Both the creep and relaxation simulations are conducted in finite element method (FEM) software. In FEM simulations, different viscoelastic properties are applied to actin filament and FLNA respectively to probe their effects on the creep and relaxation behaviour of CAFNs. It is found that the FLNA affects the viscoelastic behaviour of CAFNs greater than actin filament. In addition, the effects of applied stress on the creep strain of CAFNs as well as the effects of applied strain on the relaxation stress of CAFNs are studied respectively. Simulation results also show that CAFNs with larger actin filament volume fraction creep less, however, larger actin filament volume fraction results in more relaxation in CAFNs. The creep strain and relaxation stress of CAFNs are found to reduce and increase with the actin filament volume fraction respectively. The crosslinking density is proved to have similar influences on the creep and relaxation behaviour of CAFNs. In addition, the dependence of dynamic shear modulus of CAFNs on the frequency and amplitude of applied loads are investigated. Results indicate that the storage shear modulus of CAFNs develops a plateau at low-frequency conditions, however, the loss shear modulus of CAFNs shows an increasing trend. At high-frequency conditions, both the storage and loss moduli of CAFNs scale with the frequency of applied loads. Moreover, the storage and loss shear moduli of CAFNs remain almost constant when the amplitude of applied load is small. However, they increase with the amplitude of applied load when the applied load reaches a critical value. The simulation results obtained in this research show good agreement with the experimental measurements and theoretical predictions reported in literature.

Contents

List of Figures

List of Tables

List of Abbreviations

ABPs	Actin binding proteins
AFM	Atomic force microscopy
CAFNs	Crosslinked actin filament networks
ECM	Extracellular matrix
F-actin	Actin filament
FCC	Face centre cubic
FE	Finite element
FEM	Finite element method
FLNA	Filamin A
IFs	Intermediate filaments
MD	Molecular dynamics
MTs	Microtubules
PBCs	Periodic boundary conditions
RVE	Representative volume element
SEM	Scanning electron microscopy
2D	Two dimensional
3D	Three dimensional

Nomenclature

A	Area of the face of the representative volume element
A_{yz}	Area of the face of the representative volume element in *y-z* plane
A_c	Area of the cross section of crosslinker
A_f	Area of the cross section of actin filament
d_c	Distance between two actin filaments
E_c	Young's modulus of crosslinker
E_f	Young's modulus of actin filament
E_x	Young's modulus of crosslinked actin filament network in *x* direction
E_y	Young's modulus of crosslinked actin filament network in *y* direction
F_r	Rection force
G_{12}	Shear modulus of crosslinked actin filament network in *x-y* plane
H	Height of the representative volume element
I_c	Area moment of inertia of the cross-section of crosslinker
I_f	Area moment of inertia of the cross-section of actin filament
I_{Pc}	Polar moment of inertia of the cross-sectional area of crosslinker
I_{Pf}	Polar moment of inertia of the cross-sectional area of actin filament
k	Bending stiffness
k_{c0}	Bending stiffness of crosslinker in normal condition
k_c	Bending stiffness of crosslinker
k_{f0}	Bending stiffness of actin filament in normal condition
k_f	Bending stiffness of actin filament
l	Length of a single actin filament

L_c Length of crosslinker in dimensional analysis model

L_m Mean length of actin filament

L_t Total length of actin filaments in representative volume element

n Number of actin filaments crossing each side face of representative volume element

n_c Number of crosslinkers in representative volume element

P Force applied at the end of actin filament in dimensional analysis model

r_c Radius of the cross-section of crosslinker

r_f Radius of the cross-section of actin filament

R_F Molar ratio between filamin dimer and actin monomer

V_f Volume fraction of actin filament

W Width of the representative volume element

u Displacement in x direction

v Displacement in y direction

w Displacement in z direction

α Angle between the projection of a single actin filament in x-y plane and x axis

β Angle between a single actin filament and x-y plane

β_{ul} Up limit of the angle between a single actin filament and x-y plane

γ Applied shear strain

γ_{12} Shear strain in x-y plane

ε Normal strain

ε_x Normal strain in x direction

ε_y Normal strain in y direction

θ Angle between two actin filaments

λ_{c0} Torsional stiffness of crosslinker in normal condition

λ_c	Torsional stiffness of crosslinker
λ_{f0}	Torsional stiffness of actin filament in normal condition
λ_f	Torsional stiffness of actin filament
μ_{c0}	Axial extension stiffness of crosslinker in normal condition
μ_c	Axial extension stiffness of crosslinker
μ_{f0}	Axial extension stiffness of actin filament in normal condition
μ_f	Axial extension stiffness of actin filament
ρ_c	Crosslinking density
σ_n	Normal stress of crosslinked actin filament networks
σ_x	Normal stress in *x* direction
τ_{12}	Shear stress in *x*-*y* plane
v_c	Poisson's ratio of crosslinker
v_f	Poisson's ratio of actin filament
v_{21}	Poisson's ratio in *x*-*y* plane

Chapter 1 Introduction

1.1 Research background and objectives

As a ubiquitous intracellular architecture in eukaryotic cells, cytoskeleton plays a crucial role in maintaining the cell shape and bearing external loads. It is mainly composed of three distinct components, i.e., microtubules, intermediate filaments and actin filaments. Among the three components, actin filaments mainly locate just beneath the cell plasma membrane and can form a thin film network which is also known as cell cortex [1]. It surrounds the intracellular domain and can sensitively respond to the external physical or chemical signals. In addition, actin filaments can be crosslinked into other composite structures by different actin binding proteins (ABPs). For example, actin filaments can form lamellipodia, filopodia, stress fibres and contractile rings with different configurations to support or enable specific cell functions [2]. These complex structures always show distinct elastic properties when participating in different cell functions. Thus, to study the mechanical responses of cytoskeleton and its substructure becomes more and more imperative and important [1, 3, 4].

Changes in mechanical properties of cells can greatly affect the cell adhesion, migration and differentiation, however, the mechanical properties of cells and their cytoskeletons are not well understood. Therefore, it is essential for us to probe the mechanical properties (e.g., elastic properties, viscoelastic properties, dynamic properties) of cells, cytoskeleton and extracellular matrix.

1.2 Thesis outline

To achieve the objectives in this research, the major work of this thesis is organised as follows:

Chapter 1 briefly introduces the background and objectives of this research. The outline of this thesis is also shown in this chapter.

Chapter 2 reviews the literature of biopolymer network structures in eukaryotic cells and extracellular matrix. In addition, the methods of investigating the biopolymer networks are introduced in detail. The existing literature of mechanical properties of crosslinked actin filament networks are also reviewed in this chapter.

Chapter 3 illustrates the details in constructing three-dimensional finite element model for crosslinked actin filament network. The geometry of the network, crosslinking principle, material properties, meshing and boundary conditions are determined in this chapter.

Chapter 4 investigates the linear elastic properties of crosslinked actin filament networks by performing numerical simulations on the three-dimension model developed in Chapter 3. The isotropic properties of crosslinked actin filament networks are discussed in this chapter. Furthermore, a simple cantilever beam model is developed to conduct dimensional analysis, and the results obtained from dimensional analysis are compared with simulation results.

Chapter 5 explores the nonlinear elastic properties of crosslinked actin filament networks. The effects of actin filament volume fraction, crosslinking density and components' properties on the nonlinear elastic properties are studied in this chapter. The deformation mechanism of the crosslinked actin filament networks in large strain regime is also studied in this Chapter. The effects of the bending stiffness, torsional stiffness and tensile stiffness of crosslinkers and actin filaments on the nonlinear elastic properties of crosslinked actin filament networks are investigated separately.

Chapter 6 studies the viscoelastic properties of crosslinked actin filament networks by conducting simulations. The viscoelastic properties of actin filament and FLNA are defined. Then creep and relaxation tests are performed in commercial finite element method software. Additionally, the dynamic properties of crosslinked actin filament network are also investigated.

Chapter 7 gives the main conclusions of this research and points out the further work.

Chapter 2 Literature Review

2.1 Biopolymer networks in eukaryotic cells and extracellular matrix

Eukaryotic cells are the base of eukaryotic plants and animals with larger and more complicated form than those of prokaryotes. They are packed with different kinds of subcellular structures which play important roles in cell division, migration and gene expression. Therefore, it is important to study the mechanical behaviour of eukaryotic cells as well as their subcellular structures. Liu and Oyen [5] elucidate the importance of understanding the mechanical behaviour of cells and the mechanical interactions between cells and their surrounding environment in developing new tissues and regenerative medicines. The importance of subcellular structures on the mechanical responses and cell functions of living cells have also attracted numerous attentions during the past decades. Among the subcellular structures of eukaryotic cells, cytoskeleton is composed of filaments and tubules and form into a network-liked spatial structure which maintains the structure of the whole cell. As a porous network structure, the cytoskeleton holds an average volume fraction of 0.5% which indicates that it is possible for the free percolation of water and there is enough space for the condensation [6, 7].

The biopolymer networks also exist in extracellular matrix whose mechanical properties (e.g. stiffness) can greatly influence different cell functions just like the stiffness of cell substrate do [8]. Some diseases (e.g. tumours, atherosclerosis and fibrosis) also have a close relationship with mechanical properties of extracellular matrix [9-12]. In this section, the biopolymer network in eukaryotic cells and the extracellular matrix are introduced in detail.

2.1.1 Cytoskeleton and its components

In eukaryotic cells, cytoskeleton presents as a complex network consisting of three distinct kind of filamentous biopolymers (i.e., microtubules, microfilaments and intermediate filaments) and plays an important role in supporting cell structure and regulating various cell functions [6, 7, 13-15]. Liu and Chan [15] point out that most living cells bear intricate mechanical stimulations from both the environment and adjoining cells, and their cell functions can be regulated by cytoskeleton. It is also reported that cytoskeleton can help cells to resist deformation and transport intracellular cargo [3]. Fletcher and Mullins [3] provide a fluorescence micrograph and a schematic diagram of neurons to present the structure and elements of the cytoskeleton as shown in Figure 2.1. In Figure 2.1. (a), the neurons cells are selected to illustrate the cytoskeleton of eukaryotic cells, and the three main components (microtubules in green, intermediate filaments in purple and actin filaments in red) of the cytoskeleton of neurons are displayed. The fluorescence micrograph of the growth cone of neurons is shown in Figure 2.1. (b). The growth cone of the neurons plays an important role in the development of the nervous system. Figure 2.1. (c) and (d) show the microstructure of the axon and growth cone of the neurons. Figure 2.1. (e), (f) and (g) give the schematic diagrams of microtubules, intermediate filaments and actin filaments respectively. As microtubules, intermediate filaments and actin filaments are the three main components of cytoskeletons, their contours, functions and properties are reviewed in detail in this part.

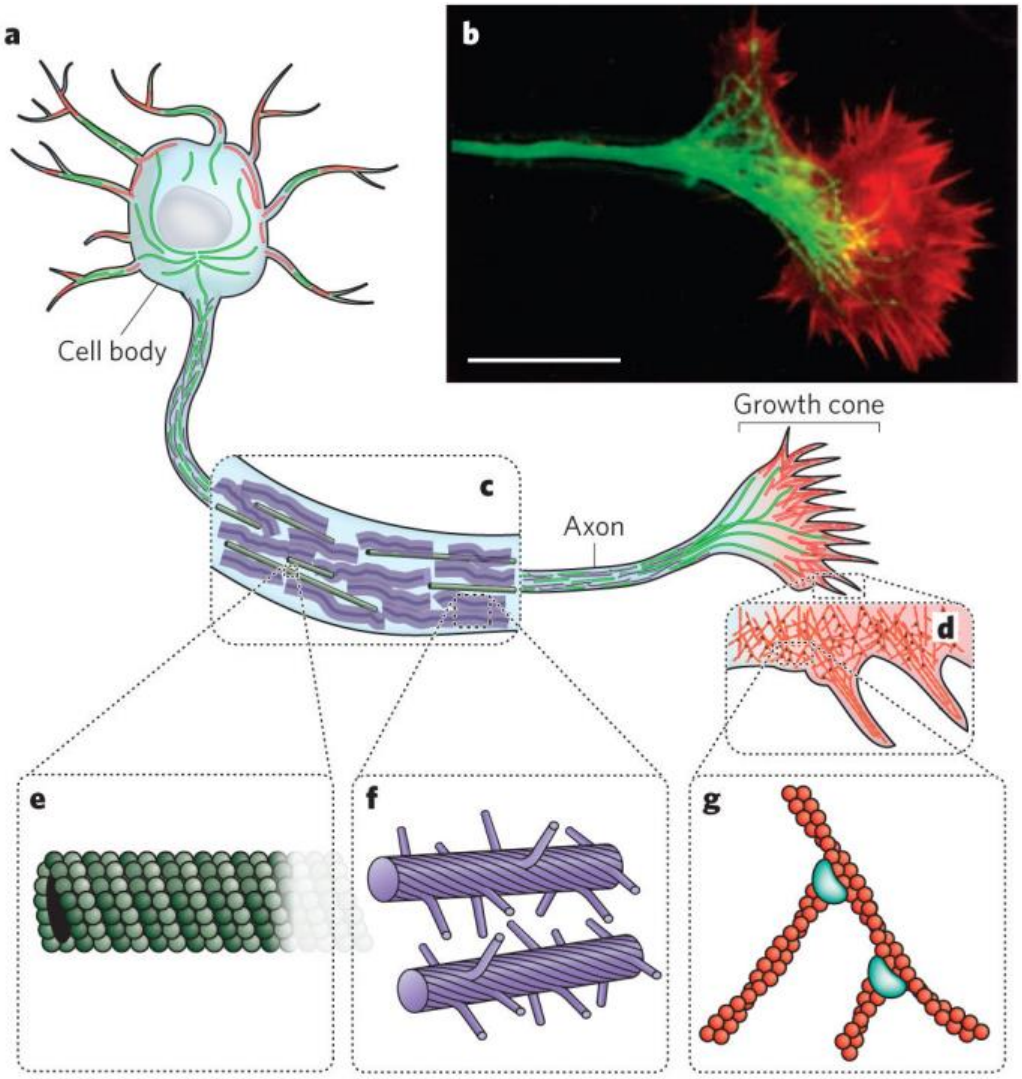

Figure 2.1. The schematic diagram and fluorescence micrograph of neurons presented by Fletcher and Mullins [3].

Among the three principal components of cytoskeleton in eukaryotic cells, the microtubules (MTs) are rigid nanoscale hollow cylinders that distribute throughout the cytoplasm (from the cell nuclear to cell membrane) with the outer diameter and inner diameter being approximate 25 nm and 17 nm respectively [13, 16]. Microtubules are made up of a kind of globular protein which is known as tubulin that is a dimer of two 50-kDa polypeptides (α-tubulin and β-tubulin). Tubulin can polymerize into linear protofilaments which will be arranged in parallel in order to be assembled around the hollow core. Typically, thirteen linear protofilaments will form into a single microtubule that can grow as long as 50 micrometres. As the tubulin dimers are in head-to-tail arrays, a polar structure with two distinct ends

will be formed when the polymerization happens. Depolymerisation will happens as well as polymerization which will results in rapid cycles of assembly and disassembly of microtubules. The confocal image of anaphase cells whose microtubules are stained by antibodies against tubulin is obtained by Rusan and Wadsworth [17] as displayed in Figure 2.2, and the microstructure of microtubules is illustrated by Hawkins et al. [16] as shown in Figure 2.3.

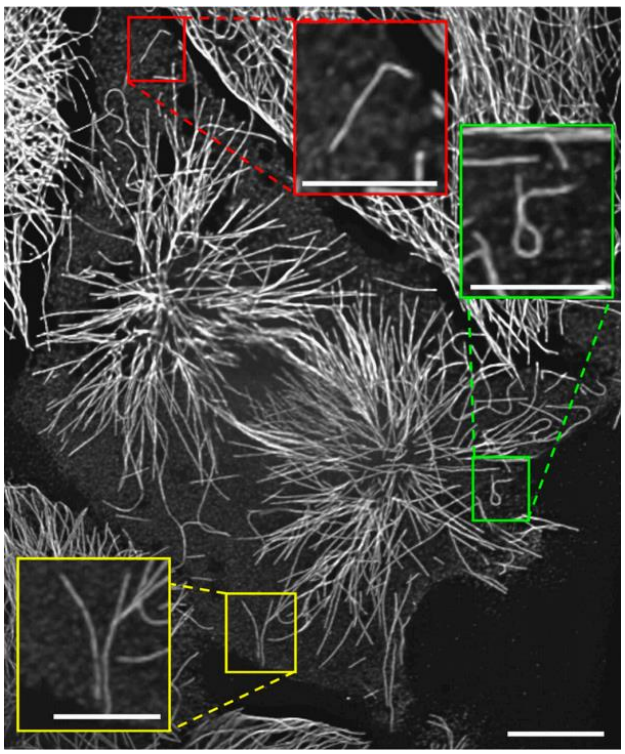

Figure 2.2. The confocal image of anaphase cells with their microtubules being stained by antibodies against tubulin [17]. The enlarged regions refer to the non-centrosome microtubules with two free ends.

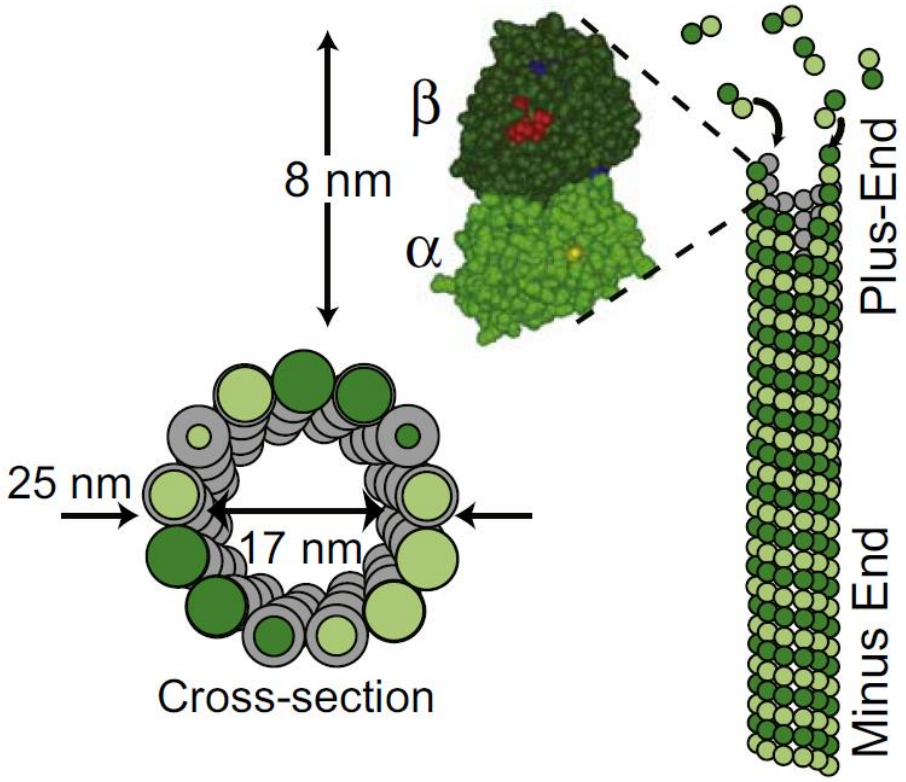

Figure 2.3. The schematic diagram of the microstructure of microtubules [16].

As the most rigid filaments in cells, microtubules have a relatively large persistence length of 5 mm, and their mechanical properties could greatly affect the cell morphology and cell functions. Due to the crucial roles of microtubules in eukaryotic cells, the mechanical properties of microtubules are widely investigated by researchers during the past decades [14, 18]. Gittes et al. [14] measured the flexural rigidity of microtubules to be $2.1\sim2.2\times10^{-23}$ N·m^2 from thermal fluctuations. Wagner et al. [18] used the oscillating rod rheometer (ORR) to measure the viscoelastic properties of microtubules and discussed the effects of the concentration on the viscoelasticity of microtubule gels. Moreover, Brangwynne et al. [19] study the ability of microtubules to bear large-scale compressive loads, and they point that the mechanically coupling between microtubules and their surrounding elastic cytoskeleton can significantly reduce their buckling wavelength as shown in Figure 2.4. Recently, Jia and Liu [20] have proposed a new perspective in measuring the flexural rigidity of microtubules from their thermal fluctuating shape by using mode analysis and principle of virtual work. Generally speaking, microtubules play important roles in various cell functions (e.g. shape

retention, cell locomotion, intracellular transport and cell mitosis) and their mechanical properties are drawing more and more attention.

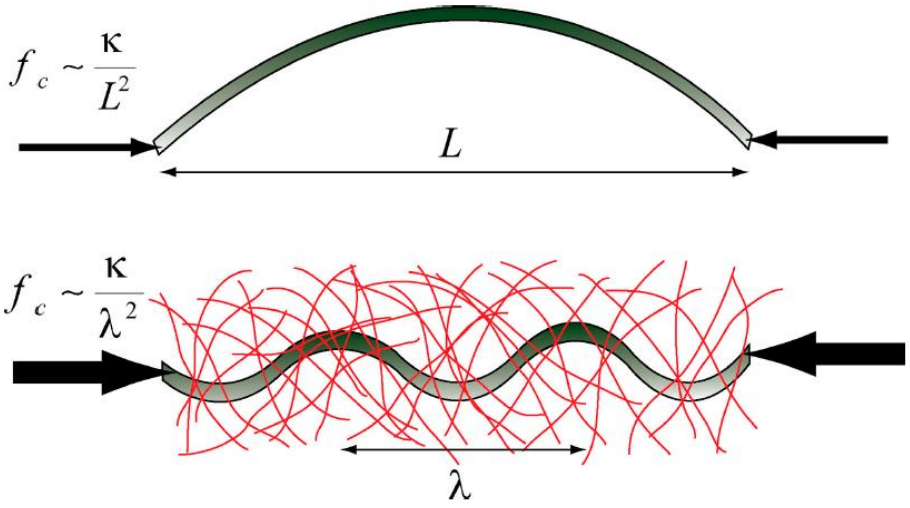

Figure 2.4. The schematic diagram of the buckling of a free single microtubule (in grey) and the buckling of a single microtubule embedded in the surrounding elastic cytoskeleton (in red) [19]. The presence of the surrounding elastic cytoskeleton results in a larger critical force and a shorter wavelength for the buckling of microtubules.

Another prominent component of cytoskeleton is intermediate filaments (IFs) that work as an important structural element in the nuclear envelope and cytoplasm of vertebrate animal cells [21, 22]. It is also reported that intermediate filaments act as a mechanical stress absorber in nucleus and an integrator for the entire cytoskeleton in cytoplasm [21]. The schematic diagram of the organization of intermediate filaments in metazoan cells is proposed by Herrmann et al. [21] as shown in Figure 2.5. It can be seen from Figure 2.5 that the microtubules, intermediate filaments and actin filaments are connected with each other by dimeric complexes of plakin-type molecules. According to the primary structure, gene structure, assembly properties and developmentally regulated tissue-specific expression patterns of the intermediate filaments, IFs are classified into five distinct groups [21, 23]. Keratins, vimentin, desmin, glial fibrillary acidic protein and neurofilament proteins are five main kinds of polypeptides that been assembled from intermediate filaments [24]. The type 1 and type 2 include the acidic and basic keratins respectively. The vimentin, desmin, peripherin and glial fibrillary acidic

protein are designated type 3. The neurofilament subunits, nestin, syncoilin and α-internexin are included in type 4. Type 5 consists of the nuclear lamins. Although different types of intermediate filaments have distinct functions in cells, they have a similar structural building plan [21].

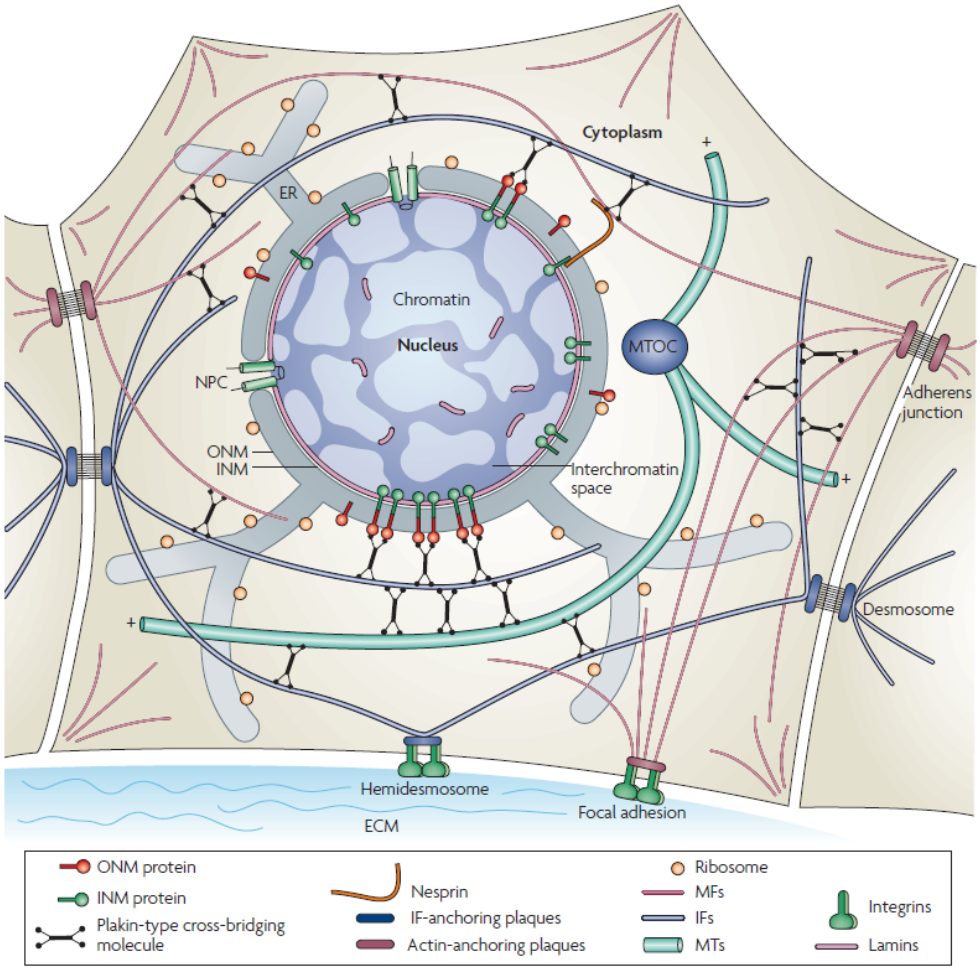

Figure 2.5. The schematic diagram of the organization of intermediate filaments (IFs) in metazoan cells [21].

With the development of electron microscopy techniques, intermediate filaments have been identified in eukaryotic cells with the diameter being 10 nm which is smaller than that of microtubules and larger than that of actin filaments [24]. Although more than 60 distinct genes can code for different kinds of intermediate filaments proteins, the intermediate filaments are all assembled with the diameter being around 10 nm. The process of the formation of intermediate filaments from dimers to mature filaments are illustrated by Godsel et al. [25] by a schematic

model as shown in Figure 2.6. In addition, the confocal image (Figure 2.7) of vimentin filaments of rat-kangaroo PtK2 cell is obtained by Chang and Goldman to illustrate the pervading of intermediate filaments in cytoplasm [23]. Intermediate filaments, together with other components, constitute the structure of eukaryotic cell cytoskeleton [26]. The main functions of intermediate filaments are bearing external/internal stress and integrating the whole cytoskeleton. It is possible to stretch IFs several times of their initial length because of their high stretchable properties which originates from their hierarchical structure that can result in a cascaded activation in different levels of deformation mechanisms [24]. However, in contrast to microtubules and actin filaments, intermediate filaments are not polar which makes them more stable than the other two components [27].

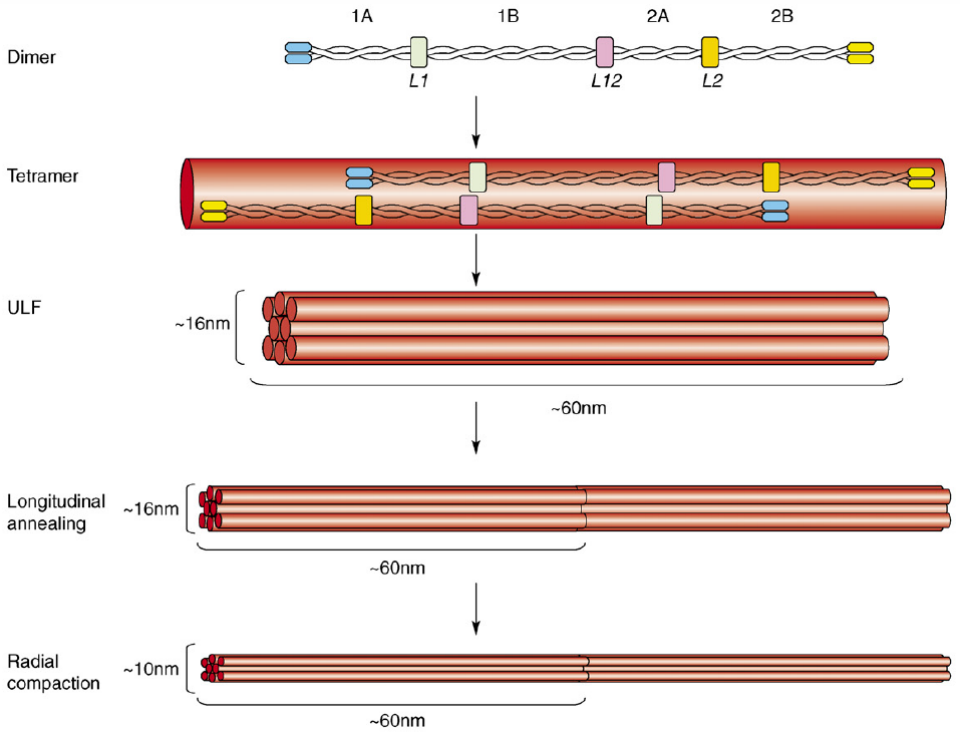

Figure 2.6. The schematic diagram of the formation of intermediate filaments [25].

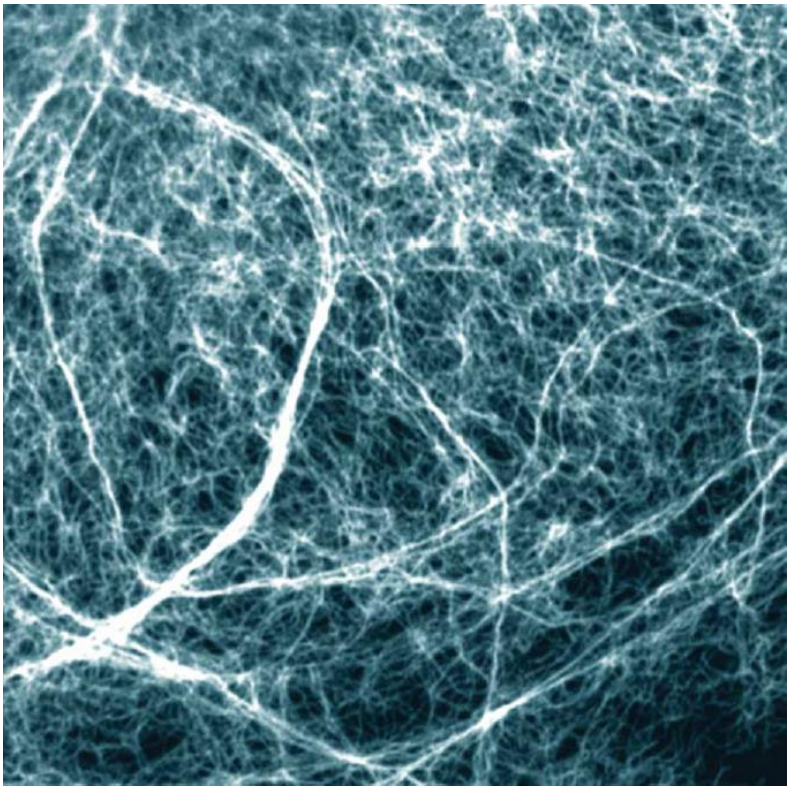

Figure 2.7. The confocal image of intermediate filaments in the cytoplasm of rat-kangaroo PtK2 cell [23].

Actin filament is the primary structural component of cytoskeleton especially in cell cortex, lamellipodium, filopodium and bundled stress fibres [28, 29] with its persistence length being 17 μm. Kim et al. [30] point out that the actin holds a very low volume fraction which is less than 1%. As the most abundant protein in eukaryotic cells, globular actin can be polymerized into actin filaments (F-actin) which is a major constituent of cytoskeleton [31]. The globular subunits of actin filaments are all arranged in the order of head-to-tail which can give actin filaments a molecular polarity and form the double helical configuration [29]. The assembly and stabilization process of actin filaments are illustrated as Figure 2.8 by Feher [32].

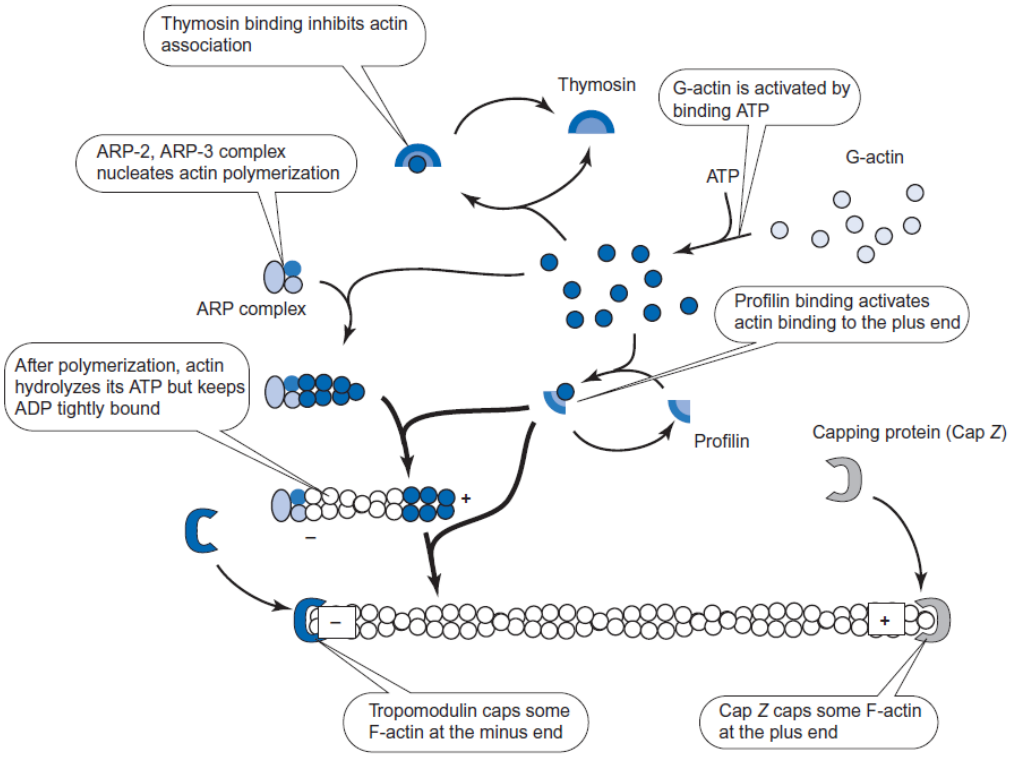

Figure 2.8. The assembly and stabilization process of actin filaments [32].

As a new kind of nano-scaled semi-flexible biopolymer with a number of striking mechanical properties [33], actin filament can form into crosslinked, branched or bundled networks in different parts of eukaryotic cells and play different roles in distinct mechanical behaviours. The different architectures formed by actin filaments and distinct actin binding proteins are schematically represented as Figure 2.9 by Blanchoin et al. [4]. Usually, actin filaments can form different network structures in two distinct dimensions (i.e., the quasi two-dimension and the three-dimension) respectively [34]. That is to say, the actin filament network in actin cortex is quasi two-dimensional and that in the bosom of cells is three-dimensional [35, 36]. Holmes et al. constructed an atomic model for actin filament on the bases of the atomic structure of actin monomers to fit the experimental observations including monomer orientations, actin-actin interactions, contacts etc. [28]. This study can help us to build up a better understanding of actin filaments as many complex cellular activities highly depend on the interactions of actin with actin and other proteins. During the experimental measuring that conducted by Gittes et al., the flexural rigidity of actin filaments is estimated to be 7.3×10^{-26} $N\cdot m^2$ [14]. According to this estimated value of flexural rigidity, the Young's modulus of actin filament can be deduced by dividing the rigidity value by the moment of inertia

(1.178×10^{-34} m^4). Then the Young's modulus of actin filament obtained by this method is 0.62 GPa which is similar to other results reported in literature [37-39]. Actin filaments mechanically support the whole cell and provide driving force for the local movement. A series of biological processes (e.g. external force sensing, cell dividing, membrane vesicle internalizing, local mobility, contraction etc.) are closely related to actin filaments [40].

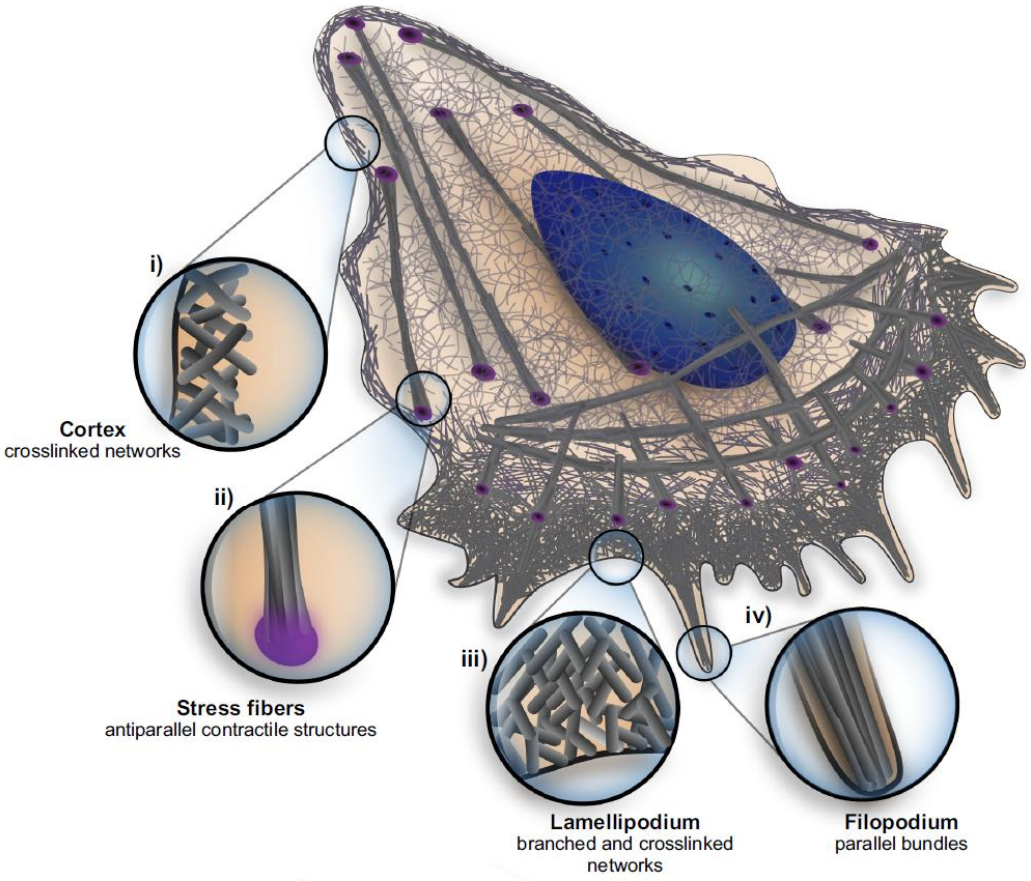

Figure 2.9. The schematic diagram of the different actin filament architectures (e.g., actin cortex, stress fibre, lamellipodium and filopodium) in different regions of a cell [4].

2.1.2 Crosslinked actin filament networks

Different kinds of actin filament structures can be formed when different actin-binding proteins bind with actin filaments and bear different cellular forces [3]. For example, crosslinked cortical networks can be formed by the combination of actin

filaments and filamin, which will provide the network structure a series of novel properties both in mechanical behaviours (e.g. strain stiffening, negative normal stress, marginal stability etc.) and physiological processes (e.g. cell shape maintaining, cell movement, external force bearing etc.). Both the nonlinear force-extension relationship of a single filament and the rearrangements of filaments in whole network can be used to explain the strain stiffing behaviour of semi-flexible biopolymer networks [41]. The electron micrographs of actin filaments crosslinked by filamin A (FLNA) and actin filament network in human blood platelet are obtained by Stossel et al. [42] and shown in Figure 2.10. Actin filaments and Arp2/3 will form into branched networks that are another primary cytoskeleton structure and mainly exist in lamellipodium to push against the plasma membrane as they grow continuously. In filopodia, actin filaments are bundled by fascin, a kind of actin bundling protein. Myosin is the actin binding protein that associates with actin filaments to form stress fibres which can generate active contractile force that play important roles in different cell behaviours. Different structures have different architectures, functions, and properties.

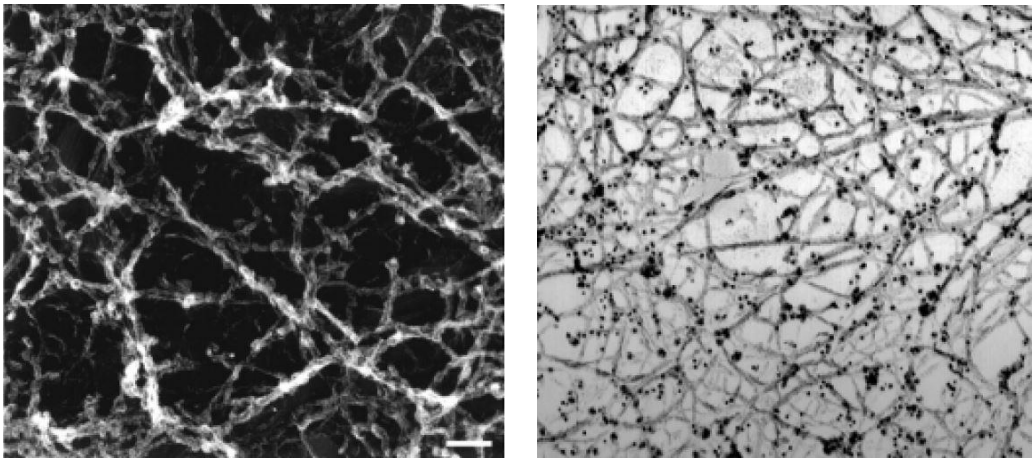

(a) (b)

Figure 2.10. (a) The Electron micrograph of rabbit skeleton muscle actin polymerized in the presence of rabbit lung macrophage FLNA, and the bars indicates 100 nm [42]. (b) the electron micrograph of actin filaments crosslinked by FLNA in human blood platelet [42].

In this research, we mainly focus on the mechanical properties of crosslinked actin filaments networks. Among those cytoskeletal networks, a dense crosslinked actin filament network lies under the cell plasma membrane and is known as cell cortex

which plays a critical role in shape control, movement, cytokinesis and mechanotransduction of the cell [1]. The microstructure of crosslinked actin network layers in sheet-like cells are captured by Xu et al. [43] by combining astigmatism imaging with a dual objective scheme as shown in Figure 2.11. As a thin actin network, cell cortex holds a thickness approximately ranging from 0.1 ~ 1 μm in different cells [1, 43-48], and keeps the mesh size ranging from 100 ~ 200 nm [1, 46, 49, 50]. The length distribution of F-actin in cells has been theoretically predicted and experimentally confirmed to be exponential by a series of previous reports [51-55]. Usually, short actin filaments with the length being about 1 μm will form into a dense isotropic network in the presence of actin-binding proteins [46]. The Young's modulus of actin filament is approximately 1 ~ 2 GPa [14, 33, 37-39, 56, 57], and the Poisson's ratio is about 0.3-0.4 [39, 56, 58]. The persistence length of actin filaments which can reflect the transverse stiffness of a single filament are known as about 17 μm [33]. The physiological lengths of actin filaments usually are less than 2 μm in living cytoskeleton [59] and can be shorter than 1 μm in motile cell cortex [48, 60, 61].

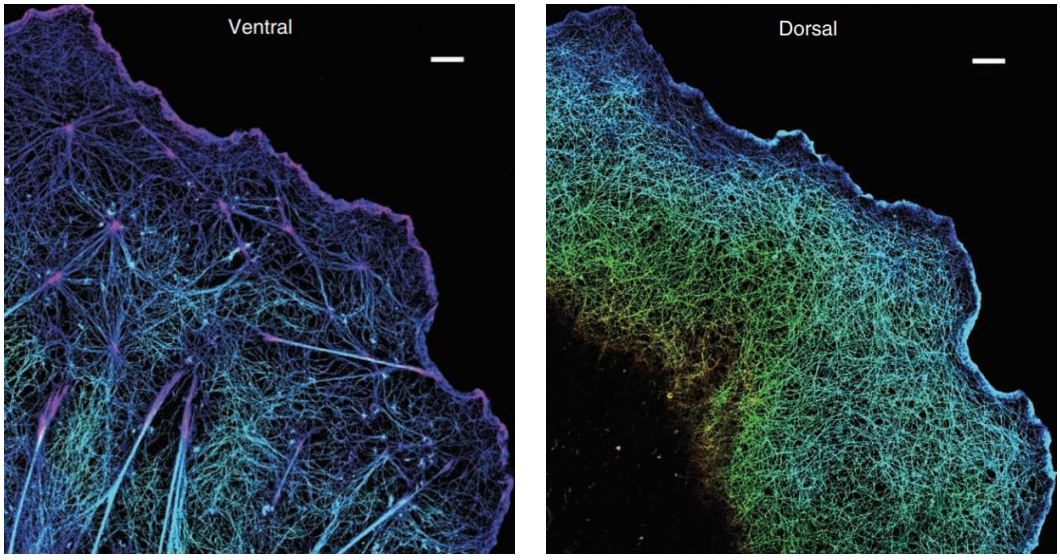

(a) (b)

Figure 2.11. The microstructure of ventral (a) and dorsal (b) actin layer in sheet-like cells, and the bars are 2 μm [43].

In addition, Gardel et al. estimate the physiological concentration of actin filaments to be 24~72 μM (i.e., μmol/L) [59], which is consistent with the concentration of 48

μM (i.e., μmol/L) reported by Nakamura et al. [62], where μM (i.e., μmol/L) is the unit of the concentration of actin monomer. Hartwig and Shevlin point out that the concentration of actin filaments in lamellae is about 12.5 mg/ml [48], however, this seems to be higher than 1.5 mg/ml that is used in other literature [63]. Koenderink et al. observe in microscopic experiments that the actin filament solutions are homogeneous and isotropic when the F-actin concentration is 23.8 μM (equivalent to 1 mg/ml) [64]. For type I collagen gel with its collagen concentration being 1 mg/ml, Lin et al. hold that the volume fraction of collagen is 0.073% [65]. Kim et al. think that the actin filament volume fraction is less than 1% which is too low for filaments to hydrodynamically interact with each other [30]. As described by Gunn, actin filaments can form into a mechanically rigid network structure at a relatively low concentration of 12~24 Mm (i.e., μmol/L) which is equivalent to a volume fraction of 0.05%~0.1% [66]. Mohrdieck et al. develop a biomimetic model to simulate the cytoskeleton network by using 0.04 as the volume fraction of actin filament and discuss the dependence of network elastic shear modulus on the actin filament volume fraction [34]. However, it seems that an actin filament volume fraction of 0.04 is larger compared with the physiological concentrations of actin filament that have been reported by other researchers.

Filamin A (FLNA), a high molecular mass actin-binding protein was first extracted from rabbit alveolar macrophages in 1975 [67]. Filamins are one kind of actin binding proteins which can crosslinked actin filaments into dynamic three-dimensional orthogonal branching networks. Filamins not only contact with other kinds of constituents in cells but also have an important relation with various of human diseases [68]. FLNA assembles two subunits into a non-covalently associated homodimer with the contour length being 160 nm [69-71]. On the microstructure scale, FLNA dimeric subunits consist of actin binding domains and a flexible part of 24 immunoglobulin repeats [70]. The electron micrograph of a single FLNA molecule is obtained by Nakamura et al. [70] as shown in Figure 2.12. And a schematic diagram to illustrate the coherent interaction of FLNA with actin filaments is also shown in Figure 2.12. In living cells, the length of actin filaments in cortical cytoskeleton is always shorter than 2 μm (or around 1 μm) with the concentration being 48 μM and the molar ratio to FLNA being 100:1 [62]. The atomic force microscope (AFM) is proved to be a powerful apparatus in measuring the mechanical properties of biological materials [72]. The mechanical properties of a single filamin A have been experimentally measured by atomic force microscopy (AFM) and an unfolding force of 50~220 pN has been obtained [73].

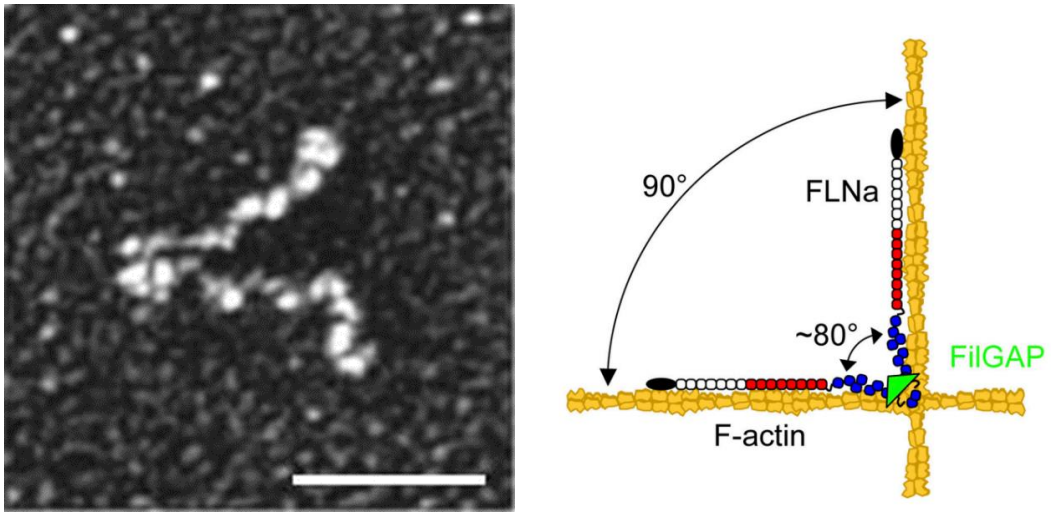

(a) (b)

Figure 2.12. (a) The electron micrograph of a single FLNA molecular, the bar indicates 50 nm [70]. (b) The schematic diagram of the coherent interaction of FLNA with actin filaments [70].

2.1.3 Extracellular matrix

The extracellular matrix (ECM) is a highly dynamic three-dimensional biopolymer network structure which consists of various macromolecules and continuously goes through controlled remodelling. It is the noncellular component that widely exists in all tissues and organs, and it not only plays a major role in supporting the surrounding cells [74, 75] but also presents crucial biochemical and biomechanical suggestions which are crucial in tissue differentiation, morphogenesis and homeostasis [76]. The extracellular matrixes in different tissues is reported to comprise different components, for example, the extracellular matrix in bone tissue consists of collagen fibres and bone mineral. The major constituents of extracellular matrix are reported to be fibrous-forming proteins (e.g., collagens, elastin and fibronectin) [77]. Theocharis et al. [77] point out that the interstitial matrix (surrounding cells) and pericellular matrix (contacting with cells) are two major types of extracellular matrix according to their different compositions and structures. The collagen is proved to be the most plentiful protein in extracellular

matrix [78], and is mostly found in fibrous tissues. Most of the collagen in human body is reported to be the type I collagen which is fibrillary and can form collagen fibres. In cartilage, collagen type II is the major constituents of the extracellular matrix. They are reported to work with other collagens and proteoglycans to form complex fibrillar structures which are crosslinked with extracellular matrix molecules [77]. The scanning electron microscopy (SEM) analysis of normal type I collagen fibre organisation in three-dimensional matrix is presented by Petropolis et al. [79] as shown in Figure 2.13.

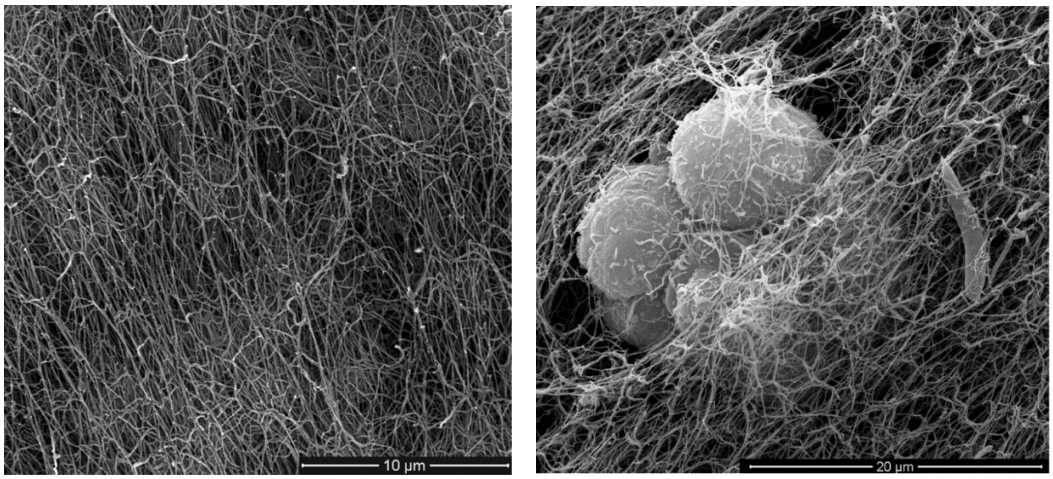

(a) (b)

Figure 2.13. (a) The scanning electron microscopy of normal type I collagen fibre organisation in three-dimensional matrix [79]. (b) The scanning electron microscopy observation of macrophages that are cultured in three-dimensional type I collagen matrix after 3 hours of interaction with *Leishmania* [79]. The three-dimensional structure of the extracellular matrix creates an effective shelter to prevent the interaction between macrophages and *Leishmania*.

The extracellular matrix can provide structural supporting for cells due to the complex mechanical interactions between them, which contributes to the integrity of tissues [80]. In addition to the structural supporting, the extracellular matrix also plays important roles in many other cell functions, such as cell adhesion, migration and signalling [75, 81] by interacting with cells. Jin et al. [82] use a novel technique to measure the contraction force of fibroblasts which are embedded in 3D collagen matrix, and find that the contraction force are highly affected by the stiffness of

collagen matrix [83]. The composition and architecture of the extracellular matrix is schematically illustrated by Griffith and Swartz [84], as shown in Figure 2.14. Therefore, it is essential to study the mechanical properties of such biopolymer network structure.

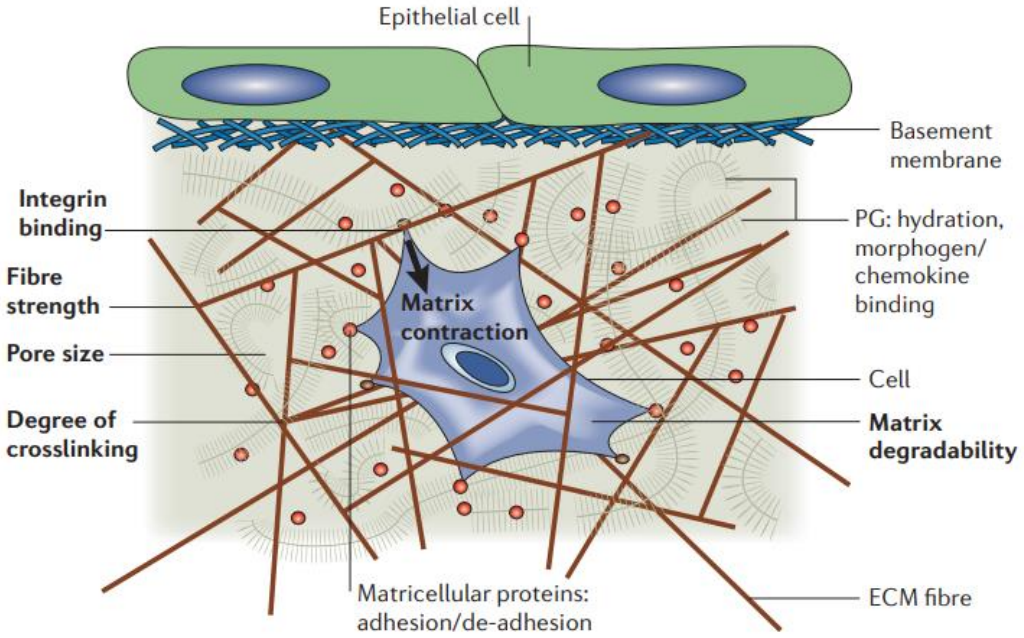

Figure 2.14. The schematic diagram of the composition and architecture of the extracellular matrix [84].

2.2 Methods to investigate biopolymer networks

In contrast to linear elastic composites, the semi-flexible biopolymer networks show a nonlinear relationship between their shear strain and shear stress. Crosslinked actin filaments networks show various novel mechanical properties because of their semi-flexible nature and special architectures. It is necessary to experimentally and theoretically analyse these properties in order to understand the mechanisms of deformation and other mechanical behaviours. During the past decades, semi-flexible biopolymers have attracted lots of attention because of their string mechanical properties which play important roles in many physiological processes [33]. Unlike flexible polymers (e.g. rubber) whose properties have been

already relatively well understood, those semi-flexible biopolymers have many mysterious properties that have not yet been completely revealed. This is the reason why semi-flexible biopolymers can motivate the continuously experimental and theoretical explorations.

Experimental [31, 59, 85-89] and theoretical [33, 90-96] analysis can use different methods to reveal the properties of semi-flexible biopolymers respectively, and both of them are very important in in studying the mechanical properties of biopolymer networks. In addition, the numerical simulation [34, 41, 47, 63, 97-99] is another effective method to investigate the mechanical behaviours of biopolymer networks. All these methods have their own advantages and disadvantages when studying the mechanical properties of biopolymer networks. For example, the experimental measuring could directly obtain the mechanical properties of biopolymer networks both *in vivo* and *in vitro* by using specific facilities (i.e., atomic force microscopy), however, it is difficult to control the culturing and polymerizing process when conducting experiments, which could result in a large discrepancy in the experimental results. In addition, conducting experiments is also time consuming and expensive. The theoretical analysis is proved to be another effective way to investigate the mechanical properties of biopolymer networks, and it could well explain the deformation mechanism of biopolymer networks by using different theories. But the microstructure of the biopolymer networks is sometimes neglected when performing theoretical analysis. In addition to the experimental measurement and theoretical analysis, numerical simulations are widely used in studying the mechanical properties of biopolymer networks. The numerical simulations show high efficiency in comparison with the experimental measurement, and the microstructure of the biopolymer networks could be taken into consideration when performing numerical simulations.

During the past decades, numerous studies have been developed to probe the mechanical properties of biopolymer networks by conducting experiments, proposing theoretical solutions and performing numerical simulations. As this research mainly focuses on the mechanical properties of crosslinked actin filament networks, the methods of studying crosslinked actin filament networks are reviewed in detail in this part.

2.2.1 Experimental measuring

Experimental measuring is an essential method to study the various properties of different materials and structures. It can provide us a lot of useful information which are measured from different experiments. For example, Ahearne et al. [100] develop a novel indentation method to measure the mechanical properties of hydrogels which are widely used in tissue engineering and regenerative medicine. During the past decades, some basic mechanical properties of a single filament have been experimentally measured by different methods [14, 37, 39]. Experimental explorations on biopolymer networks can also bring many sparkling ideas for the future design in advanced polymeric structures and composites. Janmey et al. [101] experimentally polymerize actin into actin filaments and measure the lengths of them by electron microscopy. They also measured the viscoelastic properties of actin gels by five different techniques and five different instruments using actin preparations purified in four different laboratories [85]. They found that the shear modulus of 2 mg/ml actin gels is on the order of hundred pascals (Figure 2.15 (a)) and the shear modulus of the actin gels is highly affected by the actin filament length (Figure 2.15 (b) and (c)) and the preparing process of the actin gels [85]. These findings provide significant reference to researchers to study the mechanical properties of actin filament network structures.

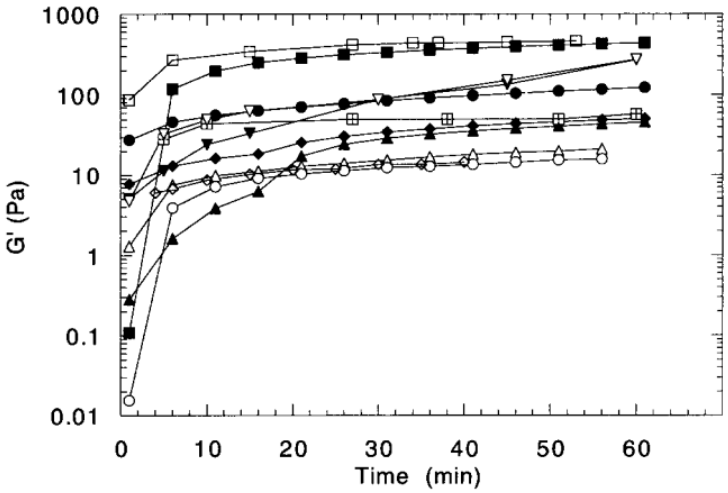

(a)

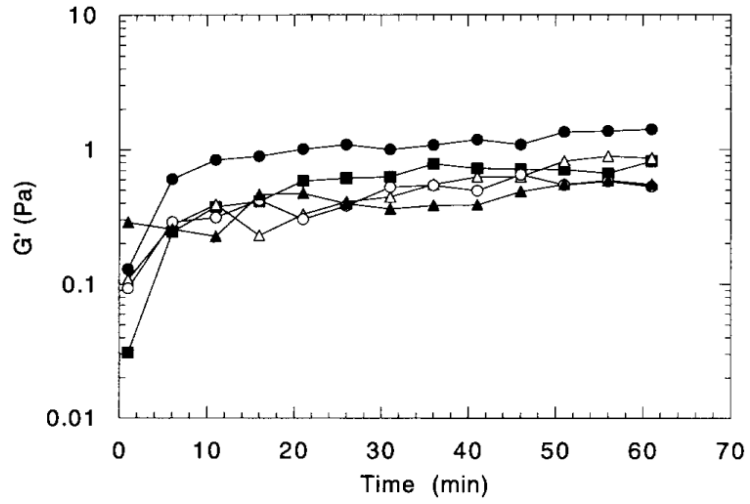

(b)

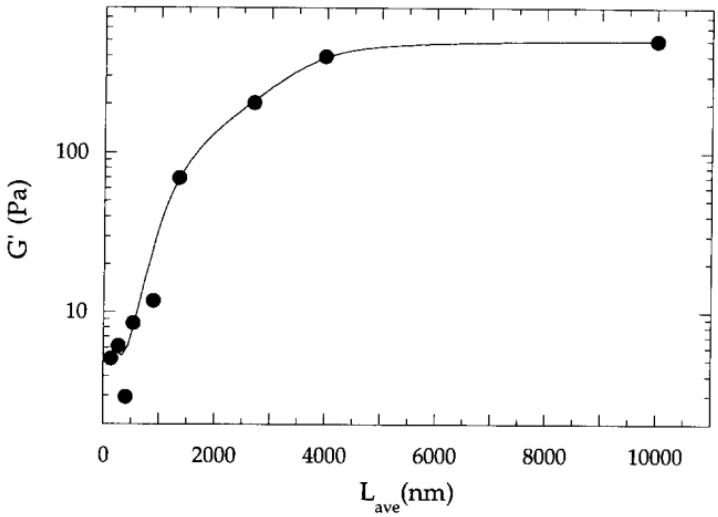

(c)

Figure 2.15. (a) The storage shear modulus (*G'*) of 2 mg/ml actin gels which are polymerized without the adding of gelsolin [85]. (b) The storage shear modulus (*G'*) of 2 mg/ml actin gels which are polymerized with the molar ratio between gelsolin and actin being 1:1000 [85]. And the average length of actin filaments in this condition is 2.7 μm. (c) The dependence of the storage shear modulus of actin filament gels on the length of actin filament [85]. The different symbols in (a) and (b) denote different acetone powders which are used to prepare actin. The solid line in (c) is the fitting curve of experimental measurements (solid circles).

The lengths of actin filaments are proved to play an important role in steric constraints [101] and mechanical properties [89] of some cytoskeleton structures

that consist of F-actin (e.g. cortex, stress fibres, branched networks etc.). Kasza et al. [89] point out that the elastic properties of actin filament networks crosslinked by the compliant actin binding proteins (e.g., filamins) are highly affected by the average length of actin filaments (Figure 2.16). From Figure 2.16 (a) and (b), it is easy to find that the average length of actin filaments could greatly affect the elastic shear modulus of actin filament networks crosslinked by filamins or NeutrAvidin protein. The experimental measurements in Figure 2.16 show that the elastic shear modulus of actin filament networks crosslinked by filamins or NeutrAvidin protein increases nonlinearly with average length of actin filaments, however, the compliant and rigid crosslinked actin filament networks show two distinct increasing trends. The slopes of the curves in Figure 2.16 (a) increase with the average length of actin filaments but the slope in Figure 2.16 (b) decrease with the average length of actin filaments.

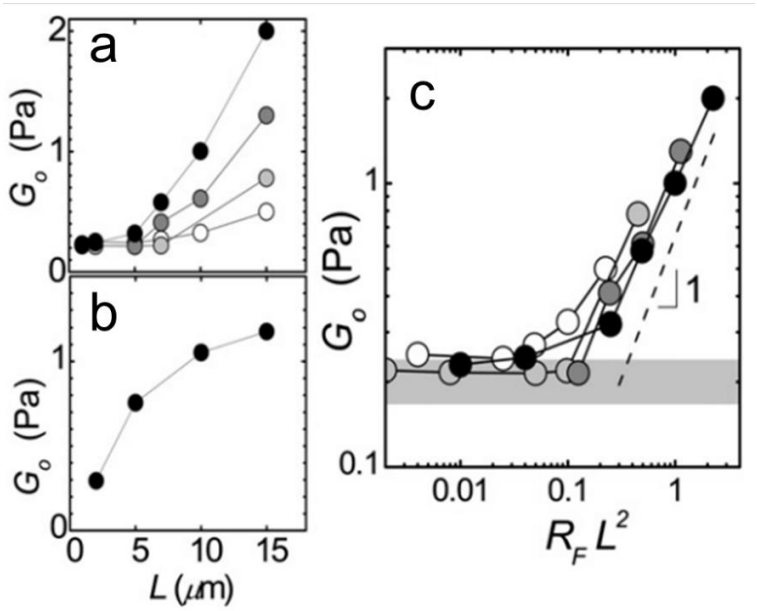

Figure 2.16. (a) The dependence of the elastic shear modulus (G_0) of compliant crosslinked actin filament networks on the average length of actin filaments [89]. (b) The dependence of the elastic shear modulus (G_0) of rigid crosslinked actin filament networks on the average length of actin filaments [89]. (c) The elastic shear modulus (G_0) of actin filament networks crosslinked by filamins at different molar ratio (R_F) between filamin dimer and actin monomer collapse onto a single curve when G_0 is plotted against $R_F L^2$ [89]. The different symbols in (a) and (c) refer to different levels of molar ratio between filamin dimer and actin monomer. The unit of $R_F L^2$ in (c) is μm^2.

Gardel et al. [31] point out that there are two different regimes when studying the elastic properties of crosslinked and bundled actin filament networks. The first regime reflects the bending of actin filaments; however, the second regime corresponds to the stretching of actin filaments. They have experimentally studied the dependence of the elastic shear modulus (G_0) of crosslinked and bundled actin filament networks on the concentration of actin and the crosslinking density (Figure 2.17). It is reported that the elasticity of the actin filament networks remains linear at lower actin concentration or crosslinking density. But it becomes nonlinear when the actin concentration or the crosslinking density increases to higher levels. In addition, the effects of the prestress on the differential elastic modulus (K') of crosslinked and bundled actin filament networks are illustrated (Figure 2.18). The differential elastic modulus (K') in Figure 2.18 is determined by superposing a small oscillatory stress ($\delta\sigma$) for a constant applied prestress (σ_0) at 0.1 Hz and measuring the response of the network to a small oscillatory stress. Then the definition of the differential elastic modulus (K') can be written as $K'(\sigma_0) = [\delta\sigma/\delta\gamma]|_{\sigma_0}$.

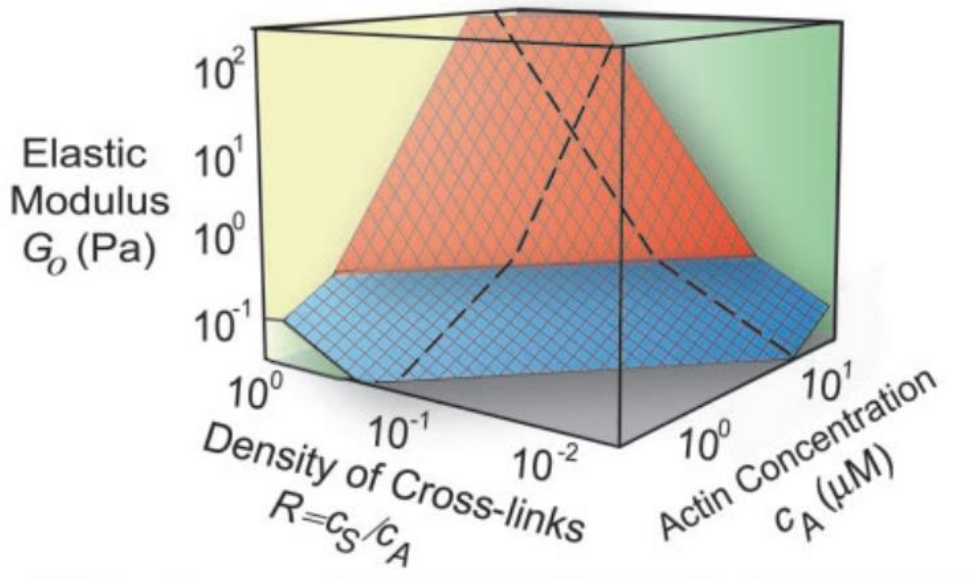

Figure 2.17. The dependence of the elastic shear modulus (G_0) of crosslinked and bundled actin filament networks on the concentration of actin and the crosslinking density [31].

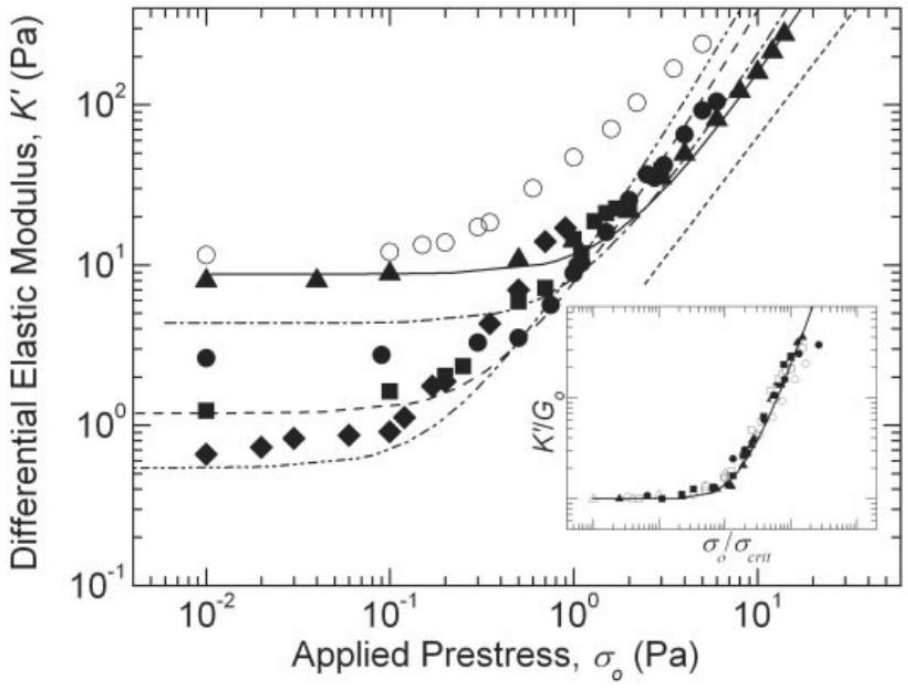

Figure 2.18. The effects of the prestress on the differential elastic modulus of crosslinked and bundled actin filament networks [31]. Different solid symbols correspond to different concentrations of actin in crosslinked actin network with the crosslinking density being fixed at 0.03. The open circles refer to the stress stiffening response of a bundled actin network. The dashed line at the right indicates $\sigma_0^{3/2}$.

Gardel et al. [59, 102] also use an *in vitro* model to study the nonlinear mechanical behaviour of crosslinked actin filament networks which has well capture the main mechanical properties of cytoskeleton of eukaryotic cells. They use different filamin mutants to form crosslinked actin filament networks to study the effects of the microstructure of filamins on the mechanical properties of actin filament networks (Figure 2.19). This behaviour has also been proved in later experimental research works that are carried out by Kasza et al. [89, 103, 104].

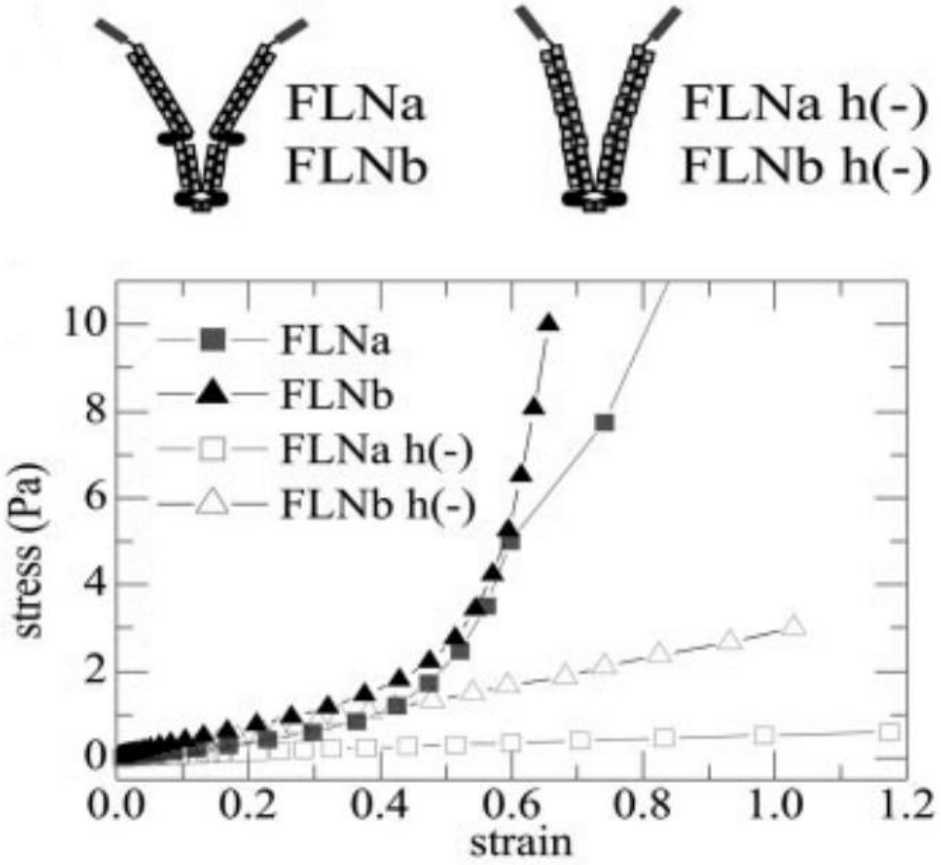

Figure 2.19. The schematic diagram of the hinged and hingeless isoforms of filamins and the stress strain relationship of crosslinked actin filament networks [59].

In summary, a large number of experiments have been conducted by researchers during the past decades to investigate the mechanical properties of crosslinked actin filament networks (CAFNs), and many meaningful results have been obtained. This not only provides us a good reference to study the properties of CAFNs and other biopolymer network structures but also helps us to design some bioinspired materials. However, there are still some issues which are difficult to be proved by conducting experiments. Therefore, theoretical analysis and numerical simulations are also applied when studying the mechanical properties of CAFNs.

2.2.2 Theoretical analysis

Theoretical analysis is another effective way to study the mechanical properties of CAFNs by applying some assumptions. During the past decades, many theories have been developed to study the mechanical properties of CAFNs.

In the classical theory, a polymer can be described by *N* bonds with each of them obeying the Gaussian distribution. When it comes to polymers whose monomeric subunits are connected by harmonic springs, Gaussian Hamiltonian is a widely used representation that can be expressed as [105]:

$$\beta H_G = \frac{1}{2b^2}\sum_{j=1}^{N}\left(\vec{r}_j - \vec{r}_{j-1}\right)^2 \tag{2.1}$$

where *b* is the distance between monomers (which is also known as Kuhn length). When a limit ($N \to \infty,\ b \to 0$) is applied to the discrete Gaussian model, the continuum form of the Gaussian Hamiltonian can be deduced as:

$$\beta H_G{}^0 = \frac{1}{2}\int_0^L \left(\frac{\partial \vec{r}}{\partial s}\right)^2 ds \tag{2.2}$$

where *L* is the total length or the contour length of a single biopolymer.

The Edwards Hamiltonian [106] for a polymer is:

$$H_E = \frac{3k_BT}{2b^2}\sum_{j=1}^{N}\left(\vec{r}_j - \vec{r}_{j-1}\right)^2 \tag{2.3}$$

where k_B is the Boltzmann's constant, *T* is the temperature. And the continuum form of Edwards Hamiltonian is:

$$H_E = \frac{3k_BT}{2b^2}\int_0^L \left|\frac{d\vec{r}\,(s)}{ds}\right|^2 ds \tag{2.4}$$

It is well known that actin filament is a typical kind of semi-flexible biopolymers which are widely exists in eukaryotic cells and can affect cell structure and function [91]. Just as its name, the semi-flexible biopolymers have a finite resistance to bending in comparison with their flexible counterparts. For a semi-flexible polymer, the Hamiltonian for its bending energy can be described in terms of its bending modulus as [33, 107]:

$$H_B = \frac{\kappa}{2}\int_0^L \left|\frac{\partial^2 \vec{r}}{\partial s^2}\right|^2 ds \tag{2.5}$$

where *k* is the bending modulus of semi-flexible polymers.

Kratky and Porod use a wormlike chain model [108] to simulate the mechanical properties of semi-flexible biopolymers including actin filaments. The wormlike chain model has also been used to analyse the stretching experiments of double-stranded DNA and a strong-stretching regime has also been observed during all the experiments [109]. The approximate interpolation formula [109] for the force-extension relationship of wormlike chain model has also been summarized from Marko and Siggia's research work as:

$$\frac{fA}{k_B T} = \frac{z}{L} + \frac{1}{4\left(1 - z/L\right)^2} - \frac{1}{4} \tag{2.6}$$

where k_B is the Boltzmann's constant, *T* is the temperature, *A* is the characteristic length over which a bend can be made with energy cost $k_B T$, *f* is the applied force that appears as a Lagrange multiplier, *z* is the end-to-end extension, *L* is the total length of a single biopolymer or the contour length. This force-extension interpolation formula has also been used to represent stretching behaviours of compliant crosslinkers in the form as follows [110, 111]:

$$f_{cl}\left(u\right) = \frac{k_B T}{l_p}\left(\frac{1}{4\left(1 - u/l_0\right)^2} - \frac{1}{4} + \frac{u}{l_0}\right) \tag{2.7}$$

When the polymer is assumed to be inextensible, the thermal fluctuation can cause a contraction in the polymer chain's end-to-end length by *u* which can be expressed as:

$$\Delta l = \int\left(\sqrt{1 + \left|\frac{\partial u}{\partial x}\right|^2} - 1\right) dx \simeq \frac{1}{2}\int\left|\frac{\partial u}{\partial x}\right|^2 dx \tag{2.8}$$

Then, by applying a tension to the free end of a one end fixed filament, the energy that produced by the tension force is:

$$H_T = \tau \Delta l = \frac{1}{2}\int \tau \left|\frac{\partial u}{\partial x}\right|^2 dx \tag{2.9}$$

In the presence of thermal fluctuations, the whole energy [33] that stored in a stretched filament is the summation of H_B and H_T and can be expressed as:

$$H = \frac{1}{2}\int\left(\kappa\left|\frac{\partial^2 u}{\partial x^2}\right|^2 + \tau\left|\frac{\partial u}{\partial x}\right|^2\right)dx \tag{2.10}$$

MacKintosh et al. [91] developed a theoretical model to study the elasticity of semiflexible biopolymer networks and illustrated the effects of the concentration of biopolymer on the storage modulus and yield strain of the network structure. According to their model, the storage shear modulus, *G'*, of the crosslinked semiflexible biopolymer gel scales with the concentration of biopolymer, c_A, as:

$$G' \sim \frac{\kappa^2}{k_B T}\left(a c_A\right)^{5/2} \tag{2.11}$$

And their theoretical predictions show good agreement with their experimental results. Their model can be used to understand the elasticity of both crosslinked biopolymer networks and entangled biopolymer solutions.

Palmer and Boyce [94] use a microstructurally informed continuum mechanics approach to develop a constitutive model for studying the microstructure and stress-strain behaviour of crosslinked actin filament networks. They used the worm-like chain model to capture the force-extension relationship of individual filaments and this force-extension behaviour is applied in the Arruda-Boyce eight-chain network model to study the mechanical properties of the three-dimensional filament networks. The results obtained from their constitutive model compare favourably with the experimental measurements of actin filament networks reported in literature. Dillen et al, [92] use affine deformation theory to study the stiffening behaviour of crosslinked biopolymer networks by taking the interaction of the filaments with the surrounding fluid into consideration which is neglected in discrete network model. The results obtained from affine network model are compare with that obtained from discrete network model. Unterberger et al, [95] propose a continuum mechanical formulation which takes the mechanical behaviour and spatial arrangement of actin filaments into account to describe the viscoelastic behaviour of actin filament networks. They model the single actin filament by using worm-like chain model and assemble the three-dimensional actin filament network by using microsphere model. And their model is validated by comparing with the measurements from rheological experiments on reconstituted actin filament gels. Menendez and Rodriguez [96] develop a microstructural model

in the framework of nonlinear continuum mechanics to study the cyclic hardening of actin filament networks crosslinked by *α*-actinin. In their model, the actin filaments are also modelled by worm-like chain model and they are crosslinked by *α*-actinin in a gelation process which is modelled as mesoscale dynamics. Their microstructure model is also validated by comparing with the experimental measurements published in literature. Meng and Terentjev [93] propose a continuum theory for equilibrium elasticity of crosslinked semiflexible filament networks to study their nonlinear elasticity. They use the three-chain constitutive model and obtain the analytical expressions of the elastic energy of the crosslinked filament networks. And their theory is proved to agree well with the measurements obtained from simple shear experiments on various filament networks.

These theoretical studies use different approaches to investigate the mechanical properties of crosslinked biopolymer networks and obtain many meaningful results which could well explain the mechanical behaviours of crosslinked biopolymer networks. Therefore, theoretical analysis is proved to be an effective method and widely used to study the mechanical responses of such biopolymer network structures. However, the theoretical analysis may not capture the precise microstructure of the biopolymer networks as it is always developed by applying many assumptions. In addition to theoretical analysis, the numerical simulation is also widely used to investigate the mechanical properties of biopolymer network structures because of its advantages in directly mimicking the precise microstructure of the biopolymer network structures. Literature about the numerical modelling of biopolymer networks are reviewed in detail in the following part.

2.2.3 Numerical modelling

In addition to the experimental and theoretical studies on the mechanical properties of crosslinked biopolymer networks, numerical simulation is another method to investigate the mechanical behaviours of crosslinked biopolymer networks. Sometimes it is difficult to get the desirable data from experimental methods, however, maybe it can be realized by numerical modelling. During the past decades, various models for both the single filament and the whole network have been established to simulate the mechanical behaviours of semi-flexible biopolymers and their network structures. In early times, researchers always

focused on two dimensional models [41, 47, 97, 98, 112-114] because of its simplicity and the quasi two dimensional structure of the cell cortex. However, there are some limitations in those simple models, for example, they cannot represent the real structure of cytoskeleton which is three dimensional in the physiological circumstances. Therefore, three dimensional models [63, 111, 115, 116] have been developed in combination with finite element method [56, 117, 118] or molecular dynamics [119] to investigate the mechanical properties of semiflexible biopolymer networks. In different models, filaments and crosslinkers are treated differently. Finite element method (FEM) is originally used to solve solid mechanics issues and can be used to study the mechanical behaviours of fibrous materials [120]. In finite element method, filaments and crosslinkers are usually modelled by beam elements which are widely used to model the mechanical responses of fibrous materials. By controlling the geometrical and material parameters of the biopolymer networks in numerical simulations, the mechanical properties of such network structures could be obtained and well understood. In this part, literature about the numerical modelling of crosslinked actin filament networks are reviewed in detail.

Among the two dimensional (2D) models for crosslinked filament networks, the Mikado model [41, 47, 97, 112] turns out to be the simplest and most widely used one. Head et al. [112] develop a two-dimensional model (Figure 2.20) to perform numerical studies on the mechanical responses of the isotropic and homogeneous network system. A large number of fibres with the same length are randomly generated in a square whose size which is large enough to contain all of the fibres. Some novel results are obtained and presented in their research. For example, when the network density is the threshold of the rigidity percolation, the elastic modulus of the network tends to decrease to zero. What is more, the affine and non-affine deformation regimes are two distinct regimes [112] that have been found in their work and these two regimes are closely related to the density of crosslink and the rigidity of fibres [97].

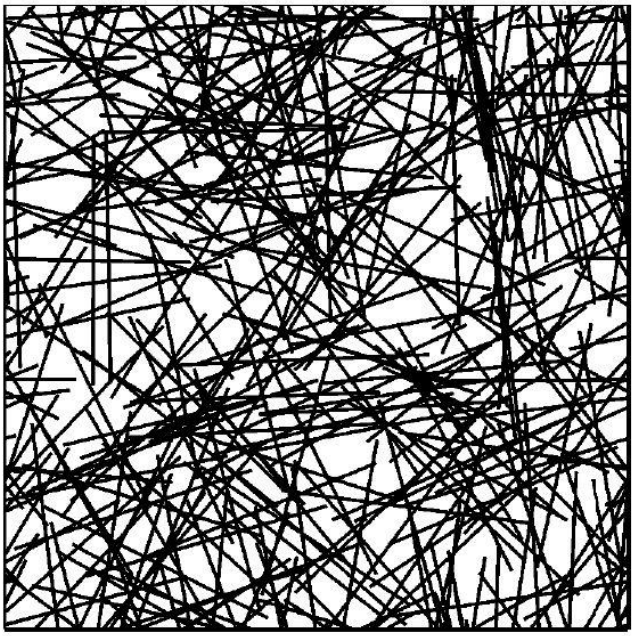

Figure 2.20. A schematic diagram of a crosslinked network in a shear cell with periodic boundary conditions are applied in both directions [112].

Head et al, [97] also use a two-dimensional network model to study the effects of connection between stiff filaments on the macroscopic mechanical properties of crosslinked filament networks. They find that the affine and nonaffine deformation regimes are related to the crosslinking density and filament rigidity. In their model, each single filament is modelled by a line segment and intersections between filaments are regarded as permanent. The energy distribution throughout the networks is illustrated in Figure 2.21.

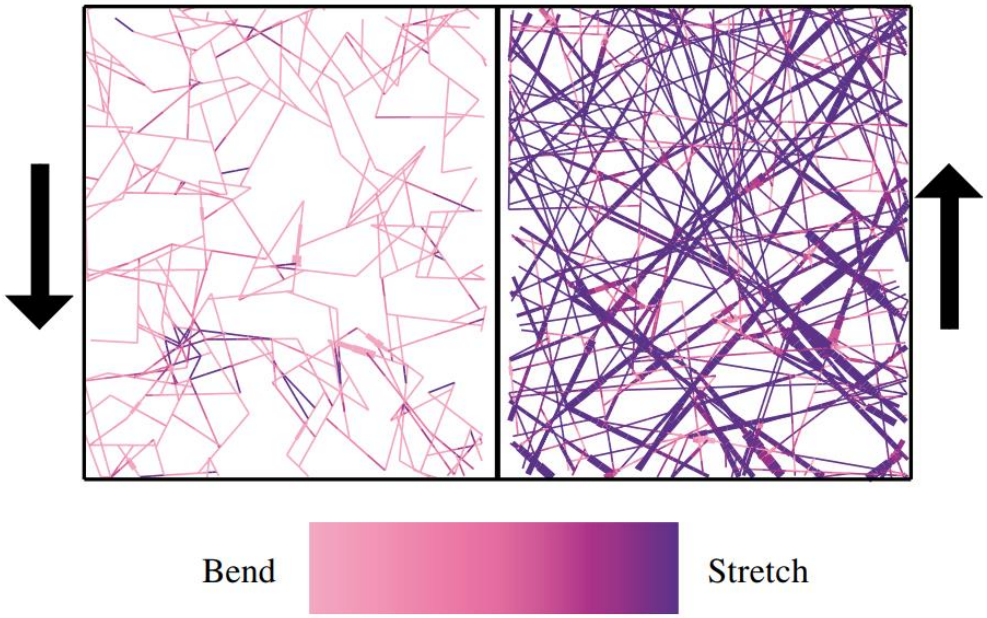

Figure 2.21. The energy distribution in the two-dimensional network model [97]. The arrows denote the given shear strain.

Wilhelm and Frey [47] also study the elastic properties of the two-dimensional random network model, and three distinct scaling regimes (i.e., critical rigidity percolation regime, homogeneously elastic regime and a novel intermediate scaling regime) are shown in their results. The model used by Wilhelm and Frey and the stress distribution in the network are shown in Figure 2.22.

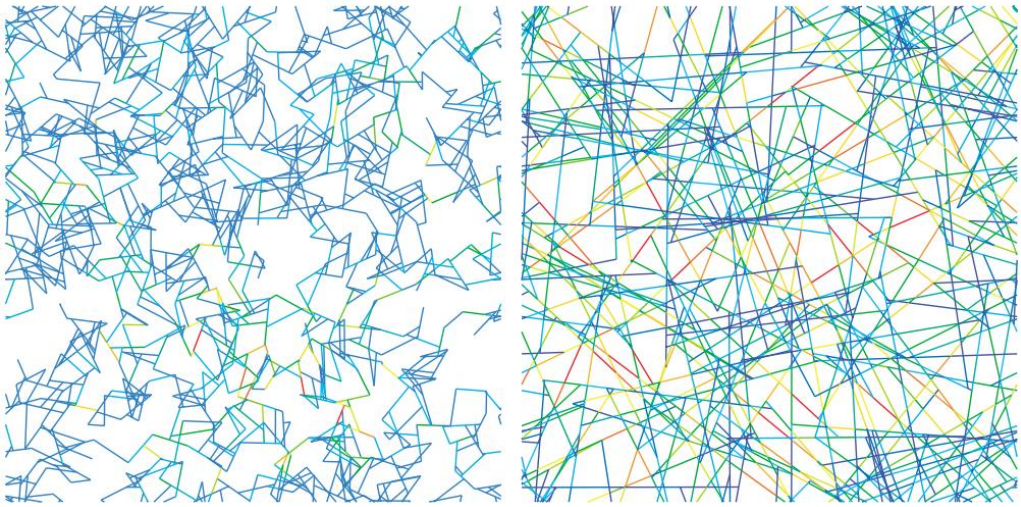

Figure 2.22. The two-dimensional network model at low and high filament densities [47]. The stress distribution in the network is shown in false colours.

Onck et al. [41] also establish a two-dimensional network model (Figure 2.23) in the similar way that Head et al. [112] used. They find that the strain stiffening behaviour of those semi-flexible biopolymer networks results from the rearrangement of the nonaffine networks. Das et al. [121] apply the effective medium theory to the analysis of mechanical behaviour of these network systems and their results can well consist with that of other theories (e.g. scaling theory) and numerical simulation. Heussinger et al. [113] use a self-consistent effective medium approach to probe the elasticity of the whole network in combination with the floppy mode in a single filament, and obtain reasonable results that consist with other simulation results. Their theory is also very useful in the study of viscoelasticity of recomposed biopolymer networks.

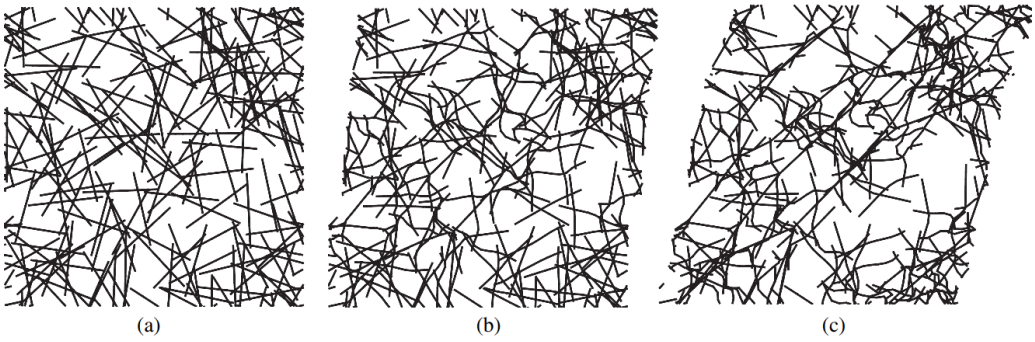

Figure 2.23. The undeformed two-dimensional network model (a), deformed configurations under intermediate shear strain (b) and under large shear strain (c).

Wei et al. [99] use a two-dimensional network model to study the effects of the physical properties of crosslinkers on the macroscopic properties of the crosslinked biopolymer networks. They use a linear spring and a rotational spring to mimic the crosslinker between two filaments and conduct a series of simulation to quantitatively reveal the effects of crosslinking molecules on the bulk behaviour of the network. The details of their model are illustrated in Figure 2.24.

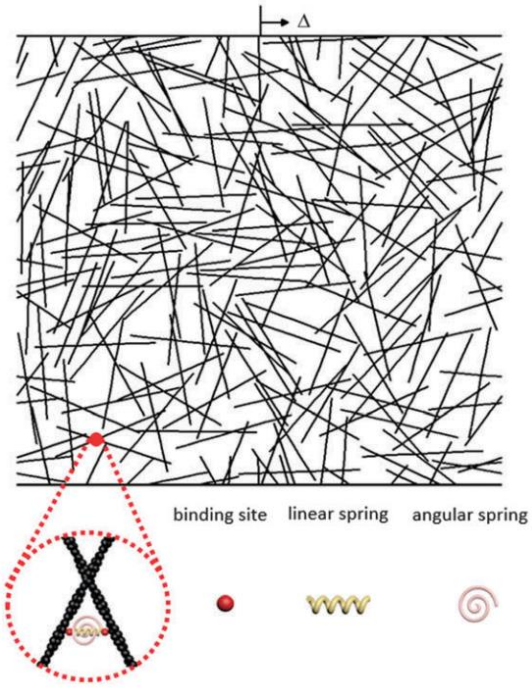

Figure 2.24. The two-dimensional network model developed by Wei et al. to study the effects of the crosslinking molecular on the mechanical behaviour of the biopolymer networks [99].

The above reviewed two-dimensional network models provide an effective way to study the mechanical properties of crosslinked biopolymer networks. Researchers obtain many useful results by conducting numerical simulations on these network models, which helps us to reveal and understand the mechanical responses of biopolymer networks. However, there are still some limitations when using two-dimensional network model to mimic the crosslinked actin filament networks as this kind of structure appears as three-dimensional (3D) in living cells. Some microstructural characteristics of the networks may be ignored when using two-dimensional models. Therefore, three-dimensional network models are also developed to study the mechanical properties of crosslinked biopolymer network structures, which could well capture the microstructure of the network. The recent research about the three-dimensional model of crosslinked biopolymer networks are reviewed in detail as follow.

Huisman et al. [63] use a three-dimensional model (Figure 2.25) to probe the influence of network architecture on the mechanical response of the whole network and find that the local configuration around crosslinks plays an important role in the nonlinear mechanical behaviours. However, crosslinks are treated as rigid in

this work, which may diverge from the compliant nature of those actin binding proteins (e.g. filamin). They also use Monte Carlo method to generate an isotropic three-dimensional network model (Figure 2.26) and study the mechanical properties of the network [115]. During this 3D model, they apply the periodic boundary conditions in the orthogonal three directions (*x*, *y* and *z*). However, they just take one kind of filaments into consideration which cannot well reflect the mechanical properties of some composite networks (e.g. vessel walls and whole cytoskeleton).

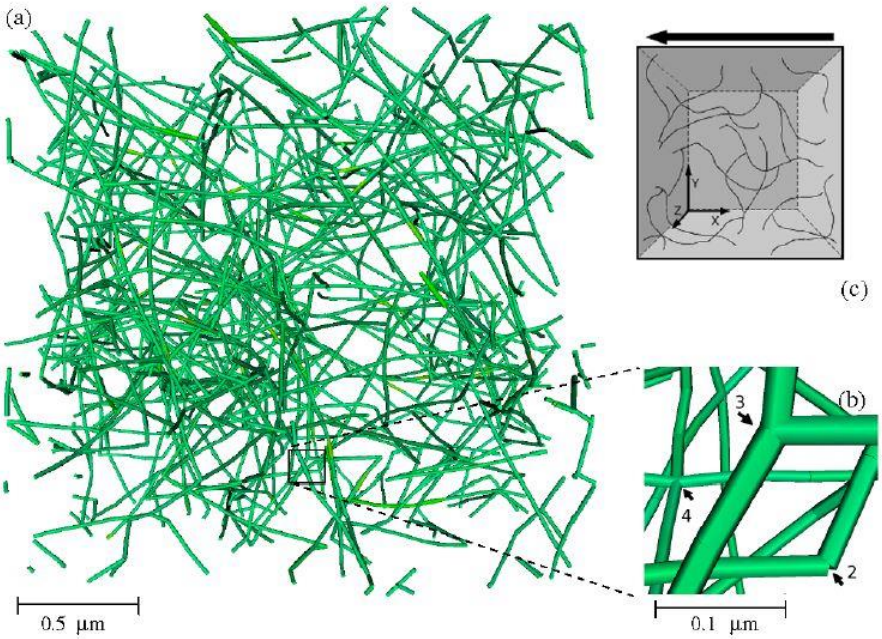

Figure 2.25. A three-dimensional model for crosslinked actin filament networks developed by Huisman et al. [63].

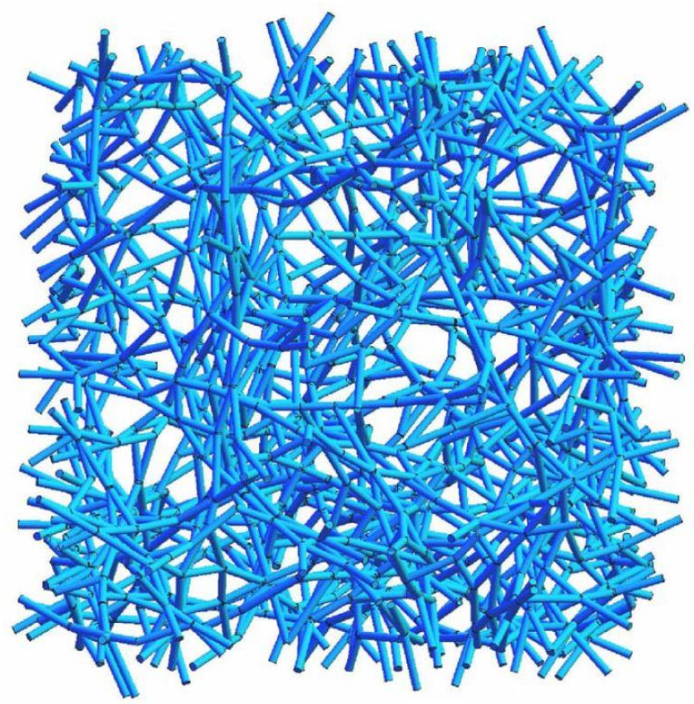

Figure 2.26. A three-dimensional isotropic, homogeneous network model generated by Monte Carlo method is used to investigate the mechanical properties of crosslinked semiflexible polymer networks by Huisman et al. [115].

A lattice-based model (Figure 2.27) is developed by Broedersz et al. [116] to explain the elasticity, criticality and isostaticity of a single filament and the whole network. Two distinct rigidity thresholds are obtained in the situations of low connectivity and high connectivity respectively. Results in this work imply that the rigidity threshold of low connectivity control the appearance of network rigidity.

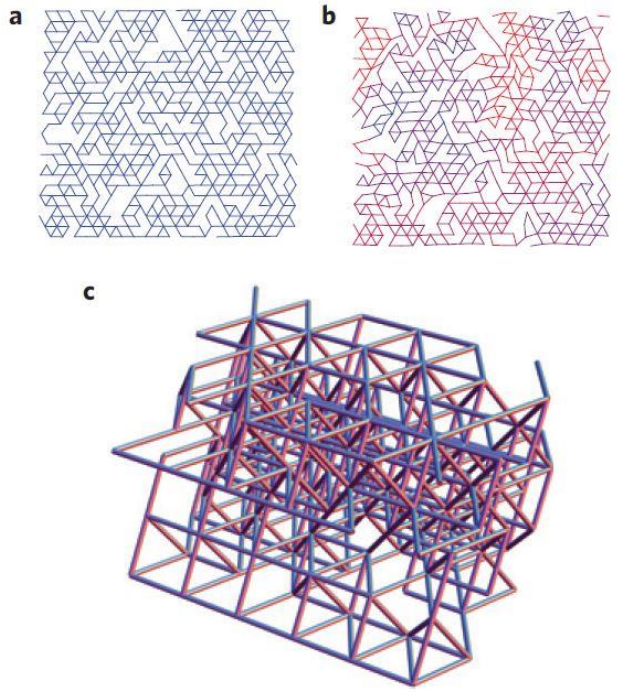

Figure 2.27. A sheared diluted triangular network with stiff filaments (a) and floppy filaments (b). (c) refers to a small section of diluted face centre cubic (FCC) network. These lattice-based models are developed by Broedersz et al. [116] to study the mechanical responses of fibre networks.

Stein et al. [122] use a three-dimensional (3D) network skeletonization algorithm to extract the geometry of *collagen-I* network, and develop a model in which collagen fibres and crosslinkers are modelled by elastic beam and torsional spring respectively to investigate the micromechanics of collagen gel. The stress-strain relationships obtained from the network model are compared with experimental measurements and agree well with experiment. They proposed that the strain stiffening behaviour of collagen network originates from the realignment of the collagen fibres in the network. Zagar et al. [123] construct a three-dimensional discrete network model to probe the elastic properties of an isotropic filamentous network. In their model, the actin filaments are treated as athermal and are interconnected by rigid crosslinkers. They find that the strain stiffening of the crosslinked actin filament networks is associated with the stretching of percolation. In addition, it is pointed out that the crosslinking density of the network could highly affect the onset of the strain stiffening of the network. Cyron et al. develop a micromechanical model (Figure 2.28) by finite element method and apply the backward Euler method to this model which shows advantages (e.g.

computational accuracy and large flexibility) over other existed models [124]. They also review other literature and find out characteristic distances that different actin binding proteins can bridge, such as 98 nm for filamin [125].

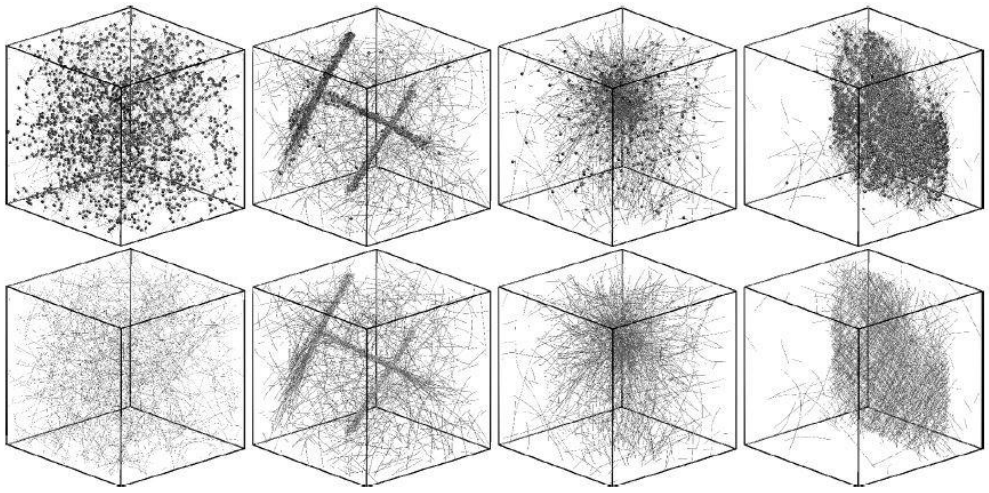

Figure 2.28. Micromechanical network models (isotropic, bundle, cluster and layer) with and without crosslinkers are reproduced by Cyron et al. [124] in finite element simulations.

In the numerical modelling, parameters of the model should be selected properly to represent the real characteristics of the components and the whole structure. For example, the dimension of the network model, the geometrical parameters of both actin filaments and crosslinkers, the crosslinking mechanism and the physical properties of components are needed to be determined when constructing the model. The details of determining the parameters used in modelling are elaborated in Chapter 3. In addition, when modelling the random composites including fibrous networks, the representative volume element (RVE) is widely used to probe the effective mechanical properties of the composite materials [126] and network structures [91, 99, 124, 127]. When using representative volume element to study the mechanical properties of crosslinked actin filament networks, the boundary conditions of the RVE model always play a crucial role in the computational accuracy controlling and surrounding constraints representing in the process of analysis. Prescribed displacement boundary conditions, mixed boundary conditions and periodic boundary conditions (PBCs) are widely used when constructing models for fibrous materials. Among these boundary conditions, the

periodic boundary conditions (PBCs) are widely used in modelling the crosslinked actin filament networks during the past years. For example, simple periodic boundary conditions [124] have been applied to simulate the real constraints around the representative volume element.

In addition to above mentioned models, there are many other models that have been developed by finite element method or molecular dynamics during recent years. These models have been used to investigate different properties of semi-flexible biopolymer networks and proved to be a complementary to the theoretical analysis and experimental study.

2.3 Mechanical properties of crosslinked actin filament networks

Although, there has been a lot of work concentrating on the mechanical properties of semi-flexible biopolymer networks, some problems still exist and need to be resolved in the future. For example, because of the semi-flexible nature of actin filaments, there is an obvious difference between the mechanical properties of actin filaments and their flexible counterparts. So, to probe the novel properties of semi-flexible biopolymers and their network structure is very essential during the following works. In early years, crosslinkers are simply assumed to be rigid [41, 63, 123] and permanently effective [41, 47, 97, 112, 128], however, this seems to be not reasonable in comparison with physiological situations. Actually, the crosslinked biopolymer networks are highly dynamic structures that experience polymerization and depolymerisation simultaneously. Actin binding proteins such as filamin A is compliant [70, 71, 73] and connect to actin filaments at two binding domains. How to properly mimic the compliant nature of those crosslinks [34, 111, 128] and their transient binding behaviour [129-131] are attracting more and more attention. In recent years, the elastic regime of crosslinked semi-flexible biopolymer networks has been well studied by scaling theory and experiments, however, there is still a lack of overall analytical theories which can reflect different mechanical responses of the whole network [33]. What is more, as a very important aspect in researching, more experiments are need to be conducted in the future to provide more information on the non-affine behaviour, marginal

bending/stretching and criticality of these networks. In addition, more efforts should be put on the viscoelasticity of the crosslinked biopolymer networks because of its importance in cell functions and motions.

To obtain the effective mechanical properties of crosslinked actin filament networks, it is essential to determine the physical properties of the components at first. Gittes et al. [14] estimate the flexural rigidity of actin filaments to be 7.3×10^{-26} Nm^2 from thermal fluctuations in shape which consistent with the results reported in literature. Isambert et al. [37] also measure the flexibility of actin filament from thermal fluctuations. Kojima et al. [39] directly measure the stiffness of single actin filament by nanomanipulation with microneedles. Furuike et al. [132] investigate the mechanical unfolding of single filamin A molecules by atomic force microscopy, and sawtooth patterns relating to the unfolding of the Ig-fold domains of filamin A molecules are observed (Figure 2.29). By stretching single filamin A molecules, Yamazaki et al. [73] obtain the force-extension relationship of filamin A dimer and find that filamin A could be reversibly unfolded by a critical external force of 50-220 pN. The role of filamin A molecules in the actin cytoskeleton is also studied in their research. In addition, Nakamura et al. [70] generate a library of filamin A fragments to study the structural properties of filamin A. Kolahi and Mofrad [133] use molecular dynamics simulations to investigate the molecular mechanical bases of filamin A in actin cytoskeleton reorganization, and find that filamin A can transduce mechanical signals and preserve topology of the in actin cytoskeleton.

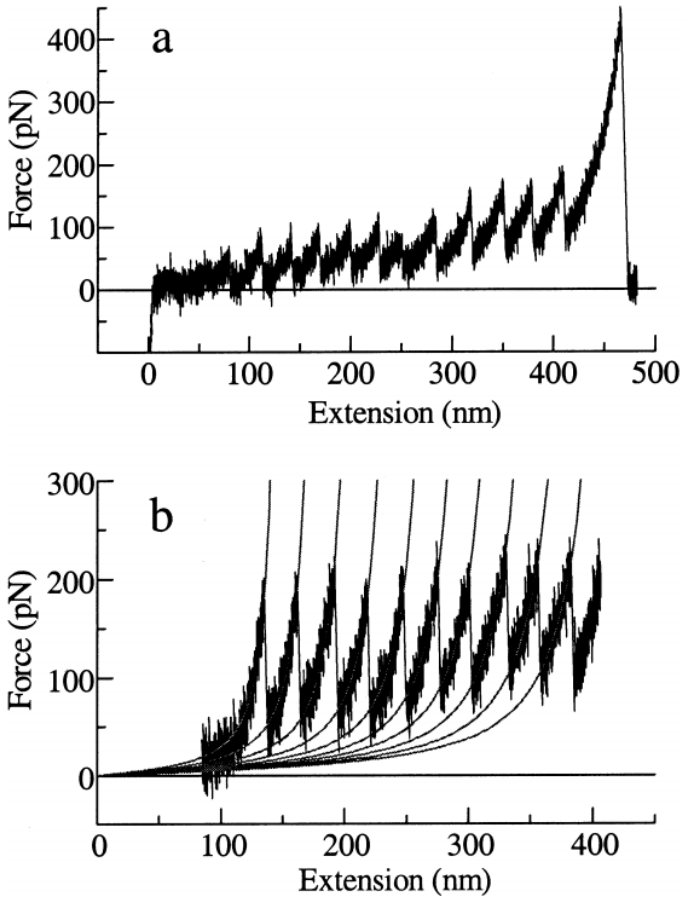

Figure 2.29. (a) The force extension curve of single filamin A molecules measured by atomic force microscopy [132]. (b) The sawtooth patterns of the force extension curve of single filamin A molecules are fitted by worm-like chain model [132].

To study the mechanical properties of crosslinked actin filament networks, both experiments and simulations are conducted by many researchers. Janmey et al. [134] polymerize three different filamentous biopolymers (i.e., tubulin, actin and vimentin) to investigate their viscoelastic properties which explain the specialized roles of these filaments in living cells. According to their measurements, actin filament networks have the highest rigidity compared with tubulin and vimentin, however, vimentin networks show lower rigidity at small strain stage but harden at large strain stage and prevent breakage [134]. Humphrey et al. [135] experimentally study the role of myosin in controlling the viscoelastic behaviour of actin filament solutions, and they find that the stress relaxation time of the actin filament solutions is obviously shortened when actin filaments are connected by myosin. To obtain these results, the elastic strength of actin filament solutions and actin-myosin networks are measured in frequency domain and the stress

relaxation experiments are conducted. Tharmann et al. [136] quantitatively study the mechanical responses of crosslinked actin filament networks by determining the dominating length scale in a single filament model and find that the crosslinker unbinding plays a crucial role in both linear and nonlinear responses of crosslinked actin filament networks. Kim et al. [119] investigate the viscoelastic properties of crosslinked actin filament networks by conducting Brownian dynamics simulations during which the storage and loss shear modulus are obtained and compared with experimental measurements as shown in Figure 2.30. In addition, the dependences of the storage and shear modulus of crosslinked actin filament networks on the frequencies of the applied loads in different crosslinking density conditions are also studied in their research as shown in Figure 2.31.

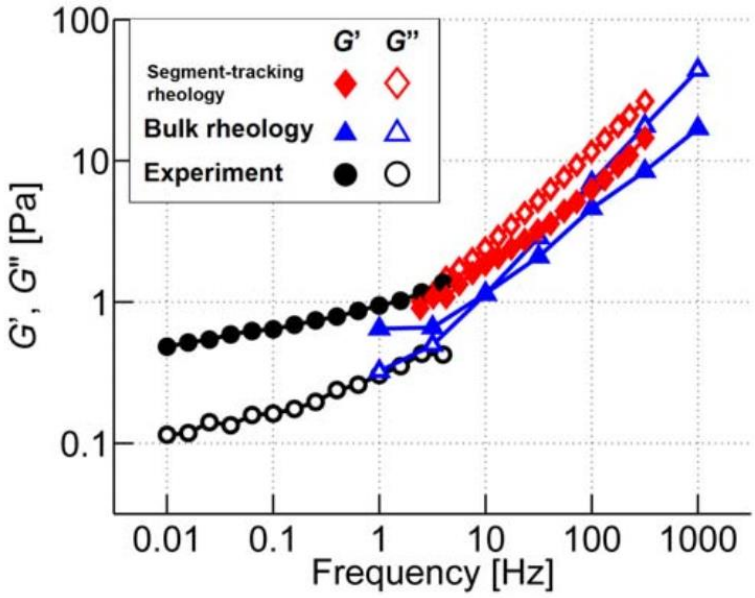

Figure 2.30. The storage shear modulus (*G'*) and loss shear modulus (*G''*) of crosslinked actin filament networks obtained from computational analysis are compared with that measured in experiments [119].

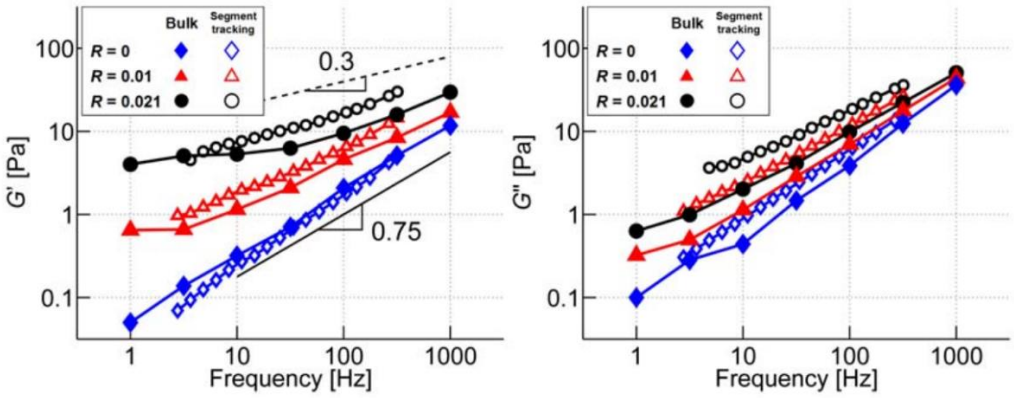

Figure 2.31. The dependences of the storage (left graph) and loss (right graph) shear modulus of crosslinked actin filament networks on the frequency of the applied loads [119]. Different crosslinking densities are applied when conducting the computational analysis.

Unterberger et al. [95] propose a continuum mechanical formulation to describe the viscoelastic properties of crosslinked actin filament networks by taking the microstructure into consideration. In their model, the actin filaments are modelled by worm-like chain model. The results obtained from the mechanical modelling are compared with experimental measurements and finite element analysis. The stress strain relationship of the crosslinked actin filament network is described by the continuum mechanical model and verified by experimental data, and the dependences of storage and loss shear modulus of the network on the amplitude of oscillational loads are also discussed as shown in Figure 2.32. In addition, creep and stress relaxation experiments are conducted by finite element modelling, and the numerical simulation results are compared with their analytical results as shown in Figure 2.33.

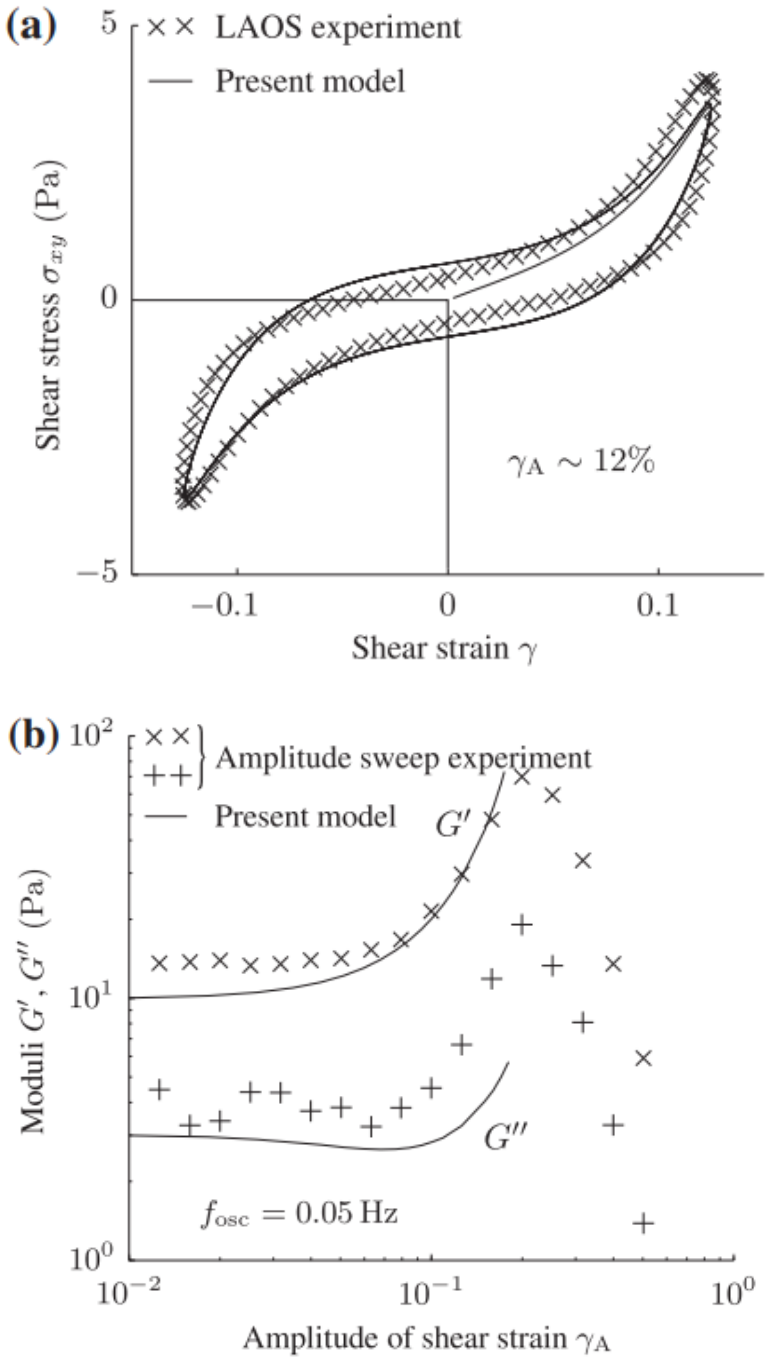

Figure 2.32. (a) The shear stress strain relationship of crosslinked actin filament networks is obtained from continuum mechanical model and compared with experimental measurements [95]. (b) The dependences of the storage and loss shear modulus of crosslinked actin filament networks on the amplitude of the applied shear strain at a constant oscillation frequency of 0.05 Hz [95].

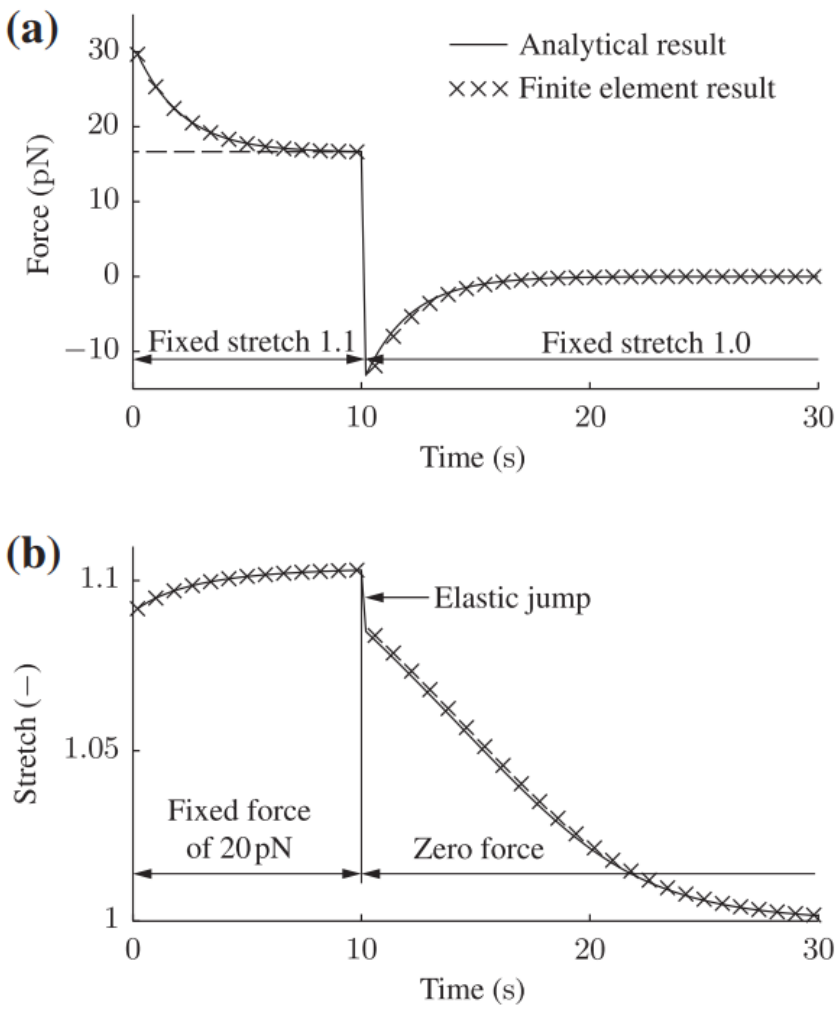

Figure 2.33. The analytical and numerical results of the force relaxation (a) and creep (b) behaviour of crosslinked actin filament networks obtained by Unterberger et al. [95].

Kim et al. [30] study the stress relaxation behaviour of crosslinked actin filament networks by applying an external stress and find that it is greatly affected by the interplay between the microstructure of the network. These results are important reference for us to study the mechanical properties of crosslinked actin filament networks and other biopolymer network structures.

Though many experiments and simulations are conducted to measure the mechanical properties of crosslinked actin filament networks, the deformation mechanism of crosslinked actin filament networks in consideration of microstructure remains poorly understood. For example, the roles of the bending, torsion and stretching of both actin filament and crosslinkers in the deformation of

the network structure have not been studied separately. These issues are studied in detail in this research by dimensional analysis and numerical simulations as shown in the following chapters.

Chapter 3 Modelling of Crosslinked Actin Filament Networks

3.1 Introduction

During the past decades, both *in vivo* and *in vitro* experiments [31, 59, 85-89] have been conducted to measure the mechanical properties of CAFNs. However, conducting experiments is time-consuming and very expensive, and external conditions can significantly affect the experimental results. Thus, theoretical [33, 90-96] and computational [34, 41, 47, 63, 97-99] models have also been developed to study the mechanical properties of CAFNs. When it comes to the methods of numerical simulation, finite element (FE) models and molecule dynamics (MD) models are widely used in studying the macro mechanical responses (e.g., elastic moduli, Poisson's ratios and stress strain relationships) of CAFNs. As MD models focus on the molecule structure of the polymer chains, they can precisely capture the mechanical responses at the scale of molecule or atom. However, this can cause much more extra costs in computation due to the extreme complexity and large scale of the model. In FE models, filaments and crosslinkers could be simply modelled by elastic beams and assembled into a network structure, which can greatly improve the computational efficiency. In addition, it is easy to control the network geometry and the material parameters in FE models.

Due to the extreme complexity of these networks and the computation limits, numerical simulations based on representative volume element (RVE) have been conducted because of their advantages in computational efficiency. During the past decades, both two dimensional (2D) models [41, 47, 55, 97, 99] and three dimensional (3D) models [34, 63, 111, 116, 124, 127] have been developed to probe the mechanical responses of CAFNs. Head et al. [97, 112] studied the elastic responses and deformation modes of crosslinked semi-flexible biopolymer

networks by constructing a 2D network model, and all of the intersections (i.e., crosslinkers) were treated as rigid connections in their models. The same treatment for crosslinker was also adopted by Wilhelm et al. [47], Onck et al. [41] and Bai et al. [55]. Thus, their models have ignored the compliant nature of the actin-binding proteins with a large contour length. Sharma et al. [110] built-up a 2D filamentous network model in which a wormlike chain crosslinker was inserted to represent the connection of two distinct filaments. Recently, Wei et al. [99] developed a 2D network model to study how the physical properties of crosslinker affect the mechanical responses of biopolymer networks, where a linear spring and a rotational spring were inserted at the intersection point of two distinct filaments.

In living cells, CAFNs always appear as 3D structure with in-plane periodicity. Therefore, 3D models are more reasonable than 2D models in mimicking the mechanical responses of CAFNs. Heidemann et al. [111] investigated the elastic properties of a 3D network that consists of rigid filaments and flexible crosslinks, where the crosslinkers were modelled as wormlike chains. Ma et al. [120] studied the mechanical behaviour of a 3D fibre-network model where the fibres were modelled by beam elements and the crosslinkers were represented by additionally inserted beam elements. Lin et al. [127] constructed a 3D RVE model to study the active stiffening behaviour of CAFNs by inserting crosslinkers and myosin-II motors at proper positions. These numerical models can help us to investigate the mechanical properties of CAFNs, however, the precise physiological geometry of filamin A (FLNA) has not been taken into consideration. In addition, using the correct mechanical properties of actin filament and FLNA is essential in finite element method (FEM) simulations. The mechanical properties of a single actin filament [14, 37, 39] and the force-extension relationship of a single FLNA [73] have been well documented.

To the best of our knowledge, the effects of components' contents and properties on the elastic properties of CAFNs remain to be understood, especially the effects of some crucial parameters. Therefore, it is necessary to develop new models that can better reflect the realistic geometry, contents and mechanical properties of the building components of CAFNs.

3.2 Network geometry and material properties

In order to study the elastic properties of crosslinked actin filament networks, a novel 3D network model is developed, and it shows good consistency with the structure of actin filament network in electron microscopy images (Figure 3.1). According to the physiological geometries of cell cortex, actin filaments and FLNA, a periodic representative volume element (RVE) is constructed with a size of $W \times W \times H$, where W is the side dimension and H is the thickness (Figure 3.2). It is reported that the majority of actin filaments in cell cortex have a physiological length less than 2 μm [46, 59, 60]. The thickness of cell cortex is reported to vary from 0.1 μm to 0.5 μm in different parts of the cell [137], for example, the average thickness of cell cortex in mitotic HeLa cells is measured to be 0.2 μm [45]. Huisman et al. [63] used a 3D model with a size of 2.5 μm to study the mechanical behaviour of CAFNs, in which the length of the actin filaments was between 0.5 μm and 2.0 μm. Chugh et al. [138] developed a 3D plate-like model to investigate the cell surface tension, and their model had a side length of 2.5 μm with the actin filament length ranging between 0.2 μm and 0.8 μm. Gong et al. [139] constructed a three dimensional model (2 μm ×2 μm ×2 μm) to investigate the mechanical responses of a crosslinked biopolymer network, and the filaments in their model had a contour length of 1.2 μm. According to the dimensions of the aforementioned models [63, 138, 139], dimensions W=2 μm and H=0.5 μm are adopted for the RVE models of CAFNs in this work. The constructed geometrical model of CAFNs in Figure 3.1 shows great similarity with the microstructure of crosslinked actin filament networks in living cells.

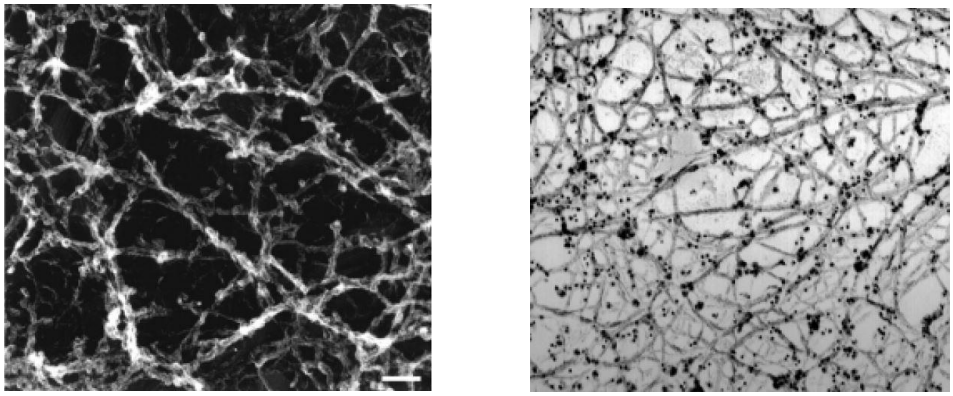

(a) (b)

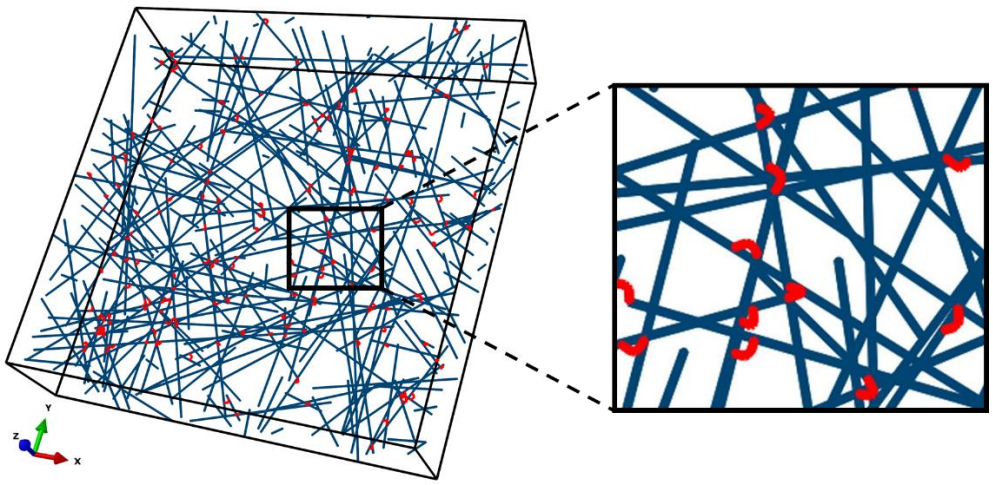

(c)

Figure 3.1. (a) Electron micrograph of actin filaments crosslinked by FLNA (the bar is 100 nm) [42]. (b) Electron micrograph of actin filament network in human blood platelet [42]. (c) The constructed 3D network model of CAFNs consisting of actin filaments (blue) and FLNA (red).

Actin filaments with the same length are usually adopted in simulations [97, 138], however, this seems not reasonable in living cells. It is reported that the length of actin filaments approximately holds an exponential distribution when polymerized in *vitro* [51, 140], and similar phenomenon is also observed in eukaryote [60]. In addition, experimental measurements show that the mean length of actin filaments in a whole cell is about 4.9 μm [141]. According to these reports, the length distribution of all filaments in a whole cell can well described by an exponential probability density function given as [55]

$$f(l,\lambda)=\begin{cases}\lambda e^{-\lambda l}, l\geq 0\\ 0, \quad l<0\end{cases}, \tag{3.1}$$

where l denotes the length of the individual actin filament and λ^{-1} is the mean length of actin filaments. It is noted that the probability density function of actin filaments length (Eq. (3.1)) is obtained for all the actin filaments in a whole cell [60], and that most actin filaments in the cell cortex are shorter than 2 μm [46, 59, 60]. In addition, FLNA tends to associate with actin filaments which are longer than 50 nm according to the binding mechanisms [70]. Thus, only actin filaments with a length between 0.05 μm and 2 μm are generated in the RVE model (the shaded region in Figure 3.2. (b)), and their mean length can be obtained as

$$L_m = \sum_{i=1}^{N} l_i \Big/ N \,, \tag{3.2}$$

where N is the total number of actin filaments generated in the RVE model and l_i is the length of filament i.

To generate a filament in a RVE, the x, y and z coordinates of its midpoint are determined by random numbers in the space of $W \times W \times H$. In addition, α is defined as the angle of turning the filament projection on the x-y plane (l_{xy}) clockwise to the positive direction of the x axis. As actin filaments are randomly oriented on the x-y plane of the RVE, α is randomly determined in the range of 0 to 2π. Moreover, β is defined as the angle between the filaments and the x-y plane. It is worth noting that some filaments have a length larger than the thickness H of the RVE, while the others have a length smaller than H. When the length of a filament is smaller than H, β is randomly determined in the range of 0 to $\pi/2$. If the length of a filament is larger than H, an upper limit value for β is defined by

$$\beta_{ul} = \arcsin\left(H/l\right). \tag{3.3}$$

In this condition, β is randomly determined in the range of 0 to β_{ul}. If part of a filament is outside the top or bottom surface of the RVE, the filament is translated in the z direction to the position with its top end on the top surface or its bottom end on the bottom surface of the RVE, as shown in Figure 3.2. (d).

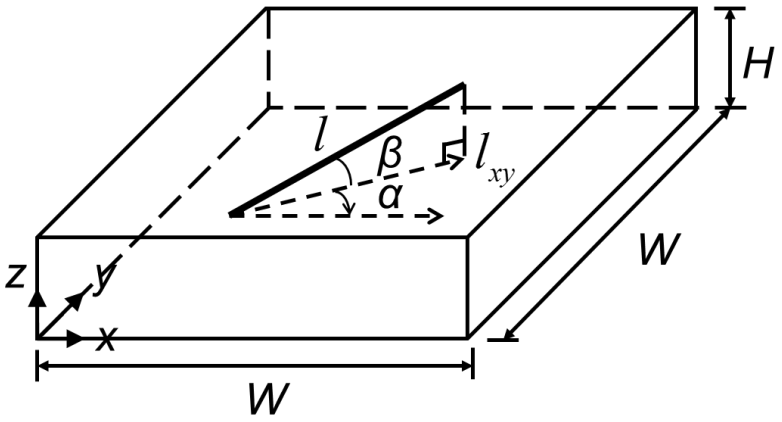

(a)

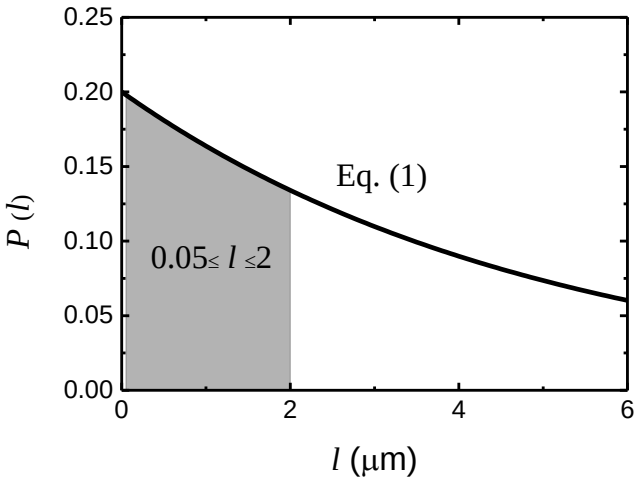

(b)

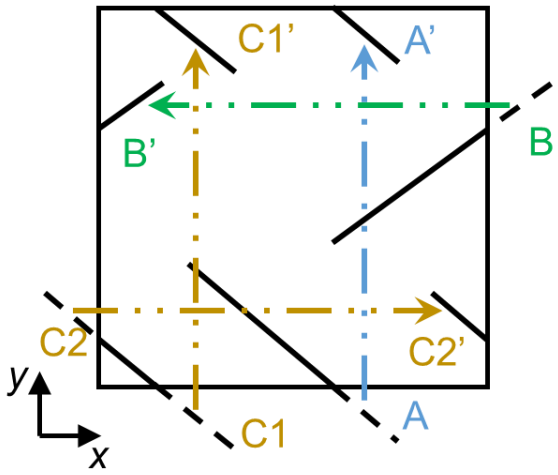

(c)

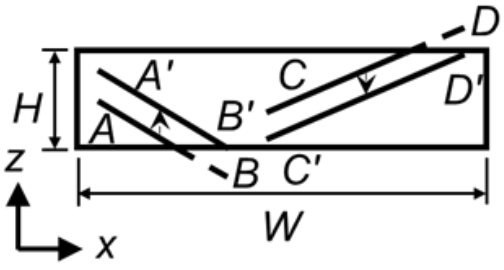

(d)

Figure 3.2. The construction details of actin filaments in RVE: (a) the position and orientation of a filament in RVE; (b) the length distribution of the actin filaments in the RVE model of CAFNs; (c) the diagrammatic sketch of how to keep periodicity of RVE in the *x* and *y* directions; (d) the method of processing out-of-plane protrusions of a filament.

The Young's modulus of actin filament E_f is measured to be about 2 GPa [14, 37, 39], and the cross-sectional area A_f is about 20 nm^2 [14, 39]. Thus, a circle cross section with a radius of 2.52 nm is adopted for the actin filaments in our model. In addition, the Poisson's ratio of actin filament is reported to range from 0.3 to 0.4 [58, 127, 142], and an average value of 0.35 is adopted in our model. For simplicity, crosslinkers are also represented by elastic rods with specific geometric and material properties. Experimental measurements show an axial extension stiffness ($\mu = EA/L$) of FLNA ranging from 5×10^{-4} $N\cdot m^{-1}$ to 1×10^{-3} $N\cdot m^{-1}$ [132], and 2×10^{-4} $N\cdot m^{-1}$ is adopted by Wei et al. [99]. The contour length of FLNA dimer is reported to be about 160 nm [70, 143]. Additionally, the radius of the circular cross-section of crosslinker is estimated to be 1.8 nm according to the microstructure of FLNA [70]. Thus, the Young's modulus of crosslinker (E_c) can be obtained as E_c=12 MPa from their axial extension stiffness (μ), cross-sectional area (A_c) and mean length (L_c). Table 3.1 shows the dimensions and the mechanical properties of actin filaments and crosslinkers which are adopted in our models of CAFNs.

Table 3.1. The geometric parameters and material properties of actin filaments and crosslinkers used in simulations.

Parameters	Actin filament	FLNA
Mean length (μm)	1	0.04
Young's modulus (Pa)	2.3E+09	1.2E+07
Poisson's ratio	0.35	0.35
Cross-sectional type	circle	circle
Cross-sectional radius (nm)	2.52	1.8
Cross-sectional area (nm^2)	19.95	10.18

According to the geometric parameters determined above, the volume fraction of actin filaments, V_f, can be specified as

$$V_f = \frac{\sum_{i=1}^{N} l_i \times A_f}{W \times W \times H}. \tag{3.4}$$

It is worth noting that it is enough to studying the linear and nonlinear elastic properties of crosslinked actin filament networks by determining the Young's moduli and Poisson's ratios of actin filament and FLNA. However, creep test data

or relaxation test data are essential when investigating the viscoelastic properties of the crosslinked actin filament networks. The viscoelastic properties of actin filament and FLNA are defined in Chapter 6 in detail.

3.3 Crosslinking principles

FLNA is a kind of actin-binding proteins that can bind actin filaments into a three-dimensional orthogonal network structure which is connected with cell membranes. This crosslinking mechanism integrates the architecture of cells and plays an important role in cell signalling and cell locomotion [144]. Filamins are also proved to bind to proteins whit diverse functions in disease progression, cell signalling, transcription, embryonic development and organ development [144]. In addition, Nakamura et al. [71] point out that filamins also have significant functions in cell migration and adhesion. Flier and Sonnenberg also point out that filamins crosslink actin filaments into orthogonal networks or bundles in different cell functions such as cell division, cell adhesion, cell migration, protein sorting, cell signalling and the maintenance of cell shape [69]. The filamins are find out to play a crucial role in the turnover of adhesion proteins in cell migration process which is important for cell contraction and cell adhesion [145]. Moreover, in forming the higher-order structures, filamins are shown to bind and crosslink actin filaments, which contributes to the phagocytosis in macrophages [146].

As FLNA has a relatively large contour length (approximately 160 nm) and an easily deformable "*V*" shape [70, 143], crosslinkers (i.e., FLNA) between two distinct filaments are modelled by deformable curved elastic rods. In addition, the angle at the FLNA dimerization point is reported to range from 50° to 110° with an average angle being about 80° [70]. According to the microstructure of FLNA and its interaction with actin filaments [70, 71, 143], two filaments are crosslinked only when their crossing angle (θ_c) is larger than 60° and their distance (d_c) is smaller than 35 nm (approximately the distance between two terminals of rod-2 segment in a FLNA dimer when the angle at the dimerization point is 120º). In order to guarantee the uniformity of crosslinking, only one crosslinker is inserted between each pair of actin filaments until the expected crosslinking density is reached. If the crosslinking density is still smaller than the expected value when all of the

available crosslinking points are crosslinked by one crosslinker, the crosslinker generation process will be repeated until the expected crosslinking density is reached. This means that some pairs of actin filaments are crosslinked by more than one crosslinker. The binding points between FLNA and actin filaments are simply treated as permanently shared nodes (i.e., both FLNA and actin filaments have the same displacements and rotations at their shared nodes). When a specific value (e.g., 35 nm) is used as the critical distance for crosslinking, interestingly, it is easy to find that large crossing angles tend to appear more frequently than smaller ones, which may explain the reason why FLNA prefers to crosslink actin filaments into orthogonal connections. Figure 3.3 shows the details of the crosslinking mechanisms.

The crosslinking density (i.e., the mean number of crosslinkers per micron length of actin filament), ρ_c, is defined as the connectivity of crosslinked actin filament networks and given by

$$\rho_c = n_c / L_t \,, \tag{3.5}$$

where n_c and L_t refer to the total number of crosslinkers and the total length of actin filaments in the RVE model, respectively. In experiments, the connectivity of the network is always controlled by tuning the molar ratio of FLNA dimers to actin monomers (R_F). Experimental results showed that 0.2 μm long actin filament contains about 76 subunits of actin monomers [60], from which we can obtain the equivalent molar ratio of FLNA to actin in our model as $R_F = \rho_c / 380$. In living cells and *in-vitro* experiments, it is proved to be a highly dynamic process for actin-binding proteins to crosslink actin filaments. Under such a circumstance, some actin filaments are crosslinked by more than one crosslinker although some actin filaments are not crosslinked. Once some actin filaments are crosslinked into a continuum path throughout the RVE, loads applied to the network can be transmitted. Although some of the actin filaments are not crosslinked at all (i.e., isolated), they are also included when calculating the nominal volume fraction of actin filaments (V_f) in Eq. (3.4). Only in this way, is the definition of the nominal volume fraction of actin filaments in this work consistent with the fact in experiments.

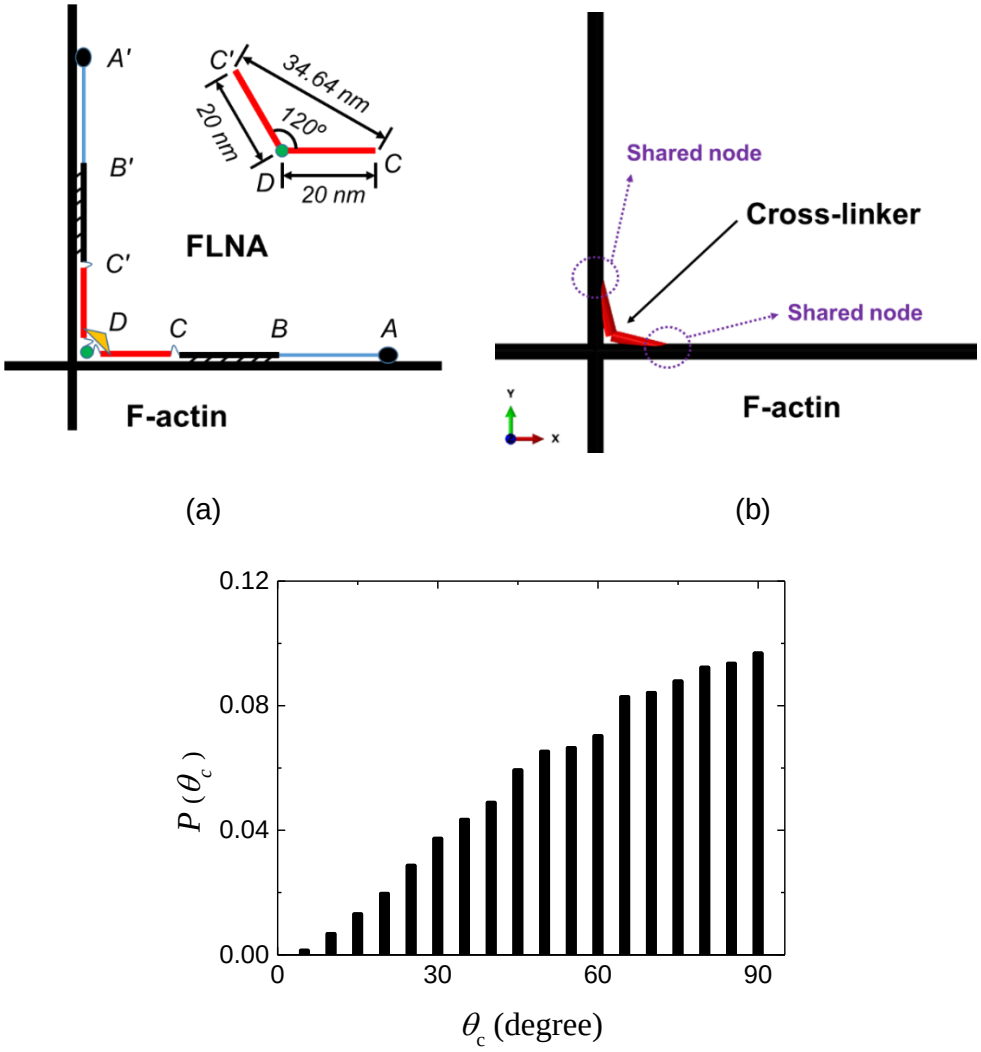

Figure 3.3. (a) Diagrammatic sketch of the microstructure of an ideally orthogonal connection formed by FLNA and actin filaments [70, 143]. Where A refers to the actin-binding domain (black solid point), AB refers to Ig1-8 of FLNA which does not bind with actin filament, BC refers to Ig9-15 of FLNA that binds with actin filament, C refers to Hinge-1 of FLNA, CD refers to Ig16-23 of FLNA which is also known as rod 2 segment, D refers to the dimerization (green solid point), the yellow solid triangle is FilGAP: a FLNA-binding RhoGTPase-activating protein. The inset shows the geometric details of rod 2 segment when the crosslinking angle is 120 degree, which determines the critical distance for crosslinking. (b) The details of a crosslinker (in red) generated in our model. Because BC and B'C' (Ig9-15) are assumed to bind with actin filament permanently in our model, only CD and C'D (Ig16-23) are presented in FE model. (c) The statistical results of probability distribution of the crossing angles (θ_c) between actin filaments in RVEs (over 100 models).

3.4 Mesh

To mesh fibres in finite element method software, there are different kinds of element types that can be used. For example, the fibres can be meshed by continuum elements or structural elements. If the fibres are meshed by continuum elements, relevant solid element types can be used. For structural elements, the beam element is usually used as the element type to mesh fibrous materials. As the actin filaments and filamins in the representative volume element model have relatively large aspect ratios, and considering the fact that solid elements always have more nodes than beam elements, beam elements show higher efficiency and are more suitable than solid elements when conducting numerical simulations in this research.

Therefore, all of the actin filaments and filamins in the RVE are meshed into Timoshenko beam elements (B32), which could successfully take into consideration the bending, torsion, axial stretching/compression, and transverse shear deformation of the beam. In consideration of the crosslinking principles as well as the computing cost, the element sizes for actin filament and FLNA are set to be 40 nm and 5 nm respectively in the FEM simulations. For simplicity, both the beam cross-sections of actin filaments and FLNA are assumed to be circles with specific areas given in Table 3.1. In addition, both actin filament and FLNA are assumed to be isotropic materials with specific Young's moduli and Poisson's ratios which are shown in Table 3.1. The meshed crosslinked actin filament network model is displayed in Figure 3.4.

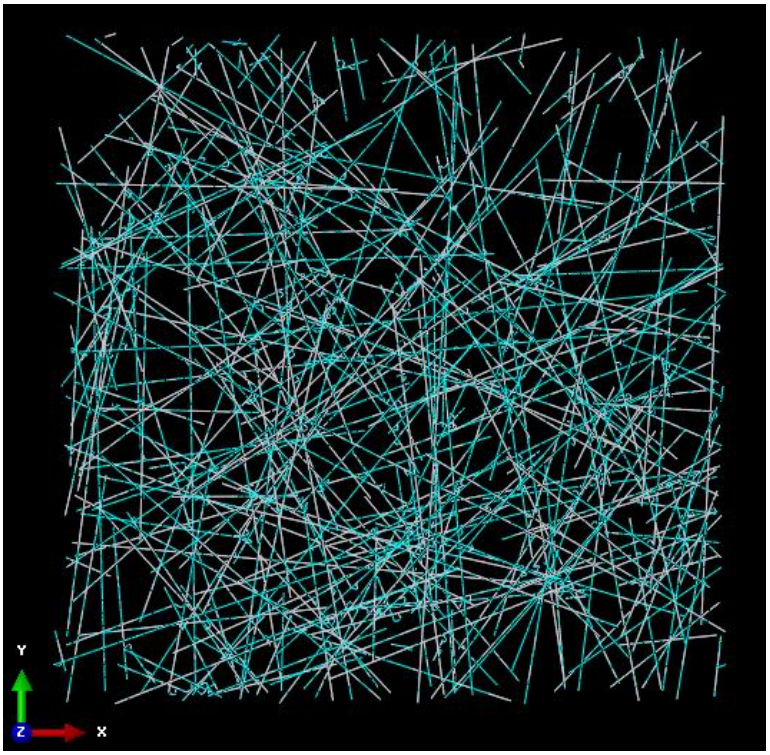

(a)

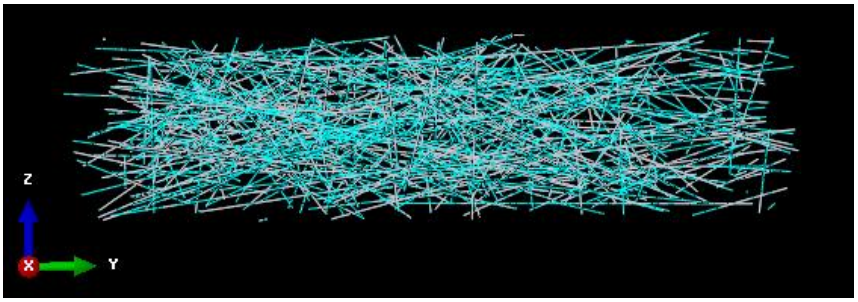

(b)

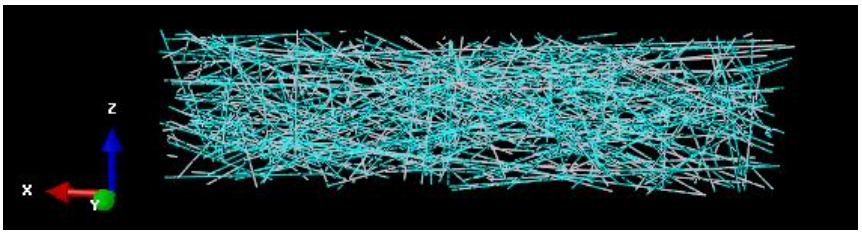

(c)

Figure 3.4. The mesh of crosslinked actin filament network model with three-node spatial Timoshenko beam elements (B32) from different perspectives. The vertical views in *z* direction (a), *x* direction (b) and *y* direction (c) are shown above respectively.

3.5 Boundary conditions

Boundary conditions are very important in studying the mechanical properties of representative volume element by performing numerical simulations. Chen et al. [147] study the effects of boundary conditions on the elastoplastic properties of two dimensional Voronoi foams and regular honeycomb. In their study, three different boundary conditions (mixed boundary conditions, prescribed displacement boundary conditions and periodic boundary conditions) are discussed. They point out that the periodic boundary conditions are more suitable for a mesh which contains open cells on its boundaries. In addition, periodic boundary conditions (PBCs) are used by Zhu et al. [148, 149] to investigate the mechanical properties of open-cell foams and two dimensional Voronoi honeycomb. The periodic boundary conditions require that the corresponding nodes on the opposite faces of the RVE hold the same displacements and rotations in all directions. The constraint equations of periodic boundary conditions used in simulations can be expressed as:

$$\begin{cases} u_i^{left} - u_j^{left} = u_{i'}^{right} - u_{j'}^{right} \\ v_i^{left} - v_j^{left} = v_{i'}^{right} - v_{j'}^{right} \\ w_i^{left} - w_j^{left} = w_{i'}^{right} - w_{j'}^{right} \\ \theta_i^{left} = \theta_{i'}^{right} \\ u_i^{top} - u_j^{top} = u_{i'}^{bottom} - u_{j'}^{bottom} \\ v_i^{top} - v_j^{top} = v_{i'}^{bottom} - v_{j'}^{bottom} \\ w_i^{top} - w_j^{top} = w_{i'}^{bottom} - w_{j'}^{bottom} \\ \theta_i^{top} = \theta_{i'}^{bottom} \end{cases}, \tag{3.6}$$

where i and j are nodes on the left or front faces of RVE model, i' and j' are the corresponding nodes on the right or back faces of RVE model, u, v and w refer to the displacements in *x*, *y* and *z* directions respectively, and θ refers to the rotations in all directions. The deformed configuration of the RVE model under periodic boundary conditions is demonstrated in Figure 3.5.

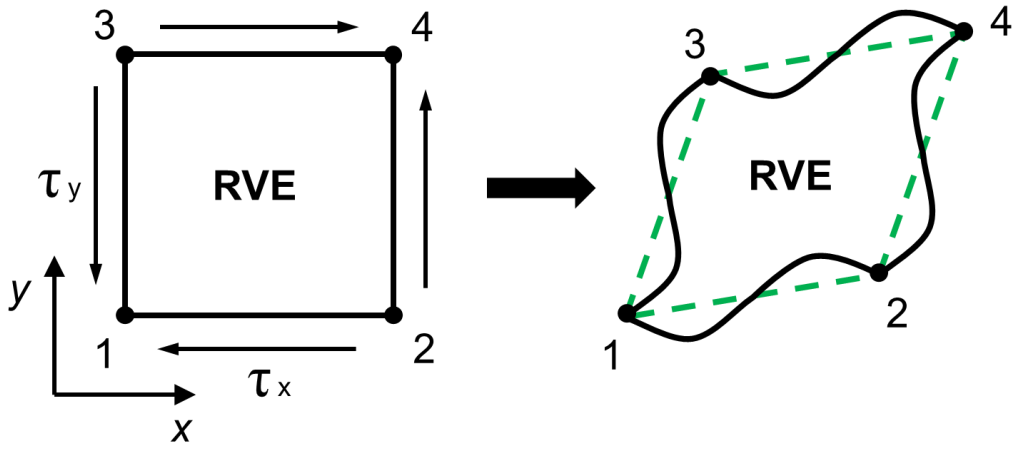

Figure 3.5. Schematic diagram of the reference (left) and deformed (right) configurations of the RVE model under periodic boundary conditions.

As the RVE model in this research is periodic in the x and y directions, periodic boundary conditions (PBCs) are more suitable for the boundaries of the RVE. For each pair of nodes on the opposite planes, the PBCs simply assume that they have the same nodal rotations, and the differences of their nodal displacements remain constants in the x, y and z directions. By simply ignoring the interactions between cell cortex and cell plasma membrane, all the nodes on the top and bottom surfaces of the RVE are left to be free (i.e., these nodes are free to displace or rotate). These boundary conditions for the nodes on the top and bottom surfaces were also adopted to study the effects of cell cortex structure on cell surface tension in reference [138].

3.6 Load

In this research, reference points are created to simplify the loading process when performing numerical simulations. By coupling the reference points with the corresponding faces of the RVE model, the displacements and rotations of the nodes on the faces of the RVE model are constraint by the displacements and rotations of the reference points. As shown in Figure 3.5, reference point 1 is set

to be at the left-bottom corner of the RVE model; reference point 2 is set to be at the right-bottom corner of the RVE model; reference point 3 is set to be at the left-top corner of the RVE model; reference point 4 is set to be at the right-top corner of the RVE model. Reference point 2 has the same coordinate with reference point 1 in y direction and z direction, and the difference between their coordinates in x direction equals the width of the RVE model (i.e., *W*). Reference point 3 has the same coordinate with reference point 1 in x direction and z direction, and the difference between their coordinates in y direction equals the width of the RVE model (i.e., *W*). Reference point 4 has the same coordinate in z direction with reference point 1, however, the differences between the coordinates of reference point 4 and reference point 1 in x direction and y direction equal the width of the RVE model (i.e., *W*). The relationship between the coordinates of the four reference points used in simulations can be expressed as

$$\begin{cases} x_2 - x_1 = W \\ y_2 = y_1 \\ z_2 = z_1 \end{cases}, \tag{3.7}$$

$$\begin{cases} x_3 = x_1 \\ y_3 - y_1 = W \\ z_3 = z_1 \end{cases}, \tag{3.8}$$

$$\begin{cases} x_4 - x_1 = W \\ y_4 - y_1 = W \\ z_4 = z_1 \end{cases}, \tag{3.9}$$

where x_i, y_i and z_i refer to the coordinates of corresponding reference point i ($i = 1, 2, 3, 4$) in *x*, *y* and *z* directions respectively.

In order to simplify the loading and post-processing, the nodes on the boundary faces of crosslinked actin filament networks are coupled with corresponding reference points, and all of the loads are applied to reference points rather than the nodes. When conducting numerical simulations, proper loads and constraints are applied on corresponding reference points to obtain the expected results. For example, to obtain the Young's moduli of crosslinked actin filament networks in x direction, reference point 1 is fixed by constraining all of its freedoms as

$$\begin{cases} u = 0 \\ v = 0 \\ w = 0 \\ \theta_x = 0 \\ \theta_y = 0 \\ \theta_z = 0 \end{cases}, \tag{3.10}$$

and a small strain, ε_x, of 0.001 is applied to reference point 2 in x direction with the other freedoms being constraint as

$$\begin{cases} u = 0.001 \\ v = 0 \\ w = 0 \\ \theta_x = 0 \\ \theta_y = 0 \\ \theta_z = 0 \end{cases}. \tag{3.11}$$

According to the periodic boundary conditions applied on the RVE model, the small strain applied to reference point 2 results in a relative displacement between the corresponding nodes on the left face and right face of the RVE model. And this applied strain can also result in a reaction force (F_r) in the opposite direction to the direction that it is applied. When completing the finite element simulations, the reaction forces of reference points could be obtained. By extracting the reaction force of reference point 2 in x direction, the effective stress that is applied to the RVE model in x direction can be expressed as

$$\sigma_x = F_r / A_{yz}, \tag{3.12}$$

where A_{yz} refers to the area of the faces of the RVE model in y-z plane (i.e., the left face or the right face of the RVE model in this research).

Then the Young's moduli of the crosslinked actin filament networks in x direction can be specified as

$$E_x = \sigma_x / \varepsilon_x. \tag{3.13}$$

In addition, when a small strain is applied to reference point 2 in x direction, the dimension of the RVE model in y direction changes due to the deformation

mechanism of materials. By extracting the strain of reference point 3 in y direction, the Poisson's ratios of crosslinked actin filament networks in this condition can be expressed as

$$\nu_{21} = -\varepsilon_x / \varepsilon_y \,. \tag{3.14}$$

Similarly, the Young's moduli of crosslinked actin filament networks in y direction can also be obtained by applying a small strain, ε_y, of 0.001 to reference 3 in y direction with reference point 1 being fixed. And the corresponding Poisson's ratio, ν_{12}, can also be obtained.

When measuring the shear modulus of crosslinked actin filament networks, reference point 1 is fixed, and a small strain of 0.0005 is applied to the reference point 2 in y direction and is applied to reference point 3 in x direction respectively. The reaction forces of reference point 3 in x direction and the reaction forces of reference point 2 in y direction equal the shear forces on the RVE model. When the reaction forces are divided by the areas of corresponding faces of the RVE model, the shear stress, τ_{12}, is obtained. To determine the in-plane shear modulus, G_{12}, of the RVE, the shear stress is divided by the shear strain that applied on the RVE. The shear strain, γ_{12}, of the RVE is the summation of the strain applied to the y direction at reference 2 and the strain applied to the x direction at reference 3. That is to say that $\gamma_{12} = 0.0005 + 0.0005 = 0.001$ when measuring the shear modulus of the RVE in this research. Therefore, the in-plane (i.e., x-y plane) shear modulus of the RVE can be expressed as

$$G_{12} = \tau_{12} / \gamma_{12} \,. \tag{3.15}$$

When studying the nonlinear elastic properties and viscoelastic properties of crosslinked actin filament networks, the loads are also applied to the corresponding reference points. The details of the loading for investigating the nonlinear elastic properties and viscoelastic properties of crosslinked actin filament networks are explained in Chapter 5 and Chapter 6 respectively.

3.7 Conclusions

In this chapter, a novel three-dimensional network model is developed in commercial finite element method software by programming to probe the mechanical properties of actin filament networks crosslinked by filamin A. In the light of the morphology of crosslinked actin filament networks in living cells, a plate-like representative volume element (RVE) model is selected as the research object in this work. Its dimensions are critically determined by considering the geometry of crosslinked actin filament network in living cells and reviewing relevant models used by other researchers. According to the physiological contour of actin filament and filamin A, actin filaments are modelled by straight elastic rods, however, the filamins are modelled by curved elastic rods. The cross sections of actin filaments and filamins are simply assumed to be circle, and the effective cross-sectional areas of actin filament and filamins are obtained according to previous reports in literature. In addition, the lengths of actin filaments are randomly determined in the reasonable range with an exponential distribution law being applied according to relevant reports in literature. The positions of actin filaments are determined by the coordinates of their midpoints and their directions. The details of processing the positions and directions of actin filaments are interpret in this chapter. The material properties (e.g., Young's moduli and Poisson's ratios) of actin filament and filamin A used in simulations are also determined and illustrated in this chapter. When studying the linear elastic and nonlinear elastic properties of crosslinked actin filament networks, it is crucial to define the material properties of the components.

The actin filaments are crosslinked into a network structure by actin binding proteins in living cells or *in vitro* gels. The actin binding proteins used in this research are filamins which have relatively large contour length. The crosslinkers in the actin filament networks are reported to play an important role in the mechanical properties of crosslinked actin filament networks. Thus, the crosslinking principles are carefully defined according to the binding mechanism between actin filaments and filamins.

In consideration of the efficiency of pre-processing and computing, beam element is used to mesh the actin filaments and filamin A during the simulations with proper element size being selected. Three nodes spatial Timoshenko beam elements (B32) are selected as the element type, which takes the shear deformation effects

into consideration. In addition, the details of the boundary conditions used in this research are also explained in this chapter. Considering the geometry of the crosslinked actin filament network and its positions in living cells, periodic boundary conditions are applied in the *x-y* plane, however, free boundary conditions are applied in the *z* direction.

Chapter 4 Linear Elastic Properties of Crosslinked Actin Filament Networks

The crosslinked actin filament networks (CAFNs) are a kind of substructure of cytoskeleton in living cells, and they can affect different cell functions. However, the linear elastic properties and the deformation mechanisms of CAFNs are not understood very well. In this chapter, numerical simulations are performed on the three-dimensional (3D) finite element (FE) model developed in Chapter 3 to mimic the mechanical responses of actin filament (F-actin) networks crosslinked by filamin A (FLNA). The simulation results indicate that although the Young's moduli of CAFNs vary in different directions for each random model, the statistical mean value is in-plane isotropic. In addition, both the crosslinking density and the actin filament volume fraction can strongly influence the linear elastic properties (e.g., shear moduli) of CAFNs. Moreover, a simple cantilever beam model has been developed to carry out the dimensional analysis on the shear stiffness of CAFNs and discuss the deformation mechanisms of CAFNs. It is found that the in-plane shear moduli of CAFNs are mainly dominated by FLNA (i.e., crosslinkers) rather than the actin filament in normal condition. Interestingly, the bending and torsion deformations of FLNA have almost the same contribution to the effective stiffness of CAFNs. In contrast, the stiffness of CAFNs is almost insensitive to the Poisson's ratios of FLNA and actin filament in the range of 0.29 to0.499. The results of the dimensional analysis are compared with the simulation outcomes.

4.1 Introduction

The crosslinked actin filament network is an important substructure of cell cytoskeleton which plays a major role in different cell functions. In recent years,

lot of attention has been paid to its striking mechanical properties. This chapter mainly focus on the elastic properties of actin filament network crosslinked by FLNA. Numerical simulations are performed on the three-dimensional finite element model developed in Chapter 3, the material properties of actin filament and FLNA used in this chapter are the same with that definite in Chapter 3.

Based on the three-dimensional finite element model developed in Chapter 3, the physiological geometry of actin filaments and FLNA are captured. By varying the components' contents and properties, the different mechanical responses of CAFNs can be obtained via finite element simulation. This model can precisely capture the elastic properties of CAFNs and can help revealing the role of CAFNs in different cell functions. The determination of the elastic constants of CAFNs is illustrated in Section 4.2; the isotropic properties of CAFNs are studied in Section 4.3; the effects of actin filament volume fraction and crosslinking density on the elastic properties of CAFNs are presented and discussed in Sections 4.4; the dimensional analysis of CAFNs is presented in Section 4.5; and the conclusions are summarized in Section 4.6.

4.2 Elastic constants of CAFNs

To study the linear elastic properties of CAFNs, it is essential to determine the relevant elastic constants (e.g., Young's moduli and Poisson's ratios). As the actin filaments are randomly distributed in the *x-y* plane, there are three orthogonal planes of elastic symmetry, and in addition, the *x-y* plane is isotropic. Thus, the crosslinked actin filament networks (CAFNs) material has only five independent elastic constants [150, 151]. Under small deformation, the stress tensor of the CAFNs is related to the strain tensor by the following relationship:

$$\begin{Bmatrix} \varepsilon_{11} \\ \varepsilon_{22} \\ \varepsilon_{33} \\ \gamma_{23} \\ \gamma_{31} \\ \gamma_{12} \end{Bmatrix} = \begin{bmatrix} \frac{1}{E_1} & -\frac{\nu_{12}}{E_1} & -\frac{\nu_{13}}{E_3} & 0 & 0 & 0 \\ -\frac{\nu_{21}}{E_1} & \frac{1}{E_1} & -\frac{\nu_{13}}{E_3} & 0 & 0 & 0 \\ -\frac{\nu_{31}}{E_1} & -\frac{\nu_{31}}{E_1} & \frac{1}{E_3} & 0 & 0 & 0 \\ 0 & 0 & 0 & \frac{1}{G_{31}} & 0 & 0 \\ 0 & 0 & 0 & 0 & \frac{1}{G_{31}} & 0 \\ 0 & 0 & 0 & 0 & 0 & \frac{1}{G_{12}} \end{bmatrix} \begin{Bmatrix} \sigma_{11} \\ \sigma_{22} \\ \sigma_{33} \\ \sigma_{23} \\ \sigma_{31} \\ \sigma_{12} \end{Bmatrix}. \quad (4.1)$$

Since the compliance matrix in Eq. (4.1) is symmetric about the leading diagonal (e.g., $v_{31}/E_1 = v_{13}/E_3$) and $G_{12} = E_1/2(1+\nu_{12})$, there are only five independent elastic constants: E_1, v_{12}, E_3, v_{31} and G_{31}. In living cells, the cell cortex (i.e., the crosslinked actin filament network) is a thin film like dense network structure that just beneath the cell plasm membrane, and it mainly bears in-plane (*x-y* plane) loads (e.g., arterial cell bears shear stress of blood flow [152] and cortical networks carry tension loads [3]) rather than those in the out-of-plane (*z* direction). In addition, it is proved that the CAFNs can deform largely in physiological conditions and present strain stiffening behaviour which is important in different cell functions (e.g., cell growth and cell migration). According to the architecture of cell cortex in living cells and the CAFNs model developed in this research, the strain stiffening (tensile or shear) behaviour of CAFNs mainly occurs in the *x-y* plane. Moreover, the actin cortex contacts with the cell plasm membrane and other substructures of cytoskeleton at the top and bottom surfaces respectively. But the constrains at these two surfaces are not clear and the boundary conditions have not been determined. Thus, only the in-plane mechanical properties are studied and presented in this research. For simplicity, reference points are set up by coupling nodes in corresponding faces of the RVE, and their reaction forces as well as displacements can be obtained from the output database. The effective engineering stress can be obtained as

$$\sigma = F/A, \quad (4.2)$$

where *F* is to the reaction force of the loaded reference point and *A* is the effective cross-sectional area of loaded plane. The effective engineering strains can be obtained by dividing the lengthening *d* by the initial side length *W* of the RVE model, and given by

$$\varepsilon = d/W \,. \tag{4.3}$$

The crosslinked actin filament networks are known to mainly bear in-plane tension and shear in different cell functions. Thus, this chapter focuses on the in-plane (i.e., *x*-*y* plane) elastic properties of CAFNs. In order to study the in-plane elastic properties of the network, a small strain (0.001) is applied to the RVE model. The effective Young's moduli (E_i) and the Poisson's ratios (ν_{ij}) of the CAFNs can be obtained by applying a small stress or strain and measuring the mechanical responses. For example, E_1 and ν_{21} can be obtained by conducting uniaxial tensile simulations and using the periodic boundary conditions.

$$\begin{cases} E_{11} = \sigma_{11}/\varepsilon_{11} \\ \nu_{21} = -\varepsilon_{22}/\varepsilon_{11} \end{cases}, \tag{4.4}$$

where σ_{11} is the effective engineering normal stress under uniaxial tension, ε_{11} is the tensile strain in the loading direction, and ε_{22} is the corresponding normal strain in the orthogonal direction. In this way, the required elastic constants of CAFNs can be determined.

4.3 In-plane isotropic properties of CAFNs

To check if the CAFNs are in-plane isotropic, a group of simulations are conducted. When studying the mechanical properties of materials and structures with random architecture, it is difficult to determine the reliable properties of these materials and structures by conducting only one test due to their stochastic geometry. Thus, the average values and standard deviations obtained from statistic data of many groups of tests are always used to estimate the real mechanical properties of these stochastic structures. For example, Zhu et al. study the elastic properties of 3D open-cell Voronoi foams [148] and 2D Voronoi honeycombs [149] by performing

finite element analysis on twenty random samples and drawing the mean and standard deviation over these twenty groups of simulation results. Lin et al. [153] also use the mean and standard deviation of ten groups of tests to estimate the elastic properties of composites reinforced by random fibre networks. The simulation results for 20 random models with a fixed actin filament volume fraction (V_f = 0.4%) and a fixed crosslinking density (ρ_c = 1.0) are listed in Table 4.1. As can be seen, although E_{11} is different from E_{22} and ν_{12} is different from ν_{21} for each of the individual random models, the statistical means of Young's moduli and Poisson's ratios are almost identical in the *x* and *y* directions (i.e., $E_{11} = E_{22}$ and $\nu_{12} = \nu_{21}$), and $G_{12} = E_{11}/[2(1+\nu_{12})]$. These results suggest that the CAFNs are in-plane isotropic, because actin filaments are randomly distributed in the *x*-*y* plane. It is worth noting that relatively high standard deviations are obtained from the statistical data due to the low volume fraction of actin filament in the model.

Table 4.1. The in-plane Young's moduli, Poisson's ratios and shear moduli of 20 periodic random RVE models with a fixed actin filament volume fraction of V_f = 0.4% and a fixed crosslinking density of ρ_c=1.0.

Model No.	E_{11} (Pa)	ν_{21}	E_{22} (Pa)	ν_{12}	G_{12} (Pa)
1	11.0289	0.1023	11.8114	0.1096	5.1154
2	18.2018	0.2432	28.1523	0.3761	13.8023
3	27.2581	0.0819	24.7734	0.0744	10.5504
4	8.5795	0.0092	7.4726	0.0080	2.4938
5	20.3106	0.3131	12.4534	0.1920	9.8949
6	27.4947	-0.0829	15.2173	-0.0459	4.3915
7	11.2361	0.0907	11.5941	0.0936	3.5636
8	19.1121	0.1014	22.3218	0.1184	11.5540
9	26.0576	0.0163	14.5517	0.0091	9.8759
10	18.1095	0.1671	26.3887	0.2434	7.1442
11	16.8870	0.1359	16.9425	0.1363	6.7550
12	9.8979	0.0545	20.4827	0.1129	3.1596
13	13.9251	0.2178	7.7709	0.1216	3.7496
14	18.3405	0.3085	6.1464	0.1034	7.5101
15	32.1869	0.2359	18.5847	0.1362	10.4478
16	14.8388	0.1350	16.6581	0.1516	9.4976
17	6.9136	0.0223	26.0117	0.0841	5.1805
18	23.8214	0.3038	14.2944	0.1823	11.3357
19	17.4011	0.2277	31.3956	0.4109	10.5491
20	7.2054	0.1364	17.7829	0.3367	6.0938
Mean	17.4403	0.1410	17.5403	0.1477	7.6332
Standard deviation	7.0455	0.1076	7.0225	0.1150	3.2406

As the CAFNs show in-plane isotropic properties, and most experiments are conducted to measure the shear modulus of CAFNs, shear simulations are performed in the following parts to study the elastic properties of CAFNs. By applying a small shear strain (0.001) to the RVE model, the effective shear modulus of RVE could be obtained. The stress distribution, strain and displacements in different directions of the RVE model could also be obtained from simulations and are demonstrated in Figure 4.1.

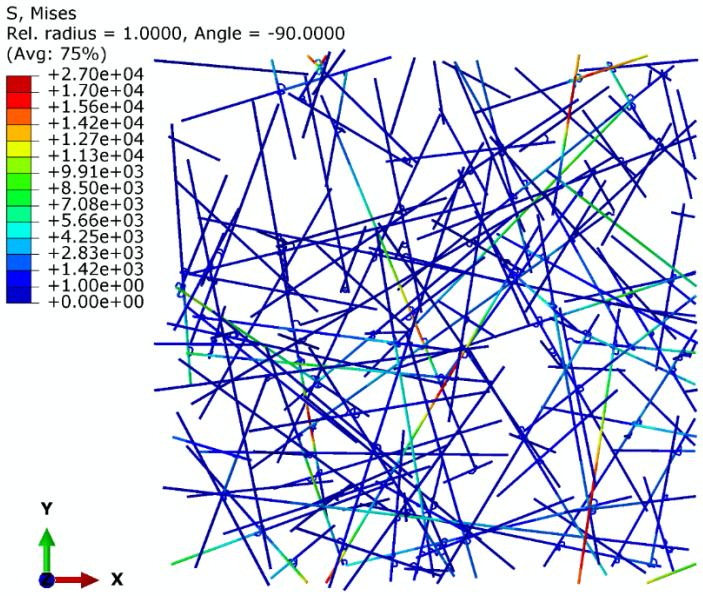

(a)

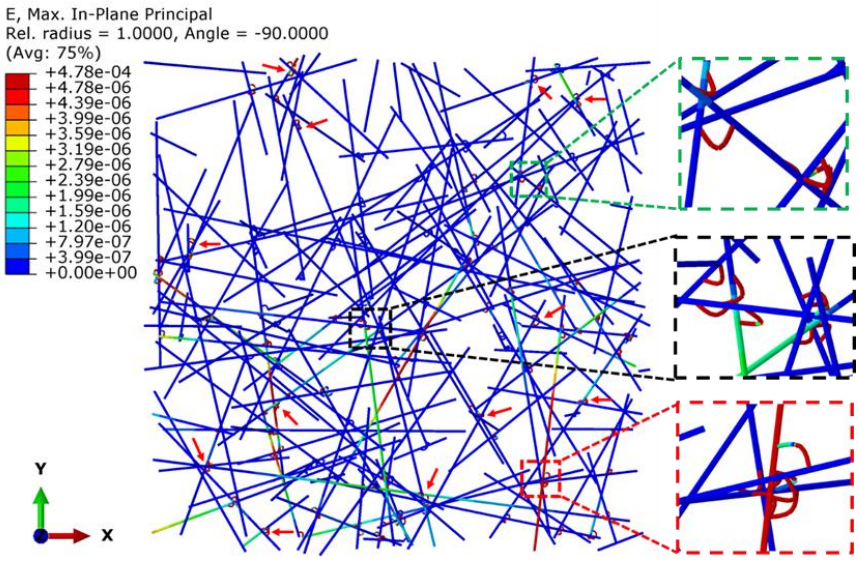

(b)

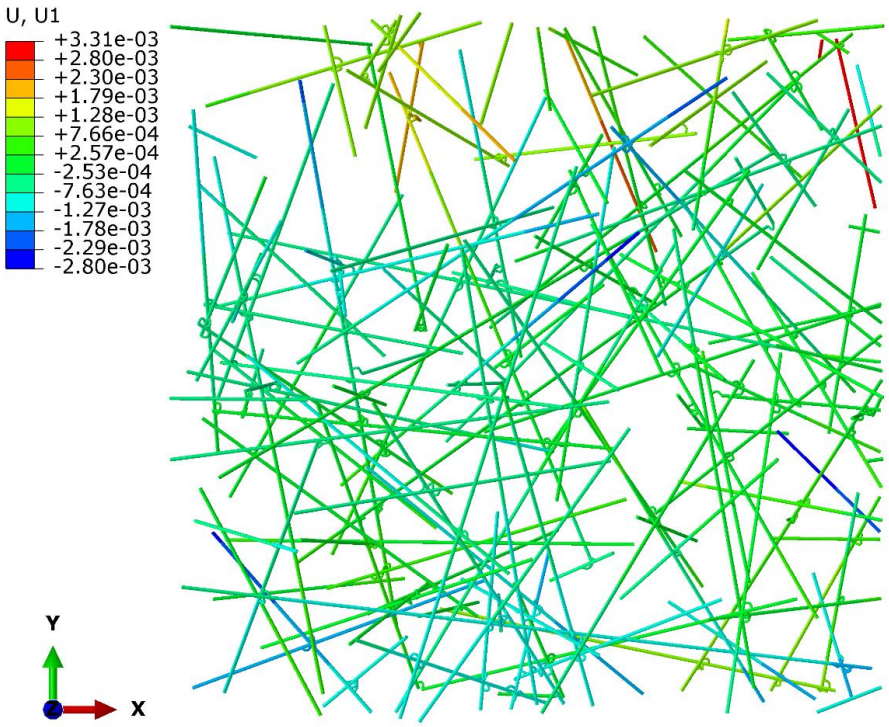
U, U1
+3.31e-03
+2.80e-03
+2.30e-03
+1.79e-03
+1.28e-03
+7.66e-04
+2.57e-04
-2.53e-04
-7.63e-04
-1.27e-03
-1.78e-03
-2.29e-03
-2.80e-03
Y
X

(c)

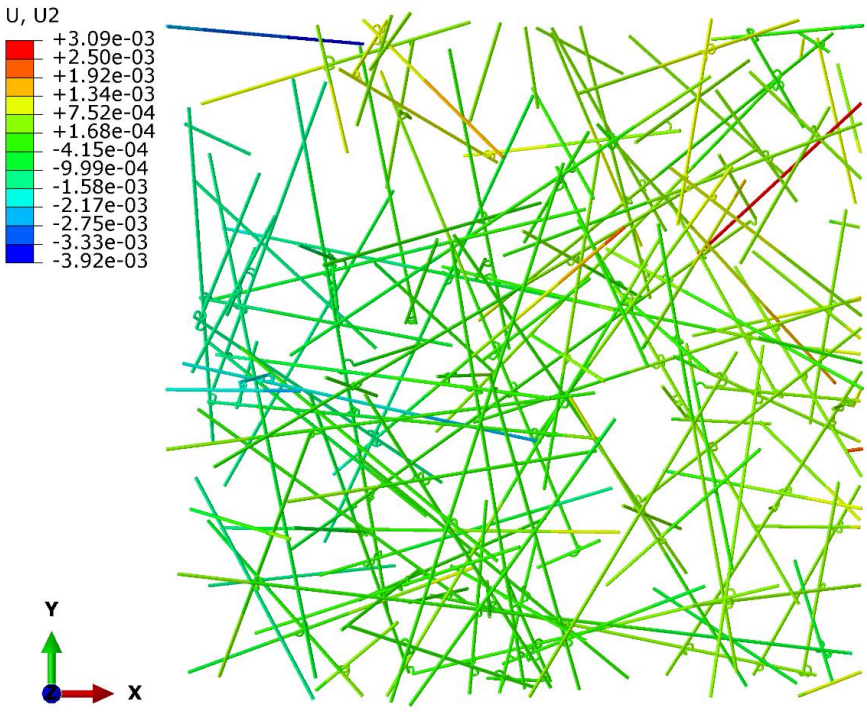
U, U2
+3.09e-03
+2.50e-03
+1.92e-03
+1.34e-03
+7.52e-04
+1.68e-04
-4.15e-04
-9.99e-04
-1.58e-03
-2.17e-03
-2.75e-03
-3.33e-03
-3.92e-03
Y
X

(d)

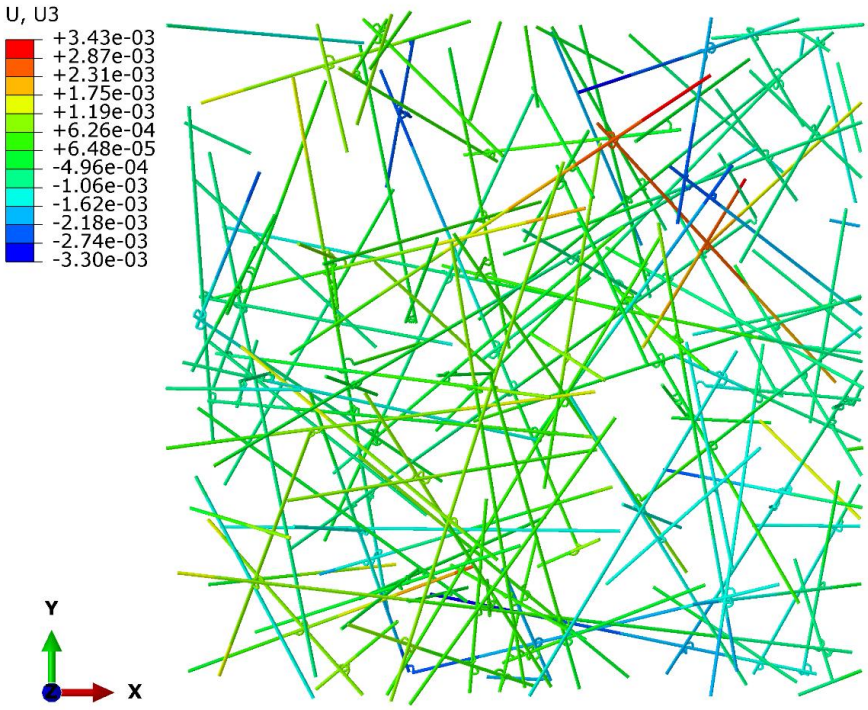

(e)

Figure 4.1. The von-Mises stress (Pa) distribution (a), strain (b) and displacements (μm) in the *x* direction (c), *y* direction (d) and *z* direction (e) of the RVE model.

It is easy to find from the von-Mises stress distribution diagram of CAFNs shown as Figure 4.1.(a) that only small number of the actin filaments (in green, yellow and red) contribute to the stress transduction through the network, however, most actin filaments almost don't bear stress. This indicates that only minority of the actin filaments are active in the small deformation regime. According to the strain distribution of CAFNs shown in Figure 4.1.(b), the crosslinkers have larger strain than actin filaments, which shows that the deformation of the CAFNs in small strain stage is mainly dominated by the crosslinkers rather than the actin filaments.

4.4 Effects of actin filament volume fraction and crosslinking density on the elastic properties of CAFNs

The actin filament volume fraction (V_f) and crosslinking density (ρ_c) of CAFNs are the two main factors that can significantly affect the elastic properties of CAFNs. In different cells or distinct regions of a single cell, the volume fraction of actin filaments (V_f) and the crosslinking density (ρ_c) are always different to meet the requirements of specific functions. Therefore, the effects of V_f and ρ_c on the in-plane shear modulus of CAFNs are investigated in this section by conducting numerical simulations. 100 models are simulated for each of the different volume fraction (or crosslinking density) conditions to obtain the statistical results, and the simulation results are presented in Figure 4.2. The results obtained from FEM simulations are compared with the experimental measurements reported in literature. The discussion of the effects of actin filament volume fraction and crosslinking density on the linear elastic properties are illustrated in detail as follow.

It is easy to find from Figure 4.2.(a) that the FEM simulation results of the in-plane shear modulus, G_{12}, is approximately proportional to $V_f^{5/2}$, which is consistent with the reports in literature [31, 91, 154]. Although strut bending is the dominant deformation mechanism in both low density random irregular Voronoi open-cell foams [148] and honeycombs [149], the shear modulus G_{12} (or Young's modulus) is proportional to V_f^2 for random irregular open-cell foams (3D) [148] and to V_f^3 for random irregular honeycombs (2D) [149]. As the geometrical structure of CAFNs (shown in Figure 3.1.(c)) is somewhat between random irregular Voronoi honeycombs (2D) [149] and random irregular Voronoi open-cell foams (3D) [148], their relationship between G_{12} and V_f is also between those of the two types of cellular materials. Figure 4.2.(b) indicates that the in-plane shear modulus of CAFNs is approximately proportional to ρ_c^2, which in general agrees with the scaling relationship of the experimental results in literature [31].

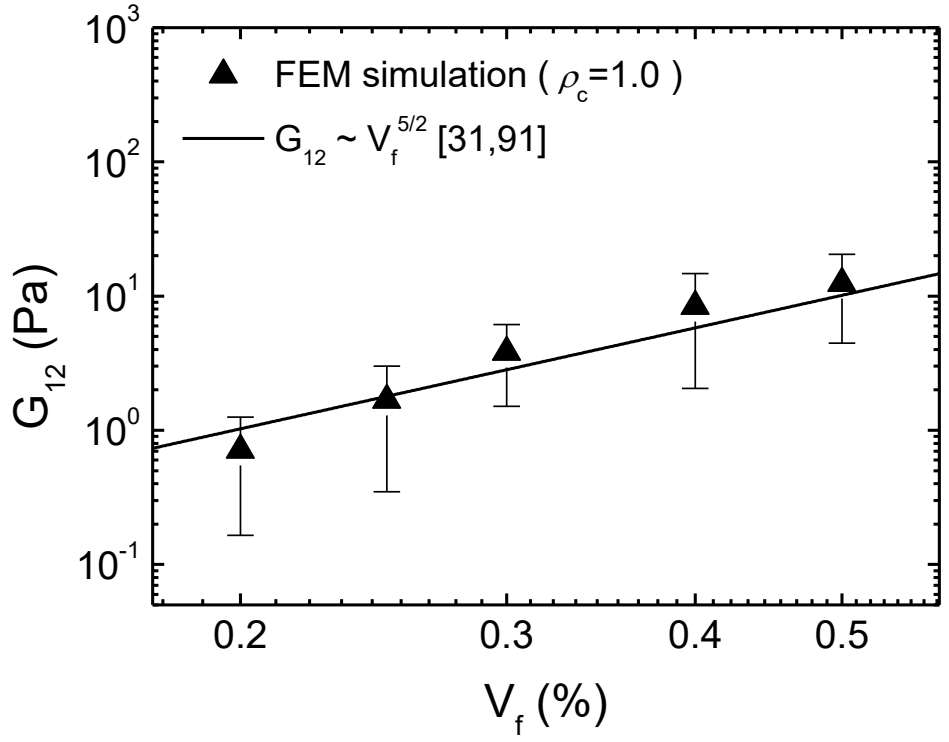

(a)

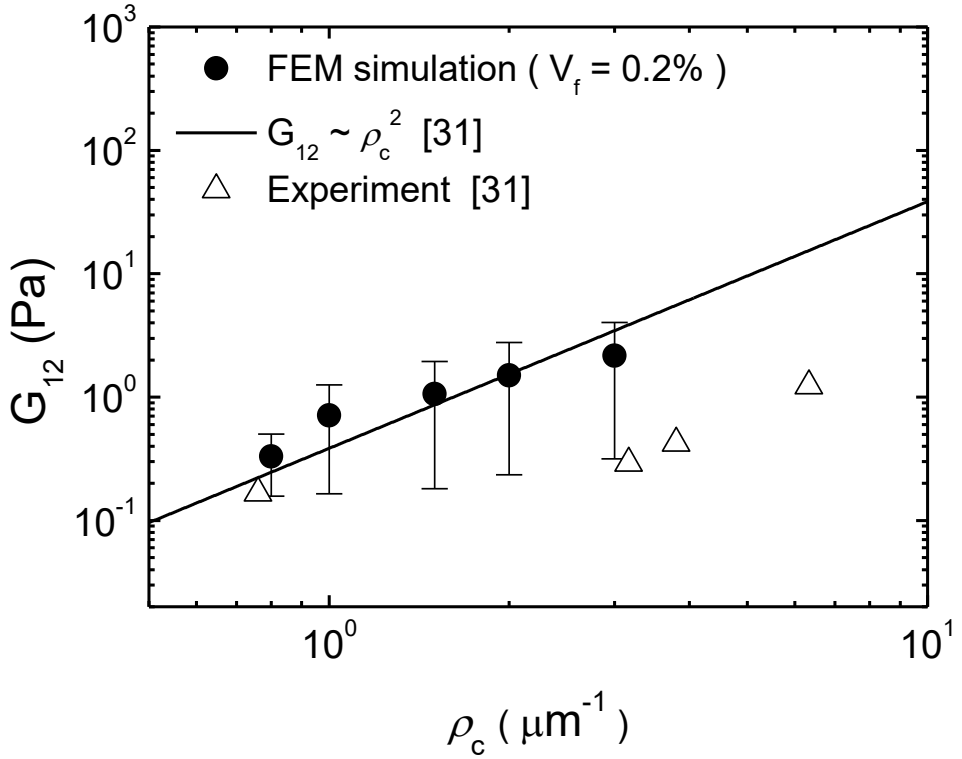

(b)

Figure 4.2. The in-plane shear modulus of CAFNs, G_{12}, scales with the actin filament volume fraction (a), and scales with the crosslinking density (b).

In addition, the simulation results of the effective in-plane shear moduli of CAFNs and the experimental measurements are listed in Table 4.2 for comparison. When conducting experiments, the crosslinking density of CAFNs is dominated by the molar ratio of FLNA dimer to actin monomer, and it is reported that 0.2 μm long actin filament contains about 76 subunits of actin monomers [60]. Thus, the equivalent molar ratio of FLNA to actin in FE model can be obtained as $R_F = \rho_c / 380$. It is worth noting that the in-plane shear moduli of CAFNs obtained from simulations are slightly larger than those obtained from experiments. This is because that it is difficult for us to perfectly match the crosslinking density in simulations and that in experiments. In experiments, the molar ratio of FLNA dimer to actin monomer corresponds to the amount of the FLNA dimer that has been added in, but some of them may be isolated. However, in computer simulations, every crosslinker is connected with actin filaments to contribute to the macro stiffness of the CAFNs.

Table 4.2. The effective in-plane shear moduli of CAFNs obtained from FEM simulations in this research are compared with the experimental measurements reported in literature.

Method	V_f	Mean length (μm)	Molar ratio (ABPs/actin)	G_{12} (Pa)	Ref.
Experiment	0.05	2.5 – 3.0	1:300	0.2	Goldmann et al. [155]
Experiment	0.05	2.0	1:100	0.2	Kasza et al. [89]
Experiment	0.05	2.0	1:100	0.1	Lee et al. [156]
Experiment	0.1	1.0	1:50	2	Kasza et al. [103]
Experiment	0.2	1.0 – 2.0	1:100	1 - 1.5	Gardel et al. [59]
Simulation	0.2	1.0	1:380	0.71	in this research
Simulation	0.2	1.0	1:190	1.50	in this research
Simulation	0.2	1.0	1:125	2.17	in this research

4.5 The dimensional analysis

The effects of the volume fraction of actin filament, V_f, and the crosslinking density, ρ_c, on the linear elastic properties of CAFNs have been studied in the previous section. In addition, the material properties of the components can also affect the

elastic properties of CAFNs. However, to our knowledge, this aspect has not been well studied. Here, we explore how the in-plane shear modulus of CAFNs depends on the elastic properties of their components by performing dimensional analysis and numerical simulations, and thus identify which component dominates the deformation of CAFNs.

It is reported that the elastic properties of CAFNs are bending dominated [13, 59] in small strain stage. However, the effect of the torsional deformation of crosslinkers on the stiffness of CAFNs has almost never been investigated. In this research, a simple L-shaped cantilever beam model is proposed to perform dimensional analysis on the shear deformation behaviour of CAFNs (Figure 4.3). In Figure 4.3, *ABC* refers to the rod 2 segment of FLNA dimer with a length of L_c=0.04 μm and it is in the *x*-*z* plane, *CD* refers to actin filament (in the *x* direction) with a length of L_f , and *P* is a very small concentrated force applied in the *y* direction at point *D*. As the dimensional analysis is mainly focused on the qualitative analysis, the main part (*BCD*) of the L-shaped cantilever beam model is simply assumed to be perpendicular to the side face of RVE. Though actin filaments may be not always perpendicular to the side face of RVE, this just influences the coefficient parameter rather than the dimensional analysis conclusions. The Young's moduli of FLNA and actin filament are E_c and E_f, and the area moments of inertia of their cross-sections are I_c and I_f, respectively.

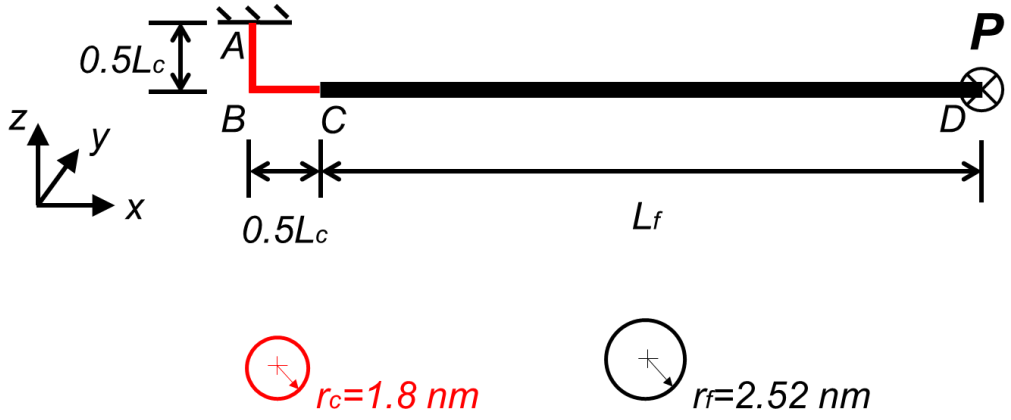

Figure 4.3. The schematic diagram of the cantilever beam model for dimension analysis. The red part (*ABC*) and black part (*CD*) refer to the crosslinker and actin filament respectively. *P* is a small concentrated force applied in y direction at point D. r_c and r_f are the radii of the cross-sections of crosslinker and actin filament respectively.

In the above cantilever beam model, when a concentrated force, *P*, is applied in the y direction at point *D*, the deflection in the *y* direction and the rotation about the *z* axis of point B are obtained as

$$y_B = \frac{P \cdot (0.5L_c)^3}{3E_c I_c}, \tag{4.5}$$

$$\theta_B = \frac{P \cdot \left(0.5L_c + L_f\right) \cdot 0.5L_c}{G_c I_{Pc}}, \tag{4.6}$$

where G_c is the shear modulus of FLNA, I_{Pc} is the second polar moment of inertia of FLNA.

The deflection in the *y* direction and the rotation about the *z* axis of point *C* can be obtained and given as

$$y_C = \frac{P \cdot (0.5 \cdot L_c)^3}{3E_c I_c} + \frac{PL_f \cdot (0.5L_c)^2}{2E_c I_c} + y_B + \theta_B \cdot 0.5L_c, \tag{4.7}$$

$$\theta_C = \frac{P \cdot (0.5L_c)^2}{2E_c I_c} + \frac{PL_f \cdot (0.5L_c)}{E_c I_c} + \theta_B. \tag{4.8}$$

Using superposition, the deflection of point *D* in the *y* direction is derived as

$$\begin{aligned} y_D &= y_C + \theta_C L_f + \frac{PL_f^3}{3E_f I_f} \\ &= \frac{P \cdot (0.5L_c + L_f) \cdot 0.5L_c L_f}{G_c I_{Pc}} + \frac{P \cdot (0.5L_c)^2 L_f}{2E_c I_c} + \frac{PL_f^2 \cdot (0.5L_c)}{E_c I_c} + \\ &\quad \frac{P \cdot (0.5L_c)^3}{3E_c I_c} + \frac{PL_f \cdot (0.5L_c)^2}{2E_c I_c} + \frac{P \cdot (0.5L_c)^3}{3E_c I_c} + \frac{P \cdot (0.5L_c + L_f) \cdot (0.5L_c)^2}{G_c I_{Pc}} + \frac{PL_f^3}{3E_f I_f} \\ &= \frac{P \cdot (0.5L_c + L_f)^2 \cdot 0.5L_c}{G_c I_{Pc}} + \frac{2P \cdot (0.5L_c)^3}{3E_c I_c} + \frac{PL_f \cdot (0.5L_c)^2}{E_c I_c} + \frac{PL_f^2 \cdot (0.5L_c)}{E_c I_c} + \frac{PL_f^3}{3E_f I_f} \end{aligned}$$

. (4.9)

In this research, The bending stiffness of actin filament (*CD*), k_f, the bending stiffness of crosslinker (*AB* and *BC*), k_{cb}, and the torsion stiffness of crosslinker (*AB*), k_{ct}, are defined as

$$\begin{cases} k_f = E_f I_f \big/ L_f^3 = E_f \pi d_f^4 \big/ (64 L_f^3) \\ k_{cb} = E_c I_c \big/ (0.5L_c)^3 = E_c \pi d_c^4 \big/ \left[64 \times (0.5L_c)^3 \right] \\ k_{ct} = G_c I_{Pc} \big/ (0.5L_c)^3 = G_c \pi d_c^4 \big/ \left[32 \times (0.5L_c)^3 \right] \end{cases}, \tag{4.10}$$

where d_f and d_c are the diameters of the circular cross sections of actin filament and crosslinker respectively, L_f and L_c are the lengths of actin filament and crosslinker respectively. In addition, I_{pc} is the polar moment of inertia of the cross-sectional area of crosslinker with $I_{Pc} = 2I_c$, and $G_c = E_c/2(1+\upsilon_c)$ is the shear modulus for the crosslinker, where υ_c is the Poisson's ratio of the crosslinker. Thus, the effective shear strain of the crosslinked actin filament networks (CAFNs) can be scaled as

$$\begin{aligned} \gamma &= \frac{y_D}{0.5L_c + L_f} \\ &= \frac{P \cdot (0.5L_c + L_f) \cdot 0.5L_c}{G_c I_{Pc}} + \frac{2P \cdot (0.5L_c)^3}{3E_c I_c \cdot (0.5L_c + L_f)} + \\ &\quad \frac{PL_f \cdot (0.5L_c)^2}{E_c I_c \cdot (0.5L_c + L_f)} + \frac{PL_f^2 \cdot (0.5L_c)}{E_c I_c \cdot (0.5L_c + L_f)} + \frac{PL_f^3}{3E_f I_f \cdot (0.5L_c + L_f)} \\ &= \frac{P \cdot (0.5L_c + L_f) \cdot 0.5L_c}{\kappa_{ct} \cdot (0.5L_c)^3} + \frac{2P \cdot (0.5L_c)^3}{3\kappa_{cb} \cdot (0.5L_c)^3 \cdot (0.5L_c + L_f)} + \\ &\quad \frac{PL_f \cdot (0.5L_c)^2}{\kappa_{cb} \cdot (0.5L_c)^3 \cdot (0.5L_c + L_f)} + \frac{PL_f^2 \cdot (0.5L_c)}{\kappa_{cb} \cdot (0.5L_c)^3 \cdot (0.5L_c + L_f)} + \frac{PL_f^3}{3\kappa_f L_f^3 \cdot (0.5L_c + L_f)} \end{aligned}, \tag{4.11}$$

To obtain the effective shear stress applied on the side face of the RVE, it is simply assumed that there are *n* actin filaments crossing each side face of the RVE model (Figure 3.1. (c)). In the RVE, actin filaments are randomly distributed, which means that they are in general not perpendicular to the side face of the RVE. But this does not influence the dimensional analysis conclusion as the dimensional analysis is mainly focused on qualitive analysis. By assuming P_i as the concentrated forces applied in the *y* direction at the ends of actin filaments which cross the side face of RVE, the effective shear force (*F*) applied on the side face of the RVE can be given as

$$F = \sum_{i=1}^{n} P_i \tag{4.12}$$

where n is the total number of actin filaments that cross one of the side faces of RVE.

Thus, the effective shear stress applied on one of the side faces of the RVE can be expressed as

$$\tau = F/WH = \sum_{i=1}^{n} P_i \Big/ WH \ , \tag{4.13}$$

where W and H are the side length and thickness of the RVE model, respectively.

Thus, the effective in-plane shear modulus of the RVE can be obtained as

$$\begin{aligned} G_{12} &= \frac{\tau}{\gamma} \\ &= \frac{3\left(0.5L_c + L_f\right)\sum_{i=1}^{n} P_i}{WHP} \\ &\quad \times \frac{k_{ct}k_{cb}k_f}{k_{ct}k_{cb} + k_f \cdot \left[3k_{cb} \cdot \left(0.5L_c + L_f\right)^2 + 2k_{ct} \cdot \left(0.5L_c\right)^2 + 3k_{ct}L_f \cdot \left(0.5L_c\right) + 3k_{ct}L_f^2\right] \Big/ \left(0.5L_c\right)^2} \end{aligned}$$

. (4.14)

In this L-shaped cantilever beam model (Figure 4.2), L_c refers to the total length of rod 2 segment in FLNA dimer (i.e., CDC' in Figure 3.3 (a)) which is reported to be 40 nm [49, 53]. L_f is the average length of actin filament segment between two neighbouring crosslinkers and given as

$$L_f = L_t / n_c \ , \tag{4.15}$$

where L_t and n_c are the total length of actin filaments and the total number of crosslinkers in the RVE model, respectively. It is easy to find that L_f is the reciprocal of the crosslinking density ρ_c. According to Eq. (4.10), the bending stiffness k_{cb} (or k_f) depends on not only the Young's modulus of crosslinker (or actin filament), but also the length of crosslinker (or actin filament). The torsion stiffness of crosslinker, k_{ct}, depends on the Young's modulus, Poisson's ratio and length of the crosslinker. In order to explore either the crosslinkers or the actin filaments dominate the stiffness (i.e., G_{12}) of the CAFNs, we fix the Poisson's ratios of crosslinker and actin filament at 0.35, the volume fraction of actin filaments at 0.2%, and the crosslinking density at 1.0.

As L_f can be obtained to be 1 μm according to Eq. (4.15), we obtain that $\left[3k_{cb}\cdot\left(0.5L_c+L_f\right)^2+2k_{ct}\cdot\left(0.5L_c\right)^2+3k_{ct}L_f\cdot\left(0.5L_c\right)+3k_{ct}L_f^2\right]\Big/\left(0.5L_c\right)^2=7803k_{cb}+7652k_{ct}$. In such a condition, the stiffnesses k_{ct}, k_{cb} and k_f only depend on E_c and E_f, respectively. By noting $3L_c\left(0.5L_c+L_f\right)\sum_{i=1}^{n}P_i\Big/WHP$ as a constant coefficient parameter, λ, Eq. (4.14) can be rewritten as

$$G_{12}=\lambda k_{ct}k_{cb}k_f\Big/\left\{L_c\cdot\left[k_{ct}k_{cb}+k_f\cdot(7803k_{cb}+7652k_{ct})\right]\right\}. \tag{4.16}$$

As the crosslinkers have a circular cross-section and are made of an isotropic material, $G_c=E_c/2(1+\nu_c)$ and $I_{Pc}=2I_c$, thus

$$k_{ct}=k_{cb}/(1+\nu_c). \tag{4.17}$$

A new symbol $k_c=k_{cb}=(1+\nu_c)k_{ct}$ is introduced to represent the amplitude of the bending stiffness of the crosslinkers, Eq. (4.16) can be rewritten as

$$G_{12}=\lambda k_c k_f\Big/\left[L_c\left(k_c+18186k_f\right)\right]. \tag{4.18}$$

Therefore, $k_c k_f\Big/\left[L_c\left(k_c+18186k_f\right)\right]$ can be used to demonstrate how the shear modulus G_{12} of CAFNs depends on the stiffnesses k_c and k_f, respectively. We respectively increase or reduce the Young's modulus of either the crosslinker or the actin filament by one or more orders, while fixing the Young's modulus of the other at the physiological level. Then different values of k_f and k_c can be obtained.

For a specific level of actin filament volume fraction and crosslinking density, the different values of k_f and k_c used for discussion are listed in Table 4.3. In order to identify either k_c or k_f dominates the stiffness (i.e., G_{12}) of the CAFNs, the values of G_{12}/λ are obtained from Eq. (4.18) and plotted against the bending stiffness of the FLNA (i.e., k_c) and the bending stiffness of the actin filament (i.e., k_f) in Figure 4.4.

Table 4.3. The values of the Young's moduli and bending stiffnesses of crosslinkers and actin filaments used for discussion in Figure 4.4.

V_f	ρ_c	E_c (Pa)	k_c (Nm^{-1})	E_f (Pa)	k_f (Nm^{-1})
0.2%	1.0	1.2×10^{4}	1.24×10^{-8}	2.3×10^{6}	7.28×10^{-11}
0.2%	1.0	1.2×10^{5}	1.24×10^{-7}	2.3×10^{7}	7.28×10^{-10}
0.2%	1.0	1.2×10^{6}	1.24×10^{-6}	2.3×10^{8}	7.28×10^{-9}
0.2%	1.0	1.2×10^{7}	1.24×10^{-5}	2.3×10^{9}	7.28×10^{-8}
0.2%	1.0	1.2×10^{8}	1.24×10^{-4}	2.3×10^{10}	7.28×10^{-7}
0.2%	1.0	1.2×10^{9}	1.24×10^{-3}	2.3×10^{11}	7.28×10^{-6}
0.2%	1.0	1.2×10^{10}	1.24×10^{-2}	2.3×10^{12}	7.28×10^{-5}

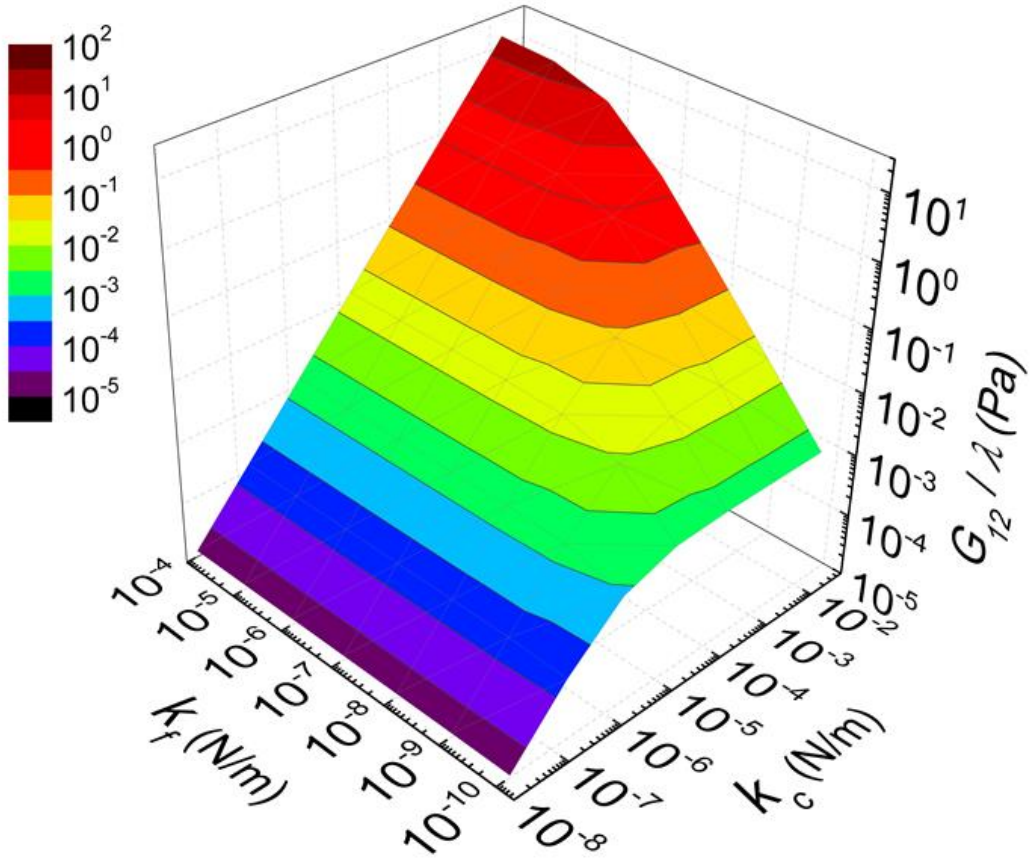

(a)

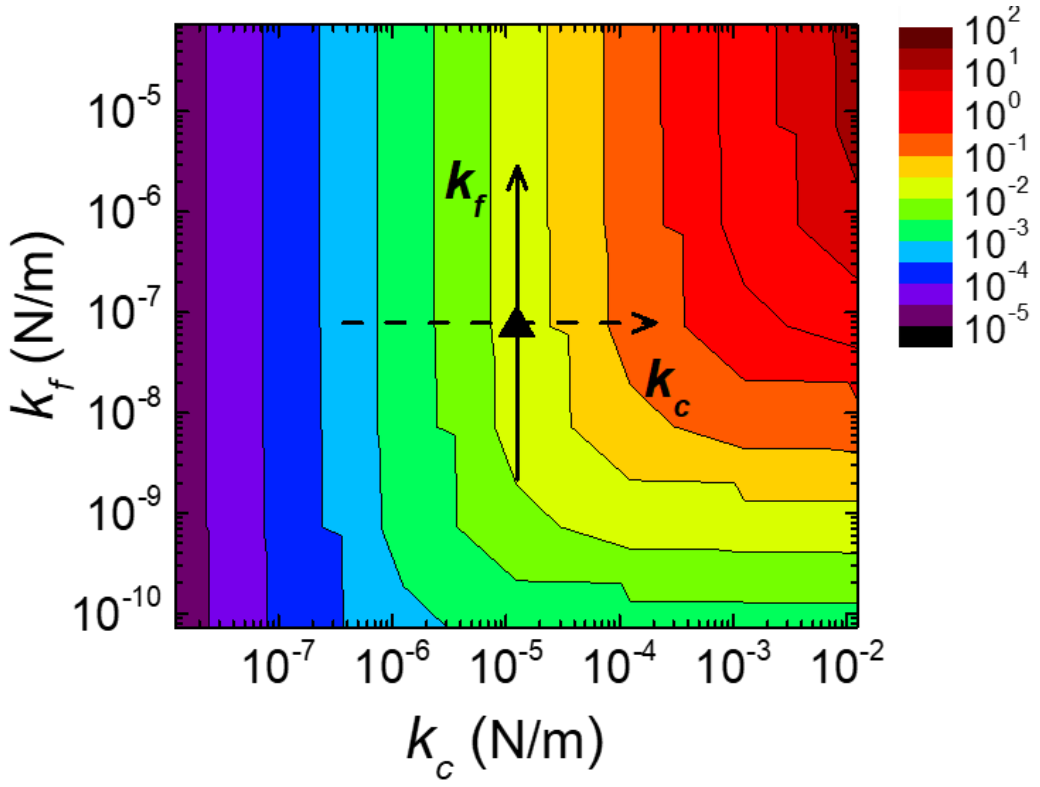

(b)

Figure 4.4. (a) Dependences of G_{12}/λ on the bending stiffness of FLNA (i.e., k_c) and the bending stiffness of actin filaments (i.e., k_f) when V_f = 0.2% and ρ_c = 1.0 μm^{-1}. (b) The plane isoline graphs of G_{12}/λ against k_c and k_f when V_f = 0.2% and ρ_c = 1.0 μm^{-1}. The solid triangle corresponds to the normal condition (i.e., the material properties are corresponding to Table 3.1). The arrow with the broken line indicates the increase of k_c , and the arrow with the solid line indicates the increase of k_f .

According to Eq. (4.10), the normal bending stiffness is $k_{c0} = 1.24\times10^{-5}$ Nm^{-1} for FLNA or $k_{f0} = 7.28\times10^{-8}$ Nm^{-1} for actin filaments. If k_f remains constant, G_{12}/λ exhibits almost a linear relationship with k_c when $k_c \ll k_f$, then the gradient drops with the further increase of k_c , and G_{12}/λ becomes a constant when $k_c \gg k_f$. On the other hand, if k_c remains constant, G_{12}/λ increases with k_f , but the gradient

drops with k_f and becomes zero when $k_f \gg k_c$. This clearly indicates that the elastic properties of CAFNs are mainly dominated by its weaker part/component. The plane isoline graph of G_{12}/λ against k_c and k_f is shown in Figure 4.4. (b), and the normal condition point (i.e., the material properties are corresponding to Table 3.1) is marked by the solid triangle. According to the plane isoline graph, when k_f is fixed at k_{f0}, it is easy to find that the small deformation stiffness of CAFNs shows a linear relationship with k_c near the normal condition point. However, when k_c is fixed at k_{c0}, the small deformation stiffness of CAFNs is not sensitive to k_f near the normal condition point. This indicates that the elastic properties of CAFNs are mainly dominated by FLNA in normal conditions.

In addition, the dependences of the in-plane shear modulus of CAFNs, G_{12}, on k_c and k_f are obtained by performing FEM simulations and shown in Figure 4.5. Considering the randomness of the RVE model, 100 models are simulated for each condition, and the statistical results (i.e., the mean results and error bars) of the 100 models are presented. It is noted that as the vertical axes are in log scale, the error bars look not symmetric about the mean values in the Figure 4.5.

In FEM simulations, the volume fraction of actin filament and the crosslinking density are the same as those used in the dimensional analysis, i.e., $V_f = 0.2\%$ and $\rho_c = 1.0$. In Figure 4.5 (a), the bending stiffness of actin filament, k_f, is fixed at k_{f0} (i.e., 7.28×10^{-8} Nm^{-1}). In Figure 4.5 (b), the bending stiffness of FLNA, k_c, is fixed at k_{c0} (i.e., 1.24×10^{-5} Nm^{-1}). In addition, different values of k_f and k_c are applied in Figure 4.5 (c) and Figure 4.5 (d) respectively to further verify the dimensional analysis results. As can be seen in Figure 4.5, the FEM simulation results of G_{12} agree well with the predictions of the dimensional analysis. The normal condition points shown in Figure 4.5 corresponds to the condition during which the material properties of actin filament and crosslinker are determined according to their normal values (i.e., materials properties shown in Table 3.1).

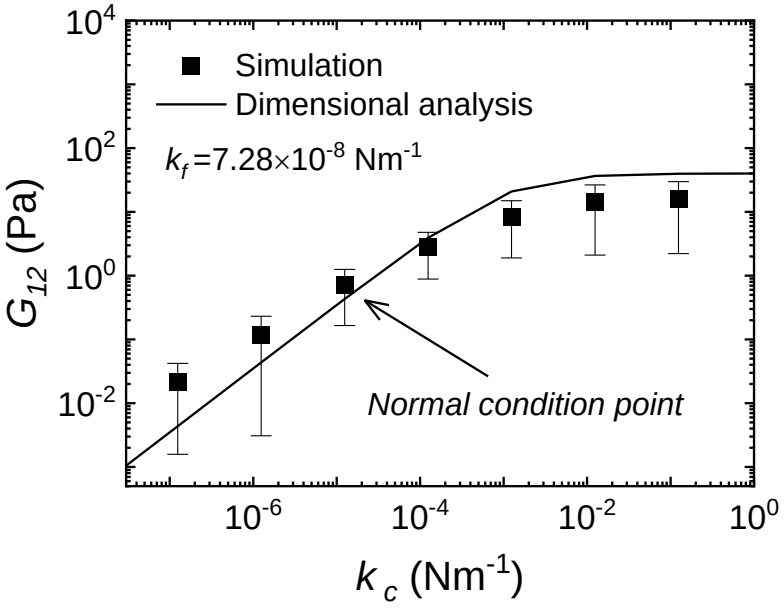
Simulation
Dimensional analysis
k_f=7.28×10^{-8} Nm^{-1}
Normal condition point
G_{12} (Pa)
k_c (Nm^{-1})
10^{4}
10^{2}
10^{0}
10^{-2}
10^{-6}
10^{-4}
10^{-2}
10^{0}

(a)

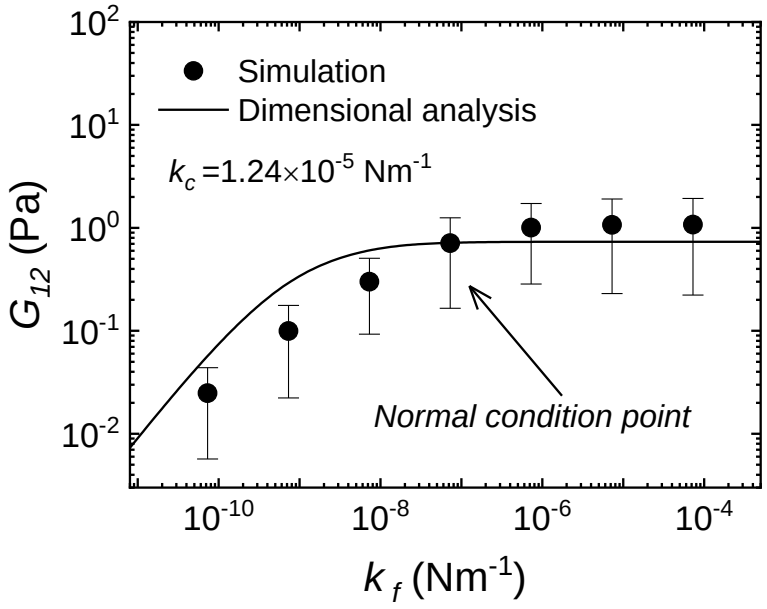
Simulation
Dimensional analysis
k_c=1.24×10^{-5} Nm^{-1}
Normal condition point
G_{12} (Pa)
k_f (Nm^{-1})
10^{2}
10^{1}
10^{0}
10^{-1}
10^{-2}
10^{-10}
10^{-8}
10^{-6}
10^{-4}

(b)

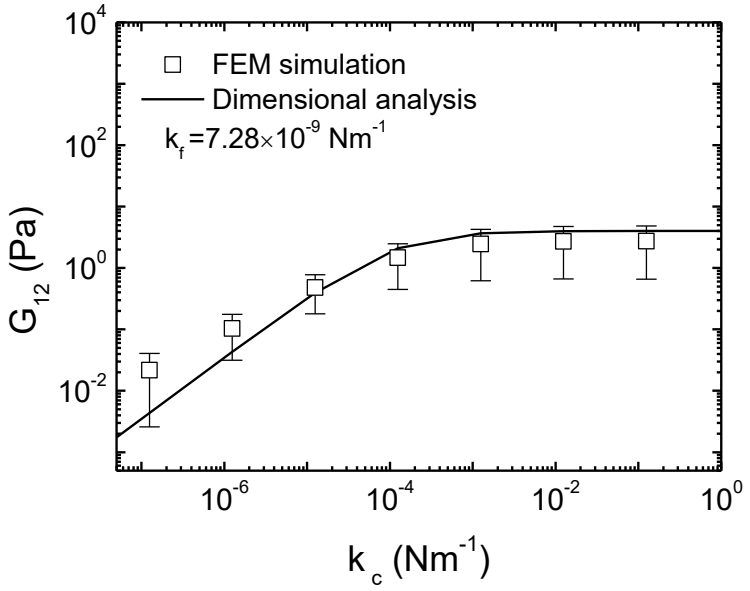

(c)

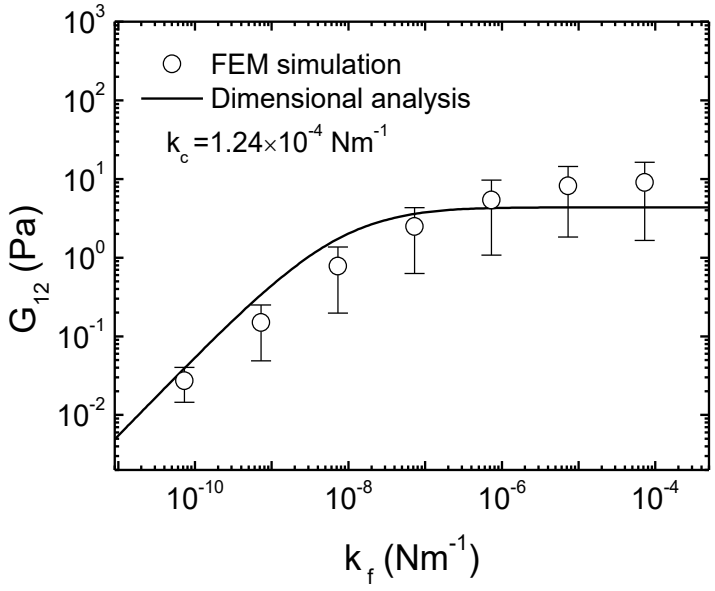

(d)

Figure 4.5. (a) The dependences of G_{12} on the bending stiffness of the crosslinker. (b) The dependences of G_{12} on the bending stiffness of the actin filament. Where V_f = 0.2%, ρ_c = 1.0 μm^{-1}. Simulation results (solid squares and solid circles) are compared with the dimensional analysis predictions (solid curves in (a) and (b)). In (a) and (b), the bending stiffness of actin filament, k_f, and the bending stiffness of crosslinker, k_c, are fixed at their normal condition values, respectively. To further verify the dimensional analysis results, the values of the bending stiffness of actin filament, k_f, and the bending stiffness of crosslinker, k_c, are chosen to be different from their normal condition values in (c) and (d).

In order to probe the effects of the Poisson's ratios of actin filament and FLNA on the in-plane shear modulus of CAFNs, one random periodic CAFNs model with an actin filament volume fraction of 0.2% and a crosslinking density of 1.0 μm^{-1} is used to do some numerical tests. For simplicity, both the actin filament and FLNA are assumed to have the same Poisson's ratio. The effects of the Poisson's ratios of actin filament and FLNA on the in-plane shear modulus of the CAFNs are illustrated by the statistic results of 100 models shown in Figure 4.6.

As can be seen from Figure 4.6. (a), the in-plane shear modulus of CAFNs, G_{12}, decreases linearly and slightly (just about 2%) when the Poisson's ratios of the actin filament and FLNA increases from 0.35 to 0.499. The change in G_{12} is because both the torsional stiffnesses and the transverse shear stiffnesses of the actin filament and FLNA decrease with the increase of the Poisson's ratios. This indicates that the stiffness of the CAFNs is almost insensitive to the Poisson's ratios of actin filament and FLNA in the range of 0.3 to 0.499.

It is worth noting that the Poisson's ratios of actin filament and FLNA are between 0.3 and 0.4 according to the experimental measurements, and the effects of the components' Poisson's ratios on the in-plane shear modulus of CAFNs are proved to be slight in this range. However, the dependences of the mechanical responses of such structures on their components' Poisson's ratios are still not clear when their components' Poisson's ratios are out of this range. Thus, it is essential to apply a larger range to Poisson's ratios (e.g., -0.999 to 0.499) when discussing the influences originating from Poisson's ratios. And this could also provide reference when designing bioinspired structures which have similar architecture with CAFNs. As shown in Figure 4.6. (b), when increasing the Poisson's ratios of actin filament and FLNA from -0.999 to 0.499, the in-plane shear modulus of CAFNs decreases about 26%.

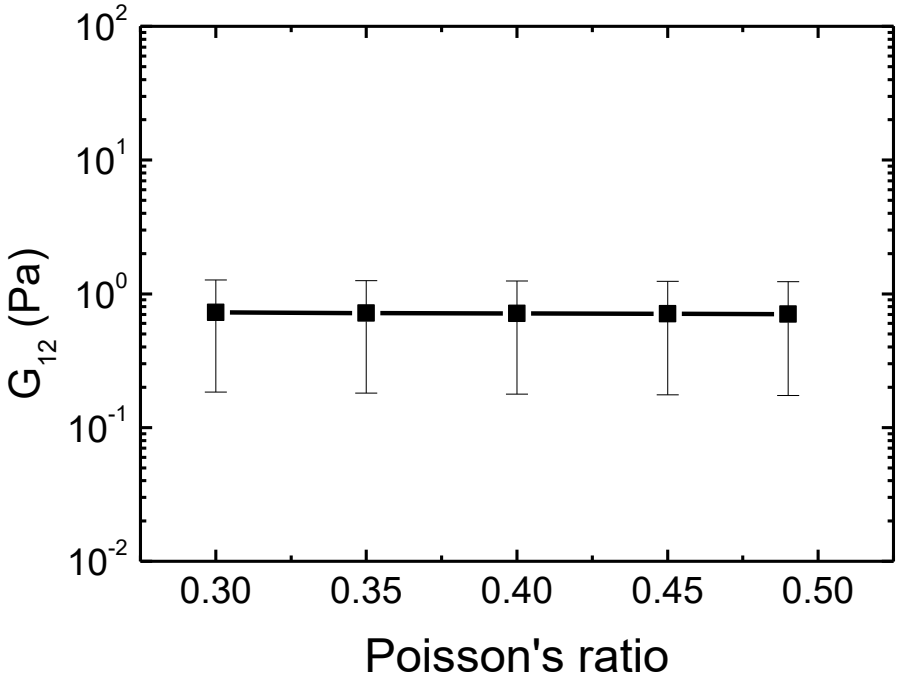

(a)

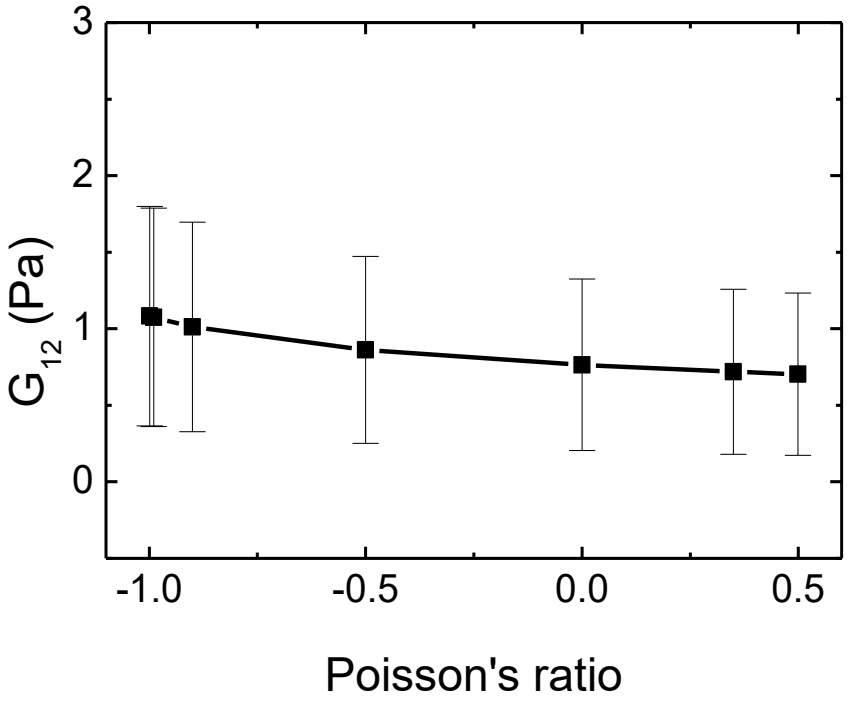

(b)

Figure 4.6. (a) The effects of the Poisson's ratios of actin filament and FLNA on the in-plane shear modulus of CAFNs when Poisson's ratios are in the range of 0.3 to 0.499 (a), and in the range of -0.999 to 0.499 (b). The statistic results are obtained from 100 random periodic FE models, where V_f = 0.2%, ρ_c = 1.0 μm^{-1}.

As the aspect ratios of the actin filaments and FLNA in our model are very large (larger than 10), the axial compression and transverse shear deformations of both the actin filaments and FLNA can fairly be ignored. To the best of our knowledge, the decoupled effects of the bending and torsion deformations of actin filaments and FLNA on the stiffness (e.g., shear modulus) of CAFNs have never been studied before. In this research, four more different cases of testing simulations on the same 100 random RVE models are conducted to explore how the stiffness of CAFNs depends on the de-coupled bending and torsion deformations of actin filaments and FLNA, and to compare these results with that obtained from the normal condition (Table 4.4). In case-1, both the bending and torsion stiffnesses of FLNA are fixed at the normal condition while both the bending and torsion stiffnesses of actin filaments are five orders larger than those of FLNA. In this case, the deformations of the actin filaments can be ignored and the stiffness of CAFNs depends on only the deformation (i.e., bending and torsion) of FLNA. In case-2, the bending stiffness of FLNA is fixed at the normal condition, and the torsion stiffness of FLNA is five orders larger than its bending stiffness (this is realized by setting the Poisson's ratio of FLNA at -0.99999). In addition, both the bending and shear stiffnesses of the actin filaments are also five orders larger than the bending stiffness of FLNA. In this case, the stiffness of CAFNs depends on only the bending deformation of FLNA. In case-3, both the bending and torsion stiffnesses of the actin filaments are fixed at the normal condition, while both the bending and torsion stiffnesses of FLNA are five orders larger than those of the actin filaments. In this case, the stiffness of CAFNs depends only on the deformation (i.e., bending and torsion) of the actin filaments. In case-4, the bending stiffness of the actin filaments is fixed at the normal condition, while the torsion stiffness of the actin filaments is five orders larger than its bending stiffness. In addition, both the bending and shear stiffnesses of FLNA are also five orders larger than those of the actin filaments. In this case, the stiffness of CAFNs depends only on the bending deformation of the actin filaments.

Table 4.4 shows the simulation results of the shear modulus of the CAFNs for the four cases, and the result obtained from the normal condition is also provided for comparison. By comparing the results of case-1 and case-3, it is very clear that the stiffness (or deformation) of CAFNs is dominated by FLNA (i.e., the crosslinkers), and that the bending and torsion deformations of the actin filaments have much smaller effects on the stiffness of CAFNs. By decoupling case-1 and

case-2, it can be found that the torsion deformation of FLNA plays almost the same important role as the bending deformation of FLNA in determining the stiffness of CAFNs. The deflection of the CAFNs given by Eq. (4.9) can be approximately expressed as

$$\begin{aligned} \mathrm{y} &= \frac{P\cdot(0.5L_c+L_f)^2\cdot 0.5L_c}{G_cI_{Pc}} + \frac{2P\cdot(0.5L_c)^3}{3E_cI_c} + \frac{PL_f\cdot(0.5L_c)^2}{E_cI_c} + \frac{PL_f^2\cdot(0.5L_c)}{E_cI_c} + \frac{PL_f^3}{3E_fI_f} \\ &\approx \frac{P\cdot(0.5L_c+L_f)^2\cdot 0.5L_c}{G_cI_{Pc}} + \frac{PL_f^2\cdot(0.5L_c)}{E_cI_c} + \frac{PL_f^3}{3E_fI_f} \end{aligned}$$

. (4.19)

This is because $L_c << L_f$. Thus, the deflection (or stiffness) resulted from the torsion deformation of the crosslinker, $\frac{P\cdot(0.5L_c+L_f)^2\cdot 0.5L_c}{G_cI_{Pc}}$, is almost the same as that resulted from the bending deformation of the crosslinker, i.e., $\frac{PL_f^2\cdot(0.5L_c)}{E_cI_c}$.

To the best of our knowledge, this is the first time to quantify the contribution of the torsion stiffness of FLNA (i.e., crosslinkers) to the stiffness of CAFNs.

Table 4.4. Effects of the bending and torsion of actin filament and FLNA on the in-plane shear modulus (G_{12}) of CAFNs. The statistic results are obtained from 100 random periodic CAFNs models, where V_f = 0.2%, ρ_c = 1.0 μm^{-1}.

Case	G_{12} (Mean) Pa	Standard deviation
Physiological	0.7189	0.5381
1	1.3866	0.8221
2	2.6386	1.5979
3	15.2351	10.4626
4	20.5075	14.7296

4.6 Conclusions

In this chapter, the effective in-plane Young's moduli, shear moduli and Poisson's ratios of the CAFNs are obtained by performing FEM simulations. The simulation results show that the CAFNs are in-plane isotropic, and the scaling relationship between the in-plane shear modulus of CAFNs and the volume fraction of actin

filament agrees well with the experimentally measured results ($G_{12} \sim V_f^{5/2}$) in literature. The in-plane shear modulus of CAFNs, G_{12}, is observed to scale with the square of the crosslinking density of CAFNs, i.e., $G_{12} \sim \rho_c^2$. By varying the actin filament volume fraction (via changing the concentration of actin) and crosslinking density (via altering the concentration of FLNA), the elastic properties of CAFNs could be optimized/tuned to meet the demanding requirements for distinct physiological functions (e.g., cell migration, cell growth and cell division).

In addition, a cantilever beam model has been developed for the dimensional analysis on the shear modulus of CAFNs. According to dimensional analysis, the in-plane shear stiffness of CAFNs is mainly dominated by FLNA, which is consistent with FEM simulation results. The FEM simulation results also indicate that the in-plane shear modulus of CAFNs is almost insensitive to the Poisson's ratios of actin filament and FLNA in the range of 0.29 to 0.499. Four more cases of testing simulations on random RVE models are performed to de-couple the influences of the torsion deformation of crosslinkers and actin filaments on the stiffness of CAFNs by altering the torsion and bending stiffnesses of crosslinkers and actin filaments, respectively. The simulation results for the first time indicate that the torsion deformation of FLNA plays almost the same important role as the bending deformation of FLNA in determining the stiffness of CAFNs. The results obtained in this research can significantly increase our understanding of the mechanical behaviours of CAFNs and have important applications in bioscience and biomedical engineering.

Chapter 5 Nonlinear Elastic Properties of Crosslinked Actin Filament Networks

In physiological conditions, cells can undergo large deformation to respond to external stimulations and to support different cell functions. When undergoing large deformation, the crosslinked actin filament networks (CAFNs) always show strong nonlinear elasticity to maintain the cell shape and integrity, which is known as strain stiffening. As the strain stiffening of the CAFNs plays a crucial role in the mechanical responses of cytoskeleton and living cells, this nonlinear elastic behaviour of CAFNs has drawn a lot of attention during the past decades. However, the effects of the components' contents and physical properties on the nonlinear elastic properties of CAFNs are not known very well. In this research, the effects of the actin filament volume fraction, crosslinking density, Young's modulus of actin filament, Young's modulus of crosslinker, Poisson's ratio of actin filament and Poisson's ratio of crosslinker on the stress strain relationship and tangent modulus of the crosslinked actin filament networks are studied. In addition, the normal stress of CAFNs is also obtained from numerical simulations, and the effects of the components' physical properties of the normal stress are discussed. In large deformation regime, the crosslinkers and actin filament can bear bending, torsion as well as stretching. Therefore, the dependences of the nonlinear elastic properties of CAFNs on the bending stiffnesses, torsional stiffnesses and tensile stiffnesses of crosslinker and actin filament are studied respectively.

5.1 Introduction

In living cells, the mechanical deformations can originate from both internal and external stresses, and the elasticity of cell cytoskeleton is proved to be enhanced

when the applied deformation is gradually increased. This behaviour of the cell cytoskeleton network is known as strain stiffening, and it is also observed in the substructures of the cytoskeleton, such as the crosslinked actin filament networks. During the past decades, the strain stiffening behaviour of cytoskeleton is proved to play a very important role in different cell functions (e.g., cell migration, cell division and cell growth) [157]. Thus, it becomes more and more pressing to investigate the nonlinear elastic properties of cytoskeleton especially the crosslinked actin filament networks. Many researchers have conducted *in vivo* or *in vitro* experiments to study this nonlinear elastic behaviour of biopolymer networks [59, 90, 104, 158-160] and obtained many meaningful results. Xu et al. [158] used reconstituted actin filament networks to study the mechanical behaviour of actin network structures and found that the elasticity of the actin filament network was regulated by the amplitude and rate of the applied loads. They also proposed a model to explain the origin of the strain stiffening of actin filament networks when strains were applied. Storm et al. [90] measured the shear moduli of different crosslinked biopolymer networks against different strain amplitudes by conducting *in vitro* experiments, and they also developed a molecular theory which explained the strain stiffening behaviour of distinct biopolymer gels by obtaining the universal stress-strain relationships at small and intermediate strain regimes. Their findings provide great implications to study the nonlinear elastic properties of cell cytoskeleton and other biopolymer network structures. Gardel et al. [59] measured the stress-strain relationships of actin filament networks reconstituted *in vitro*, and they used different filamin mutants to crosslink the actin filaments into networks to replicate the mechanical properties of living cells. The dependences of the differential modulus of the crosslinked actin filament networks on the prestress are also discussed in their work. Kasza et al. [104] also used purified actin filament networks to conduct *in vitro* experiments to investigate the nonlinear elastic properties of stiff biopolymers connected by flexible crosslinkers. They found that the nonlinear elastic properties of crosslinked actin filament networks are regulated by the concentration of crosslinkers in the network, and a model of rigid rods connected with multiple compliant linkers is proposed to account for this behaviour. These studies on the nonlinear elastic properties of crosslinked actin filament networks provide implications to understand the mechanical responses of cytoskeleton and living cells.

However, due to the extreme complexity and instability of these biopolymer network systems, sometimes it is difficult to systematically study their mechanical

properties just by experimental measurements. Therefore, theoretical analysis [90, 93, 111, 161] and numerical modelling [111, 119] have also been developed to investigate the nonlinear elastic properties of crosslinked biopolymer network structures. Numerical modelling is proved to be a highly efficient method to mimic both the architecture and physical properties of complex structural systems by applying assumptions when constructing the model. In addition, using numerical simulations makes it possible to study the effects of some crucial factors (e.g., actin filament length, actin filament volume fraction, crosslinking density and physical properties of components) on the mechanical behaviours of CAFNs by tuning corresponding parameters in simulations. But these effects may not be revealed by simply using some hyperelastic material models such as the Mooney-Rivlin model and Arruda-Boyce model. During the past decade, different theories (e.g., Molecular Dynamics and Finite Element Method) have been applied to develop numerical models to investigate the mechanical properties of material or structures. The Molecular Dynamics uses the Newton's equations of motion to obtain the time evolution of a set of interacting atoms, which can precisely capture the microstructure of biopolymers. However, this also results in the remarkable complexity when constructing crosslinked actin filament network models by Molecular Dynamics. This makes it difficult for us to construct a large-scale network model by this method, and this also increases the computational cost when conducting numerical simulations. In Finite Element Methods (FEM), materials can be assumed to be homogeneous and be partitioned into finite elements with specific properties, which makes it easy to compute the model at low cost [120]. Therefore, FEM models can be used to mimic the mechanical behaviour of crosslinked actin filament networks. Because of the large scale and extreme complexity of the crosslinked actin filament networks in living cells, representative volume element is always selected when constructing models. Therefore, the nonlinear elastic properties of crosslinked actin filament networks are studied in this chapter by conducting finite element method simulations, and the simulation results are compared with experimental measurements.

In this chapter, the nonlinear elastic properties of CAFNs are studied by conducting numerical simulations. According to the results of numerical simulations, it can be demonstrated that the nonlinear elastic properties of crosslinked actin filament networks can be greatly influenced by the actin filament volume fraction, crosslinking density and components' properties. In Section 5.2, the stress strain relationship of crosslinked actin filament networks is obtained and

compared with experimental measurements. In Section 5.3, the effects of actin filament volume fraction and crosslinking density on the nonlinear elastic properties of CAFNs are studied. In Section 5.4, the effects of components' properties on the nonlinear elastic properties of CAFNs are illustrated. In Section 5.5, the negative normal stress of CAFNs is discussed. The dependences of the nonlinear elastic properties on the bending stiffnesses, torsional stiffnesses and tensile stiffnesses of crosslinkers and actin filaments are discussed in Section 5.6. This can partially reveal the deformation mechanism of crosslinked actin filament networks in large strain regime. Conclusions are drawn in Section 5.7.

5.2 Stress strain relationship of CAFNs

During the past decades, the force-extension relationships of single filamin A [132] and actin filament [162] are characterized by atomic force microscopy and microfabricated cantilevers respectively. According to the force-extension curve of filamin A molecule in aqueous solution measured by AFM [132], sawtooth patterns corresponding to the unfolding of Ig-fold domains of filamin A are observed and the unfolding force of the Ig-fold domains of the filamin A is about 100 pN. The molecular rupture force between single actin filament and filamin A measured by Ferrer et al. [163] ranges from 40pN to 80 pN which is smaller than the unfolding force of filamin A. This means that the filamin A does not unfold before the onset of the rupture between actin filament and filamin A. The force-extension curve of filamin A molecule is nonlinear when the applied force is small, which highly relates to the curved contour of filamin A in experiments. However, the force-extension curve of filamin A tends to be linear when the applied force is increased (before unfolding), which indicates that the filamin A is stretched to be straight at this stage. In this research, the crosslinker (i.e., filamin A) is modelled by curved beam (with linear elastic material properties) whose force-extension curve is also nonlinear due to its curved contour, which is consistent with the force-extension curve of filamin A measured in experiments [132]. Liu and Pollack point out that the force-extension relationship of a single actin filament is nonlinear in low-tension range and become linear at moderate-tension and high-tension ranges [162]. The nonlinearity of the force-extension curve of actin filament in low-tension range also originates from the curved contour of actin filament in experiments. However, the

actin filament is modelled by straight beam in this research, which indicates the absence of the nonlinear stretching stage at low-tension range. Thus, the actin filaments are assumed to be linear elastic materials as they are straight in this research. In addition, this chapter mainly focuses on the nonlinearity of CAFNs caused by the rearranging of the microstructure of CAFNs. Thus, when studying the nonlinear elastic properties of CAFNs, the actin filament and crosslinker are also assumed to be isotropic and linear elastic materials. That is the nonlinearity (i.e., strain stiffening) of CAFNs studied in this chapter originates from the rearrangement of the microstructures. Their material properties are determined according to literature and shown in Table 3.1.

When a relatively large shear strain is incrementally applied to the RVE models of CAFNs during the simulations, nonlinear stress strain curves are obtained though actin filament and crosslinker are assumed to be linear elastic materials in this chapter. This nonlinear elastic behaviour of CAFNs originates from the changes in the microstructure of CAFNs rather than the material properties of actin filament and crosslinker. The effects of the nonlinearity of the materials properties (e.g., viscoelastic properties) of actin filament and crosslinker on the nonlinear mechanical behaviour (e.g., viscoelastic behaviour) of CAFNs are studied in Chapter 6.

By conducting numerical simulations, the shear stress strain curve of CAFNs with specific actin filament volume fraction and crosslinking density is obtained and shown in Figure 5.1. In this research, the tangent modulus is defined as the slope (i.e., $d\sigma/d\gamma$) of the shear stress-strain curve at any specific stress or strain. Thus, the tangent modulus of CAFNs can be obtained from the shear stress strain curve of CAFNs shown in Figure 5.1. Then, the tangent modulus of CAFNs is also shown in Figure 5.1. Gardel et al. [59] experimentally measure the stress-strain relationships of crosslinked actin filament networks with a stress-controlled rheometer. By comparing with the experimental measurements, the shear stress-strain curve and tangent shear modulus of CAFNs obtained from FEM simulations show good agreement with the experimental results reported in literature [59]. During the small strain stage, the shear stress increases almost linearly with the applied strain, which results in a constant tangent modulus. Then, the shear stress increases nonlinearly with the applied strain. This nonlinear increase in the stress strain curve consequently results in a nonlinear increase of the tangent modulus. It is easy to find that the tangent modulus could be enhanced by several orders of magnitude when the applied strain reaches 0.5. This nonlinear elastic behaviour

is also known as strain stiffening which plays an important role in the mechanical response of the CAFNs.

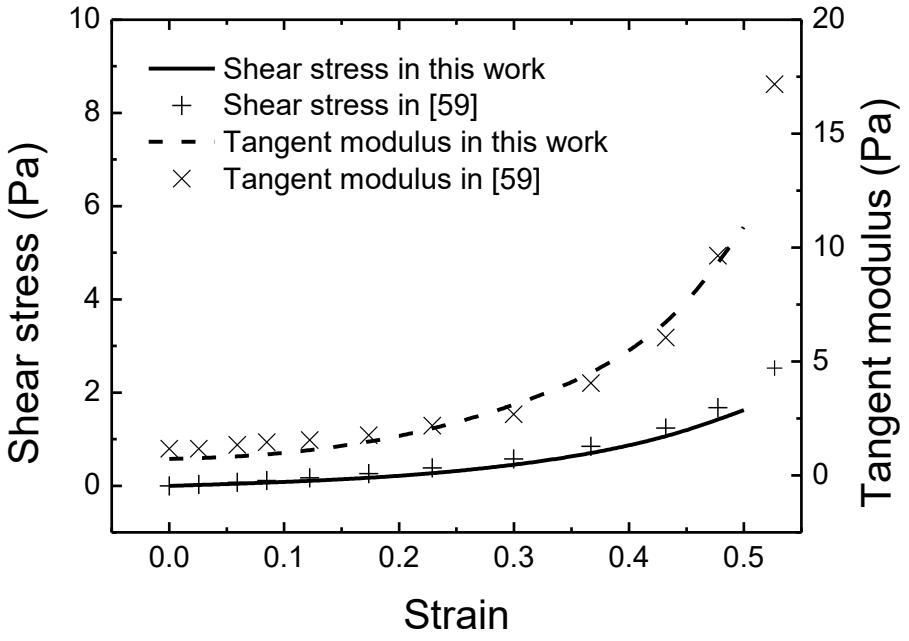

Figure 5.1. The shear stress strain relationship and tangent modulus of CAFNs. The volume fraction of actin filament, V_f, is 0.2%, and the crosslinking density, ρ_c, is 3.0 μm^{-1}.

5.3 Effects of components' content

5.3.1 Effects of actin filament volume fraction on the nonlinear elastic properties of CAFNs

The volume fraction of actin filaments can no doubt influence the mechanical properties of crosslink biopolymer networks. The effects are studied by applying different volume fraction of actin filaments to the model with the crosslink density being controlled at a constant level.

In this Section, the influences of actin filament volume fraction on the nonlinear elastic properties of CAFNs are studied (Figure 5.2) by conducting numerical

simulations. Our simulation results show that larger V_f and shear strain result in larger tangent modulus (Figure 5.2. (b)). When the volume fraction of actin filament is increased from 0.2% to 0.3%, the tangent modulus of CAFNs increases by about one order of magnitude. If the volume fraction of actin filaments is continuously improved from 0.3% to 0.4%, the tangent modulus of the network increases to about two times of that for 0.3% volume fraction. This indicates that the influence of volume fraction of actin filaments on the nonlinear elasticity of CAFNs is more crucial when the volume fraction of actin filaments is small.

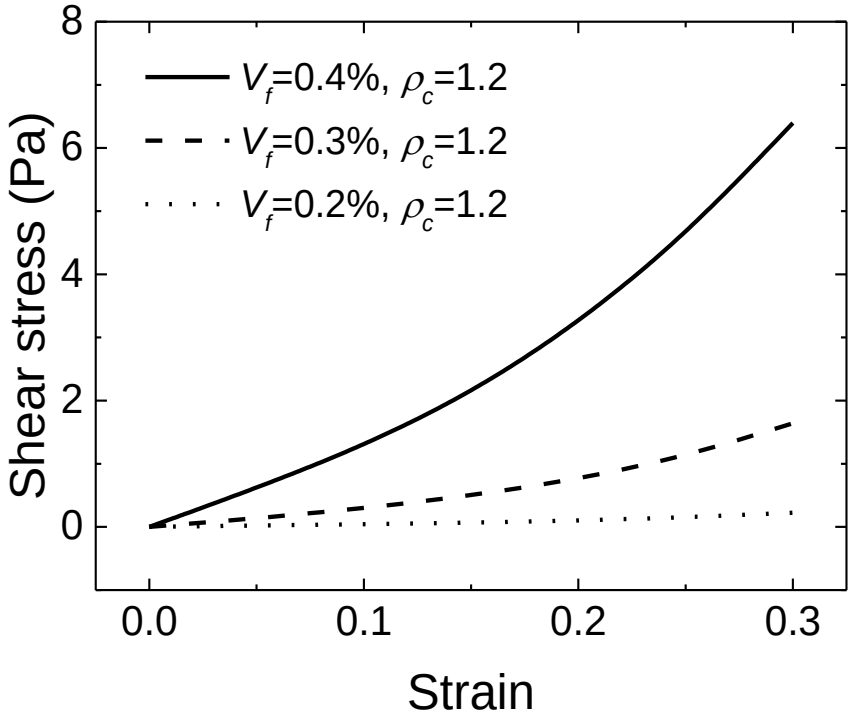

(a)

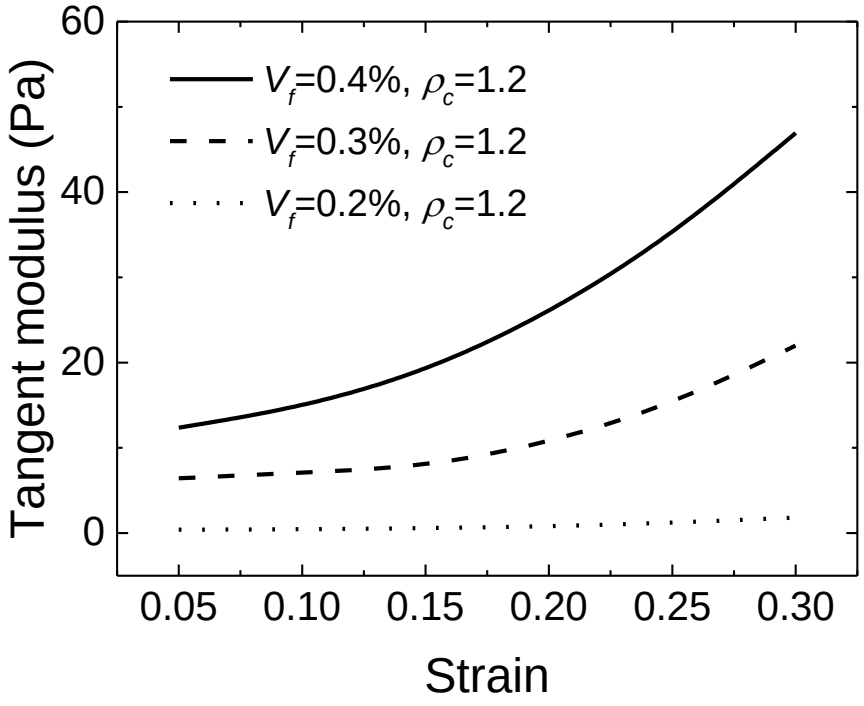

(b)

Figure 5.2. Dependences of the shear stress strain relationship (a) and tangent modulus (b) of CAFNs on the actin filament volume fraction. Where the unit of the crosslinking density μm^{-1}.

5.3.2 Effects of crosslinking density on the nonlinear elastic properties of CAFNs

The crosslinking density can greatly influence the mechanical properties of crosslinked actin filament networks. In this part, three different levels of crosslinking density (ρ_c=1.0 μm^{-1}, 1.2 μm^{-1} and 1.5 μm^{-1}) are applied to models with the same volume fraction (0.3%) and mean length (1 μm) of filaments. By conducting numerical simulations, the dependence of stress and tangent modulus on strain are obtained and shown in Figure 5.3. From the stress strain curve, it is easy to find that the stress increases nonlinearly with the improvement of applied strain, and networks with larger crosslink density hold larger stress. In addition, the stress strain curves are linear when the strain is small, however, they become nonlinear when the applied strain is large enough. This nonlinear elastic property

is also known as strain stiffening which plays an important role in the mechanical response of the biopolymer networks. According to the stress strain curves shown in Figure 5.3. (a), the crosslinking density has great effects on the nonlinear elastic properties of crosslinked actin filament networks. In addition, the tangent moduli of the crosslinked actin filament networks are also greatly influenced by the crosslinking density as shown in Figure 5.3. (b). It can also be found that the tangent modulus of CAFNs increase nonlinearly with the crosslinking density. By increasing the crosslinking density, ρ_c , from 1.0 μm^{-1} to 1.2 μm^{-1}, the shear stress and tangent modulus increase over three times (Figure 5.3), and they continuously increase two times when ρ_c is further increased from 1.2 μm^{-1} to 1.5 μm^{-1}. In summary, it can be seen that larger crosslinking density results in larger shear stress and larger tangent modulus. Thus, the crosslink density can greatly influence the nonlinear elasticity of crosslinked biopolymer networks.

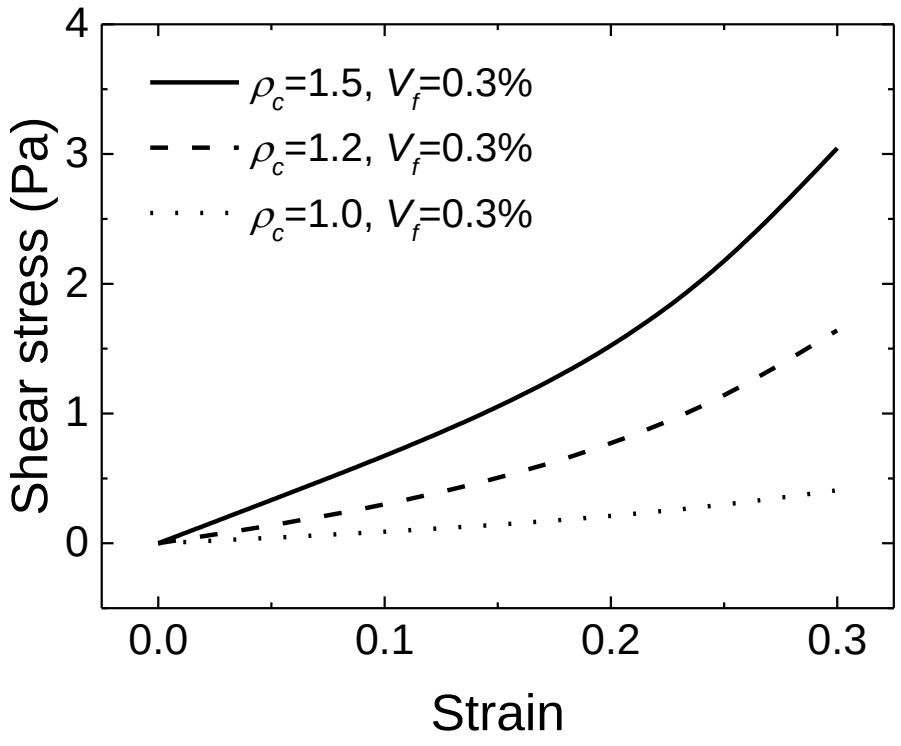

(a)

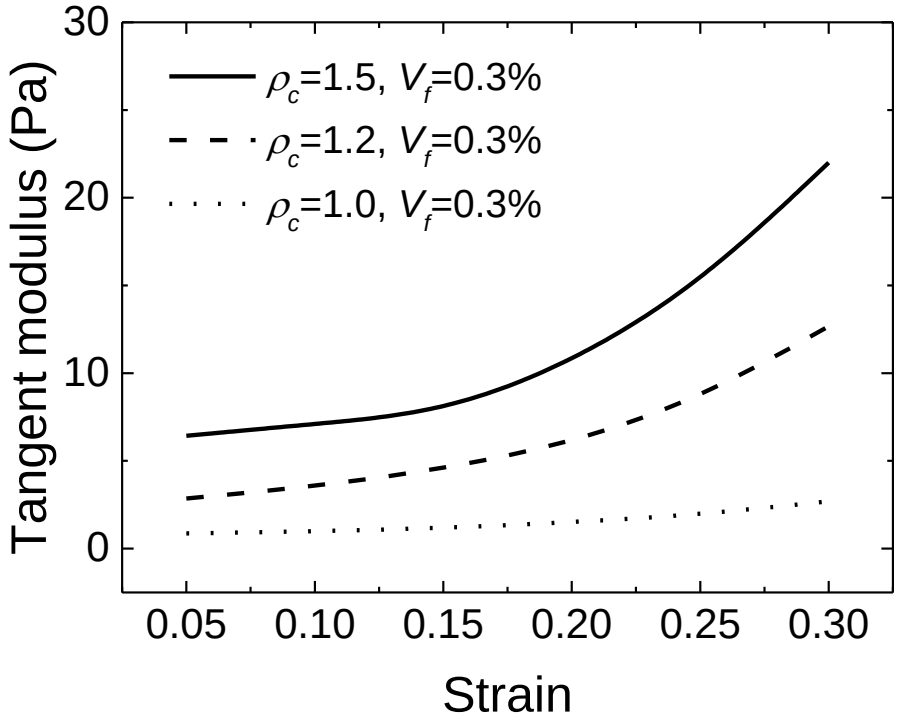

(b)

Figure 5.3. Dependences of the shear stress strain relationship (a) and tangent modulus (b) of CAFNs on the crosslinking density. Where the unit of the crosslinking density μm^{-1}.

5.4 Effects of components' properties

5.4.1 Effects of components' Young's moduli on the nonlinear elastic properties of CAFNs

In order to probe the effects of components' elasticity on the nonlinear elastic properties of CAFNs, different Young's moduli are adopted for FLNA and actin filament respectively. Our simulation results show that the Young's moduli of FLNA and actin filaments can greatly affect the shear stress strain relationship of CAFNs (Figure 5.4). The larger the Young's moduli, the larger the shear stress and the tangent modulus of the CAFNs. When the Young's modulus of FLNA (E_c) is increased from 12 MPa to 120 MPa, the shear stress/tangent modulus at small

strain stage (γ = 0.001) increases about three times and continuously increases with the strain (approximate four times at γ = 0.2). When the Young's modulus of FLNA (E_c) is decreased by one order of magnitude to 1.2 MPa, the shear stress/tangent modulus at small strain stage (γ = 0.001) decreases to about one fourth and continuously decreases with the strain (approximate one fifth at γ = 0.2). When we decrease the Young's modulus of actin filament (E_f) by one order of magnitude to 230 MPa, the shear stress/tangent modulus at small strain stage (γ = 0.001) reduces by two thirds. However, in large strain stage, the decrease of shear stress/tangent modulus becomes smaller and smaller in comparison with the small strain stage (about 50% at γ = 0.2). By continuously reducing E_f from 230 MPa to 23 MPa, the shear stress/tangent modulus at small strain stage (γ = 0.001) reduces by three fourths. However, at γ = 0.2, the shear stress/tangent modulus decreases by about two thirds. These results suggest that both the Young's moduli of FLNA and actin filaments can greatly affect the nonlinear elastic properties of CAFNs. However, the nonlinear elastic properties of CAFNs are mainly dominated by FLNA.

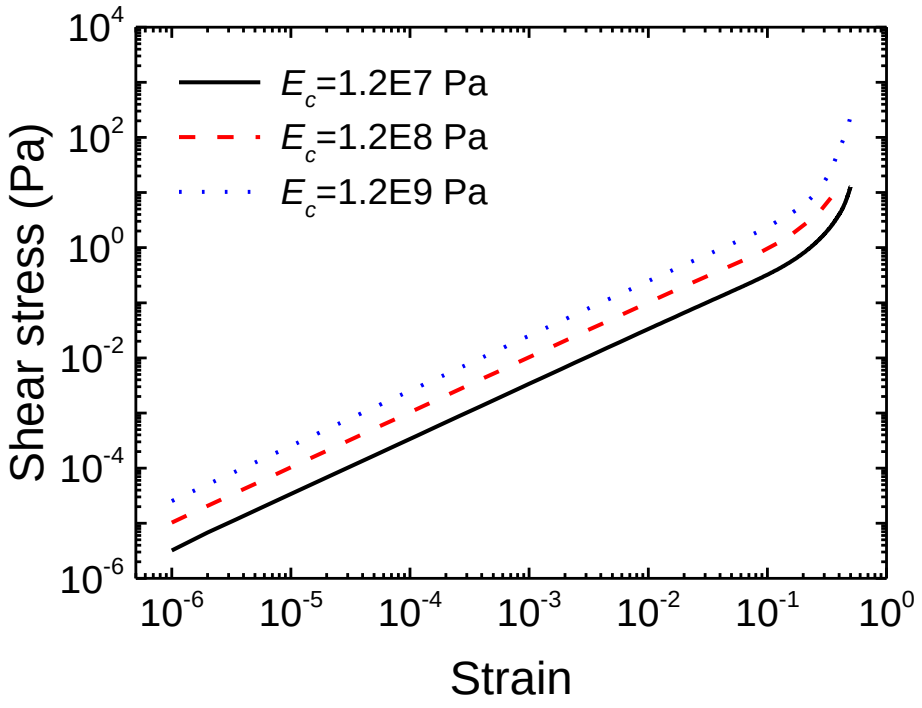

(a)

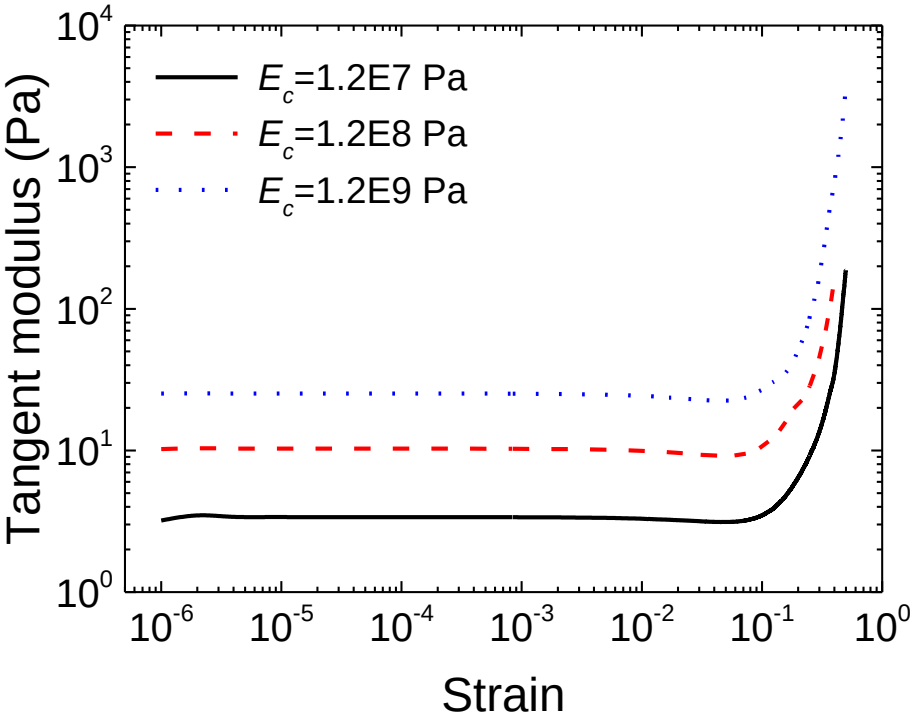
Tangent modulus (Pa)
Strain
E_c=1.2E7 Pa
E_c=1.2E8 Pa
E_c=1.2E9 Pa

(b)

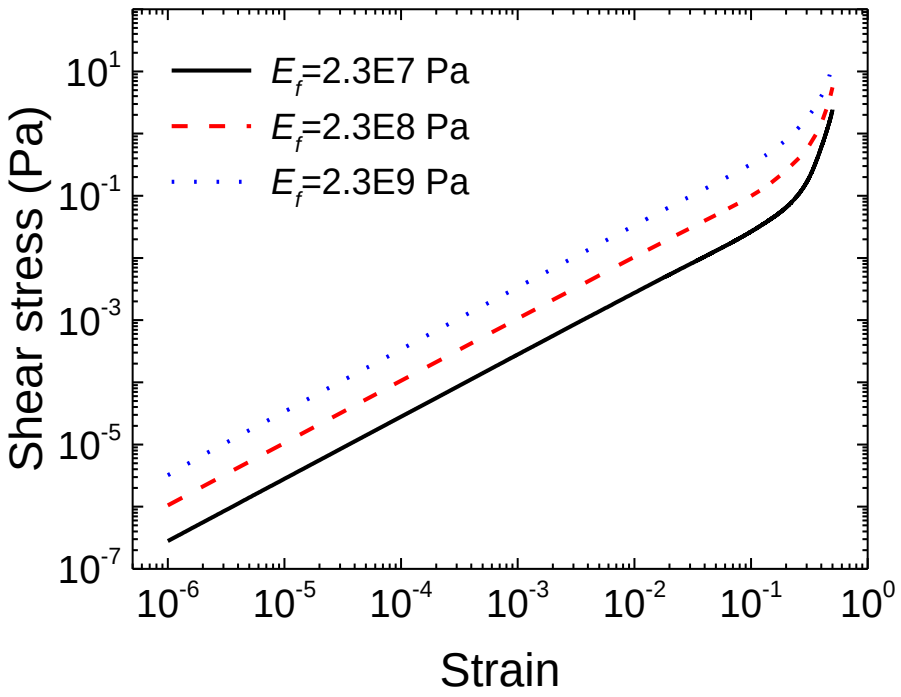
Shear stress (Pa)
Strain
E_f=2.3E7 Pa
E_f=2.3E8 Pa
E_f=2.3E9 Pa

(c)

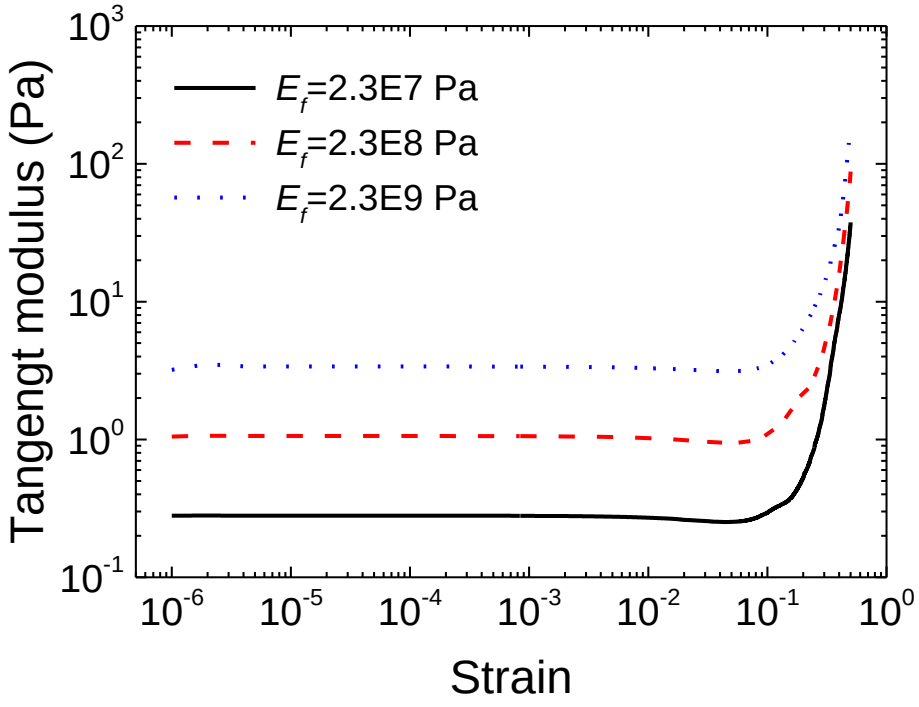

(d)

Figure 5.4. Dependence of the shear stress strain relationship and tangent modulus of CAFNs on E_c (a-b) and E_f (c-d), where V_f=0.3%, ρ_c=1.2 μm^{-1}. In (a) and (b), the Young's modulus of actin filament is fixed at 2.3 GPa. In (c) and (d), the Young's modulus of FLNA is fixed at 12 MPa.

5.4.2 Effects of components' Poisson's ratios on the nonlinear elastic properties of CAFNs

The effects of the Poisson's ratios of crosslinker and actin filament on the nonlinear elastic properties of crosslinked actin filament networks are studied by applying different values to the Poisson's ratios of crosslinker and actin filament when performing numerical simulations. For simplicity, the Poisson's ratios of crosslinker and actin filament are assumed to be the same in simulations. When the Poisson's ratios of crosslinker and actin filament are decreased from 0.49 to -0.9, the shear stress of crosslinked actin filament networks increase slightly (Figure 5.5 (a)). According to the shear stress strain relationship of crosslinked actin filament networks, the tangent modulus of the crosslinked actin filament networks can be obtained and shown as Figure 5.5 (b). It is easy to find that the tangent modulus of the crosslinked actin filament networks also increases slightly when the

Poisson's ratios of crosslinker and actin filament are decreased. This indicates that the Poisson's ratios of the components have slight influences on the nonlinear elastic properties of CAFNs when they are in the range of -0.9 to 0.49. The changes of the nonlinear elastic properties of crosslinked actin filament networks caused by the variation of the Poisson's ratios of crosslinker and actin filament can be attributed to the increases of the shear moduli of crosslinkers and actin filaments.

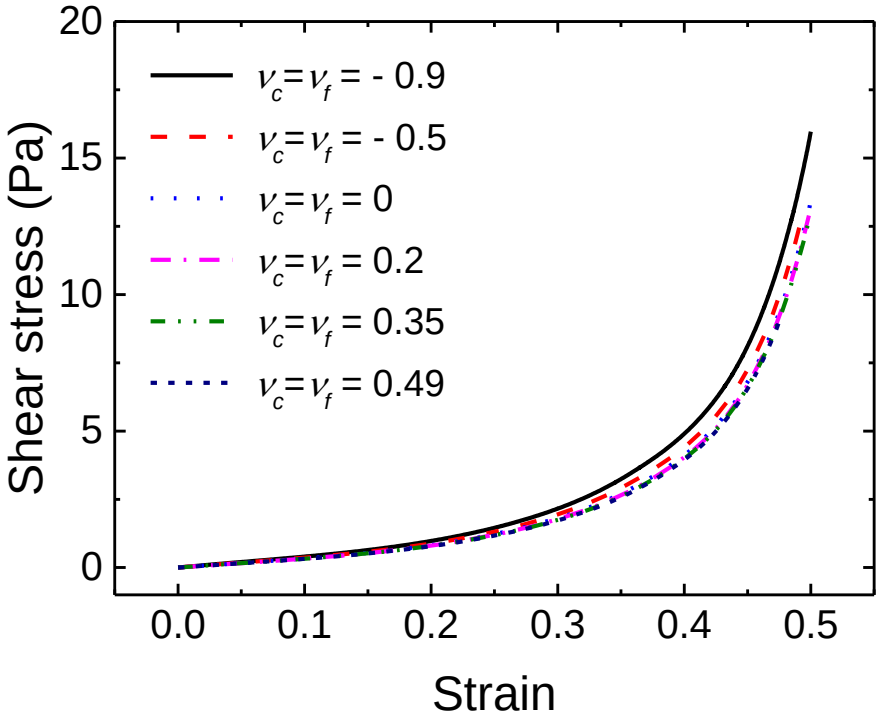

(a)

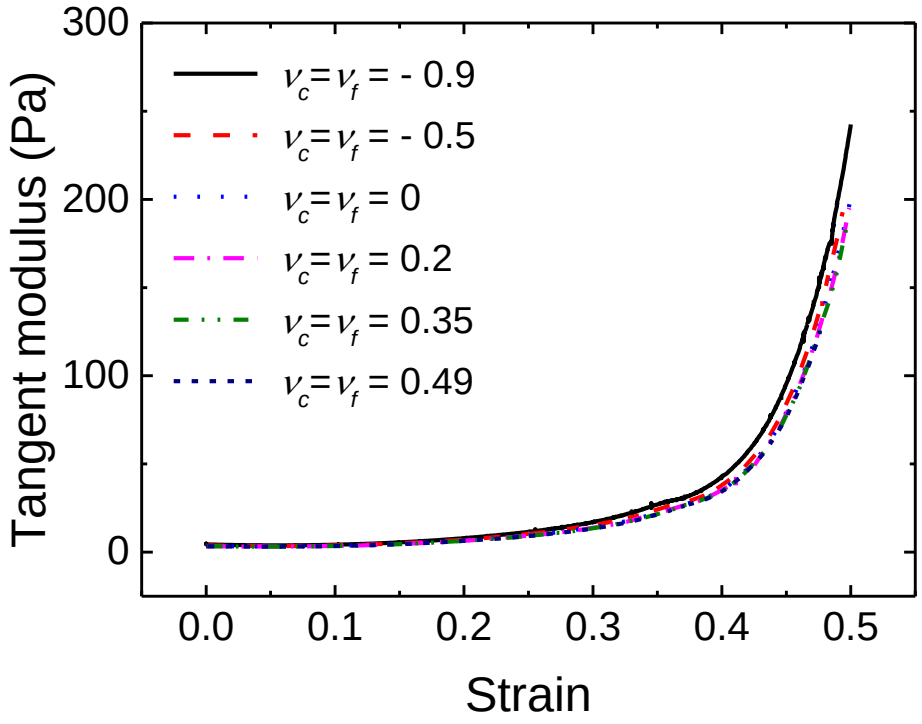

(b)

Figure 5.5. Dependence of the shear stress strain relationship (a) and tangent modulus (b) of CAFNs on the Poisson's ratios of actin filament and FLNA, where V_f=0.3%, ρ_c=1.2 μm^{-1}.

5.5 The negative normal stress of CAFNs

When shear deformations are applied to materials, most of them are reported to expand in the direction perpendicular to the applied shear strain [164]. This could result in the positive normal stress in the direction perpendicular to the applied shear strain. However, crosslinked biopolymer networks are reported to exhibit opposite trend during which the normal stresses are negative. Due to the strain stiffening behaviour of the crosslinked biopolymer networks, the normal stresses of crosslinked biopolymer networks, σ_n, could be as large as the shear stresses. Thus, it is important to study the negative normal stress of crosslinked actin filament networks. In this section, the shear stress and normal stress of crosslinked actin filament networks are obtained by performing numerical simulations on the three-dimensional model developed in Chapter 3. A network

model with the actin filament volume fraction being 0.3% and the crosslinking density being 1.2 is used to conduct simulations in this section and the results are shown is Figure 5.6. According to the simulation results, the shear stress of the crosslinked actin filament networks increases nonlinearly with the applied shear strain. The normal stress of the crosslinked actin filament networks is negative, and its absolute value increase gradually with the applied shear strain. The absolute value of the normal stress is comparable with the value of the shear stress of crosslinked actin filament networks. This indicates that the normal stress is important in the deformation of the crosslinked actin filament networks.

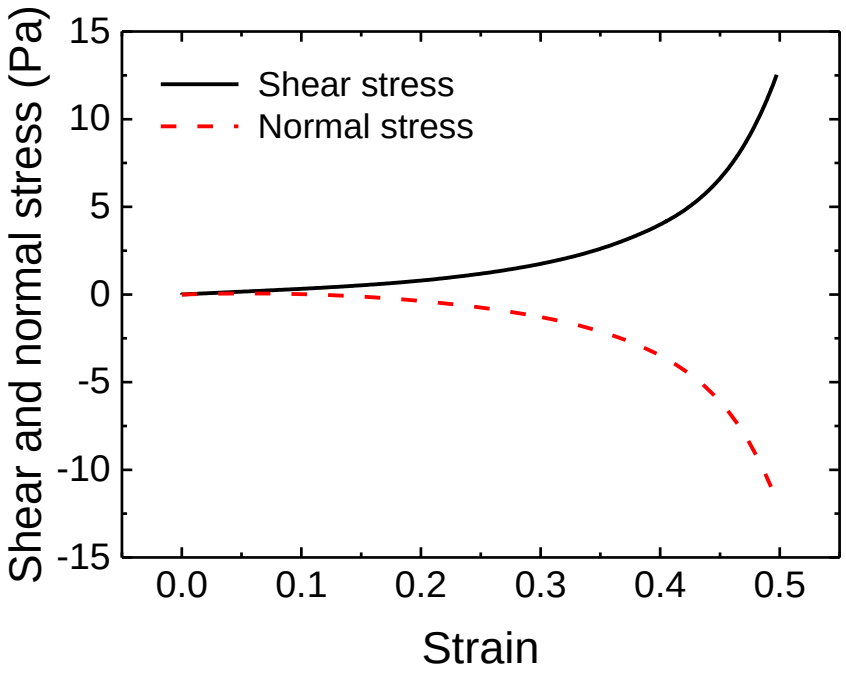

Figure 5.6. The shear (solid black curve) and normal (dash red curve) stresses of CAFNs as the strain is gradually increased, where V_f=0.3%, ρ_c=1.2 μm^{-1}.

The effects of the Young's moduli and Poisson's ratios of actin filaments and crosslinkers on the normal stress of crosslinked actin filament networks are also studied in this section, and the results are displayed in Figure 5.7 and Figure 5.8 respectively. According to Figure 5.7 (a), the influences of the Young's modulus of crosslinker on the normal stress of crosslinked actin filament networks can be revealed by changing the material properties (i.e., Young's modulus) of crosslinker in numerical simulations. When increasing the Young's modulus of crosslinker, the absolute value of the negative normal stress increases nonlinearly. The Young's

modulus of actin filament has similar effects on the normal stress of crosslinked actin filament networks as the Young's modulus of crosslinker has. However, the absolute value of the normal stress of the crosslinked actin filament networks changes more when changing the Young's modulus of crosslinker compared with changing the Young's modulus of actin filament. This indicates that the crosslinkers play a more crucial role in affecting the normal stress of crosslinked actin filament networks compared with actin filaments.

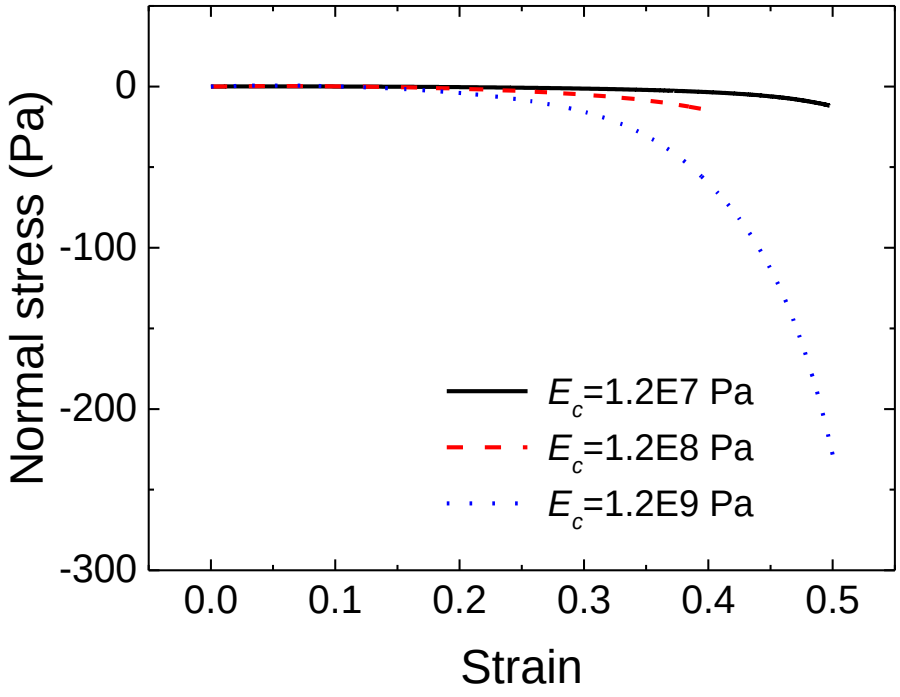

(a)

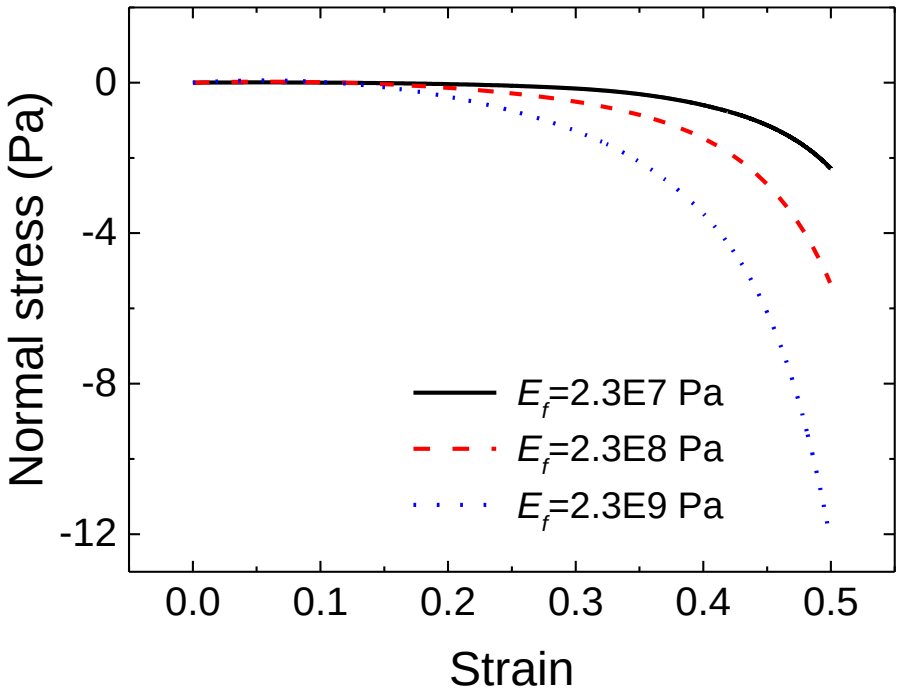

(b)

Figure 5.7. Dependence of the normal stress of CAFNs on the Young's modulus of FLNA (a) and actin filament (b), where V_f=0.3%, ρ_c=1.2 μm^{-1}.

In addition, the effects of the Poisson's ratios of crosslinker and actin filament on the normal stress of crosslinked actin filament networks are also studied (Figure 5.8). When conducting numerical simulations, the Poisson's ratios of crosslinker and actin filament are simply assumed to be the same. By changing the Poisson's ratios of crosslinker and actin filament from -0.9 to 0.49, the absolute values of the normal stress of crosslinked actin filament networks just has a small change. This indicates that the Poisson's ratios of crosslinker and actin filament have small influences on the normal stress of crosslinked actin filament networks. It is interesting that the absolute value of the normal stress of crosslinked actin filament networks increases when the Poisson's ratios of crosslinker and actin filament are decreased. It is easy to find that decreasing the Poisson's ratios can result in the increase of the shear moduli of materials, which can further lead to the increase of the torsional stiffness of crosslinker and actin filament. The stiffnesses of the crosslinked actin filament networks are also enhanced because of the increase of the torsional stiffnesses of the components, which can well explain the increase of the absolute value of the normal stress.

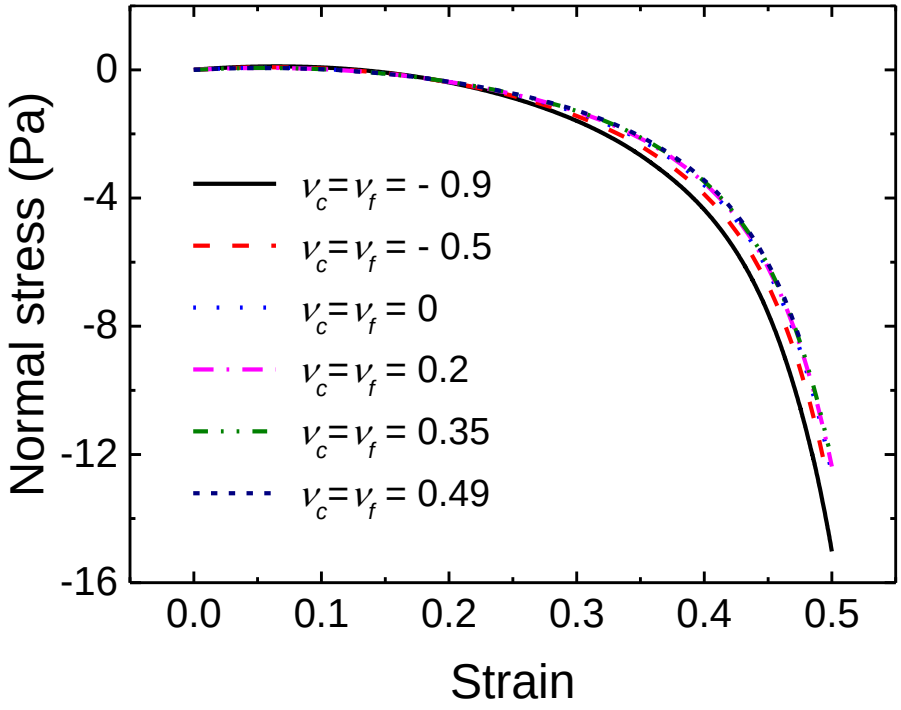

Figure 5.8. Dependence of the normal stress of CAFNs on the Poisson's ratios of actin filament and FLNA, where V_f=0.3%, ρ_c=1.2 μm^{-1}.

5.6 Deformation mechanism in large strain regime

In physiological conditions, living cells can bear large deformations in response to external and internal mechanical signals. When applying large strains to the crosslinked actin filament networks, they exhibit nonlinear mechanical responses which play an important role in various cell functions. Thus, the deformation mechanisms of crosslinked actin filament networks in large strain regime are worth to be studied. The deformation mechanisms of crosslinked actin filament networks in small strain regime are discussed in Chapter 4, however, the deformation mechanisms of crosslinked actin filament networks in large strain regime are not known very well. In this section, the deformations of crosslinkers and actin filaments are split into three main parts (i.e., bending, torsion and tension), and their effects on the stress-strain relationships and tangent modulus of crosslinked

actin filament networks are investigated separately by conducting numerical simulations.

5.6.1 Effects of components' bending stiffness on the stress strain relationship of CAFNs

When constructing the numerical simulations, both actin filaments and crosslinkers are modelled by deformable elastic beams with large aspect ratio. The bending deformation of beams with large aspect ratio is proved to take a considerable part of the total deformation in small strain regime. However, its role in large strain regime remains unclear. In this part, the effects of the bending stiffnesses of crosslinkers and actin filaments on the nonlinear elastic properties of crosslinked actin filament networks are studied respectively. In this research, κ_c and κ_f are defined as the bending stiffnesses of crosslinkers and actin filaments respectively:

$$\begin{cases} k_c = E_c I_c / (0.5 L_c)^3 \\ k_f = E_f I_f / L_f^3 \end{cases}, \tag{5.1}$$

where I_c and I_f are the area moments of inertia of the cross-sections of crosslinker and actin filament respectively. In addition, κ_{c0} and κ_{f0} are defined as the bending stiffnesses of crosslinker and actin filament in normal conditions (i.e., the material properties of crosslinker and actin filament are chosen from Table 3.1) respectively. By simultaneously tuning the values of Young's moduli, Poisson's ratios and radius of crosslinker and actin filament, the bending stiffnesses of crosslinker and actin filament can be changed with the torsional stiffnesses and tensile stiffnesses of crosslinker and actin filament being fixed at constant values. For example, when increasing the Young's modulus by two orders of magnitude and decreasing the radius by one order of magnitude, the bending stiffness decreases by two orders of magnitude, however, the tensile stiffness doesn't change. Then, increasing the value of $1/(1+\nu)$ by two orders of magnitude can make the torsional stiffness to be constant. In this way, only the bending stiffness is changed, and the effects of bending stiffness on the deformation of CAFNs can be obtained.

During the simulations, the bending stiffnesses of crosslinkers, κ_c, or actin filaments, κ_f, is decreased by one order with the torsional stiffnesses and tensile stiffnesses of crosslinkers and actin filaments being fixed. The stress-strain curves and tangent moduli of crosslinked actin filament networks at different levels of κ_c and κ_f are obtained and displayed in Figure 5.9 and Figure 5.10 respectively. According to the simulation results, both the bending stiffness of crosslinker and the bending stiffness of actin filament can affect the nonlinear elastic properties of crosslinked actin filament networks. In the range of strain studied in this research (i.e., 0 to 0.5), the bending of crosslinkers is proved to play a more important role in the nonlinear elastic properties of CAFNs compared with the bending of actin filament. This indicates that both the bending of crosslinkers and the bending of actin filaments contribute to the nonlinear deformation of the crosslinked actin filament networks.

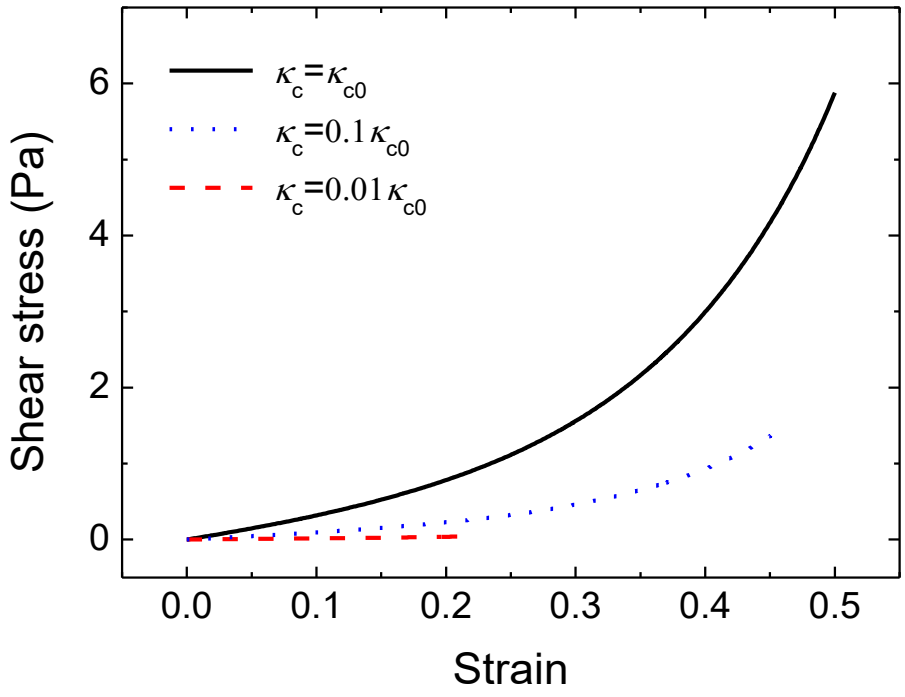

(a)

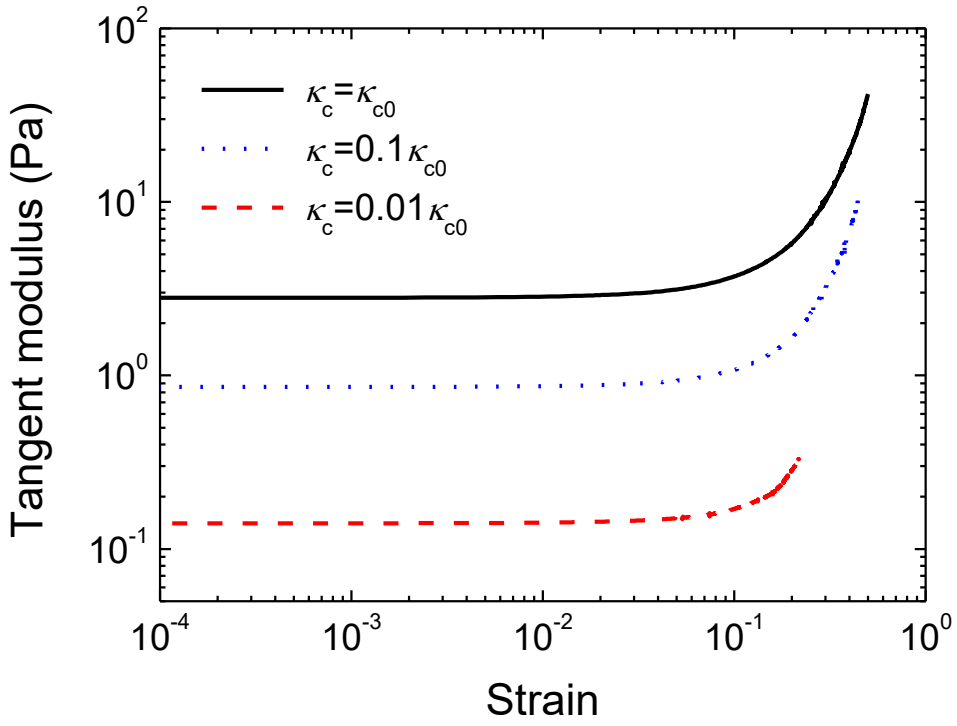

(b)

Figure 5.9. (a) The effects of the bending stiffness of crosslinkers on the stress strain relationship of crosslinked actin filament networks. (b) The effects of the bending stiffness of crosslinkers on the tangent modulus of crosslinked actin filament networks. Where V_f=0.3%, ρ_c=1.2 μm^{-1}.

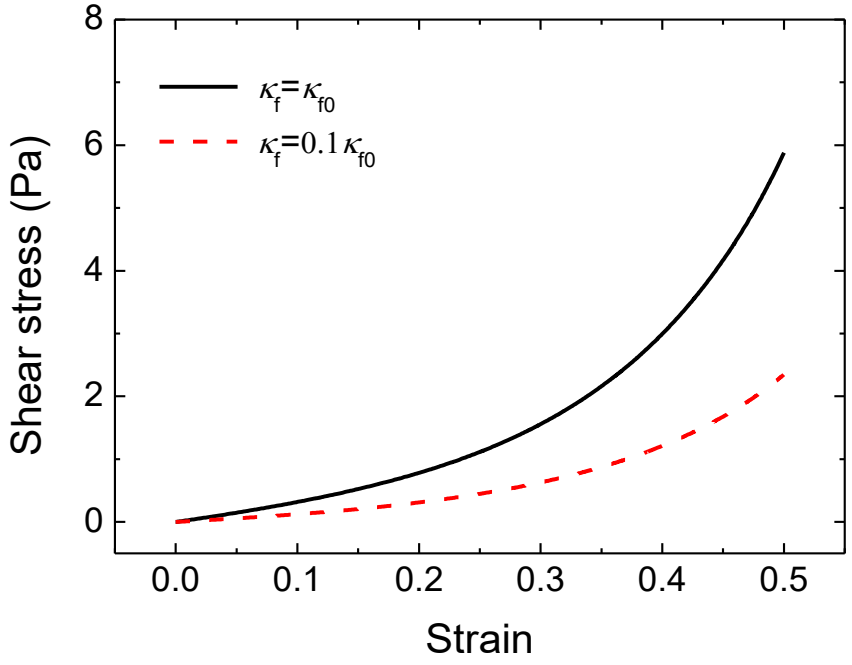

(a)

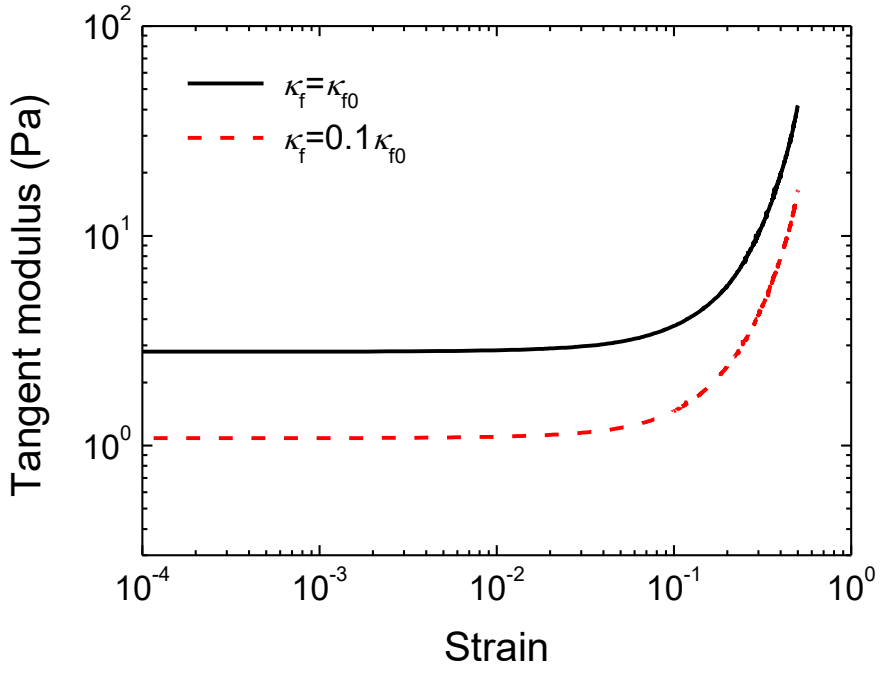

(b)

Figure 5.10. (a) The effects of the bending stiffness of actin filament on the stress strain relationship of crosslinked actin filament networks. (b) The effects of the bending stiffness of actin filament on the tangent modulus of crosslinked actin filament networks. Where V_f=0.3%, ρ_c=1.2 μm^{-1}.

5.6.2 Effects of components' torsional stiffness on the stress strain relationship of CAFNs

In addition to the bending of crosslinkers and the bending actin filaments, the torsion of crosslinker and the torsion of actin filament also contribute to the deformation of crosslinked actin filament networks. In this research, λ_c and λ_f are defined as the torsional stiffnesses of crosslinkers and actin filaments respectively:

$$\begin{cases} \lambda_c = G_c I_{Pc} \\ \lambda_f = G_f I_{Pf} \end{cases}, \tag{5.2}$$

where I_{Pc} and I_{Pf} are the polar moments of inertia of the cross-sectional areas of crosslinker and actin filament respectively. In addition, λ_{c0} *and* λ_{f0} are defined as

the torsional stiffnesses of crosslinker and actin filament in normal conditions (i.e., the material properties of crosslinker and actin filament are chosen from Table 3.1) respectively. By simultaneously tuning the values of Young's moduli, Poisson's ratios and radius of crosslinker and actin filament, the torsional stiffnesses of crosslinker and actin filament can be changed with the bending stiffnesses and tensile stiffnesses of crosslinker and actin filament being fixed at constant values.

The effects of the torsional stiffness of crosslinkers, λ_c, and the torsional stiffness of actin filaments, λ_f, on the nonlinear elastic properties of crosslinked actin filament networks are studied respectively by conducting numerical simulations. During the FEM simulations, the torsional stiffnesses of crosslinkers and actin filaments are varied with their bending stiffnesses and tensile stiffnesses being fixed. The stress-strain curves and tangent moduli of crosslinked actin filament networks are obtained from numerical simulations and are displayed in Figure 5.11 and Figure 5.12.

According to Figure 5.11, when increasing the torsional stiffness of crosslinkers by one order of magnitude, the shear stress of the crosslinked actin filament networks increase about 30%. However, when the torsional stiffness of crosslinkers is continuously increased by one order of magnitude, the shear stress of the crosslinked actin filament networks just increase a little. The torsional stiffness of crosslinkers has similar effects on the tangent modulus of crosslinked actin filament networks. This indicates that the torsional stiffness of crosslinkers plays a considerable role in the nonlinear elastic properties of crosslinked actin filament networks.

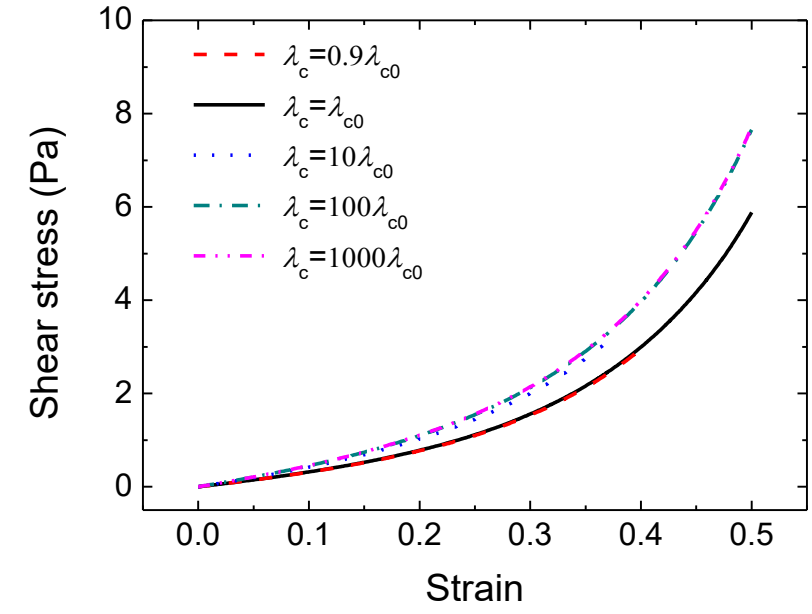

(a)

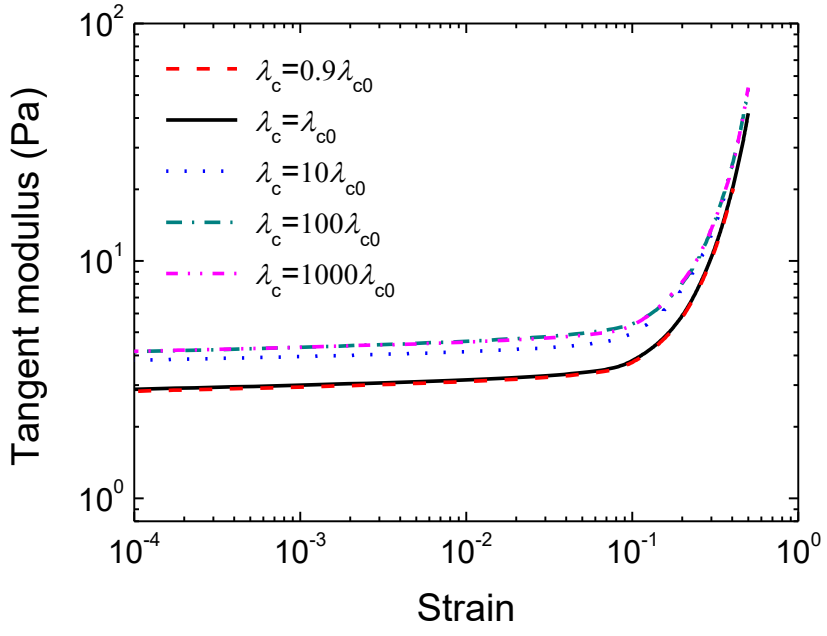

(b)

Figure 5.11. (a) The effects of the torsional stiffness of crosslinkers on the stress strain relationship of crosslinked actin filament networks. (b) The effects of the torsional stiffness of crosslinkers on the tangent modulus of crosslinked actin filament networks. Where V_f=0.3%, ρ_c=1.2 μm^{-1}.

The effects of the torsional stiffness of actin filaments on the nonlinear elastic properties are studied separately by fixing the bending stiffness and tensile

stiffness of actin filaments at normal condition. When the torsional stiffness of actin filaments is increased by one order of magnitude, the shear stress and tangent modulus of crosslinked actin filament networks almost do not change. This demonstrates that the nonlinear elastic properties of crosslinked actin filament networks are not sensitive to the torsional stiffness of actin filaments.

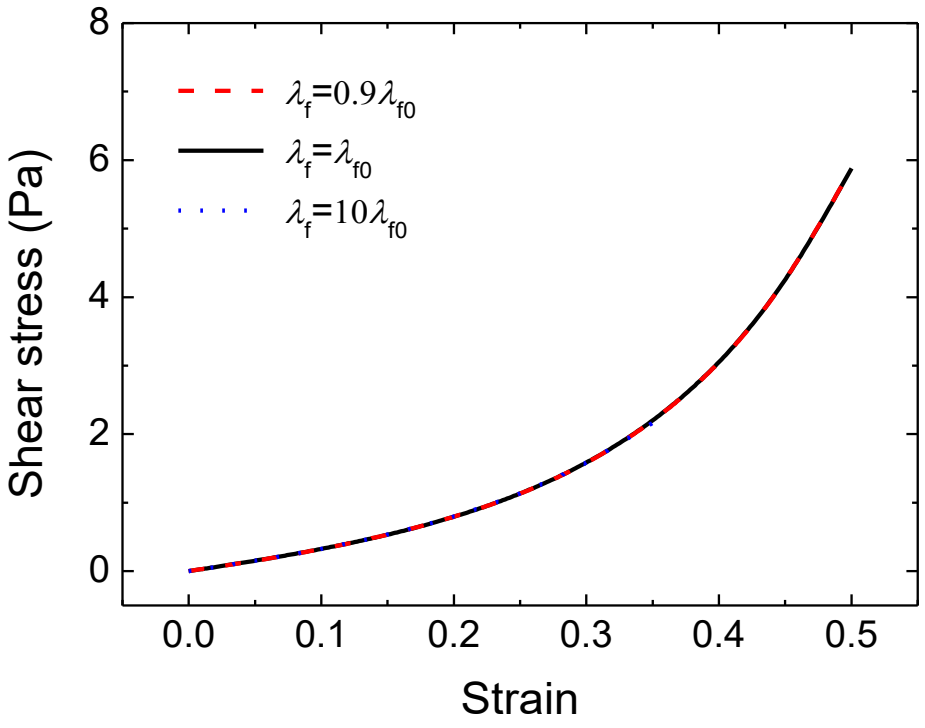

(a)

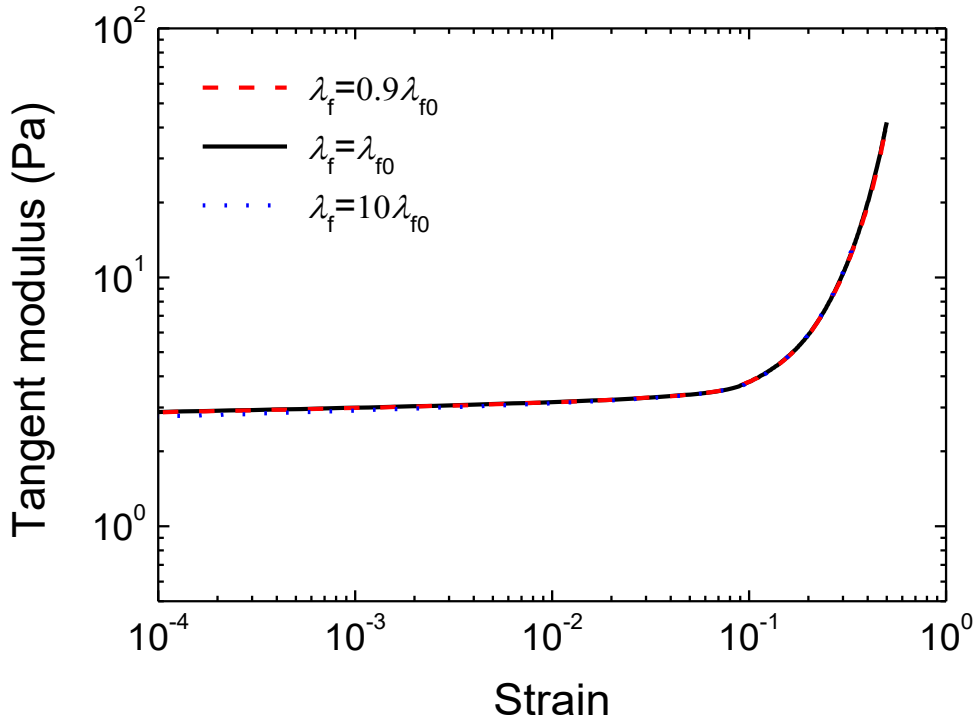

(b)

Figure 5.12. (a) The effects of the torsional stiffness of actin filament on the stress strain relationship of crosslinked actin filament networks. (b) The effects of the torsional stiffness of actin filament on the tangent modulus of crosslinked actin filament networks. Where V_f=0.3%, ρ_c=1.2 μm^{-1}.

5.6.3 Effects of components' tensile stiffness on the stress strain relationship of CAFNs

In large strain regime, the stretching of crosslinkers and actin filaments cannot be ignored. In this research, μ_c *and* μ_f are defined as the tensile stiffnesses of crosslinkers and actin filaments respectively:

$$\begin{cases} \mu_c = E_c A_c \\ \mu_f = E_f A_f \end{cases}, \tag{5.3}$$

where A_c and A_f are the cross-sectional areas of crosslinker and actin filament respectively. In addition, μ_{c0} *and* μ_{f0} are defined as the tensile stiffnesses of crosslinker and actin filament in normal conditions (i.e., the material properties of

crosslinker and actin filament are chosen from Table 3.1) respectively. By simultaneously tuning the values of Young's moduli, Poisson's ratios and radius of crosslinker and actin filament, the tensile stiffnesses of crosslinker and actin filament can be changed with the bending stiffnesses and torsional stiffnesses of crosslinker and actin filament being fixed at constant values.

Thus, the effects of the axial tensile stiffnesses of crosslinkers, μ_c, and actin filaments, μ_f, on the nonlinear elastic properties of crosslinked actin filament networks are studied by change their values in simulations, and results are shown in Figure 5.13 and Figure 5.14. For example, when investigating the influences of the tensile stiffness of crosslinkers, μ_c, on the nonlinear elastic properties of crosslinked actin filament networks, μ_c is increased or decreased by one order of magnitude with the bending stiffness and torsional stiffness of crosslinkers being fixed. Thus, the effects of the tensile stiffness of crosslinkers on the nonlinear elastic properties of CAFNs can be split. According to the simulation results shown in Figure 5.13, decreasing the tensile stiffness of crosslinkers can result in the decrease of the shear stress and tangent modulus of crosslinked actin filament networks. However, in the range of applied strain studied in this research (i.e., 0 to 0.5), the shear stress and tangent modulus of crosslinked actin filament networks almost do not change when the tensile stiffness of crosslinkers is increased by one order or two orders of magnitude.

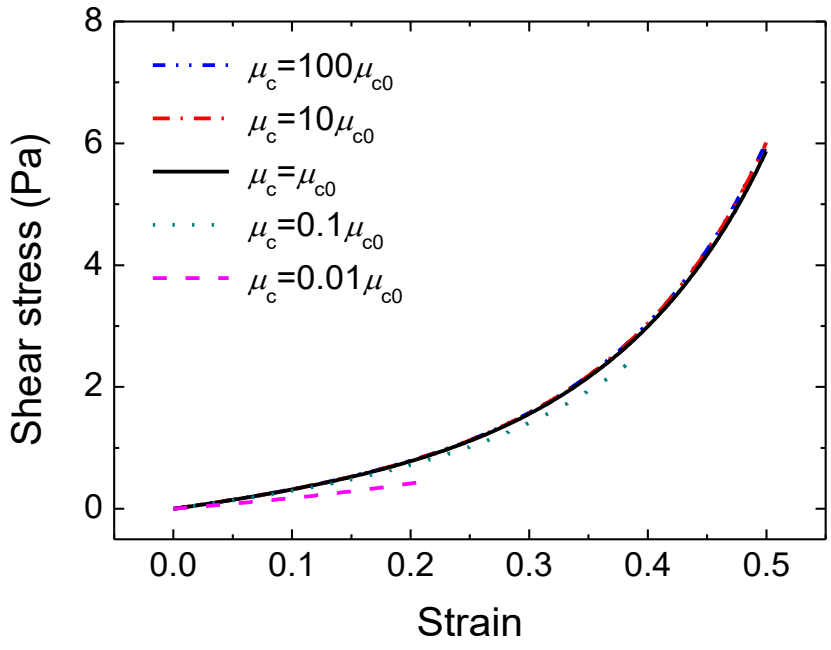

(a)

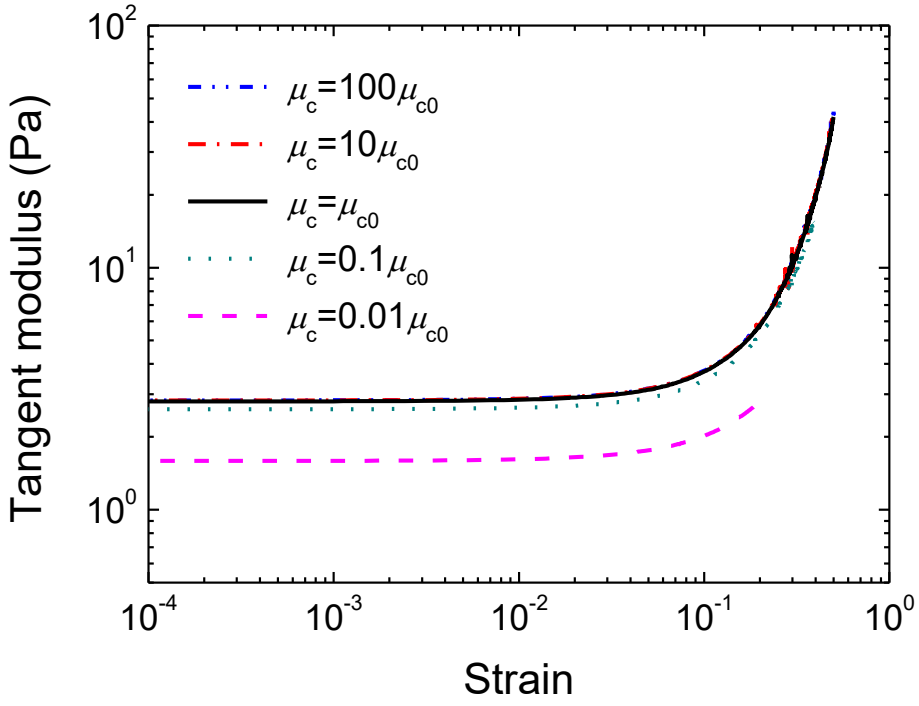

(b)

Figure 5.13. (a) The effects of the tensile stiffness of crosslinkers on the stress strain relationship of crosslinked actin filament networks. (b) The effects of the tensile stiffness of crosslinkers on the tangent modulus of crosslinked actin filament networks. Where V_f=0.3%, ρ_c=1.2 μm^{-1}.

Similarly, the effects of the tensile stiffness of actin filaments, μ_c, on the nonlinear elastic properties of crosslinked actin filament networks are also studied by performing numerical simulations. However, when decreasing the tensile stiffness of actin filaments by one order or two orders of magnitude, the shear stress and tangent modulus of crosslinked actin filament networks almost do not change. Due to the convergence of the simulations, the situations of increasing the tensile stiffness of actin filaments are not obtained.

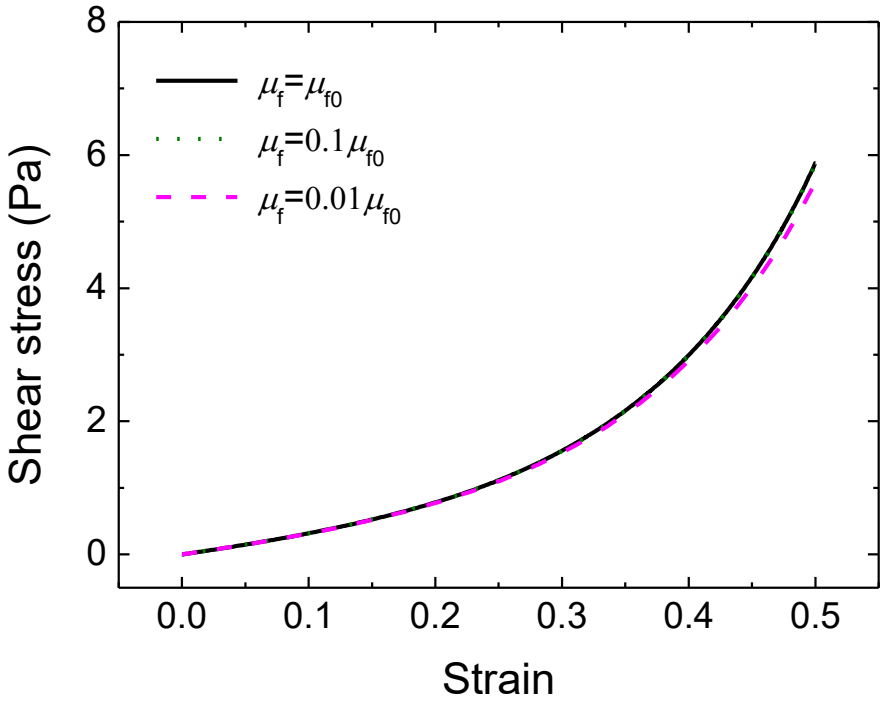

(a)

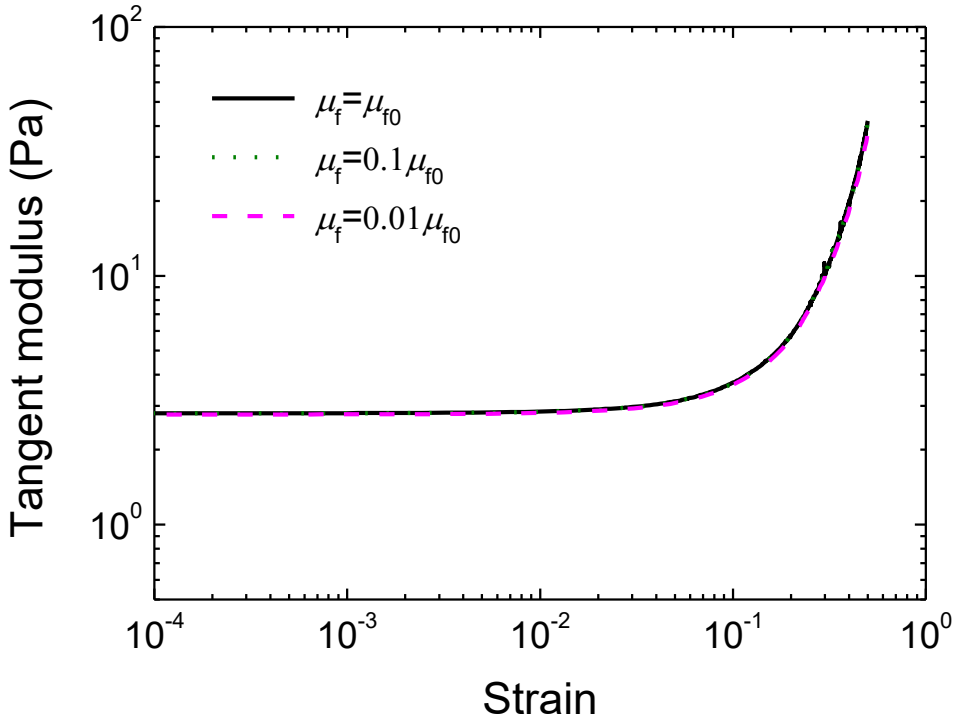

(b)

Figure 5.14. (a) The effects of the tensile stiffness of actin filament on the stress strain relationship of crosslinked actin filament networks. (b) The effects of the tensile stiffness of actin filament on the tangent modulus of crosslinked actin filament networks. Where V_f=0.3%, ρ_c=1.2 μm^{-1}.

In summary, in the range of applied strain studied in this research (i.e., 0 to 0.5), the bending, torsion and tension of crosslinkers are proved to make considerable contribution to the deformation of crosslinked actin filament networks. However, for actin filaments, only the bending is proved to contribute to the deformation of crosslinked actin filament networks. The nonlinear elastic properties of crosslinked actin filament networks seem not sensitive to the torsional stiffness and tensile stiffness of actin filaments at least in the range of applied strain studied in this research.

5.7 Conclusions

By conducting numerical simulations on the three-dimensional network model developed in Chapter 3, the nonlinear elastic properties of crosslinked biopolymer network systems are investigated systematically. The simulation results show that the nonlinear elastic properties of crosslinked actin filament networks can be greatly affected by the volume fraction of actin filaments and the crosslinking density. In addition, the physical properties (e.g., Young's modulus and Poisson's ratio) of components (i.e., actin filament and FLNA) can also influence the nonlinear elastic properties of CAFNs. In addition, the deformation mechanism of crosslinked actin filament networks in larger strain regime is studied by varying the bending stiffness, torsional stiffness and tensile stiffness of crosslinkers and actin filaments.

The influences of actin filament volume fraction and crosslinking density on the nonlinear elasticity (e.g., stress strain curve and tangent modulus) of the crosslinked actin filament network systems are studied by changing the parameters when conducting simulations. The simulation results show that the crosslinking density can greatly influence the stress strain curve and tangent modulus of the crosslinked actin filament networks. Larger crosslinking density can result in earlier appearance of the nonlinear elasticity and stronger stiffness, which indicates that the crosslinking density greatly enhances the stiffening behaviour of the crosslinked actin filament networks. The volume fraction of actin filaments has similar effects on the nonlinear elastic properties of the crosslinked

actin filament networks as crosslinking density does. The volume fraction of actin filaments can also enhance the stress strain relationship and tangent modulus of CAFNs obviously. These results provide valuable reference for studying the mechanical properties of biopolymer network systems and designing biological composite structures. For example, by varying the geometry parameters of the network, the mechanical properties of the network can be optimized to ideal state to meet the physiological requirements for distinct cell functions.

The influences of the physical properties of components on the nonlinear elasticity is studied by varying the Young's moduli and Poisson's ratios of crosslinkers (i.e., FLNA) and actin filaments. For the Young's modulus of crosslinker, three different levels of values (E_c=1.2 MPa, 12 MPa and 120 MPa) are applied to investigate its effects on the nonlinear elastic properties of crosslinked actin filament networks. According to the results obtained from simulations, it is easy to find that the trend of the stress strain relationship does not change when the Young's modulus of crosslink is improved by two orders of magnitude. And the trend of the differential shear modulus of the network has not been influenced by the increase of the Young's modulus of crosslink. However, the absolute values of the shear stress and tangent modulus of the crosslinked actin filament networks are enhanced when the Young's modulus of crosslinker is increased. This indicates that the Young's modulus of crosslinker can only influence the nonlinear elastic properties of the crosslinked actin filament networks in quantity. The Young's modulus of actin filament is proved to have similar influences on the nonlinear elastic properties of CAFNs as the crosslinkers have. The effects of the Poisson's ratios of crosslinkers and actin filaments on the nonlinear elastic properties are studied by varying the Poisson's ratios in the range of -0.9 to 0.49, and the simulation results indicate that the Poisson's ratios of the components just have slight influences on the nonlinear elastic properties of crosslinked actin filament networks.

The negative normal stress of the crosslinked actin filament networks is also obtained from the simulations, and the effects of the Young's moduli and Poisson's ratios of crosslinkers and actin filaments are discussed. According to the simulation results, both the Young's modulus of crosslinker and the Young's modulus of actin filament can greatly influence the negative normal stress of crosslinked actin filament networks. In addition, the Poisson's ratios of crosslinkers and actin filaments are also proved to affect the negative normal stress of crosslinked actin filament networks.

The deformation mechanism of the crosslinked actin filament networks in large strain regime is also studied in this Chapter. The effects of the bending stiffness, torsional stiffness and tensile stiffness of crosslinkers and actin filaments on the nonlinear elastic properties of crosslinked actin filament networks are investigated separately. The bending, torsion and tension of the crosslinkers are proved to contribute to the deformation of the crosslinked actin filament networks when large strains are applied. The bending of actin filaments is also proved to contribute to the deformation of the crosslinked actin filament networks, however, the contributions of the torsion and tension of actin filaments to the deformation of crosslinked actin filament networks are slight.

Chapter 6 Viscoelastic Properties of Crosslinked Actin Filament Networks

6.1 Introduction

Most of the biopolymer networks are viscoelastic and their mechanical properties are highly dependent on time and frequency. In living cells, the viscoelastic behaviour of crosslinked actin filament networks (CAFNs) could greatly affect the mechanical responses of cells, and different cell functions. Thus, it is important to study the viscoelasticity of CAFNs. FEM simulation is proved to be a highly efficient method to mimic both the architecture and physical properties of complex structural systems by constructing 3D models. In FEM simulations, it is possible to study the effects of some crucial factors (e.g., actin filament length, actin filament volume fraction, crosslinking density and physical properties of components) on the viscoelastic behaviours of CAFNs by tuning corresponding parameters. It is worth noting that some mechanical models such as Maxwell model, Kelvin model and Kelvin-Voigt model can also be used to mimic the viscoelastic responses of materials and structures, however, it is difficult to reveal the effects of some crucial factors (e.g., actin filament length, actin filament volume fraction, crosslinking density and physical properties of components) on the viscoelastic behaviours of CAFNs by using these mechanical models. Thus, the viscoelastic properties of actin filament (F-actin) networks crosslinked by filamin A (FLNA) are investigated by conducting FEM simulations on the three-dimensional (3D) finite element random network model in this chapter. Both creep and relaxation simulations are conducted on this model. In FEM simulations, different viscoelastic properties are applied to actin filament and FLNA respectively to probe their effects on the creep and relaxation behaviour of CAFNs. It is found that FLNA affect the viscoelastic behaviour of CAFNs greater than actin filament. In addition, the effects of applied stress on creep strain and the effects of applied strain on relaxation stress are studied respectively. Simulation results also show that

CAFNs with larger actin filament volume fraction creep less, however, larger actin filament volume fraction results in more relaxation in CAFNs. The creep strain and relaxation stress are found to reduce and increase with the actin filament volume fraction respectively. The crosslinking density is proved to have the similar effects on the creep and relaxation behaviour of CAFNs. In addition, the dependences of dynamic shear moduli of CAFNs on the frequency and amplitude of applied loads are investigated. Results indicate that the storage shear modulus develops a plateau at low-frequency conditions, and the loss shear modulus shows an increasing trend. At high-frequency conditions, both the storage and loss moduli scale with the frequency of applied loads. Moreover, the storage and loss shear moduli remain almost constant when the amplitude of applied load is small. However, they increase with the amplitude of applied load when the applied load reaches a critical value. The simulation results obtained in this research show good agreement with the experimental measurements and theoretical predictions.

In this Chapter, the details of material properties used in the finite element (FE) model are illustrated in Section 6.2. In Section 6.3, the creep behaviour of CAFNs is investigated by conducting numerical simulation on the model built in commercial finite element method software (ABAQUS). The effects of applied stress, actin filament volume fraction and crosslinking density on the creep behaviour of CAFNs are discussed. In Section 6.4, the relaxation behaviour of CAFNs is also studied by conducting numerical simulation. The influences of applied strain, actin filament volume fraction and crosslinking density on the relaxation behaviour of CAFNs are presented. In Section 6.5, the dynamic properties of CAFNs are obtained and compared with the experimental measurements and theoretical predictions. Conclusions are elaborated in Section 6.6.

6.2 Material properties

In ABAQUS, viscoelastic materials can be defined as linear viscoelastic or nonlinear viscoelastic. And the linear viscoelasticity can be defined as time domain viscoelasticity and frequency domain viscoelasticity. The time domain viscoelastic material model can be used only in conjunction with linear elastic behaviour or

hyperelastic behaviour to define the continuum elastic material properties. However, to the best of our knowledge, there is little rheological tests on a single actin filament or filamin until now. Though there are hyperelastic material models (e.g., Mooney-Rivlin model, Polynomial model, Neo-Hookean Model, Marlow model, Ogden model and Arruda-Boyce model) provided in ABAQUS to reflect the material nonlinearity of actin filament or crosslinker, they are not applied in this research in consideration of the lack of some crucial material parameters. In addition, according to the discussion on material defining in Chapter 5, both actin filament and crosslinker are assumed to be linear elastic. Thus, when studying the viscoelastic properties of CAFNs, the actin filament and crosslinker are assumed to be homogeneous isotropic and linear viscoelastic materials. And the material properties of actin filament and crosslinker are defined according to the normalized creep compliance of actin filament networks reported in literature [59] in conjunction with the elastic properties shown in Table 3.1. It is reported that the volume fraction of actin filament in 1 mg/ml actin gel is approximately 0.1% [165], which indicates that the mass and volume of actin filament in 1 ml gel are 1 mg and 0.001 ml respectively. Therefore, the density of actin filament is estimated to be 1 g/cm^3 in this research according to the above-mentioned actin filament volume fraction in actin gel. As there is little literature mentioning the density of FLNA, it is simply assumed that the density of FLNA is also 1 g/cm^3, which is the same with that of actin filament.

When studying the viscoelastic properties of CAFNs in this chapter, the actin filament and FLNA are regarded as viscoelastic materials in FEM simulations. The FE model used for simulation is introduced in Chapter 3. The geometry of the model as well as the elastic properties (i.e., Young's moduli and Poisson's ratios) of the components used in this chapter are the same as that introduced in Chapter 3. In ABAQUS, the viscoelastic properties of the components are also need to be defined. In ABAQUS, the components' viscoelastic properties are defined in this section.

To define the viscoelastic properties of actin filament and FLNA in simulation, the creep or relaxation test data of actin filament or FLNA are essential. Mechanical tests have been conducted on single actin filament [166] and single FLNA [132] to probe their material properties, however, no creep or relaxation tests have been carried out to obtain their viscoelastic properties. In this research, the creep test data of actin filament network [59, 134] are used to define the viscoelastic properties of actin filament and FLNA approximately during the FEM simulations.

In ABAQUS, the creep test data of viscoelastic materials are expressed by specifying the normalized shear compliances, $\overline{J(t)} = J(t)/J(0)$, which are displayed in Figure 6.1. The normalized creep compliances of actin filament ($J_F(t)/J_F(0)$) and FLNA ($J_C(t)/J_C(0)$) used in simulations are defined according to the normalized shear compliances shown in Figure 6.1.

In Figure 6.1, J_B refers to the normalized creep compliance of actin filament network obtained from literature [59], J_A and J_C are assumed according to J_B for comparison. When defining the viscoelastic properties of actin filament and FLNA, it can be assumed that the FLNA has the same or different normalized creep compliance with actin filament. The different combinations of normalized creep compliance for actin filament and FLNA are illustrated in Table 6.1. By applying different cases to the FEM simulations, the effects of FLNA and actin filament on the viscoelastic properties of CAFNs can be revealed.

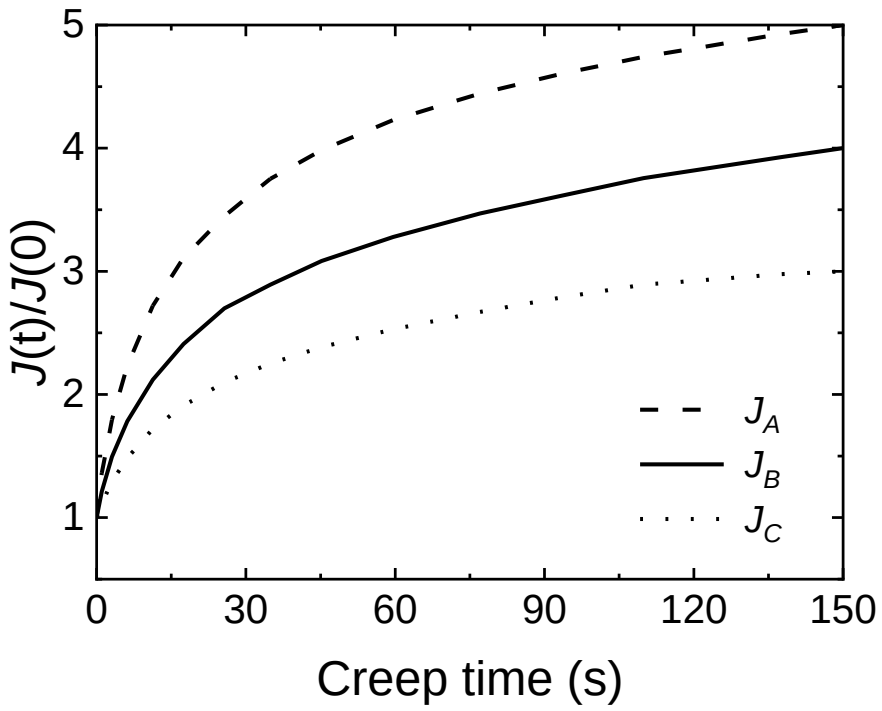

Figure 6.1. The normalized shear creep compliances used for defining the viscoelastic properties of actin filament and FLNA in FEM simulations. J_B is the normalized creep compliance of actin filament network obtained from literature [59], J_A and J_C are assumed according to J_B.

Table 6.1. The viscoelastic properties of actin filament and FLNA used for different cases in FEM simulations. J_A, J_B and J_C are illustrated in Figure 6.1. J_B refers to the normalized creep compliance of actin filament network obtained from literature [59], J_A and J_C are assumed according to J_B.

Case No.	$J_F(t)/J_F(0)$	$J_C(t)/J_C(0)$
1	J_B	J_A
2	J_B	J_B
3	J_B	J_C
4	J_A	J_B
5	J_C	J_B

6.3 Creep

Creep is an important mechanical behaviour of viscoelastic materials and structures, for example, it is reported that the crosslinked actin filament networks (CAFNs) show an obvious viscoelastic properties [30, 59, 136]. Gardel et al. experimentally applied a shear stress of 0.03 Pa to the in-vitro reconstituted FLNA-actin filament network to study its creep behaviour [59]. In our research, the creep tests on CAFNs are carried out by performing FEM simulations, and five different cases of viscoelastic material properties (i.e., Case 1, Case 2, Case 3, Case 4 and Case 5 elaborated in Table 6.1) are applied to the components.

When performing the creep simulations, a shear stress of 0.03 Pa is applied to CAFNs in a second, and is kept constant in the following time. By monitoring the corresponding shear strain, γ, over time, the creep curves of CAFNs can be obtained (Figure 6.2. a). It can be found that the five creep curves obtained from five different cases are almost identical. The creep compliances of CAFNs ($J(t)$) are deduced and then are normalized by their initial values ($J(0)$), and the normalized creep compliances of crosslinked actin filament networks and shown in Figure 6.2. (b). Gardel et al. [59] conduct creep tests on crosslinked actin filament networks with a stress-controlled rheometer by applying a constant stress

for 150 seconds and measuring the resultant strain over this time. According to Figure 6.2. (b), it can be seen that the normalized creep compliances obtained from FEM simulations in this research agree in general with the experimental measurements [59], which indicates that the RVE model developed in this research can well mimic the creep behaviour of CAFNs. However, there is a difference between creep curves obtained from simulation and experiments in quantity. This is due to the fact that the viscoelastic properties of actin filament and FLNA used in FEM simulations are not as accurate as the actual ones which have not been measured until now. Another reason is that it is difficult to perfectly match the conditions in simulations and in experiments, especially the crosslinking level. The molar ratio of FLNA dimer to actin monomer, R_F, in experiments corresponds to the total FLNA dimer that has been added in, but some of them may not connect with actin filaments. In contrast, all of the crosslinkers are active in simulations, i.e., every crosslinker has successfully connected with two distinct actin filaments to contribute to the mechanical responses of CAFNs. In addition, according to Figure 6.2. (b), it is easy to find that FLNA affects the normalized creep compliance of CAFNs more than actin filament.

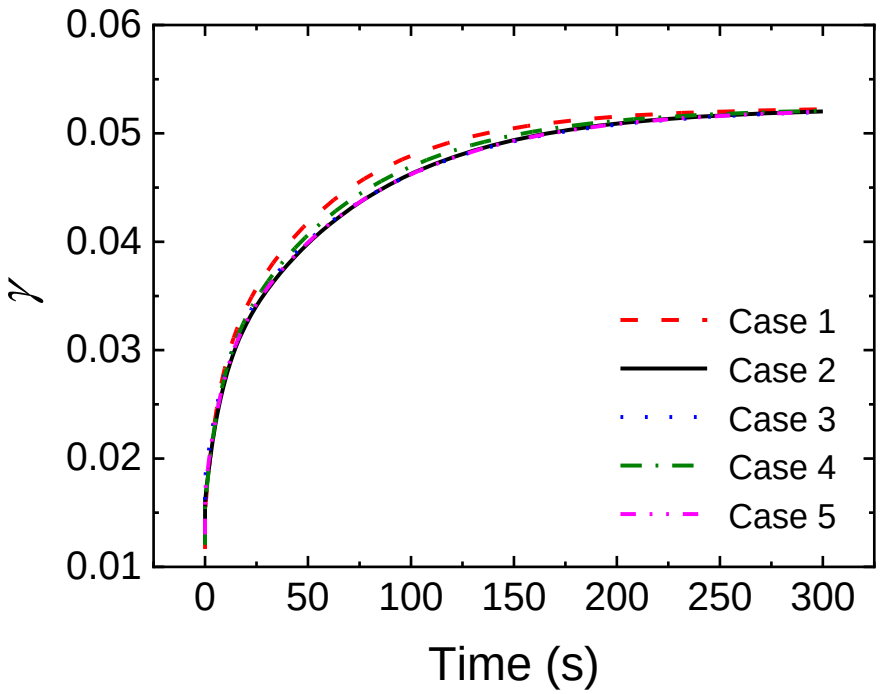

(a)

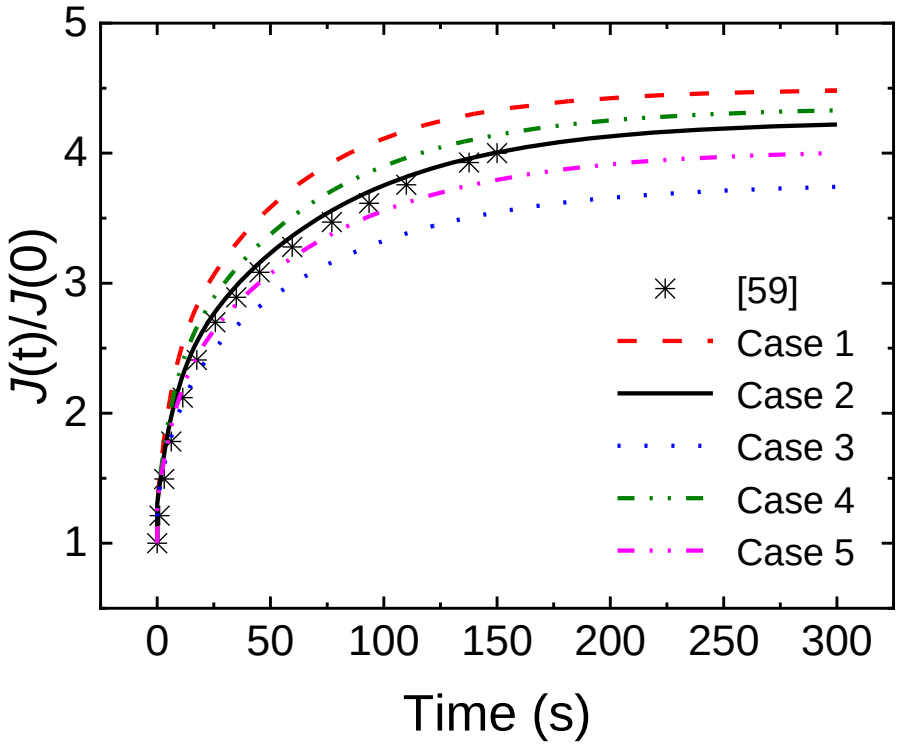

(b)

Figure 6.2. (a) The creep curves of crosslinked actin filament networks (CAFNs) obtained by performing FEM simulations with different cases of material combinations (i.e., five cases defined in Table 6.1) being applied. In FEM simulations, a constant shear stress, $\tau_0 = 0.03$ Pa is applied to CAFNs during the creep process. (b) The normalized creep compliances obtained from FEM simulations are compared with the experimentally measured results [59], where the creep compliances are normalized by their initial values. In FEM simulations, the volume fraction of actin filaments (V_f) is 0.2% and the crosslinking density (ρ_c) is 3.0 μm^{-1}.

6.3.1 Effects of applied stress on the creep behaviour of CAFNs

In physiological conditions, CAFNs exhibit different mechanical responses to different loads, however, little research has been conducted to investigate the effects of applied stress on the creep behaviour of CAFNs. In this part, five different levels of shear stresses (0.03 Pa, 0.06 Pa, 0.09 Pa, 0.12 Pa and 0.15 Pa),

τ, are applied when conducting FEM simulations. According to Figure 6.2. (a), the CAFNs have similar creep behaviours when different cases of viscoelastic properties are applied to the components of CAFNs. In this part, the viscoelastic properties of actin filament and FLNA are defined according to Case 2 (i.e., actin filament and FLNA have the same normalized creep compliance). Then, five creep curves are obtained from the simulation results and presented in Figure 6.3. In general, higher level of shear stress results in larger creep shear strain. However, the creep shear strain level does not increase linearly with the increase of applied shear stress. To further explore the effects of applied stress on the creep behaviour of CAFNs, the shear strains are isochronally displayed. Results show that the shear strains increase significantly with the applied shear stress at small stress stage, however, the slopes tend to decrease with the increase of the applied shear stress. The decrease of the slopes in Figure 6.3. (b) is due to the strain stiffening mechanism of CAFNs [90]. This indicates that the increase of applied stress plays a major role in the increase of creep shear strain level. And a nonlinear relationship between shear strain and applied shear stress is observed in the creep tests on CAFNs.

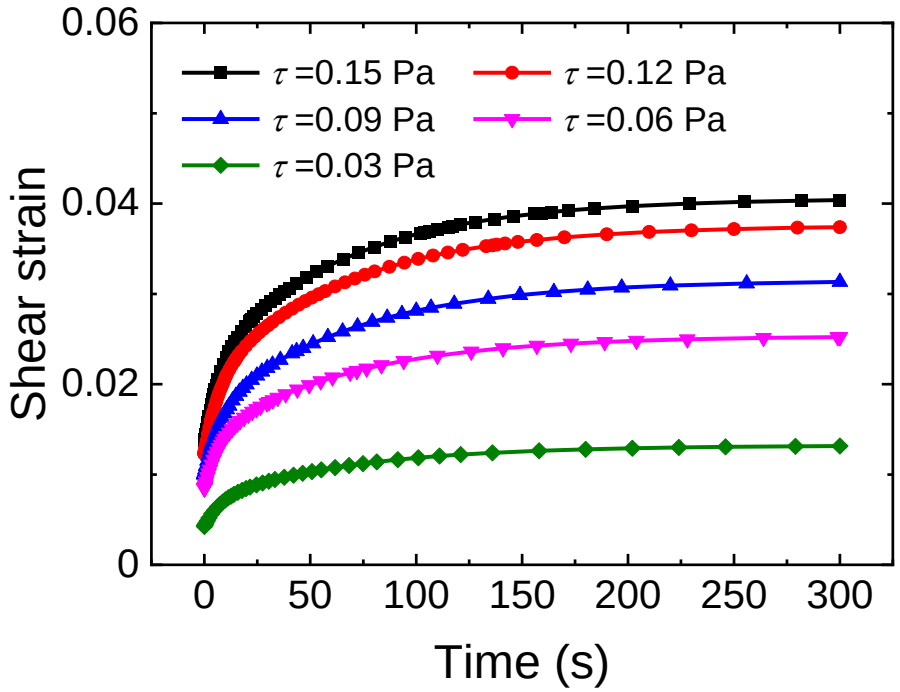

(a)

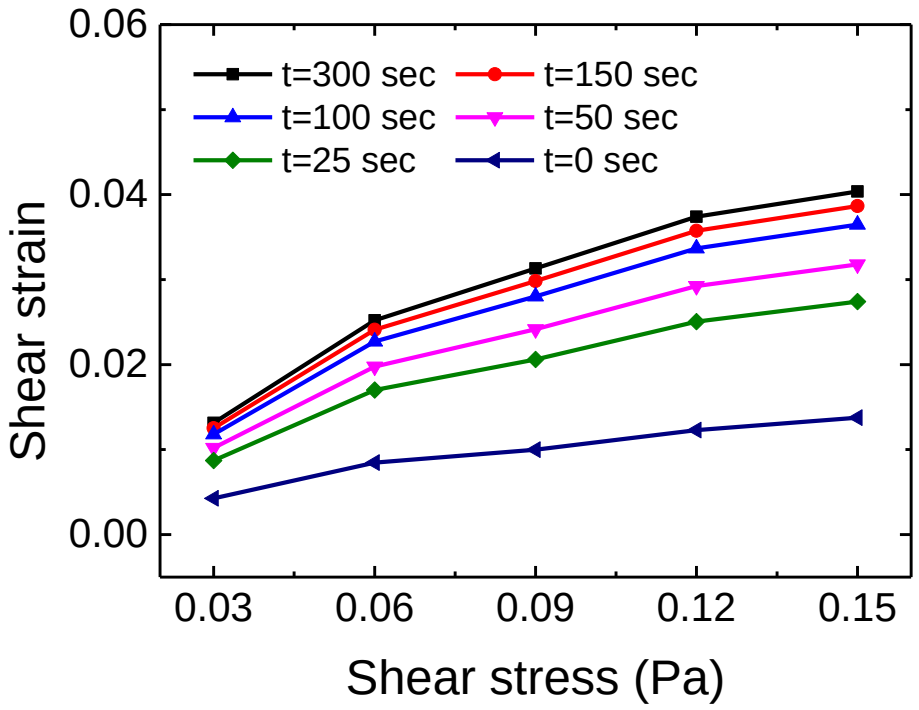

(b)

Figure 6.3. (a) The creep tests of CAFNs with various applied stresses. The volume fraction of actin filament is 0.3%, and the crosslinking density is 1.2 μm^{-1}. (b) The isochronal display of creep shear strain at specific time points as a function of applied shear stress.

6.3.2 Effects of actin filament volume fraction and crosslinking density on the creep behaviour of CAFNs

As an extremely complex network structure, the microstructure of CAFNs can no doubt affect its creep behaviour. Thus, the effects of actin filament volume fraction (V_f) and crosslinking density (ρ_c) on the creep behaviour of CAFNs are investigated by varying relevant parameters in FEM simulations. For simplicity, the viscoelastic properties of actin filament and FLNA are assumed to be the same (i.e., Case 2), and the shear stress is fixed at 0.03 Pa in creep simulations. Five levels of actin filament volume fraction (0.2%, 0.25%, 0.3%, 0.35% and 0.4%) are considered to study its effects on the creep behaviour of CAFNs with the crosslinking density being fixed at 1.2 μm^{-1} (Figure 6.4. (a)). The creep shear strain

data shown in Figure 6.4. (a) is comparable with the creep shear strain obtained in experiment [59]. When V_f is increased, the creep shear strain at a specific time decreases nonlinearly. To study the effects of crosslinking density (ρ_c) on the creep behaviour of CAFNs, five crosslinking density conditions (1.0, 1.5, 2.0, 2.5 and 3.0) are adopted (see Figure 6.4. b), and the volume fraction of actin filament (V_f) is fixed at 0.3%. Similarly, larger crosslinking density results in a lower creep strain level. This is because that increasing actin filament volume fraction (V_f) or crosslinking density (ρ_c) can enhance the stiffness of CAFNs, and stiffer CAFNs creep less when exposed to a specific stress level. This can well explain the reduction in creep strain level when V_f or ρ_c is increased.

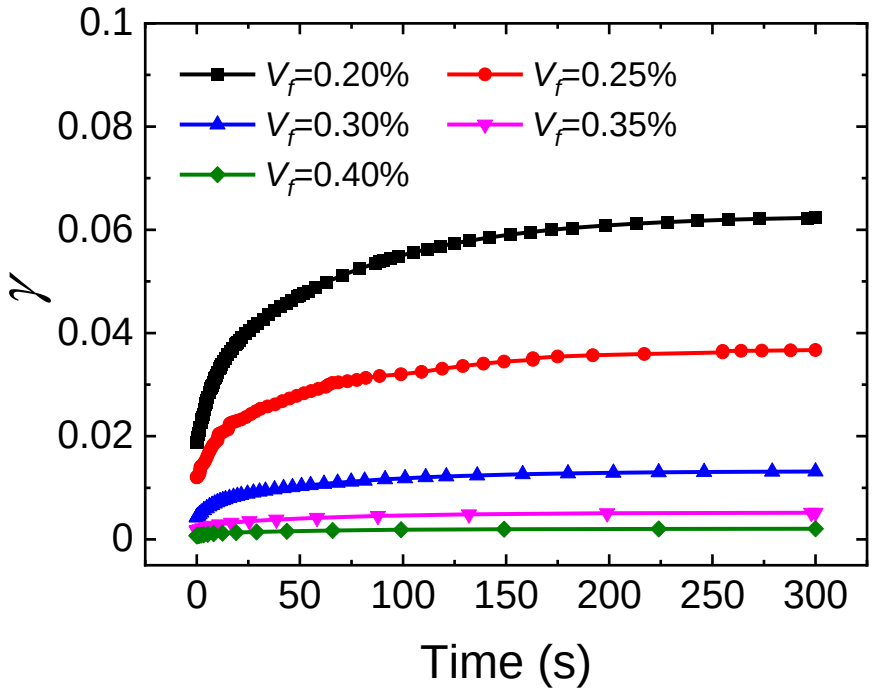

(a)

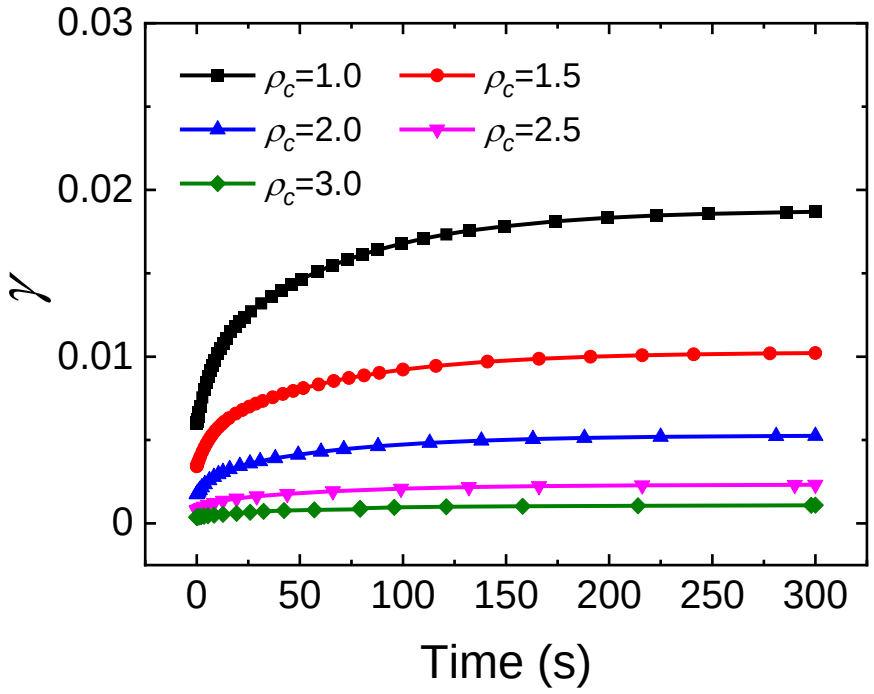

(b)

Figure 6.4. (a) Effects of actin filament volume fraction on the creep behaviour of CAFNs with the crosslinking density being 1.2 μm^{-1}. (b) Effects of crosslinking density on the creep behaviour of CAFNs with the volume fraction of actin filament being 0.3%.

6.4 Relaxation

Relaxation is another important rheological behaviour of viscoelastic materials and structures. In this part, the relaxation behaviour of CAFNs is studied by performing FEM simulations on RVE models with $V_f = 0.2\%$ and $\rho_c = 3.0$ μm^{-1} which are the same with that used in creep simulations in Figure 6.2. According to the creep test data displayed in Figure 6.2, a shear stress of 0.03 Pa results in an instantaneous shear strain of about 0.01 to 0.02. Therefore, in order to keep consistent with the stress level and strain level in creep test, the shear strain used in relaxation simulation is chosen to be 0.02. In stress relaxation simulations, five different cases of viscoelastic properties for actin filament and FLNA (i.e., five cases defined in Table 6.1) are adopted. Then a constant shear strain ($\gamma_0 = 0.02$) is

applied to CAFNs in a second, and the shear stress is measured over time (Figure 6.5.). It is easy to find that the relaxation shear stresses obtained from five different cases are almost identical except for the initial values. Results also show that the shear stress decreases fast in a relatively short time and then develops a steady stage during which the shear stress just decreases a little in a relatively long period. Humphrey et al. [135] perform bulk stress relaxation experiments on actin networks with a commercial fluid rheometer and measure the relaxation stress over time. In addition, Nam et al. [167] conduct stress relaxation experiments on collagen gels with an AR-G2 stress-controlled rheometer. In order to compare simulation results with experimental measurements and theoretical predictions, the stress relaxation data is normalized by the initial shear stress (i.e., the maximum shear stress after loading). The five cases of normalized relaxation stresses obtained from our simulations are almost identical and show good agreement with experimental measurements [167] and analytical results [95]. However, the normalized relaxation stress obtained from entangled actin filament solution [135] is obviously smaller than our simulation results in quantity. This is because that actin filaments in our model are crosslinked by actin binding proteins (i.e., FLNA), which is different from the microstructure of entangled actin filament solution. This indicates that the presence of crosslinkers plays a major role in the relaxation behaviour of CAFNs. It is worth noting that the FLNA has greater influences on the relaxation behaviour of CAFNs according to Figure 6.5. (b).

In this section, the influences of applied strain (γ_0), actin filament volume fraction (V_f) and crosslinking density (ρ_c) on the stress relaxation behaviour of CAFNs are investigated by conducting FEM simulations. As the relaxation simulation results corresponding to the five different cases just have little difference, FLNA and actin filament are simply assumed to have the same normalized creep compliance (i.e., Case 2) in this section.

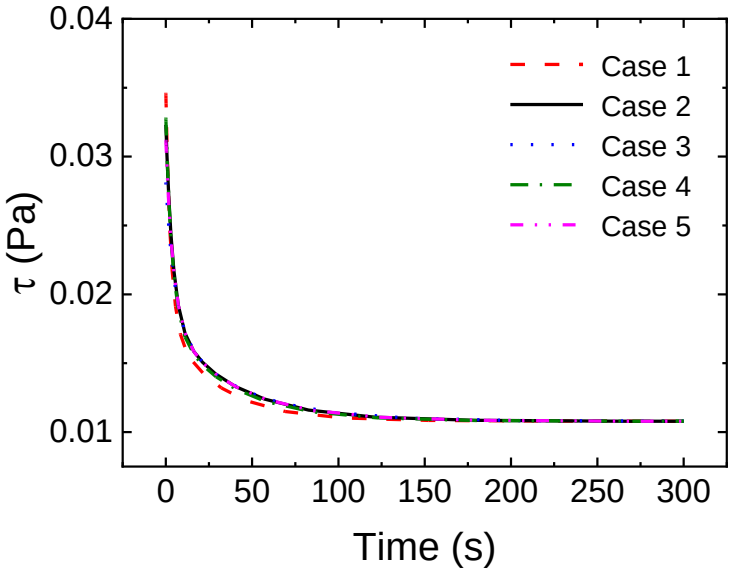

(a)

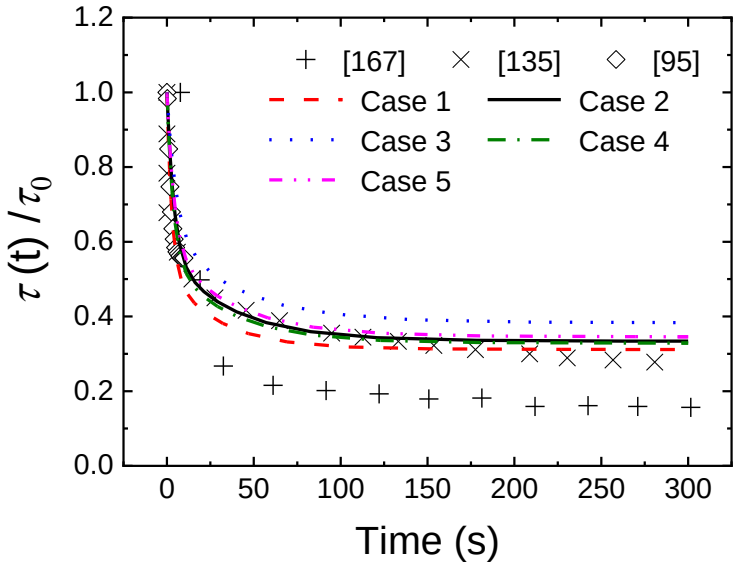

(b)

Figure 6.5. (a) The relaxation behaviour of crosslinked actin filament networks (CAFNs) obtained by performing FEM simulation with different cases of material combinations (i.e., five cases defined in Table 6.1) being applied. In FEM simulations, a constant shear strain, $\gamma_0 = 0.02$, is applied to CAFNs during the relaxation process. (b) The normalized relaxation stress of CAFNs in FEM simulation is compared with stress relaxation data of collagen gel [167], entangled actin filament solution [135] and theoretical predictions of cross-linked actin network [95]. In FEM simulations, the volume fraction of actin filament (V_f) is 0.2% and the crosslinking density (ρ_c) is 3.0 μm^{-1}.

6.4.1 Effects of applied strain on the relaxation behaviour of CAFNs

When different levels of shear strain are applied, the CAFNs show different relaxation behaviours. In order to reveal the implications of applied strain (γ_0) for the relaxation behaviour of CAFNs, seven levels of shear strain (0.02, 0.04, 0.06, 0.08, 0.10, 0.15 and 0.20) are applied to CAFNs ($V_f = 0.2\%$, $\rho_c = 3.0\ \mu m^{-1}$) in FEM simulations (Figure 6.6). Then, seven stress relaxation curves are obtained by measuring the relaxation shear stress over time. It is clear that the relaxation shear stress level of larger applied shear strain is higher than that of smaller applied shear strain, indicating that the relaxation shear stress of CAFNs is enhanced by the increase of applied shear strain. When the relaxation shear stresses in Figure 6.6. (a) are normalized by their initial shear stresses (the shear stresses at 0 second) respectively, they collapse onto one single curve as shown in Figure 6.6. (b), which indicates that the level of applied strain just influences the relaxation behaviour of CAFNs in quantity rather than in quality. When increasing the applied strain, the enhancement in the rate of stress relaxation observed by Nam et al. [167] is not found in our simulation. This is due to the fact that the unbinding between actin filament and FLNA is not taken into consideration in our model. The isochronal displays of relaxation shear stress and relaxation shear modulus (Figure 6.6. (c) and (d)) indicate that the relaxation shear stress and relaxation shear modulus increase nonlinearly over the applied shear strain, which is also observed in the relaxation of open-cell polymer foams [168]. This strain stiffening phenomenon observed in the relaxation behaviour of CAFNs is consistent with previous reports [90]. According to the isochronal displays of relaxation shear stress and relaxation shear modulus shown in Figure 6.6, the strain stiffening exists throughout the relaxation process and does not diminish during our FEM simulations. This difference between our simulation and Nam's experimental results is also because of the happening of the unbinding between actin filament and FLNA in living cells or reconstructed actin filament networks.

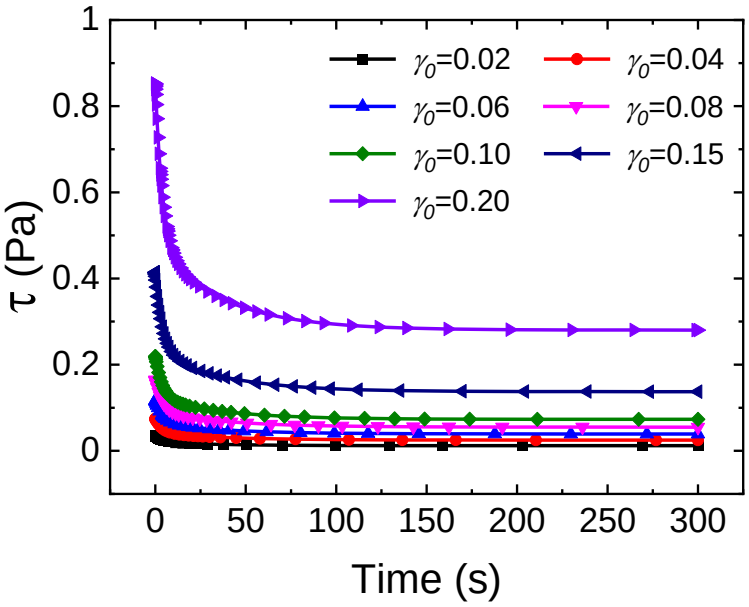
τ (Pa)
Time (s)
γ0=0.02
γ0=0.04
γ0=0.06
γ0=0.08
γ0=0.10
γ0=0.15
γ0=0.20

(a)

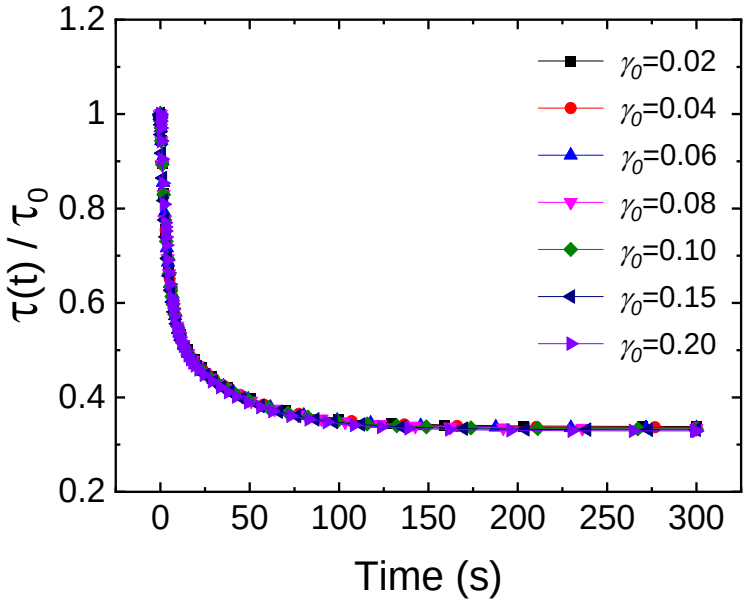
τ(t) / τ0
Time (s)
γ0=0.02
γ0=0.04
γ0=0.06
γ0=0.08
γ0=0.10
γ0=0.15
γ0=0.20

(b)

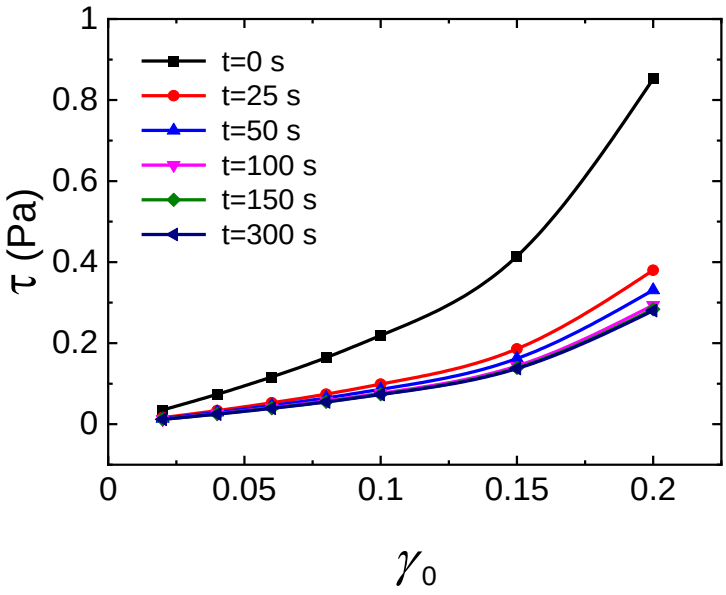

(c)

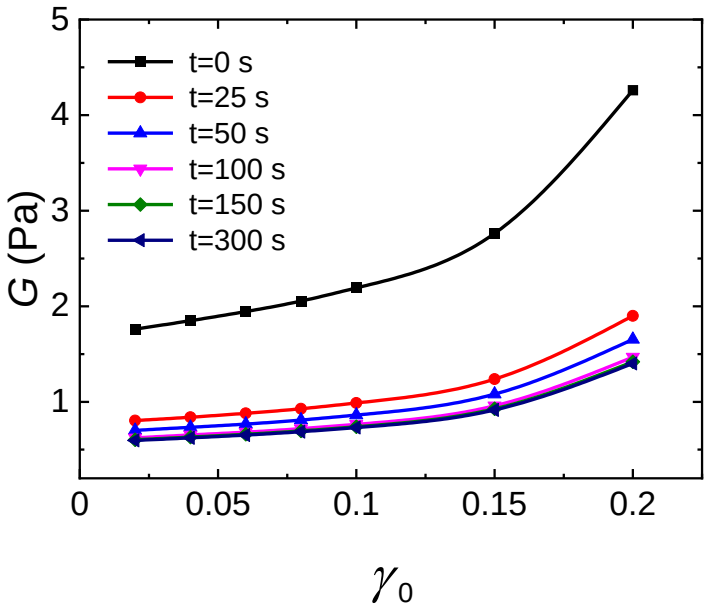

(d)

Figure 6.6. (a) The relaxation shear stress, $\tau(t, \gamma_0)$, of the crosslinked actin filament networks (CAFNs) is measured as a function of time for various applied strains (γ_0). The actin filament volume fraction, V_f, is 0.2%, and the crosslinking density, ρ_c, is 3.0 μm^{-1}. (b) Normalized relaxation shear stress of CAFNs at different applied strains. (c) The isochronal display of relaxation shear stress, $\tau(t, \gamma_0)$, at specific time points as a function of applied strain (γ_0). (d) The isochronal display of relaxation shear modulus, $G(t, \gamma_0)$, at specific time points as a function of applied strain (γ_0).

6.4.2 Effects of actin filament volume fraction and crosslinking density on the relaxation behaviour of CAFNs

The effects of actin filament volume fraction (V_f) and crosslinking density (ρ_c) on the relaxation behaviour of CAFNs are also studied by conducting a series of FEM simulations. By varying the parameters used in simulations, different actin filament volume fraction and crosslinking density can be obtained. When fixing the crosslinking density of CAFNs at 1.2 μm^{-1}, five groups of simulations are conducted with different volume fractions (0.20%, 0.25%, 0.30%, 0.35% and 0.40%) of actin filament being applied. Simulation results displayed in Figure 6.7. (a) indicate that larger V_f can result in larger relaxation shear stress. In addition, the relaxation shear stresses at specific time points increase nonlinearly with the volume fraction of actin filament. When studying the effects of crosslinking density on the relaxation behaviour of CAFNs, the actin filament volume fraction is fixed at 0.3%, and five levels (1.0, 1.5, 2.0, 2.5 and 3.0) of crosslinking density are considered. As the CAFNs achieve larger crosslinking density, their relaxation shear stress shows higher value. In addition, a nonlinear increase in the relaxation shear stress is also observed when increasing the crosslinking density of CAFNs.

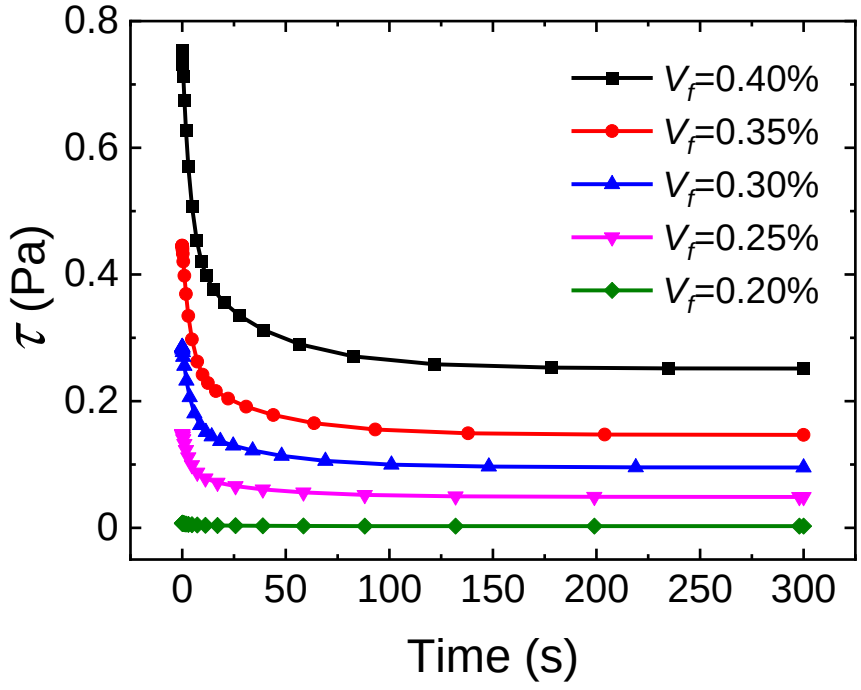

(a)

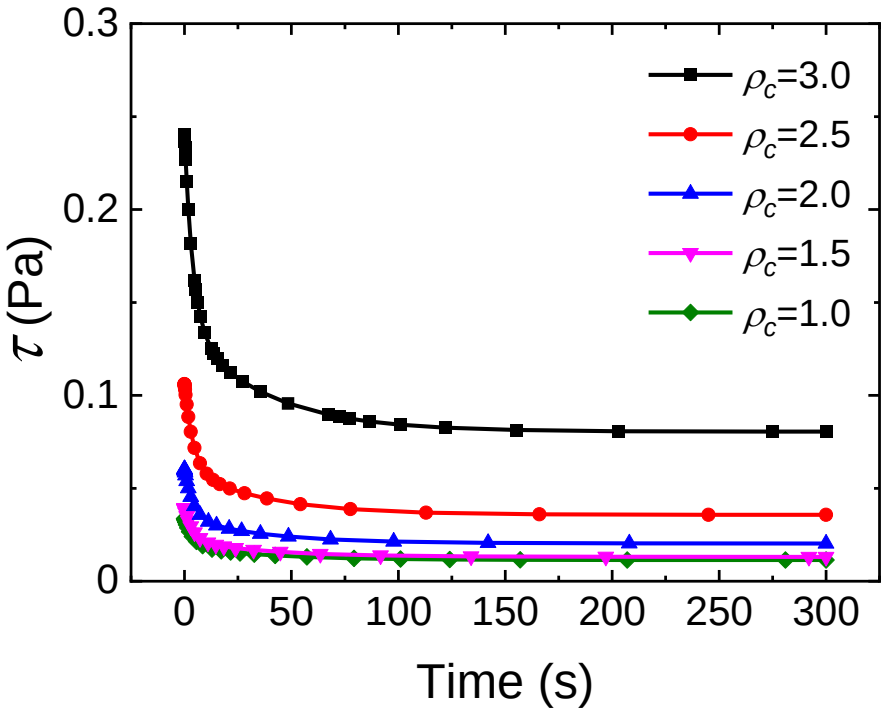

(b)

Figure 6.7. (a) Effects of actin filament volume fraction on the relaxation behaviour of CAFNs with $\rho_c = 1.2\,\mu m^{-1}$. (b) Effects of crosslinking density on the relaxation behaviour of CAFNs with $V_f = 0.3\%$.

6.5 Dynamic properties

In physiological conditions, cells are proved to be viscoelastic and highly dynamic, which is essential for many cell functions. For viscoelastic materials, it is established that a phase lag exhibits in their strains. When an oscillational shear strain is applied, the shear stress, $\tau(t)$, and the shear strain, $\gamma(t)$, in viscoelastic materials can be represented by expressions as

$$\begin{cases} \gamma(t) = \gamma_A \sin(\omega t) \\ \tau(t) = \tau_A \sin(\omega t + \delta) \end{cases} \tag{6.1}$$

Where $\omega = 2\pi f$, *f* is the frequency of applied shear strain, *t* is the time, δ is the phase lag between the shear stress and shear strain, γ_A is the amplitude of applied shear strain and τ_A is the amplitude of shear stress. In viscoelastic materials, the storage modulus measures the stored energy which represents the elastic portion; the loss modulus measures the energy dissipated as heat which represents the viscous portion. The shear storage modulus, G', and the shear loss modulus, G'', are defined as follow:

$$\begin{cases} G' = \dfrac{\tau_A}{\gamma_A}\cos\delta \\ G'' = \dfrac{\tau_A}{\gamma_A}\sin\delta \end{cases}, \tag{6.2}$$

And the complex shear modulus, G^*, is defined as

$$G^* = G' + iG'' \tag{6.3}$$

Where i is the imaginary unit.

The CAFNs show obvious dynamic properties due to their viscoelastic components and extremely complex structure. And the dynamic properties of CAFNs may affect various cell functions a lot. Experiments have been conducted to probe the dynamic properties of CAFNs by researchers [59, 87, 102]. In this paper, the dynamic properties of CAFNs are studied by measuring their storage and loss shear moduli via performing FEM simulations over the abovementioned RVE model. Specifically, both the effects of load frequency and load amplitude on

the storage and shear modulus of CAFNs are studied by carrying out numerical simulations. The simulation results are discussed and compared with experimental measurements.

6.5.1 Effects of load frequency on the dynamic shear modulus of CAFNs

As CAFNs are highly dynamic structures, the mechanical properties of CAFNs are highly dependent on the load frequency [59, 87]. Theoretical models predict that the dynamic shear modulus (G^*) of semi-flexible biopolymer network system scales with load frequency as $G^* \sim \omega^{3/4}$ [169, 170]. In order to investigate the effects of load frequency, f, on the dynamic shear modulus of CAFNs, loads with different frequencies (0.001 Hz to 100 Hz) are applied when conducting FEM simulations. According to the simulation results shown in Figure 6.8, the storage shear modulus, G', is find to be much larger than the loss shear modulus, G'', at low frequency conditions (0.001 Hz to 0.1 Hz). However, with the increase of load frequency, the loss shear modulus increases fast and becomes comparable with the storage shear modulus when the load frequency reaches 1 Hz. It is worth noting that the storage shear modulus of CAFNs almost keeps constant in the range of 0.01 Hz to 1 Hz, which presents to be a plateau in the curve. In addition, both the storage shear modulus and loss shear modulus scale with frequency as $G' \sim \omega^{3/4}$ and $G'' \sim \omega^{3/4}$ when the load frequency is larger than 1 Hz, which could be easily observed. Gardel et al. [59] measure the storage shear modulus and loss shear modulus of crosslinked actin filament networks with a stress-controlled rheometer by applying a sufficiently small oscillatory stress and measuring the resulting deformation. As shown in Figure 6.8, the FEM simulation results show agreement with the experimental measurements [59] in quantity at low frequency ranges of 0.001 Hz to 1 Hz. In the range of frequency from 0.001 Hz to 1 Hz, the transition to the scaling relationship of $G' \sim \omega^{3/4}$ and $G'' \sim \omega^{3/4}$ doesn't appear because the frequency level of the applied oscillatory load is not high enough. The scaling relationships of $G' \sim \omega^{3/4}$ and $G'' \sim \omega^{3/4}$ at high frequency ranges (i.e., over 1 Hz) obtained from the FEM simulations are generally consistent with that predicted theoretically [169, 170] and measured experimentally [87]. It is worth

noting that the transition to the scaling relationship (i.e., $G' \sim \omega^{3/4}$ and $G'' \sim \omega^{3/4}$) can occur at different frequencies. For example, the scaling relationship observed by Gittes and MacKintosh [169] occurs when the frequency is more than 1 Hz, however, the transition to the scaling relationship occurs between 1 Hz to 10 Hz according to the simulations performed by Kim et al. [119]. In addition, it is difficult to recognise the precise point at which the transition to the $\omega^{3/4}$ regime occurs as the frequency level is discretely increased. The occurrence of the transition to the $\omega^{3/4}$ regime can be affected by some factors, for example, the length of actin filament [87]. But the effects of such factors on the transitions to the $\omega^{3/4}$ regime are not discussed in this research. In this section, the parameters (e.g., actin filament volume fraction, crosslinking density and actin filament length) are selected to be at specific values which may different from that used in some experiments. This is the reason why there are differences between the transitions to the $\omega^{3/4}$ regime in this research and previously reported experiments.

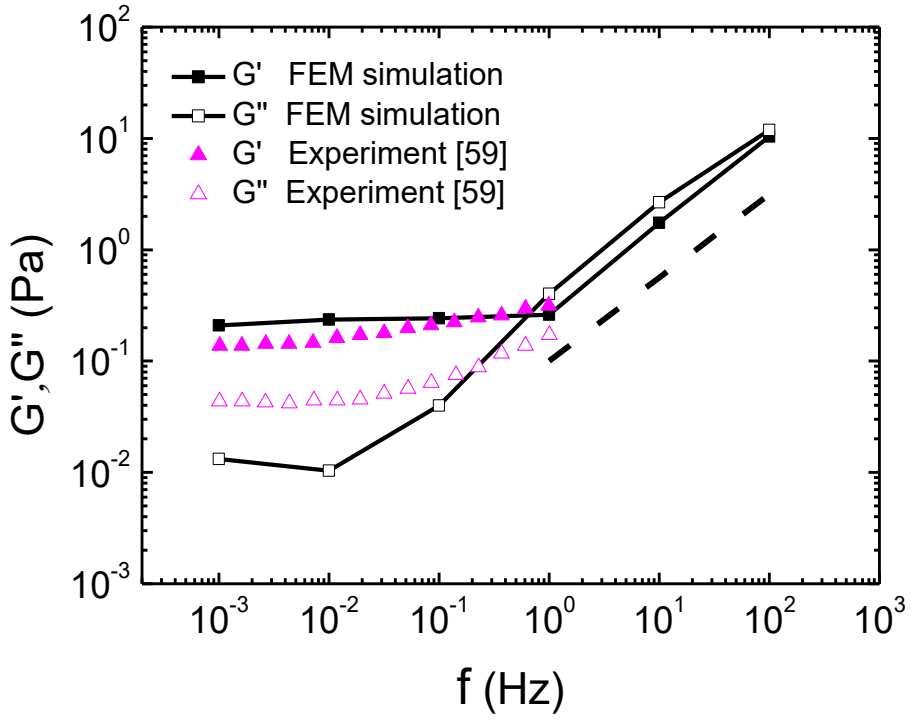

Figure 6.8. The storge and loss shear moduli of the crosslinked actin filament networks (CAFNs) as a function of the load frequency with $V_f = 0.2\%$, $\rho_c = 3.0$ μm^{-1} and $\gamma = 0.001$. The broken line has a slope of 0.75.

6.5.2 Effects of load amplitude on the dynamic shear modulus of CAFNs

The amplitude of applied loads is another factor that can influence the dynamic properties of CAFNs. Thus, shear strains, with different amplitudes are applied in FEM simulations to investigate the effects of load amplitude, γ, on the dynamic shear modulus of CAFNs. Unterberger et al. [95] and Gardel et al. [102] study the dependence of the dynamic modulus of crosslinked actin filament networks on the amplitude of applied loads by performing experiments with a stress-controlled rheometer. In order to compare FEM simulation results with experimental measurements [102], the amplitude of applied shear strains are changed from 0.01 to 1. Both the storage shear modulus (G') and loss shear modulus (G'') of the CAFNs are obtained from numerical simulations and shown in Figure 6.9. According to the simulation results presented in Figure 6.9, the storage shear modulus (G') is insensitive to the amplitude of the applied strain until $\gamma = 0.1$, after which it starts to increase nonlinearly. The increase of the storage shear modulus can be mainly attributed to the strain stiffening behaviour of CAFNs. And this shows good agreement with experimental measurements [95, 102].

In addition, it is easy to find that the storage shear modulus (G'') in experiments shows a decrease trend after the amplitude of applied shear strain reaches 0.9 [102], which is caused by the failure of the network in large strain regime. However, this decrease trend does not appear in FEM simulations as the failure of materials and the unbinding between actin filament and FLNA have not been taken into consideration in this research. For the loss shear modulus (G'') of the CAFNs, the FEM simulation results demonstrate that it increases at larger strains (γ > 0.4), which indicates that the viscous properties of CAFNs are enhanced by the increase of strain amplitude. Similar dependence of G'' on the amplitude of applied shear strain is also observed in the shear rheology experiment on collagen gels [167].

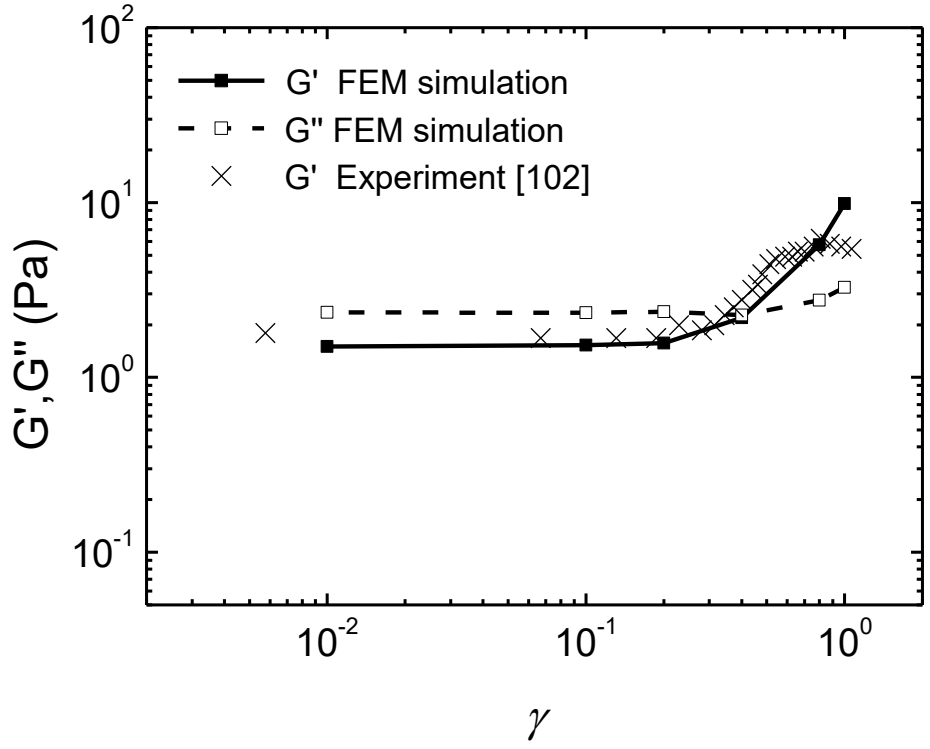

Figure 6.9. Amplitude-dependent storage shear modulus (G') and loss shear modulus (G'') of the crosslinked actin filament networks with $V_f = 0.2\%$ and $\rho_c = 1.0$ μm^{-1}. The frequency of applied shear strain is 0.5 Hz.

6.6 Conclusions

In summary, the viscoelastic properties of CAFNs are investigated by performing FEM simulations over the three-dimensional FE model developed in this research. Simulation results show good agreement with experimental measurements and theoretical predictions. This indicates that the FE model could well mimic the viscoelastic behaviours of CAFNs. Revealing the viscoelastic and dynamic properties of CAFNs greatly helps us to understand the mechanical behaviours of crosslinked actin filament networks in physiological conditions.

The creep and relaxation behaviour of CAFNs are studied by conducting numerical simulations, and results are compared with experimental measurements and theoretical predictions. By applying different viscoelastic properties to actin filament and FLNA, the creep curves and relaxation curves of CAFNs just change

a little. But it is worth noting that FLNA has greater influences on the normalized creep compliance and normalized relaxation stress of CAFNs than actin filament. According to the simulation results, the level of applied stress could greatly influence the creep behaviour of CAFNs. Larger applied stress results in larger creep strain at specific time points. According to the isochronal display of creep shear strain at specific time points, the creep shear strain shows a nonlinear relationship with the applied stress, which is due to the strain/stress stiffening of CAFNs. In addition to applied stress, the volume fraction of actin filament (V_f) and the crosslinking density (ρ_c) could also affect the creep behaviour of CAFNs. Results show that the creep behaviour of CAFNs is obviously undermined when the volume fraction of actin filament or the crosslinking density is increased.

Similarly, the level of applied strain, volume fraction of actin filament (V_f) and crosslinking density (ρ_c) could also affect the relaxation behaviour of CAFNs. According to the simulation results, applying larger shear strain could result in larger shear stress, and the shear stress increases nonlinearly with the applied shear strain. However, when the stress relaxation curves of different applied strains are normalized by their initial stresses respectively, they collapse onto a single curve. This indicates that the applied strain just influences the relaxation behaviour of CAFNs in quantity in this research. Because the unbinding between actin filaments and FLNA is simply ignored in the FE model. Larger volume fraction of actin filament and crosslinking density could also result in larger shear stress in relaxation simulations.

The dependences of dynamic shear modulus of CAFNs on the frequency and amplitude of applied loads are also studied. It is found that a plateau is formed in the storage shear modulus before the load frequency reaches 1 Hz. After that, the storage shear modulus increases nonlinearly with the load frequency. At high frequency conditions, both the storage and loss shear moduli of CAFNs scale with the load frequency as $G' \sim \omega^{3/4}$ and $G'' \sim \omega^{3/4}$, which is consistent with previous experimental measurements and theoretical predictions. In addition, the dynamic shear moduli of CAFNs are not sensitive to the amplitude of applied loads in small strain stage, however, they increase nonlinearly with the amplitude of applied loads in large strain stage. This phenomenon shows good agreement with experimental measurements.

Chapter 7 Conclusions and Further Research

7.1 Conclusions

This research systematically investigates the mechanical properties of crosslinked actin filament networks (CAFNs) by conducting numerical simulations as well as performing dimensional analysis. A three-dimensional network model is developed according to the microstructure of the crosslinked actin filament networks in living cells. The actin filaments (F-actin) in the model are generated with random lengths and orientations, and they are modelled by deformable elastic beams. The crosslinkers (i.e., FLNA) in the model are represented by curved beams which can precisely capture the physiological contour of filamins in living cells. Novel crosslinking principles are applied when constructing the model to mimic the real interactions between actin filament and crosslinker. The linear elastic, nonlinear elastic and viscoelastic properties of crosslinked actin filament networks are revealed in this research by performing simulations, and the simulation results are compared with experimental measurements and theoretical predictions reported in literature.

The linear elastic properties of crosslinked actin filament networks are obtained in this research by performing numerical simulations on the three-dimensional network model, and the simulation results are compared with experimental measurements reported by other researchers. The crosslinked actin filament networks are proved to be transversely isotropic as the orientations of actin filaments in plane are determined by random numbers. The effective in plane shear moduli of the crosslinked actin filament networks obtained from simulations show good agreement with the experimental results in literature. As the mechanical properties of actin filament gels can be greatly affected by the concentrations of actin monomers and actin binding proteins added in the gels, the effects of the volume fraction of actin filaments and the crosslinking density on the effective elastic properties of crosslinked actin filament networks are

investigated in this research by conducting numerical simulations. According to the simulations, the effective in plane shear moduli of the crosslinked actin filament networks scale with the volume fraction of actin filaments as $G \sim V_f^{2.5}$, which is in consistence with the experimental results. In addition, the effective in plane shear moduli of the crosslinked actin filament networks are proved to scale with the crosslinking density of the networks as $G \sim \rho_c^{\ 2}$, which is also observed in experiments. This indicates that both the actin filament volume fraction and the crosslinking density can greatly affect the linear elastic properties of the crosslinked actin filament networks. To reveal the deformation mechanism of the crosslinked actin filament networks in small strain regime, a simple cantilever beam model is proposed to perform the dimensional analysis. The deformation of the cantilever beam model can be obtained by applying the principle of superposition. The effects of the bending stiffnesses of the crosslinkers and actin filaments on the effective in plane shear modulus of the crosslinked actin filament networks are investigated by varying the Young's moduli of the crosslinkers and actin filaments respectively. It is easy to find that the dimensional analysis results agree well with the simulation results, and the bending stiffness of crosslinkers is proved to has greater effects on the elastic properties of CAFNs than the bending stiffness of actin filaments has. Moreover, the torsion of the crosslinkers is also taken into consideration in this research. Interestingly, both the dimensional analysis results and the simulation results demonstrate that the torsional stiffness of the crosslinkers has considerable effects on the linear elastic properties of crosslinked actin filament networks.

In living cells, the cytoskeleton always deforms largely to respond to the external and internal mechanical signals. In this way, the happening of different cell functions can be guaranteed and the cell integrity can be maintained. When large stress or strain is applied, the crosslinked actin filament networks are reported to present nonlinear elastic properties, which is also known as strain stiffening. As the nonlinear elastic properties play a major role in the mechanical behaviours of crosslinked actin filament networks, the nonlinear elasticity of CAFNs is studied by conducting numerical simulations in this research. When performing simulations, a large shear strain is applied to the three-dimensional network model and the shear stress can be obtained. The stress strain relationships and tangent moduli of the crosslinked actin filament networks are obtained from simulations and show good agreement with the experimental measurements. This demonstrates that the three-dimensional network model developed in this

research can precisely capture the nonlinear elastic behaviour of the crosslinked actin filament networks. Then the effects of the actin filament volume fraction and crosslinking density on the nonlinear elastic properties of the crosslinked actin filament networks are studied by varying the corresponding parameters when performing the simulations. Simulation results indicate that both the actin filament volume fraction and the crosslinking density can greatly affect the nonlinear elastic properties of crosslinked actin filament networks. In addition, the effects of the Young's moduli and Poisson's ratios of the components on the nonlinear elastic properties of CAFNs are also revealed. It is easy to find that the nonlinear elastic properties of CAFNs can be greatly affected by the Young's moduli of actin filaments and crosslinkers, however, the Poisson's ratios of actin filaments and crosslinkers just have slight influences on the stress strain relationships and tangent moduli of the CAFNs in the range of -0.9 to 0.49. Crosslinked actin filament networks are proved to show negative normal stress when a shear strain or shear stress is applied. This phenomenon is also observed in this research, and the effects of the components' physical properties on the negative normal stress of CAFNs are investigated. In addition, the deformation mechanism of crosslinked actin filament networks in large strain regime is studied. The bending, torsion and tension of crosslinkers and actin filaments are split to reveal their effects on the nonlinear elastic properties of crosslinked actin filament networks. According to the simulation results, the bending stiffness, torsional stiffness and tensile stiffness of crosslinkers have considerable effects on the nonlinear elastic properties of crosslinked actin filament networks. The bending stiffness of actin filaments is also proved to have large effects on the nonlinear elastic properties of crosslinked actin filament networks; however, the torsional stiffness and tensile stiffness of actin filaments almost do not affect the nonlinear elasticity at least in the range of applied astrain studied in this research.

The crosslinked actin filament networks are also proved to be highly dynamic structures which present obvious viscoelastic properties. This suggests that their mechanical properties are time dependent and can be influenced by the frequencies of the applied loads. The viscoelastic properties of crosslinked actin filament networks are found to play a major role in different cell functions; however, they are not known very well. Thus, it is necessary to study the viscoelastic properties of crosslinked actin filament networks. In this research, the viscoelastic properties of crosslinked actin filament networks are obtained by performing numerical simulations, and the material properties of crosslinkers and actin

filaments are determined according to the experimental measurements in literature. It is worth noting that another several cases of material properties are assumed and applied to crosslinkers and actin filaments to reveal the roles of crosslinkers and actin filaments in the viscoelastic behaviour of crosslinked actin filament networks. Simulation results indicate that the crosslinkers have larger effects on the creep behaviour of CAFNs than actin filaments have, and the simulation results show good agreement with the experimental measurements reported in literature. Then, the effects of the applied stress on the creep behaviour of CAFNs are investigated by varying the levels of applied stresses. Larger applied stress results in larger creep strain, and the isochronal display of creep strain at specific time points indicates that there exists a nonlinear elastic relationship between the applied stress and creep strain which originates from the strain stiffening of CAFNs. In addition, the dependences of the creep behaviour of CAFNs on the actin filament volume fraction and crosslinking density are also revealed according to simulation results. It can be found that both the actin filament volume fraction and the crosslinking density can greatly affect the creep behaviour of CAFNs. As another important viscoelastic behaviour, the relaxation of crosslinked actin filament networks is also studied in this research. Different cases with various material properties of crosslinkers and actin filaments are simulated, and the simulation results are compared with experimental measurements. The relaxation tests demonstrate that the crosslinkers have greater effects on the relaxation behaviour of CAFNs than actin filaments have. And the levels of the applied shear strains can also affect the relaxation behaviour of CAFNs. The isochronal display of the relaxation shear stress and relaxation shear modulus at specific time points are as functions of the applied shear strains, and nonlinear relationships are observed in these functions. The nonlinear relationships between the relaxation shear stress (or relaxation shear modulus) and applied shear strain can be well explained by the strain stiffening behaviour of CAFNs. There is no doubt that the actin filament volume fraction and crosslinking density can also greatly affect the relaxation behaviour of CAFNs. Finally, the dependences of the storage and loss shear modulus of the crosslinked actin filament networks on the frequency and amplitude of the applied loads are investigated in detail by conducting numerical simulations. According to the simulation results, a plateau is formed in the storage shear modulus of CAFNs before the load frequency reaches 1 Hz. Then the storage shear modulus of CAFNs increases nonlinearly with the load frequency. At high frequency conditions, both the storage and loss shear moduli of CAFNs scale with the load frequency as $G' \sim \omega^{3/4}$ and $G'' \sim \omega^{3/4}$, which

agrees well with experimental measurements and theoretical predictions reported in literature. In addition, both the storage shear modulus and loss shear modulus of CAFNs are not sensitive to the amplitude of applied loads in small strain stage, however, they increase nonlinearly with the amplitude of applied loads in large strain stage. This phenomenon is also observed in experiments.

In summary, a novel three-dimensional network model is developed in this research, and the microstructure of this model can precisely capture the characteristics of the crosslinked actin filament networks in living cells. This model can also mimic the mechanical behaviours of crosslinked actin filament networks as well as other biopolymer networks with similar structures. And the simulation results obtained from this model are compared with experimental measurements and theoretical predictions reported in literature. In addition, some other interesting results are also obtained by performing numerical simulations and dimensional analysis on this three-dimensional network model. This indicates that this model can be used to investigate the mechanical properties of crosslinked actin filament networks and provide good reference in constructing numerical models for such complex network systems. And the results obtained in this research can also help us to understand the mechanical responses of crosslinked actin filament networks in living cells.

7.2 Further research

This research has investigated the linear elastic, nonlinear elastic and viscoelastic properties of the crosslinked actin filament networks by conducting numerical simulations on a three-dimensional network model which is developed according to the microstructure of crosslinked actin filament networks in living cells. Yet there are more to be considered when constructing the models and conducting simulations. The details of further research needed to be done are demonstrated as follow.

Firstly, the connections between crosslinkers and actin filaments are assumed to be permanent, which means that the unbinding and rebinding between crosslinkers and actin filaments are not taken into consideration in this research. In living cells, the cytoskeleton and its substructures are proved to be highly

dynamic. The polymerization and depolymerization of actin filaments as well as the binding, unbinding and rebinding between crosslinkers and actin filaments can be observed throughout the whole life cycle of living cells. However, due to the extreme complexity in constructing the network models and conducting simulations, these issues are not taken into consideration in this research. In future research, these points need to be included to optimize the three-dimensional FEM models of crosslinked actin filament networks.

Secondly, the crosslinked actin filament networks always connected with other biopolymer structures (e.g., actin filament bundles, stress fibres, branched actin filament networks, intermediate filaments and microtubules) to form the cytoskeleton. This research mainly focuses on the mechanical properties of crosslinked actin filament networks, however, the coordination between these distinct biopolymer structures is not discussed. Thus, the role of the coordination between these distinct biopolymer structures in different cell functions worth to be investigated in the future.

Thirdly, the crosslinked actin filament networks are embedded in viscoelastic cytoplasm in living cells, which indicates that the cytoplasm may constrain the deformation of crosslinked actin filament networks. Yet this is not discussed in this research. To better understand the interactions between the crosslinked actin filament networks and cytoplasm in living cells, a model includes both the network and cytoplasm need to be developed in the future research.

Finally, the crosslinked actin filament networks are observed to be just beneath the cell plasm membrane, which indicates that the cell plasm membrane may also has effects on the mechanical responses of the crosslinked actin filament networks. And the crosslinked actin filament networks are reported to connect with the extracellular matrix by specific proteins crossing the cell plasm membrane. To study the dependences of the mechanical properties of living cells on the extracellular matrix, the extracellular matrix and cell plasm membrane are also need to be include in the model. These works are also considered to be included in the future research.

References

[1] Salbreux, G., G. Charras, and E. Paluch, *Actin cortex mechanics and cellular morphogenesis.* Trends Cell Biol, 2012. 22(10): p. 536-545.

[2] Nobes, C.D. and A. Hall, *Rho, Rac, and Cdc42 GTPases regulate the assembly of multimolecular focal complexes associated with actin stress fibers, lamellipodia, and filopodia.* Cell, 1995. 81: p. 53-62.

[3] Fletcher, D.A. and R.D. Mullins, *Cell mechanics and the cytoskeleton.* Nature, 2010. 463(7280): p. 485-492.

[4] Blanchoin, L., et al., *Actin dynamics, architecture, and mechanics in cell motility.* Physiol Rev, 2014. 94: p. 235-263.

[5] Liu, K.-K. and M.L. Oyen, *Nanobiomechanics of living materials.* Interface Focus, 2014. 4(2): p. 20140001.

[6] Pollard, T.D., *Purification of a Calcium-sensitive Actin Gelation Protein from Acanthamoeba.* J Biol Chem, 1981. 256(14): p. 7666-7670.

[7] Alt, W., A. Deutsch, and G. Dunn, *Dynamics of Cell and Tissue Motion*. 2012: Birkhäuser Basel. 336.

[8] Discher, D.E., P. Janmey, and Y. Wang, *Tissue Cells Feel and Respond to the Stiffness of Their Substrate.* Science, 2005. 310(5751): p. 1139-1143.

[9] NM, v.P., et al., *Association Between Arterial Stiffness and Atherosclerosis.* Stroke, 2001. 32(2): p. 454-460.

[10] Huang, S. and D.E. Ingber, *Cell tension, matrix mechanics, and cancer development.* Cancer Cell, 2005. 8(3): p. 175-176.

[11] Georges, P.C., et al., *Increased stiffness of the rat liver precedes matrix deposition: implications for fibrosis.* Am J Physiol Gastrointest Liver Physiol, 2007. 293: p. G1147–G1154.

[12] Levental, K.R., et al., *Matrix crosslinking forces tumor progression by enhancing integrin signaling.* Cell, 2009. 139(5): p. 891-906.

[13] Cooper, G.M., *The Cell: A Molecular Approach*. 2nd edition ed. 2000: Sunderland (MA): Sinauer Associates.

[14] Gittes, F., et al., *Flexural rigidity of microtubules and Actin Filaments Measured from Thermal Fluctuations in Shape.* J. Cell Biol, 1993. 120(4): p. 923-934.

[15] Liu, K.-K. and V. Chan, *Nanoengineering life: from cell to tissue.* Interface Focus, 2011. 1(5): p. 699-701.

[16] Hawkins, T., et al., *Mechanics of microtubules.* J Biomech, 2010. 43(1): p. 23-30.

[17] Rusan, N.M. and P. Wadsworth, *Centrosome fragments and microtubules are transported asymmetrically away from division plane in anaphase.* J Cell Biol, 2005. 168(1): p. 21-28.

[18] Wagner, O., et al., *Viscoelastic Properties of f-actin, Microtubules, f-actin/α-actinin, and f-actin/Hexokinase Determined in Microliter Volumes with a Novel Nondestructive Method.* Biophysical Journal, 1999. 76: p. 2784-2796.

[19] Brangwynne, C.P., et al., *Microtubules can bear enhanced compressive loads in living cells because of lateral reinforcement.* J Cell Biol, 2006. 173(5): p. 733-741.

[20] Jia, K. and X. Liu, *Measuring the flexural rigidity of actin filaments and microtubules from their thermal fluctuating shapes: A new perspective.* Journal of the Mechanics and Physics of Solids, 2017. 101: p. 64-92.

[21] Herrmann, H., et al., *Intermediate filaments: from cell architecture to nanomechanics.* Nat Rev Mol Cell Biol, 2007. 8(7): p. 562-573.

[22] Steinert, P.M. and D.R. Roop, *Molecular and Cellular Biology of Intermediate Filaments.* Ann. Rev. Biochem, 1988. 57: p. 593-625.
[23] Chang, L. and R.D. Goldman, *Intermediate filaments mediate cytoskeletal crosstalk.* Nat Rev Mol Cell Biol, 2004. 5(8): p. 601-613.
[24] Lazarides, E., *Intermediate filaments as mechanical integrators of cellular space.* Nature, 1980. 283: p. 249-256.
[25] Godsel, L.M., R.P. Hobbs, and K.J. Green, *Intermediate filament assembly: dynamics to disease.* Trends Cell Biol, 2008. 18(1): p. 28-37.
[26] Fuchs, E. and K. Weber, *Intermediate Filament: Structure, Dynamics, Function and Disease.* Annu. Rev. Biochem., 1994. 63: p. 345-382.
[27] Goldman, R.D., et al., *Inroads into the structure and function of intermediate filament networks.* J Struct Biol, 2012. 177(1): p. 14-23.
[28] Holmes, K.C., et al., *Atomic model of the actin filament.* Nature, 1990. 347: p. 44-49.
[29] Pollard, T.D. and G.G. Borisy, *Cellular Motility Driven by Assembly and Disassembly of Actin Filaments.* Cell 2003. 112: p. 453-465.
[30] Kim, T., M.L. Gardel, and E. Munro, *Determinants of fluidlike behavior and effective viscosity in cross-linked actin networks.* Biophys J, 2014. 106(3): p. 526-534.
[31] Gardel, M.L., et al., *Elastic Behavior of Cross-Linked and Bundled Actin Networks.* Science, 2004. 304: p. 1301-1305.
[32] Feher, J., *2.1 - Cell Structure*, in *Quantitative Human Physiology*, J. Feher, Editor. 2012, Academic Press: Boston. p. 75-90.
[33] Broedersz, C.P. and F.C. MacKintosh, *Modeling semiflexible polymer networks.* Rev Mod Phys, 2014. 86(3): p. 995-1036.
[34] Mohrdieck, C., et al., *Biomimetic models of the actin cytoskeleton.* Small, 2007. 3(6): p. 1015-1022.
[35] Lodish, H., et al., *Molecular Cell Biology*. 6th ed. 2008: W. H. Freeman. 1120.
[36] Laurent, V.M., et al., *Tensegrity Behaviour of Cortical and Cytosolic Cytoskeletal Components in Twisted Living Adherent Cells.* Acta Biotheoretica, 2002. 50: p. 331-356.
[37] Isambert, H., et al., *Flexibility of Actin Filaments Derived from Thermal Fluctuations.* J Biol Chem, 1995. 270(19): p. 11437-11444.
[38] Gardel, M.L., et al., *Mechanical Response of Cytoskeletal Networks.* Methods in Cell Biology, 2008. 89: p. 487-519.
[39] Kojima, H., A. Ishuima, and T. Yanagida, *Direct measurement of stiffness of single actin filaments with and without tropomyosin by in vitro nanomanipulation.* Proc Natl Acad Sci U S A, 1994. 91: p. 12962-12966.
[40] Pollard, T.D. and J.A. Cooper, *Actin, a Central Player in Cell Shape and Movement.* Science, 2009. 326: p. 1208-1212.
[41] Onck, P.R., et al., *Alternative explanation of stiffening in cross-linked semiflexible networks.* Phys Rev Lett, 2005. 95(17): p. 178102.
[42] Stossel, T.P., et al., *Filamins as intergrators of cell mechanics and signalling.* Nat Rev Mol Cell Biol, 2001. 2: p. 138-145.
[43] Xu, K., H.P. Babcock, and X. Zhuang, *Dual-objective STORM reveals three-dimensional filament organization in the actin cytoskeleton.* Nat Methods, 2012. 9(2): p. 185-188.
[44] Charras, G.T., et al., *Reassembly of contractile actin cortex in cell blebs.* J Cell Biol, 2006. 175(3): p. 477-490.
[45] Clark, A.G., K. Dierkes, and E.K. Paluch, *Monitoring actin cortex thickness in live cells.* Biophys J, 2013. 105(3): p. 570-580.

[46] Eghiaian, F., A. Rigato, and S. Scheuring, *Structural, mechanical, and dynamical variability of the actin cortex in living cells.* Biophys J, 2015. 108(6): p. 1330-1340.
[47] Wilhelm, J. and E. Frey, *Elasticity of stiff polymer networks.* Phys Rev Lett, 2003. 91(10): p. 108103.
[48] Hartwig, J.H. and P. Shevlin, *The Architecture of Actin Filaments and the Ultrastructural Location of Actin-binding Protein in the Periphery of Lung Macrophages.* J. Cell Biol, 1986. 103: p. 1007-1020.
[49] Morone, N., et al., *Three-dimensional reconstruction of the membrane skeleton at the plasma membrane interface by electron tomography.* J Cell Biol, 2006. 174(6): p. 851-862.
[50] Charras, G.T., et al., *Life and times of a cellular bleb.* Biophys J, 2008. 94(5): p. 1836-1853.
[51] Kawamura, M. and K. Maruyama, *Electron Microscopic Particle Length of F-Actin Polymerized in Vitro.* J Biochem, 1970. 67(3): p. 437-457.
[52] Edelstein-Keshet, L. and G.B. Ermentrout, *Models for the Length Distributions of Actin Filaments I. Simple Polymerization and Fragmentation.* Bulletin of Mathematical Biology, 1998. 60: p. 449-475.
[53] Biron, D. and E. Moses, *The Effect of a-Actinin on the Length Distribution of F-Actin.* Biophysical Journal, 2004. 86: p. 3284-3290.
[54] Grazi, E. and S. Pozzati, *Protein osmotic pressure modulates actin filament length distribution.* J Theor Biol, 2008. 251(3): p. 411-420.
[55] Bai, M., et al., *On the role of the filament length distribution in the mechanics of semiflexible networks.* Acta Biomater, 2011. 7(5): p. 2109-2118.
[56] Lin, S., et al., *Active stiffening of F-actin network dominated by structural transition of actin filaments into bundles.* Composites Part B: Engineering, 2016.
[57] Janmey, P.A., J.X. Tang, and C.F. Schmidt, *Actin Filaments.* 1999.
[58] Tseng, Y., et al., *Functional synergy of actin filament cross-linking proteins.* J Biol Chem, 2002. 277(28): p. 25609-25616.
[59] Gardel, M.L., et al., *Prestressed F-actin networks cross-linked by hinged filamins replicate mechanical properties of cells.* Proc Natl Acad Sci U S A, 2006. 103(6): p. 1762-1767.
[60] Podolski, J.L. and T.L. Steck, *Length Distribution of F-actin in Dictyostelium discoideum.* J Biol Chem, 1990. 265: p. 1312-1318.
[61] Medalia, O., et al., *Macromolecular Architecture in Eukaryotic Cells Visualized by Cryoelectron Tomography.* Science, 2002. 298: p. 1209-1213.
[62] Nakamura, F., et al., *Comparison of filamin A-induced cross-linking and Arp2/3 complex-mediated branching on the mechanics of actin filaments.* J Biol Chem, 2002. 277(11): p. 9148-9154.
[63] Huisman, E.M., et al., *Three-dimensional cross-linked F-actin networks: relation between network architecture and mechanical behavior.* Phys Rev Lett, 2007. 99(20): p. 208103.
[64] Koenderink, G.H., et al., *An active biopolymer network controlled by molecular motors.* Proc Natl Acad Sci U S A, 2009. 106(36): p. 15192-15197.
[65] Lin, S. and L. Gu, *Influence of Crosslink Density and Stiffness on Mechanical Properties of Type I Collagen Gel.* Materials, 2015. 8(2): p. 551-560.
[66] Gunn, R.B., *Cell physiology of blood*. Society of General Physiologists, 41st Annual Symposium. Vol. 43. 1988: Rockefeller University Press. 402.
[67] Hartwig, J.H. and T.P. Stossel, *Isolation and Properties of Actin, Myosin, and a New Actin-binding Protein in Rabbit Alveolar Macrophages.* J Biol Chem, 1975. 250(25): p. 5696-5705.

[68] Yuanyi Feng, C.A.W., *The many faces of filamin A versatile molecular scaffold for cell motility and signalling.* Nature Cell Biology, 2004. 6: p. 1034-1038.
[69] van der Flier, A. and A. Sonnenberg, *Structural and functional aspects of filamins.* Biochim Biophys Acta, 2001. 1538: p. 99-117.
[70] Nakamura, F., et al., *Structural basis of filamin A functions.* J Cell Biol, 2007. 179(5): p. 1011-1025.
[71] Nakamura, F., T.P. Stossel, and J.H. Hartwig, *The filamins: Organizers of cell structure and function.* Cell Adhesion & Migration, 2011. 5(2): p. 160-169.
[72] Zhu, X., et al., *Determination of work of adhesion of biological cell under AFM bead indentation.* J Mech Behav Biomed Mater, 2016. 56: p. 77-86.
[73] Yamazaki, M., S. Furuike, and T. Ito, *Mechanical response of single filamin A (ABP-280) molecules and its role in the actin cytoskeleton.* J Muscle Res Cell Motil, 2002. 23: p. 525-534.
[74] Bonnans, C., J. Chou, and Z. Werb, *Remodelling the extracellular matrix in development and disease.* Nat Rev Mol Cell Biol, 2014. 15(12): p. 786-801.
[75] Hynes, R.O., *The Extracellular Matrix: Not Just Pretty Fibrils.* Science, 2009. 326: p. 1216-1219.
[76] Frantz, C., K.M. Stewart, and V.M. Weaver, *The extracellular matrix at a glance.* Journal of Cell Science, 2010. 123(24): p. 4195-4200.
[77] Theocharis, A.D., et al., *Extracellular matrix structure.* Adv Drug Deliv Rev, 2016. 97: p. 4-27.
[78] Di Lullo, G.A., et al., *Mapping the ligand-binding sites and disease-associated mutations on the most abundant protein in the human, type I collagen.* J Biol Chem, 2002. 277(6): p. 4223-4231.
[79] Petropolis, D.B., et al., *Leishmania amazonensis promastigotes in 3D Collagen I culture: an in vitro physiological environment for the study of extracellular matrix and host cell interactions.* PeerJ, 2014. 2: p. e317.
[80] Siamantouras, E., et al., *Nanomechanical Investigation of Soft Biological Cell Adhesion using Atomic Force Microscopy.* Cellular and Molecular Bioengineering, 2015. 8(1): p. 22-31.
[81] Hynes, R.O., *Integrins: Bidirectional, Allosteric Signaling Machines.* Cell, 2002. 110: p. 673-687.
[82] Jin, T., et al., *A novel collagen gel-based measurement technique for quantitation of cell contraction force.* J R Soc Interface, 2015. 12(106).
[83] Jin, T., et al., *Collagen matrix stiffness influences fibroblast contraction force.* Biomedical Physics & Engineering Express, 2016. 2(4): p. 047002.
[84] Griffith, L.G. and M.A. Swartz, *Capturing complex 3D tissue physiology in vitro.* Nat Rev Mol Cell Biol, 2006. 7(3): p. 211-224.
[85] Janmey, P.A., et al., *The Mechanical Properties of Actin Gels.* J Biol Chem, 1994. 269: p. 32503-32513.
[86] Wagner, B., et al., *Cytoskeletal polymer networks: the molecular structure of cross-linkers determines macroscopic properties.* Proc Natl Acad Sci U S A, 2006. 103(38): p. 13974-13978.
[87] Koenderink, G.H., et al., *High-frequency stress relaxation in semiflexible polymer solutions and networks.* Phys Rev Lett, 2006. 96(13): p. 138307.
[88] Sharma, A., et al., *Strain-controlled criticality governs the nonlinear mechanics of fibre networks.* Nature Physics, 2016. 12(6): p. 584-587.
[89] Kasza, K.E., et al., *Actin filament length tunes elasticity of flexibly cross-linked actin networks.* Biophys J, 2010. 99(4): p. 1091-1100.
[90] Storm, C., et al., *Nonlinear elasticity in biological gels.* Nature, 2005. 435(7039): p. 191-194.

[91] MacKintosh, F.C., J. Kas, and P.A. Janmey, *Elasticity of semiflexible biopolymer networks.* Phys Rev Lett, 1995. 75(24): p. 4425-4428.
[92] van Dillen, T., P.R. Onck, and E. Van der Giessen, *Models for stiffening in cross-linked biopolymer networks: A comparative study.* J Mech Phys Solids, 2008. 56(6): p. 2240-2264.
[93] Meng, F. and E.M. Terentjev, *Nonlinear elasticity of semiflexible filament networks.* Soft Matter, 2016. 12(32): p. 6749-6756.
[94] Palmer, J.S. and M.C. Boyce, *Constitutive modeling of the stress-strain behavior of F-actin filament networks.* Acta Biomater, 2008. 4(3): p. 597-612.
[95] Unterberger, M.J., et al., *Viscoelasticity of cross-linked actin networks: experimental tests, mechanical modeling and finite-element analysis.* Acta Biomater, 2013. 9(7): p. 7343-7353.
[96] López-Menéndez, H. and J.F. Rodríguez, *Microstructural model for cyclic hardening in F-actin networks crosslinked by α-actinin.* J Mech Phys Solids, 2016. 91: p. 28-39.
[97] Head, D.A., A.J. Levine, and F.C. MacKintosh, *Deformation of cross-linked semiflexible polymer networks.* Phys Rev Lett, 2003. 91(10): p. 108102.
[98] Missel, A.R., et al., *Affine-nonaffine transition in networks of nematically ordered semiflexible polymers.* Phys Rev E Stat Nonlin Soft Matter Phys, 2010. 82(4 Pt 1): p. 041907.
[99] Wei, X., et al., *Response of biopolymer networks governed by the physical properties of cross-linking molecules.* Soft Matter, 2016. 12(9): p. 2537-2541.
[100] Ahearne, M., et al., *Characterizing the viscoelastic properties of thin hydrogel-based constructs for tissue engineering applications.* J R Soc Interface, 2005. 2(5): p. 455-463.
[101] Janmey, P.A., et al., *Structure and mobility of actin filaments as measured by quasielastic light scattering, viscometry, and electron microscopy.* J Biol Chem, 1986. 261: p. 8357-8362.
[102] Gardel, M.L., et al., *Stress-dependent elasticity of composite actin networks as a model for cell behavior.* Phys Rev Lett, 2006. 96(8): p. 088102.
[103] Kasza, K.E., et al., *The cell as a material.* Curr Opin Cell Biol, 2007. 19(1): p. 101-107.
[104] Kasza, K.E., et al., *Nonlinear elasticity of stiff biopolymers connected by flexible linkers.* Phys Rev E Stat Nonlin Soft Matter Phys, 2009. 79(4 Pt 1): p. 041928.
[105] Bhattacharjee, S.M., A. Giacometti, and A. Maritan, *Flory theory for polymers.* J Phys Condens Matter, 2013. 25(50): p. 503101 (503131pp).
[106] Doi, M. and S.F. Edwards, *The theory of polymer dynamics*. Current Opinion in Solid State and Materials Science. 1986, Oxford, UK: Oxford University Press.
[107] Meng, F. and E. Terentjev, *Theory of Semiflexible Filaments and Networks.* Polymers, 2017. 9(2): p. 52.
[108] Kratky, O. and G. Porod, *Röntgenuntersuchung gelöster Fadenmoleküle.* Recueil des travaux chimiques des Pays Bas., 1949. 68(12): p. 1106-1122.
[109] Marko, J.F. and E.D. Siggia, *Stretching DNA.* Macromolecules, 1995. 28: p. 8759-8770.
[110] Sharma, A., et al., *Elastic response of filamentous networks with compliant crosslinks.* Phys Rev E Stat Nonlin Soft Matter Phys, 2013. 88(5): p. 052705.
[111] Heidemann, K.M., et al., *Elasticity of 3D networks with rigid filaments and compliant crosslinks.* Soft Matter, 2015. 11(2): p. 343-354.
[112] Head, D.A., A.J. Levine, and F.C. MacKintosh, *Distinct regimes of elastic response and deformation modes of cross-linked cytoskeletal and semiflexible polymer networks.* Phys Rev E Stat Nonlin Soft Matter Phys, 2003. 68(6 Pt 1): p. 061907.

[113] Heussinger, C., B. Schaefer, and E. Frey, *Nonaffine rubber elasticity for stiff polymer networks.* Phys Rev E Stat Nonlin Soft Matter Phys, 2007. 76(3 Pt 1): p. 031906.

[114] Shahsavari, A.S. and R.C. Picu, *Size effect on mechanical behavior of random fiber networks.* Int J Solids Struct, 2013. 50(20-21): p. 3332-3338.

[115] Huisman, E.M., C. Storm, and G.T. Barkema, *Monte Carlo study of multiply crosslinked semiflexible polymer networks.* Phys Rev E Stat Nonlin Soft Matter Phys, 2008. 78(5 Pt 1): p. 051801.

[116] Broedersz, C.P., et al., *Criticality and isostaticity in fibre networks.* Nat Phys, 2011. 7(12): p. 983-988.

[117] Chen, X., et al., *Predictive assembling model reveals the self-adaptive elastic properties of lamellipodial actin networks for cell migration.* Commun Biol, 2020. 3(1): p. 616.

[118] Wang, X., et al., *The elastic properties and deformation mechanisms of actin filament networks crosslinked by filamins.* J Mech Behav Biomed Mater, 2020. 112: p. 104075.

[119] Kim, T., et al., *Computational analysis of viscoelastic properties of crosslinked actin networks.* PLoS Comput Biol, 2009. 5(7): p. e1000439.

[120] Ma, Y.H., et al., *The elasto-plastic behaviour of three-dimensional stochastic fibre networks with cross-linkers.* J Mech Phys Solids, 2018. 110: p. 155-172.

[121] Das, M., F.C. MacKintosh, and A.J. Levine, *Effective Medium Theory of Semiflexible Filamentous Networks.* Phys Rev Lett, 2007. 99: p. 038101.

[122] Stein, A.M., et al., *The micromechanics of three-dimensional collagen-I gels.* Complexity, 2011. 16(4): p. 22-28.

[123] Žagar, G., P.R. Onck, and E. Van der Giessen, *Elasticity of Rigidly Cross-Linked Networks of Athermal Filaments.* Macromolecules, 2011. 44(17): p. 7026-7033.

[124] Cyron, C.J., et al., *Micromechanical simulations of biopolymer networks with finite elements.* J Comput Phys, 2013. 244: p. 236-251.

[125] Castellani, L., et al., *Structure of filamin and the F-actin-heavy merofilamin complex.* Journal of Muscle Research & Cell Motility, 1981. 2: p. 193-202.

[126] Kanit, T., et al., *Determination of the size of the representative volume element for random composites: statistical and numerical approach.* International Journal of Solids and Structures, 2003. 40(13-14): p. 3647-3679.

[127] Lin, S., et al., *Active stiffening of F-actin network dominated by structural transition of actin filaments into bundles.* Composites Part B: Engineering, 2017. 116: p. 377-381.

[128] Zagar, G., P.R. Onck, and E. van der Giessen, *Two fundamental mechanisms govern the stiffening of cross-linked networks.* Biophys J, 2015. 108(6): p. 1470-1479.

[129] Lieleg, O., et al., *Cytoskeletal polymer networks: viscoelastic properties are determined by the microscopic interaction potential of cross-links.* Biophys J, 2009. 96(11): p. 4725-4732.

[130] Norstrom, M. and M.L. Gardel, *Shear thickening of F-actin networks crosslinked with non-muscle myosin IIB.* Soft Matter, 2011. 2011(7): p. 3228-3233.

[131] Yao, N.Y., et al., *Stress-enhanced gelation: a dynamic nonlinearity of elasticity.* Phys Rev Lett, 2013. 110(1): p. 018103.

[132] Furuike, S., T. Ito, and M. Yamazaki, *Mechanical unfolding of single filamin A (ABP-280) molecules detected by actomic force microscopy.* FEBS Letters, 2001. 498: p. 72-75.

[133] Kolahi, K.S. and M.R. Mofrad, *Molecular mechanics of filamin's rod domain.* Biophys J, 2008. 94(3): p. 1075-1083.

[134] Janmey, P.A., et al., *Viscoelastic Properties of Vimentin Compared with Other Filamentous Biopolymer Networks.* J. Cell Biol, 1991. 113: p. 155-160.
[135] Humphrey, D., et al., *Active fluidization of polymer networks through molecular motors.* Nature, 2002. 416(6879): p. 413-416.
[136] Tharmann, R., M.M. Claessens, and A.R. Bausch, *Viscoelasticity of isotropically cross-linked actin networks.* Phys Rev Lett, 2007. 98(8): p. 088103.
[137] Bray, D. and J.G. White, *Cortical flow in animal cells.* Science, 1988. 239(4842): p. 883-888.
[138] Chugh, P., et al., *Actin cortex architecture regulates cell surface tension.* Nat Cell Biol, 2017. 19(6): p. 689-697.
[139] Gong, B., et al., *Cross-linked biopolymer networks with active motors: Mechanical response and intra-network transport.* J Mech Phys Solids, 2019. 127: p. 80-93.
[140] Sept, D., et al., *Annealing Accounts for the Length of Actin Filaments Formed by Spontaneous Polymerization.* Biophys J, 1999. 77: p. 2911-2919.
[141] Burlacu, S., P.A. Janmey, and J. Borejdo, *Distribution of actin filament lengths measured by fluorescence microscopy.* Am J Physiol Cell Physiol, 1992. 262(3): p. C569-C577.
[142] Schmidt, F.G., F. Ziemann, and E. Sackmann, *Shear field mapping in actin networks by using magnetic tweezers.* Eur Biophys J., 1996. 24: p. 348-353.
[143] Ehrlicher, A.J., et al., *Mechanical strain in actin networks regulates FilGAP and integrin binding to filamin A.* Nature, 2011. 478(7368): p. 260-263.
[144] Zhou, A.X., J.H. Hartwig, and L.M. Akyurek, *Filamins in cell signaling, transcription and organ development.* Trends Cell Biol, 2010. 20(2): p. 113-123.
[145] Kim, H. and C.A. McCulloch, *Filamin A mediates interactions between cytoskeletal proteins that control cell adhesion.* FEBS Lett, 2011. 585(1): p. 18-22.
[146] Shizuta, Y., et al., *Purification and properties of filamin, and actin binding protein from chicken gizzard.* J. Biol. Chem., 1976. 251(21): p. 6562-6567.
[147] Chen, C., T.J. Lu, and N.A. Fleck, *Effect of imperfections on the yielding of two-dimensional foams.* Journal of the Mechanics and Physics of Solids, 1999. 47: p. 2235-3372.
[148] Zhu, H.X., J.R. Hobdell, and A.H. Windle, *Effects of cell irregularity on the elastic properties of open-cell foams.* Acta Mater, 2000. 48: p. 4893-4900.
[149] Zhu, H.X., J.R. Hobdell, and A.H. Windle, *Effects of cell irregularity on the elastic properties of 2D Voronoi honeycombs.* J Mech Phys Solids, 2001. 49(4): p. 857-870.
[150] Zhu, H.X., *Size-dependent elastic properties of micro- and nano-honeycombs.* J Mech Phys Solids, 2010. 58(5): p. 696-709.
[151] Zhu, H.X., et al., *Size-dependent and tunable elastic properties of hierarchical honeycombs with regular square and equilateral triangular cells.* Acta Mater, 2012. 60(12): p. 4927-4939.
[152] Chiu, J.J. and S. Chien, *Effects of Disturbed Flow on Vascular Endothelium: Pathophysiological Basis and Clinical Perspectives.* Physiol Rev, 2011. 91(1): p. 327-387.
[153] Lin, X., et al., *The elastic properties of composites reinforced by a transversely isotropic random fibre-network.* Composite Structures, 2019. 208: p. 33-44.
[154] Lin, Y.C., et al., *Origins of elasticity in intermediate filament networks.* Phys Rev Lett, 2010. 104(5): p. 058101.
[155] Goldmann, W.H., et al., *Viscoelasticity of actin-gelsolin networks in the presence of filamin.* Eur. J. Biochem., 1997. 246: p. 373-379.
[156] Lee, H., et al., *Passive and active microrheology for cross-linked F-actin networks in vitro.* Acta Biomater, 2010. 6(4): p. 1207-1218.

[157] Huang, S. and D.E. Ingber, *The structural and mechanical complexity of cell-growth control.* Nature Cell Biology, 1999. 1(5): p. E131-E138.

[158] Xu, J., Y. Tseng, and D. Wirtz, *Strain Hardening of Actin Filament Networks.* The Journal of Biological Chemistry, 2000. 275(46): p. 35886-35892.

[159] Kang, H., et al., *Nonlinear Elasticity of Stiff Filament Networks Strain Stiffening, Negative Normal Stress, and Filament Alignment in Fibrin Gels.* J. Phys. Chem. B, 2009. 113: p. 3799-3805.

[160] Piechocka, I.K., et al., *Multi-scale strain-stiffening of semiflexible bundle networks.* Soft Matter, 2016. 12: p. 2145-2156.

[161] Broedersz, C.P., C. Storm, and F.C. MacKintosh, *Nonlinear elasticity of composite networks of stiff biopolymers with flexible linkers.* Phys Rev Lett, 2008. 101(11): p. 118103.

[162] Liu, X. and G.H. Pollack, *Mechanics of F-Actin Characterized with Microfabricated Cantilevers.* Biophysical Journal, 2002. 83: p. 2705-2715.

[163] Ferrer, J.M., et al., *Measuring molecular rupture forces between single actin filaments and actin-binding proteins.* Proc Natl Acad Sci U S A, 2008. 105: p. 9221-9226.

[164] Janmey, P.A., et al., *Negative normal stress in semiflexible biopolymer gels.* Nat Mater, 2007. 6(1): p. 48-51.

[165] MacKintosh, F.C. and P.A. Janmey, *Actin gels.* Current Opinion in Solid State & Materials Science, 1997. 2(3): p. 350-357.

[166] Tsuda, Y., et al., *Torsional rigidity of single actin filaments and actin–actin bond breaking force under torsion measured directly by in vitro micromanipulation.* Proc. Natl. Acad. Sci. USA, 1996. 93: p. 12937-12942.

[167] Nam, S., et al., *Strain-enhanced stress relaxation impacts nonlinear elasticity in collagen gels.* Proc Natl Acad Sci U S A, 2016. 113(20): p. 5492-5497.

[168] Zhu, H.X. and N.J. Mills, *Modelling the creep of open-cell polymer foams.* J Mech Phys Solids, 1999. 47: p. 1437-1457.

[169] Gittes, F. and F.C. MacKintosh, *Dynamic shear modulus of a semiflexible polymer network.* Phys Rev E Stat Nonlin Soft Matter Phys, 1998. 58(2): p. R1241-R1244.

[170] Morse, D.C., *Viscoelasticity of tightly entangled solutions of semiflexible polymers.* Phys Rev E Stat Nonlin Soft Matter Phys, 1998. 58(2): p. R1237-R1240.

Publications

Journal papers

Xiaobo Wang, Hanxing Zhu, Yongtao Lu, Zuobin Wang and David Kennedy, The elastic properties and deformation mechanisms of actin filament networks crosslinked by filamins, Journal of the Mechanical Behavior of Biomedical Materials, 2020, 112, 104075.

Xiaobo Wang, Hanxing Zhu, and David Kennedy, The deformation mechanisms of crosslinked actin filament networks under large deformation, in preparation

Xiaobo Wang, Hanxing Zhu, and David Kennedy, Investigation on viscoelastic properties of actin filament networks crosslinked by filamins, in preparation

Conference papers

Wang, X., Zhu, H. And Kennedy, D. 2018. Effects of crosslink geometry on the elastic properties of nano-structured biopolymer networks. Presented at: 6th European Conferences on Computational Mechanics, Glasgow, UK, 10-15 June 2018.

Wang, X., Zhu, H. And Kennedy, D. 2019. Viscoelastic properties of crosslinked actin filament networks. Presented at: 12th EBSA Biophysics Congress, 10th ICBP-IUPAP Biophysics Congress, Madrid, Spain, 20-24 July 2019.

Wang, X., Zhu, H. And Kennedy, D. 2020. Nonlinear elastic properties of crosslinked actin filament networks. Presented at: Cardiff Institute for Tissue Engineering & Repair Annual Scientific Meeting (CITER ASM), Cardiff, UK, 14-15 September 2020, ISSN: 2634-100X.